THÈSE

présentée à

L'Université Bordeaux I

Ecole Doctorale des Sciences Physiques et de l'Ingénieure

par

Yek Wah LAM
(Yi Hua LAM 藍乙華)

Pour obtenir le grade de

DOCTEUR

Spécialité Astrophysique, Plasmas, Nucléaire

Isospin Symmetry Breaking in sd Shell Nuclei

Soutenue le 13 decembre 2011

Après avis de:

M. Piet Van ISACKER	DR, CEA, GANIL	**Rapporteur externe**
M. Frederic NOWACKI	DR, CNRS, IHPC, Strasbourg	**Rapporteur externe**

Devant la commission d'examen formée de:

M. Bertram BLANK	DR, CNRS, CEN Bordeaux-Gradignan	**Président**
M. Michael BENDER	DR, CNRS, CEN Bordeaux-Gradignan	**Directeur de thèse**
M. Van Giai NGUYEN	DR, CNRS, IPN, Orsay	**Examinateurs**
M. Piet Van ISACKER	DR, CEA, GANIL	
M. Frederic NOWACKI	DR, CNRS, IHPC, Strasbourg	
Mme. Nadezda SMIRNOVA	Maître de Conférences, Université Bordeaux I	

Dedicated to my beloved wife Mei Chee Chan (陳美芝),
and my dear son Yu Xuan Lam (藍豫謨),
without whose consistent encouragement
and total sacrifice, this thesis
would have never been
touched by the light.

And dedicated to the late Peik Ching Ho (何碧清),
my grandma who loved me most,
and lost her beloved hubby
during WW2, and rebuilt
our family determinantly.

Acknowledgments

As a mechanical engineering graduate, I opted not to follow the ordinary trend of graduates. Most of them have a rather easy life with high income, whereas I have chosen a different path of life – pursuing theoretical physics career – the so-called abnormal path in ordinary Malaysians perspective. And I have to be ready that there is no guarantee for the future...

No matter how many impedences and how challenging the path is, I keep my faith on Him and trust His guidance. I thank God for His grace and faithful love. Throughout the moment I pursue the PhD thesis, He has sent many angels to me, like Patrick AURENCHE (LAPTH, Annecy) whom I knew since 2003, and Vincent BRETON (LPC, Clermont-Ferrand) known in 2007. I appreciate their consistent concerns about my stay and research work in France, and Vincent's prayers.

Moreover, I am deeply indebted to Nadya A. SMIRNOVA, who is my sister in Christ, and is my sister in life and nuclear physics. Special thank to her, Etienne CAURIER, and Frederic NOWACKI for introducing me to nuclear shell model; and Piet Van Isacker for fruitful discussion in dynamical symmetry breaking and Wigner's supermultiplet theory. Meanwhile, I would like to thank Michael BENDER, who is the mean-field approach expert, and seems to be my big brother, who fight for me with the bureaucratics. He works together with Philippe QUENTIN, Bernard HASS, and Arnaud GAUFFIER for securing financial support from the embassy of France in Malaysia.

Besides, I thank Bertram BLANK and Jérôme GIOVINAZZO for the calculation of experimental uncertainties, as well as fruitful discussions about isospin-forbidden proton emissions; and Johnny PINSON and Catherine SEZNEC for I.T. support.

I thank Benoit AVEC in sharing his knowledge of mean-field approach, and Julien LE BLOAS for his workstation, hence I managed to push many results during the last stage of PhD; and Patricia GABINSKI for her support to file a lawsuit to la CAF about their discriminate decision on my beloved son. Finally, I won the lawsuit.

Special thanks for the juniors, who work in other laboratories, have helped me to obtain some very important articles. They are Casey CHEW Soo Hoon (周淑芬) (TU Munich, Germany), Marc CHEONG (Monash Univ., Australia), and HOANG Ngoc Duy (Lund Univ., Sweden).

張建華賀贈乙華弟兄蘿薛
抄借——张悦《洰湖山寺》

學案寂歷常倚道，虛谷若懷誦書聲，
核理未能雲外賞，太初豈是世中情，
書山踏盡千重出，答辯靈台一片明，
巢由若悟箇中意，不願蘿薛易簪纓。

LAM Yi Hua (藍乙華)

Contents

Contents

Contents

"Nature seems to take advantage of the simple mathematical representations of the symmetry laws. When one pauses to consider the elegance and the beautiful perfection of the mathematical reasoning involved and contrast it with the complex and far reaching physical consequences, a deep sense of respect for the power of the symmetry laws never fails to develop."
Chen Ning Yang (楊振寧).

Contents

Chapter 1

Isospin Symmetry and Its Breaking in Nuclear Structure

Contents

The isospin symmetry is an approximate, but very useful symmetry of atomic nuclei. It takes advantage of the similarity between a proton and a neutron, considering them as two different charge states of a nucleon. Indeed the masses of the proton and the neutron are very close, $m_p = 938.272013(23)\mathrm{MeV/c^2}$ and $m_n = 939.565379(21)\mathrm{MeV/c^2}$ [1], and the mass ratio is about one, i.e., $m_n/m_p = 1.001378$. In addition, as we will show later in this chapter, the nuclear forces are to a good level of approximation charge-independent, i.e. the strong proton-proton, neutron-neutron and proton-neutron interactions may roughly be considered identical.

For many years, the isospin symmetry has been serving as a stringent guideline for the construction of the nucleon-nucleon interaction. Some nuclear models (such as the shell model) explicitly implement the isospin scheme to simplify the calculations. Eigenstates of an isospin-invariant Hamiltonian can be characterized by additional quantum numbers related to the isospin. This proposes a classification scheme for nuclear states, as well as for baryons and mesons in particle physics.

Nevertheless, the isospin symmetry is broken by electromagnetic interactions, isospin non-conserving component of strong force, and differences in proton and neutron masses. The degree of the breaking is small compared to the nuclear scale, however, it should be explicitly taken

into account for the description of isospin-forbidden phenomena. In this thesis, we develop isospin non-conserving shell-model Hamiltonians capable to precisely describe the experimentally measured isospin-symmetry breaking effects.

In this chapter we first briefly sketch the isospin formalism, then we explain how the isospin symmetry in a many-nucleon system (nucleus) is broken and we indicate the physics motivation for the theoretical study of isospin-symmetry breaking.

1.1   Isospin Formalism

The isospin formalism was proposed by Heisenberg [2], soon after discovery of the neutron by Chadwick [3]. Assuming that the proton and the neutron have very similar masses, he proposed to consider them as two different charge states of the same particle, a nucleon. To distinguish between them he introduced a new variable, t_z, assigning $t_z = +1/2$ to the neutron and $t_z = -1/2$ to the proton. The mathematical formalism of the isospin used by Heisenberg is analogous to the formalism of the intrinsic spin devised by Pauli.

There is nowadays a lot of experimental evidence for the validity of the isospin concept in nuclear physics. The nucleon-nucleon interaction possesses a genuine isospin symmetry confirmed by experiment.

First, experimental data on $^1S_0$ scattering lengths in two-nucleon isospin-1 system (proton-proton, proton-neutron and neutron-neutron) are not very different after electromagnetic effects are removed [4]:

$$a_{pp}^N = -17.3 \pm 0.4 \text{ fm}, \quad a_{nn}^N = -18.95 \pm 0.40 \text{ fm}, \quad a_{np}^N = -23.740 \pm 0.020 \text{ fm}. \tag{1.1}$$

Indeed, if the Coulomb interaction between two protons is ignored, the strong nuclear interaction in a neutron-neutron and a proton-proton system is the same. This property is referred to as *charge symmetry* of the nuclear force. At a higher level of approximation, the strong nuclear neutron-neutron, proton-proton, and neutron-proton interactions can be considered the same, leading to the *charge independence* of the nuclear force [5, 6, 7].

These properties of the nuclear interaction are confirmed by experimental nuclear spectra. Let us consider *mirror nuclei*, i.e. a pair of nuclei which transform into each other by interchanging their proton and neutron numbers. In general, they have very similar energy level schemes relative to their ground states. The difference in their binding energies is mainly due to the different Coulomb energy in two mirror systems. As an example, we present the low-lying energy spectra of $^{33}_{16}\text{S}_{17}$ and $^{33}_{17}\text{Cl}_{16}$ in Fig. 1.1. Thus, substitution of all neutron-neutron bonds by proton-proton bonds and vice versa almost does not alter the energy levels. This is the manifestation of the charge symmetry of the nuclear force.
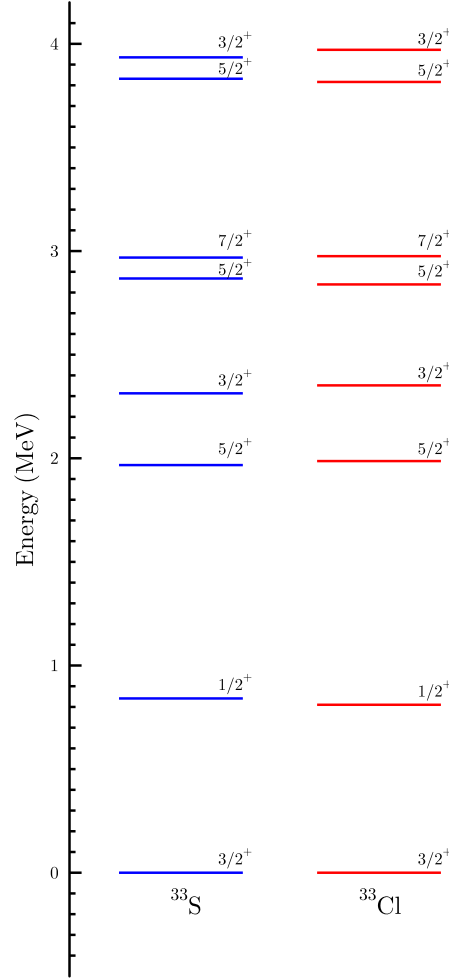
Figure 1.1: *Comparison of the level schemes of the mirror nuclei $^{33}_{16}\text{S}_{17}$ and $^{33}_{17}\text{Cl}_{16}$.*
This plot shows only positive-parity levels. The excitation energies of the states with the same total angular momentum J and parity π exhibit close similarity in mirror nuclei.

Similarly, we can consider the low-energy spectra of three isobars, which include an $N = Z$ nucleus and a neighboring mirror pair. As an example, excitation energies of low-lying states in $^{34}_{16}\text{S}_{18}$, $^{34}_{17}\text{Cl}_{17}$, and $^{34}_{18}\text{Ar}_{16}$ are shown in Fig. 1.2. As was discussed above, the spectra of mirror nuclei are similar, but in addition we find analogous states (of the same spin and parity and similar excitation energy) among the low-lying states in ^{34}Cl (only these analogue states are shown in Fig. 1.2). The difference in the binding energies of the isobars is mainly due to the different Coulomb energy. The similarities of the spectra allow us to conclude that the total nuclear interaction energy of the many-nucleon system is (almost) invariant under interchange of neutron-neutron, neutron-proton, and proton-proton interactions. This is the confirmation of the charge independence of the nuclear force.
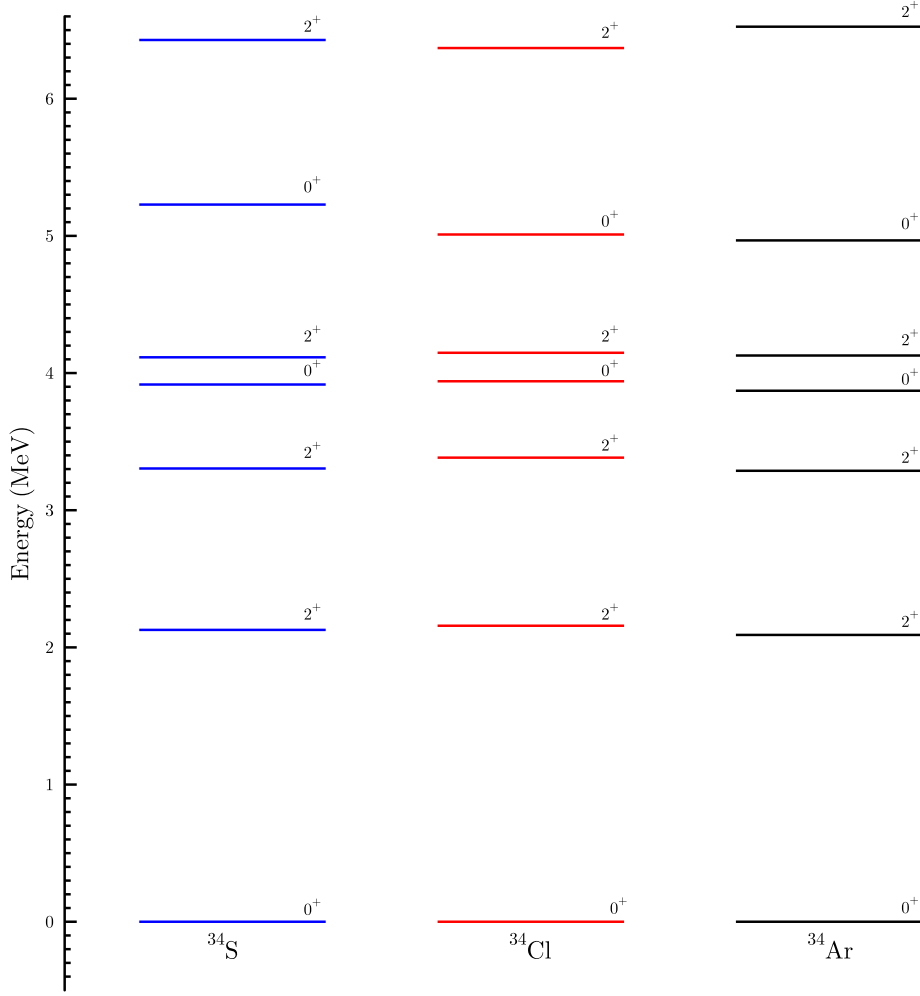
Figure 1.2: *Comparison of the level schemes of $^{34}_{16}S_{18}$ and $^{34}_{18}Ar_{16}$, and partial level schemes of $^{34}_{17}Cl_{17}$. The excitation energies of the states with the same total angular momentum J and parity π exhibit close similarity in these three nuclei.*

The isospin space (isospace) is an abstract space, spanned by the vectors (isospinors) representing proton and neutron states. In a matrix representation,

$$|p\rangle = \begin{pmatrix} 0 \\ 1 \end{pmatrix} , \qquad |n\rangle = \begin{pmatrix} 1 \\ 0 \end{pmatrix} . \tag{1.2}$$

The isospin operator is a vector $\vec{t}$, defined by its three components

$$t_x = \frac{1}{2} \begin{pmatrix} 0 & 1 \\ 1 & 0 \end{pmatrix} , \qquad t_y = \frac{1}{2} \begin{pmatrix} 0 & -i \\ i & 0 \end{pmatrix} , \qquad t_z = \frac{1}{2} \begin{pmatrix} 1 & 0 \\ 0 & -1 \end{pmatrix} , \tag{1.3}$$

where t_x, t_y, and t_z, respectively, project the nucleon state on the x-, y-, and z-axis in the isospace. These t_x, t_y, and t_z operators obey the SU(2) commutation relations,

$$[t_x, t_y] = i t_z , \tag{1.4}$$

with cyclic permutations; whereas the SU(2) Casimir operator[1] $\vec{t}^2 = t_x^2 + t_y^2 + t_z^2$ commutes with the SU(2) generators,

$$\left[\vec{t}^2, t_i\right] = 0, \quad \text{for} \quad i = x, y, z. \tag{1.5}$$

The eigenvalue of $\vec{t}^2$ is $t(t+1)$. Acting with t_z on a proton state or on a neutron state given in Eq.(1.2), we obtain

$$t_z |p\rangle = \frac{1}{2} \begin{pmatrix} 1 & 0 \\ 0 & -1 \end{pmatrix} \begin{pmatrix} 1 \\ 0 \end{pmatrix} = -\frac{1}{2} |p\rangle, \qquad t_z |n\rangle = \frac{1}{2} \begin{pmatrix} 1 & 0 \\ 0 & -1 \end{pmatrix} \begin{pmatrix} 1 \\ 0 \end{pmatrix} = \frac{1}{2} |n\rangle. \tag{1.6}$$

The eigenvalues of t_z are thus $-1/2$ for the proton and $+1/2$ for the neutron. High-energy physicists use opposite signs for the eigenvalues of t_z for the proton and the neutron. Other than t_x, t_y, and t_z operators, we may introduce ladder operators t_+ and t_- defined as

$$t_+ \equiv t_x + it_y, \qquad t_- \equiv t_x - it_y, \tag{1.7}$$

which obey the commutation relations:

$$[t_z, t_\pm] = \pm t_\pm, \qquad [t_+, t_-] = 2t_z. \tag{1.8}$$

These isospin ladder operators t_+ and t_- are also called raising and lowering operators, respectively. They transform a proton state into a neutron state and vice versa,

$$
\begin{aligned}
t_+ |p\rangle &= |n\rangle, & t_- |p\rangle &= 0, \\
t_- |n\rangle &= |p\rangle, & t_+ |n\rangle &= 0.
\end{aligned}
\tag{1.9}
$$

These operations are useful to describe the β-decay.

The electric charge operator in the isospin formalism reads $Q = e(1 - 2t_z)/2$, and acquires the following form in matrix representation :

$$Q = e \begin{pmatrix} 0 & 0 \\ 0 & 1 \end{pmatrix}, \tag{1.10}$$

with e denoting the proton charge. This charge operator is deduced from the relations below

$$\frac{1}{2}(1 - 2t_z) |p\rangle = |p\rangle, \qquad \frac{1}{2}(1 - 2t_z) |n\rangle = 0. \tag{1.11}$$

The isospin operator and its z-component of a many-nucleon system can be constructed from nucleonic isospin operators as

$$\vec{T}_{\text{total}} = \sum_{i=1}^{A} \vec{t}_i, \qquad T_z = \sum_{i=1}^{A} t_{z_i}, \tag{1.12}$$

---

[1] A Casimir operator (or a Casimir invariant) is an operator which commutes with all elements of a Lie algebra [8]. Eq.(1.4) shows that isospin operators t_x, t_y, and t_z form a Lie algebra τ, and $\vec{t}^2$ commutes with all operators of τ. A Casimir operator can be a linear, quadratic, cubic, quartic, ..., form in the elements t_i.

where A is the nuclear mass number or the total number of nucleons in a nucleus. The components of $\vec{T}$ obey similar commutation relations as those given in Eq.(1.5). The eigenvalue of the $\vec{T}^2$ operator is $T(T+1)$. If A is even, the total isospin quantum number T is an integer, if A is odd, T is half-odd-integer. For each value of T, there are $(2T+1)$ eigenstates of $\vec{T}^2$, characterized by different T_z values. They form a so-called *isospin multiplet* (or *isobaric multiplet*) of states with

$$T_z = -T, -T+1, \ldots, T-1, T. \tag{1.13}$$

An isospin multiplet with $T = 1/2$, $T = 1$, $T = 3/2$ and $T = 2$ is a doublet, a triplet, a quartet (or a quadruplet) and a quintet of states, respectively.

For a nucleus with Z protons and N neutrons, $T_z = \frac{1}{2}(N-Z)$, while the total isospin can have the following values compatible with T_z:

$$T = |T_z|, |T_z|+1, |T_z|+2, \ldots, \frac{1}{2}A. \tag{1.14}$$

Generally, ground states of all nuclei have the isospin $T = |T_z|$, except for some $N = Z$ odd-odd nuclei.

If the Hamiltonian $\mathscr{H}_0$ of an A-nucleon system is isospin-invariant (it does not include the Coulomb interaction and nucleon-nucleon interactions are assumed to be charge-independent), i.e.

$$[\mathscr{H}_0, \vec{T}] = 0, \tag{1.15}$$

its eigenstate states can be characterized by the isospin quantum number T and its projection T_z. Thus, the isospin formalism can be used in the classification of nuclear states. Denoting the Hamiltonian eigenstates as $|\alpha, T, T_z\rangle$, where α defines other relevant quantum numbers (J, π, etc, including A), we get

$$\vec{T}^2 |\alpha, T, T_z\rangle = T(T+1) |\alpha, T, T_z\rangle,$$
$$T_z |\alpha, T, T_z\rangle = T_z |\alpha, T, T_z\rangle. \tag{1.16}$$

States in the isobars, having the same α and T quantum numbers, but different T_z values are called *isobaric analogue states* (IAS). As an example, let us return to isospin triplets of states in $A = 34$ nuclei, illustrated above. The states of the same J^π and excitation number are $T = 1$ states (IAS). In the spectrum of $^{34}_{17}\mathrm{Cl}_{17}$, there are also $T = 0$ states which do not have analogues in neighboring isobars. In principle, at higher excitation energy one can find states with higher T-values, i.e. $T = 2$ which are members of an isobaric quintet of states. These states are not shown in the figure.

All member states of an isospin multiplet can be transformed to one another by the total isospin raising and/or lowering operators

$$T_\pm \equiv T_x \pm iT_y = \sum_{i=1}^{A} (t_x(i) \pm it_y(i)), \tag{1.17}$$

which are given by the summation of single-nucleon isospin raising and lowering operators Eq.(1.7). These total isospin ladder operators satisfy the following commutation relations

$$[T_z, T_\pm] = \pm T_\pm \,, \qquad [T_+, T_-] = 2T_z \,. \tag{1.18}$$

Applying these ladder operators to a nuclear state $|\alpha, T, T_z\rangle$ we get

$$T_\pm |\alpha, T, T_z\rangle = \sqrt{T(T+1) - T_z(T_z \pm 1)} \, |\alpha, T, T_z \pm 1\rangle \,. \tag{1.19}$$

To conclude, let us remark that the fact that the Hamiltonian commutes with the T_z operator implies that the electric charge is conserved ($[\mathscr{H}_0, Q] = 0$).

1.2 Isospin Symmetry Breaking

The isospin symmetry is only an approximate symmetry of a nuclear Hamiltonian due to the presence of electromagnetic interactions, isospin non-conserving strong force, and difference in nucleonic masses. The largest source of the isospin symmetry breaking is the Coulomb interaction between protons.

Isospin-symmetry breaking (ISB) in nuclear states can be explained by the idea of dynamical symmetry breaking[2] [9].

1.2.1 Perturbation theory analysis

Coulomb interaction

The Coulomb force acting between protons is the main source of the isospin-symmetry breaking in an atomic nucleus. The Coulomb interaction represented in the isospin formalism has the form:

$$V_{coul} = \sum_{i<j} \frac{Q_i Q_j}{|\vec{r}_i - \vec{r}_j|} = e^2 \sum_{i<j} \left(\frac{1}{2} - t_z(i)\right)\left(\frac{1}{2} - t_z(j)\right)\frac{1}{|\vec{r}_i - \vec{r}_j|} \,, \tag{1.20}$$

---

[2] The physical meaning of dynamical symmetry breaking in this context is different from the one described in condensed matter and particle physics. The latter symmetry breaking is a special form of spontaneous symmetry breaking.

and can be expanded as a sum of isoscalar, isovector, and isotensor operators [9, 10],

$$
\begin{aligned}
V_{coul} &= \sum_{q=0,1,2} V_{coul}^{(q)} \\
&= V_{coul}^{(0)} + V_{coul}^{(1)} + V_{coul}^{(2)} \\
&= e^2 \sum_{i<j} \left(\frac{1}{4} + \frac{1}{3} \vec{t}(i) \cdot \vec{t}(j) \right) \frac{1}{|\vec{r}_i - \vec{r}_j|} \\
&\quad - \frac{e^2}{2} \sum_{i<j} (t_z(i) + t_z(j)) \frac{1}{|\vec{r}_i - \vec{r}_j|} \\
&\quad + e^2 \sum_{i<j} \left(t_z(i)t_z(j) - \frac{1}{3} \vec{t}(i) \cdot \vec{t}(j) \right) \frac{1}{|\vec{r}_i - \vec{r}_j|} .
\end{aligned}
\tag{1.21}
$$

where q corresponds to the rank of tensor in isospace. All these operators are 0-components of rank-q isotensors, since the electric charge is conserved.

The effect of the Coulomb interaction can be treated within perturbation theory. In the lowest-order approximation, the isospin symmetry turns out to be broken in a dynamical way [9]. The isoscalar term $V_{coul}^{(0)}$ is invariant with respect to isospin SU(2) group, whereas the isovector term $V_{coul}^{(1)}$ and the isotensor term $V_{coul}^{(2)}$ are invariant with respect to isospin SO(2), a subgroup of SU(2). $V_{coul}^{(1)}$ and $V_{coul}^{(2)}$ contain the operators T_z and T_z^2, respectively.

In the lowest order of perturbation theory, the energy shift of a given member of an isobaric multiplet due to the Coulomb interaction is expressed by the expectation value of the Coulomb interaction in this state, namely,

$$
E_{coul}(\alpha, T, T_z) = \langle \alpha, T, T_z | V_{coul} | \alpha, T, T_z \rangle .
\tag{1.22}
$$

Applying the Wigner-Eckart theorem [11], we can factor out the T_z dependence, to obtain the following expression:

$$
\begin{aligned}
E_{coul}(\alpha, T, T_z) &= \langle \alpha, T, T_z | \sum_{q=0,1,2} V_{coul}^{(q)} | \alpha, T, T_z \rangle \\
&= \sum_{q=0,1,2} (-1)^{T-T_z} \begin{pmatrix} T & q & T \\ -T_z & 0 & T_z \end{pmatrix} \langle \alpha, T \| V_{coul}^{(q)} \| \alpha, T \rangle \\
&= E_{coul}^{(0)}(\alpha, T) + E_{coul}^{(1)}(\alpha, T)T_z + E_{coul}^{(2)}(\alpha, T)(3T_z^2 - T(T+1)),
\end{aligned}
\tag{1.23}
$$

where

$$
\begin{aligned}
E_{coul}^{(0)}(\alpha, T) &= \frac{1}{\sqrt{2T+1}} \langle \alpha, T \| V_{coul}^{(0)} \| \alpha, T \rangle , \\
E_{coul}^{(1)}(\alpha, T) &= \frac{1}{\sqrt{T(2T+1)(T+1)}} \langle \alpha, T \| V_{coul}^{(1)} \| \alpha, T \rangle , \\
E_{coul}^{(2)}(\alpha, T) &= \frac{1}{\sqrt{T(2T+3)(2T+1)(T+1)(2T-1)}} \langle \alpha, T \| V_{coul}^{(2)} \| \alpha, T \rangle .
\end{aligned}
\tag{1.24}
$$

The matrix elements with two bars denote reduced matrix elements (in isospin space).

Thus, in lowest-order perturbation theory, the diagonal matrix elements of the Coulomb interaction $\langle \alpha, T, T_z | V_{coul} | \alpha, T, T_z \rangle$ are given by a quadratic form of T_z, c.f. Eq.(1.23), while the off-diagonal isospin mixing matrix elements of the Coulomb interaction $\langle \alpha, T, T_z | V_{coul} | \alpha, T', T_z \rangle$ are neglected. In this case, V_{coul} is assumed not to mix states $|\alpha, T, T_z\rangle$ having different values of T ($T = T_z, T_z+1, \ldots$), and isospin T is still a good quantum number. However, the $(2T+1)$-fold degeneracy is now removed. The isobaric multiplet is thus splitted in $(2T+1)$ components.

We make use of Eq.(1.23) to obtain the mass excess of an isospin-T multiplet member in a specific state defined by α:

$$M(\alpha, T, T_z) = \frac{1}{2}(M_n + M_H)A + (M_n - M_H)T_z + \langle \alpha, T, T_z | \mathscr{H}_0 | \alpha, T, T_z \rangle + E_{coul}(\alpha, T, T_z), \quad (1.25)$$

where M_n and M_H are the neutron mass and hydrogen mass, respectively. From hereon, $\mathscr{H}_0$ represents the isospin-invariant nuclear Hamiltonian (having charge-independent interactions only). Therefore, Eq.(1.25) can be recast as

$$M(\alpha, T, T_z) = a(\alpha, T) + b(\alpha, T)T_z + c(\alpha, T)T_z^2, \quad (1.26)$$

which is the famous *isobaric multiplet mass equation* (IMME) [12, 13], where

$$
\begin{aligned}
a(\alpha, T) = {} & \frac{1}{2}(M_n + M_H)A \\
& + \langle \alpha, T, T_z | \mathscr{H}_0 | \alpha, T, T_z \rangle \\
& + E_{coul}^{(0)}(\alpha, T) - T(T+1)E_{coul}^{(2)}(\alpha, T), \\
b(\alpha, T) = {} & \Delta_{nH} - E_{coul}^{(1)}(\alpha, T), \\
c(\alpha, T) = {} & 3E_{coul}^{(2)}(\alpha, T).
\end{aligned}
\quad (1.27)
$$

The expressions for the coefficients $a(\alpha, T)$, $b(\alpha, T)$, and $c(\alpha, T)$ for $T = 1/2, 1, 3/2, 2$ are given in the next chapter. The neutron-hydrogen mass difference is $\Delta_{nH} = M_n - M_H = 782.347$ keV (c.f. Table A.2 of Appendix A). Experimentally, the values of $a(\alpha, T), b(\alpha, T)$, and $c(\alpha, T)$ are ~100 MeV, 3–15 MeV, and ~200–300 keV, respectively.

Charge-dependence of the NN interaction

The discussion above is also valid if instead of the Coulomb interaction we consider two-body charge-dependent nuclear forces. Evidence for the charge-symmetry breaking and charge-independence breaking in the NN interaction comes from scattering experiments. First, there is a small difference between v_{pp}^N and v_{nn}^N (e.g., different scattering lengths in $^1S_0$ channel: $a_{pp}^N - a_{nn}^N = 1.65 \pm 0.60$ fm [4]) which implies *charge-symmetry breaking* (or *charge-asymmetry*) of the NN interaction. Second, there is an even more substantial difference between v_{pp}^N and v_{nn}^N from one side and v_{pn}^N from the other side (e.g., different singlet scattering lengths: $(a_{pp}^N + a_{nn}^N)/2 - a_{np}^N = 5.6 \pm 0.6$ fm) which corroborates the *charge-independence breaking* of the NN

interaction. Detailed consideration and theoretical studies of these effects can be found in Refs. [4, 14, 15, 16]

The existence of non-vanishing charge-dependent NN forces may result in a non-negligible isospin-symmetry breaking component of the effective NN interaction, which should be taken into account when solving a many-body problem. Similar to the Coulomb interaction, isospin-symmetry breaking two-body nuclear forces are tensors of rank 1 and 2 in isospin space. Since their magnitude is even smaller than that of the Coulomb interaction, we can exploit the same technique of the perturbation theory as explained in the previous section. Therefore, instead of V_{coul} in Eq.(1.23), we can use a charge-dependent part of the nuclear Hamiltonian, which may include both the Coulomb interaction and charge-dependent forces of nuclear origin, V_{CD}, i.e.

$$H_{CD} = V_{coul} + V_{CD}.$$

1.2.2 Exact treatment: Isospin Impurities in Nuclear States

The Coulomb interaction and charge-dependent nuclear forces do not commute with the isospin operator,

$$[\mathscr{H}_0 + H_{CD}, \vec{T}] \neq 0, \qquad [\mathscr{H}_0 + H_{CD}, \vec{T}^2] \neq 0. \tag{1.28}$$

Therefore the total Hamiltonian is not invariant under rotations in isospace and the isospin is not conserved. Furthermore, the isospin symmetry is also violated if we take into account the neutron-proton mass difference, $\Delta M = M_n - M_p$, which causes the kinetic operator for nucleons not to commute with $\vec{T}$ and with $\vec{T}^2$ [7].

Let us call this total Hamiltonian the *isospin non-conserving* (INC) *Hamiltonian* H_{INC}. Its charge-dependent part, H_{CD}, is due to the Coulomb interaction between protons, the neutron-proton mass difference and effective nuclear charge-dependent interactions. The eigenstates of an INC Hamiltonian are admixture of different isospin eigenstates. Therefore, we speak about *isospin impurities* in nuclear states.

1.3 Physics Motivation

The degree of isospin non-conservation due to the Coulomb interaction and charge-dependent nuclear forces is small compared to nuclear effects. However, a precise description of the ISB in nuclear states is crucial when the nucleus is considered as a laboratory to test the fundamental symmetries underlying the Standard Model of the electroweak interaction. One of the important applications is the calculation of so-called nuclear-structure corrections to the nuclear β-decay. These corrections arise due to isospin mixing in nuclear states which should be evaluated within a nuclear many-body model.

In particular, high-precision theoretical values of nuclear structure corrections to superallowed $0^+ \to 0^+$ β-decay rates are of major interest. Combined with various radiative corrections, they serve to extract an absolute $\mathscr{F}t$-value from observed ft-values of these purely Fermi transitions for nuclear beta decay. The constant $\mathscr{F}t$ would confirm the conserved vector current (CVC) hypothesis and would allow one to deduce the nuclear weak-interaction coupling constant, G_F. The ratio of the latter to the weak-interaction coupling constant extracted from the muon decay results in V_{ud}, which is the upper-left matrix element of the Cabibbo-Kobayashi-Maskawa (CKM) quark-mixing matrix. The upper row of the CKM matrix is the one which provides a stringent test for the unitarity, with V_{ud} being the major contributor (around ~94%). The breakdown of the unitarity would signify a possibility of new physics beyond the Standard Model, see Ref. [17] for a recent review.

Nowadays, ft-values for thirteen $0^+ \to 0^+$ β^+-transitions among $T = 1$ analogue states are known with a precision better than 0.1%. The largest uncertainty on the extracted $\mathscr{F}t$ value (which is about 0.4%) is due to the ambiguous calculation of the nuclear-structure correction [18]. Therefore, an accurate theoretical description of isospin mixing in nuclear states is of primary importance.

Similarly, theoretical calculations of nuclear-structure corrections to Fermi β-decay are necessary to extract the absolute $\mathscr{F}t$ value and V_{ud} matrix element from mixed Fermi/Gamow-Teller transitions in mirror $T = 1/2$ nuclei [19].

Moreover, nuclear-structure corrections to Gamow-Teller β-decay matrix elements are required in studies of asymmetry of Gamow-Teller β-decay rates of mirror transitions with the aim to constrain the value of the induced tensor term in the axial-vector weak current [20, 21].

Apart from these applications for studies of fundamental interactions, precise modelling of the Coulomb and charge-dependent nuclear forces is required to describe observed mirror energy differences (MED)[3] [22] and splittings of the isobaric multiplets, amplitudes of experimentally measured isospin-forbidden processes, such as β-delayed nucleon emission [23], Fermi β-decay to non-analogue states, $E1$-transitions in self-conjugate nuclei [24] or isoscalar $E1$-components extracted from $E1$-transitions between analogue states [25] and so on. The charge-dependent effective interaction is indispensable for understanding the structure of proton-rich nuclei with important consequences for astrophysical applications.

At the same time, the theoretical calculation of the isospin-symmetry breaking within a microscopic model represents a great challenge. Various approaches have been developed to deal with the problem.

The first shell-model estimations of isospin mixing date back to the 60's [26, 27], including its implication for a nuclear β-decay [20, 26, 28]. The most recent work within the shell model related to the construction of realistic INC effective Hamiltonians constrained by the experimental data (mass splittings of isobaric multiplets) [29, 30]. Another approach based on

---

[3] The difference in excitation energy between excited IAS states of a pair of mirror nuclei.

the analysis of the MED in pf-shell nuclei is given in Ref. [31].

The common feature of the shell-model approaches is that the transition matrix elements calculated within the INC scheme are divided into two parts. First, there is a contribution from the isospin-symmetry breaking effects in the configuration mixing of basis states, constructed from spherical harmonic-oscillator single-particle wave functions within the model space (valence space). This is obtained via the diagonalization of an effective one- plus two-body Hamiltonian that does not conserve the isospin. Second, in the calculation of transition rates one has to change the single-particle harmonic-oscillator wave functions to realistic spherically-symmetric wave functions obtained from a finite-well nuclear potential plus Coulomb potential (to account for the isospin violation outside the model space). Applications of the shell model to superallowed beta decay can be found in Refs. [17, 18, 32] and references therein, while corrections to Gamow-Teller β-decay in mirror systems have been evaluated in Refs. [20, 21]). Numerous applications to the isospin-forbidden proton emission and to the structure of proton-rich nuclei can be found in the literature (e.g. Refs. [33, 34, 35]).

The problem of the ISB was intensively studied in the framework of self-consistent mean-field theories within the Hartree-Fock + Tamm-Dankoff or random-phase approximation (RPA) in 90's [36, 37, 38, 39]. Recently, more advanced studies have been performed within the relativistic RPA approach [40], as well as within the angular-momentum-projected and isospin-projected Hartree-Fock model [41, 42].

Some other many-body techniques have recently been applied to deal with the isospin non-conservation. In particular, the isospin mixing in nuclei around $N \approx Z \approx 40$ has been evaluated by variation-after-projection techniques on the Hartree-Fock-Bogoliubov basis with a realistic two-body force in Ref. [43]. Isospin-symmetry violation in light nuclei, applied to the case of superallowed β decay of ^{10}C has been calculated within the *ab-initio* no-core shell model [44], while effects of the coupling to the continuum on the isospin mixing in weakly-bound light systems were studied in the Gamow shell-model approach [45]. The relation between the isospin impurities and the isovector giant monopole resonance was explored by Auerbach [46], with consequent application to the calculation of nuclear-structure corrections to superallowed β-decay [47].

Up to now, the approaches mentioned above do not agree on the magnitude of isospin impurities in nuclear states and predict largely different values for the corrections to nuclear β-decay. Given the importance of the problem we have decided to revise the existing INC shell-model Hamiltonians. First, since the work of Ref. [30], more experimental data of higher precision have been accumulated on the properties of isobaric multiplets (mass-excess data and level schemes), on isospin-forbidden particle emission, on nuclear radii and so on. Development of the computer power and shell-model techniques allows us to access larger model spaces [48]. In addition, more precise new nuclear Hamiltonians have been designed (e.g. Refs. [49, 50, 51]), as well as new approaches to account for short-range correlations [52, 53]. The purpose of this thesis is to present an updated set of globally-parametrized INC Hamiltonians for sd-shell nuclei, and to show their quantitative implication to calculations of isospin-forbidden processes in nuclei.

Chapter 2 is devoted to the shell-model formalism and explains the scheme to construct an isospin non-conserving Hamiltonian. The compilation of the database on experimentally determined coefficients of the isobaric-mass multiplet equation is presented in Chapter 3. Chapter 4 contains the results obtained in the sd-shell. Staggering effects of IMME coefficients are shown and explained in Chapter 5. In Chapter 6 we explore the extension of the IMME beyond the quadratic form in $T = 2$ multiplets. In Chapter 7, we present a new set of nuclear structure corrections for superallowed $0^+ \rightarrow 0^+$ Fermi β-decay, as well as a few cases of Fermi transitions to non-analogue states (configuration-mixing part). In Chapter 8 we calculate proton widths for several cases of isospin-forbidden proton emission. The thesis is summarized in the last chapter.

Chapter 2

Nuclear Shell Model and the Construction of Isospin Non-Conserving Hamiltonian

Contents

In this chapter, the basics of the nuclear shell model is briefly presented. We discuss the fundamental concepts of the nuclear shell model in tackling truncated many-body problems. Then, we concentrate on the formalism of constructing the isospin non-conserving Hamiltonian and discuss possible candidates for the isospin-symmetry breaking terms in the charge-dependent Hamiltonian. Furthermore, we illustrate the implementation of recently developed short-range correlation (SRC) schemes in adjusting the harmonic-oscillator wave functions used in the calculation of the two-body matrix elements of the isospin-symmetry breaking terms.

2.1   Nuclear Shell Model

The nuclear shell model was introduced by Mayer [54] and by Jensen *et al.* [55] in 1949, to solve the puzzle of observed regularities of the nuclear properties related to N and Z numbers, i.e., $2, 8, 20, 28, 50, \ldots$, the so-called *magic numbers*. The set of magic numbers obtained in the shell model matches the experimental data. Since then, the shell model has continued to be developed [48, 56]. The shell model provides a precise description of low-energy nuclear structure of light, medium-light and medium-mass nuclei, and their decay modes.

The shell model assumes that in first-order approximation, every nucleon in an A-nucleon system moves independently in an average potential. This mean potential is produced by $A(A-1)/2$ pairs of NN interactions in the nuclear medium. Usually, NNN and higher-body interactions are effectively described by in-medium NN interactions. The NN interaction in a nuclear medium is different from the free NN interaction [57, 58]. The free nuclear NN interaction is strongly repulsive at short distances and is attractive at larger distances; and it includes non-central and spin-dependent forces. It strongly binds two nucleons to around a constantly balanced distance, ~1 fm. Fig. 2.1 schematically displays the hierarchy of scales determining the type of NN potentials. If the distance between the two nucleons is larger than ~1.5 fm, the NN interaction can be described by the one-pion exchange potential (OPEP); whereas, at distances ~0.8 – 1.5 fm, the two-pion exchange potential (TPEP) dominates the NN interaction [59, 60]. For distances below ~0.5 fm, the NN interaction becomes a hard-core potential, and a non-relativistic formalism is not applicable anymore in this region, because the interaction energies are very high. Multi-pion exchange or a heavy-meson exchange potential is needed, and/or the NN interaction at this short distance is given as a parametrized form fitted to experimental data [60].
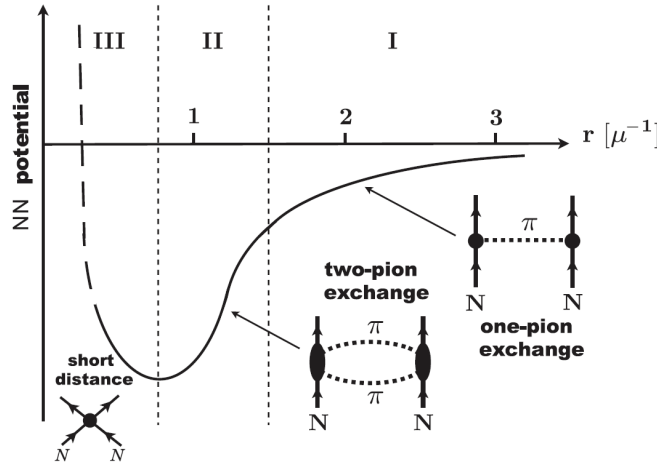
Figure 2.1:   *Schematic plot of meson exchange theories describing the NN potentials in different regions. The NN distance r is given in units of the pion's Compton wavelength $\mu^{-1} \approx 1.4$ fm. Adapted from Ref. [59, 60].*

If $A(A-1)/2$ pairs of nucleons form a nuclear system, the binding energy per nucleon of this nuclear system, BE/A, may naively be estimated as

$$\frac{BE}{A} \propto E_{NN}\frac{A-1}{2}\,, \tag{2.1}$$

where E_{NN} is the binding energy of two nucleons. Experimentally, however, the BE/A values throughout the whole nuclear chart are roughly constant, ~8 MeV [61], except for light nuclei. We may accept that the estimate $BE/A \approx 8$ MeV is applicable to most nuclei. When all nucleons in a nucleus are at the equilibrium distance, the density of the nucleus saturates inside the nucleus. Within the interaction range (~1 fm), a nucleon bound in the nucleus receives NN interactions from the adjacent nucleons. Since the nuclear density is roughly the same inside the nucleus, the mean effect of such NN interactions should be constant causing the mean potential to become constant too. At the same time, nucleons at the nuclear surface should feel less the mean effect, since they are surrounded by fewer neighboring nucleons. Hence, in the vicinity of nuclear surface, the mean potential should decrease.

A number of physics arguments support the idea of the mean field in an atomic nucleus. Indeed, the empirical mean free path of nucleons is larger than 3 fm [57]. Hence, a non-relativistic form of NN interaction is applicable for the derivation of the mean potential. In addition, the ratio of the volume occupied by nucleons of a given nucleus to the total volume of the nucleus is low

$$\frac{V_{occ}}{V_{nucleus}} \approx \left(\frac{r_{core}}{2r_0}\right)^3 \approx 0.5\times10^{-2}\,,\text{ with }r_{core}\approx 0.4\text{ fm, and }r_0\approx 1.2\text{ fm.} \tag{2.2}$$

Consequently, a nucleus is almost transparent for nucleons.

There are a number of experimental facts that confirm the existence of shell structure in nuclei.

- Nuclear masses, plotted as a function of N or Z, exhibit a pattern of deviations from predictions of the liquid-drop model indicating more binding for $Z, N = 2, 8, 20, 28, 50, 82$ and $N = 126$ and less binding for nuclei in the middle of the regions between two of these numbers (Fig. 2.2).

- Even-even nuclei near the β-stability valley with $Z = 8, 20, 28, 50, 82$, and an appropriate corresponding number of neutrons $N = 8, 20, 28, 50, 82, 126$, possess substantially higher excitation energies for the first-excited state compared to other nuclei (Fig. 2.3). The similar situation occurs in atomic physics: the atoms with fully filled electronic (sub)shells have higher-lying first-excited states compared to atoms with partially filled electronic shells, giving rise to a corresponding set of magic numbers.

- Shell structure is evidenced in the discrete strength distribution in nucleon-transfer reactions, for example, the pick-up reaction ^{208}Pb(^{3}He,d)^{209}Bi shown in Fig. 2.4, in nucleon (two-nucleon) separation energies and so on.

At the same time, nuclear shell structure is different from atomic shell structure, because (i) the nuclear mean field is different from the Coulomb potential in an atom; (ii) protons and neutrons (two different types of fermions) coexist; and (iii) there is only the center-of-mass and no specific central point in a nucleus, whereas an atom has the central Coulomb field produced by the atomic nucleus.
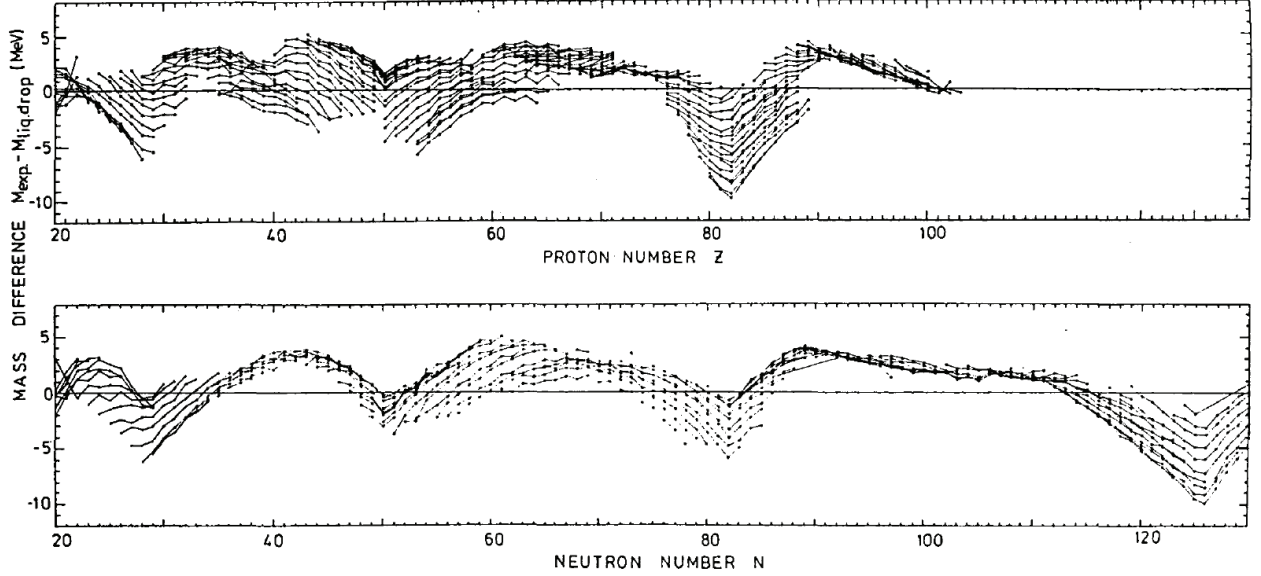
Figure 2.2: *Deviation of nuclear masses from their mean (liquid drop) values as a function of Z or N.* Adapted from Ref. [57, 62].

The nuclear shell model uses solutions from a spherically symmetric potential to construct many-body basis states. This helps us to study nuclear properties with the advantage of spherical symmetry. Suppose that a nucleon propagates in a spherically symmetric potential. The propagation is described by the one-body Schrödinger equation

$$(K + U(r))\phi_a(\vec{r}) = \epsilon_a \phi_a(\vec{r}) \,, \tag{2.3}$$

where a represents a set of quantum numbers; K is the kinetic energy operator; $U(r)$ is a spherical mean potential governing this single nucleon; and ϵ_a are the discrete single-particle energies. The single-particle wave functions $\phi_a(\vec{r})$ are the solutions of the one-body Schrödinger equation. Although the single-particle motion seems to resemble electrons in the potential well of a hydrogen-like atom, we have to keep in mind that it does not possess a central charge. The wave functions $\phi_a(\vec{r})$ form a complete set of orthonormal states

$$\int \phi_{a'}^*(\vec{r})\phi_a(\vec{r})d\vec{r} = \delta_{a'a} = \begin{cases} 1, & \text{for } a' = a \,, \\ 0, & \text{for } a' \neq a \,. \end{cases} \tag{2.4}$$

For a non-interacting A-particle system, the Hamiltonian is given by a sum of independent-particle Hamiltonians Eq.(2.3), i.e.

$$H_0 = \sum_{i=1}^{A}(K_i + U(r_i)) = \sum_{i=1}^{A} h_0(i) \,. \tag{2.5}$$
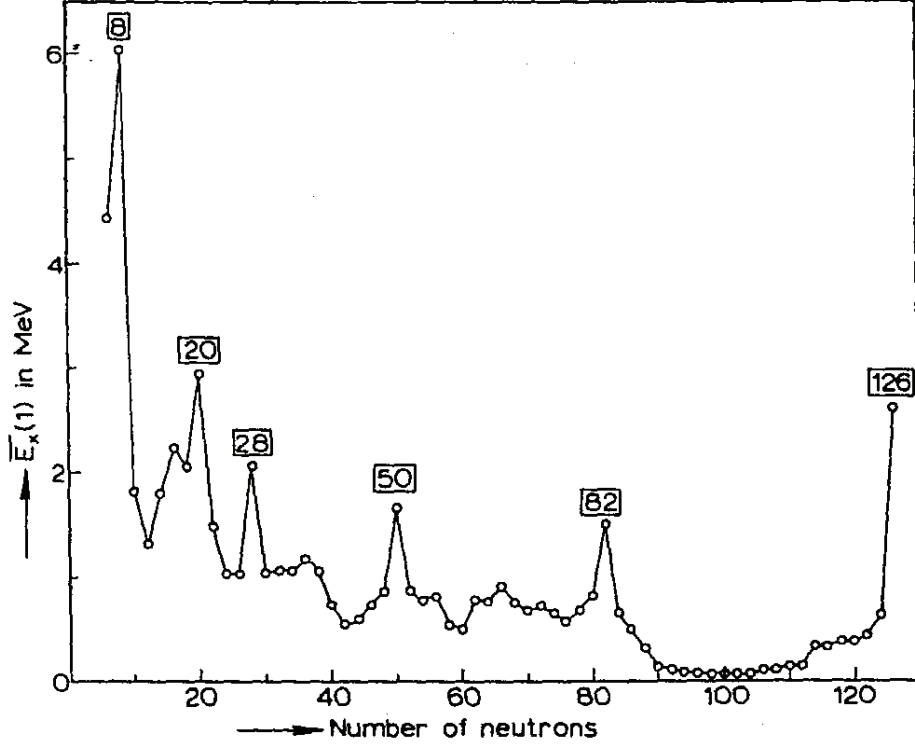
Figure 2.3: *The neutron magic numbers.*
The average excitation energies of the first-excited states in doubly-even nuclei (mainly a $J^\pi = 2^+$ level) plotted as a function of the neutron number N. Adapted from Ref. [57, 63].

However, a nucleus is a system of strongly interacting fermions, therefore the Hamiltonian should consist of nucleonic kinetic energies and nucleonic interactions

$$H = \sum_{i=1}^{A} K_i + \frac{1}{2} \sum_{i,j=1}^{A} V_{ij} \,, \tag{2.6}$$

and $\frac{1}{2}$ is inserted at the two-body interaction terms to avoid double counting. Three-body and higher-body terms are neglected here. We may formally introduce a single-particle potential $U(r)$ and rewrite the Hamiltonian as

$$
\begin{aligned}
H &= \sum_{i=1}^{A} [K_i + U(r_i)] + \left(\frac{1}{2} \sum_{i,j=1}^{A} V_{ij} - \sum_{i=1}^{A} U(r_i) \right) \\
&= H_0 + H_{\text{residual}} \\
&= \sum_{i=1}^{A} h_0(i) + H_{\text{residual}} \,,
\end{aligned}
\tag{2.7}
$$

where H_{residual} denotes the residual interaction. One can use the Hartree-Fock (HF) method to obtain the best mean field $U(r)$. Instead, in the shell model, one chooses $U(r)$ to be a simple schematic potential. Then the residual interaction is diagonalized in the basis given by the eigenfunctions of H_0.
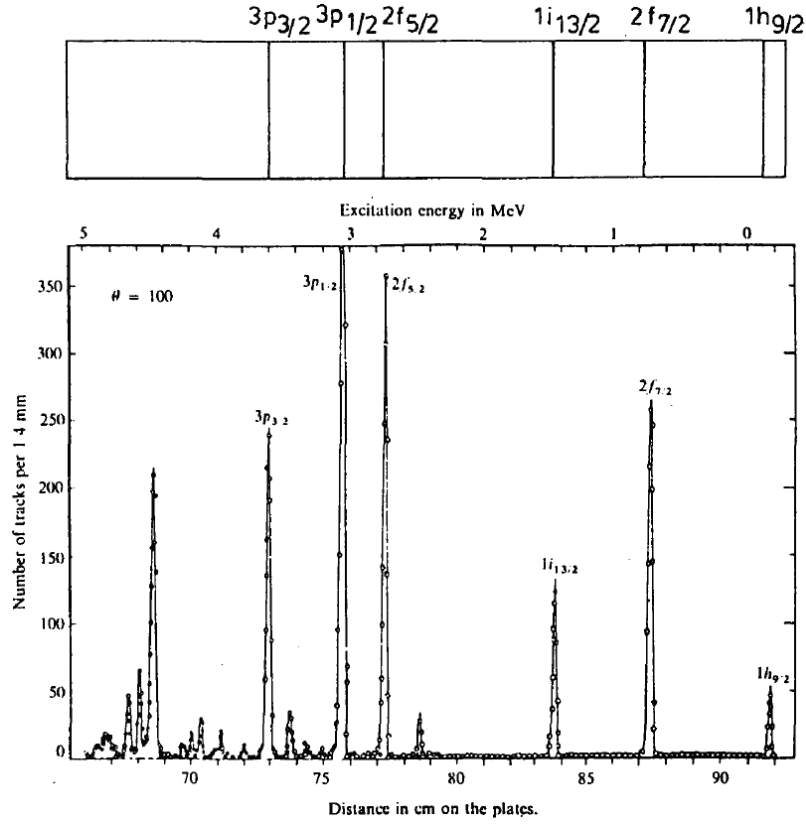
Figure 2.4: *Single-nucleon states in ^{209}Bi.*
The upper figure displays the proton single-nucleon states corresponding to the spectra in the figure below. The lower figure shows the spectra obtained from the pick-up reaction ^{208}Pb(^{3}He,d)^{209}Bi. Adapted from Ref. [57].

For example, one may employ an often called realistic Woods-Saxon (WS) potential,

$$U_{WS}(r) = \frac{V_0}{1 + e^{(r-R_0)/a}}, \tag{2.8}$$

where $V_0 \approx -50$ MeV is the potential well depth, $R_0 = r_0 A^{1/3}$ with $r_0 = 1.2$ fm, and a is the diffuseness, $a \approx 0.7$ fm. We can obtain the eigenstates of the WS potential by numerical calculation.

In practice, the potential $U(r)$ of choice is the analytically solvable harmonic oscillator (HO) potential (due to its numerous symmetries and characteristic properties),

$$U_{HO}(r) = \frac{1}{2} M_N \omega^2 r^2, \tag{2.9}$$

where M_N is the nucleon mass, and ω is the oscillator frequency.

The Schrödinger equation for a nucleon in the harmonic oscillator potential is

$$h_0 \phi(r) = \left(-\frac{\hbar^2}{2M_N} \nabla^2 + \frac{1}{2} M_N \omega^2 r^2 \right) \phi(\vec{r}) = \epsilon \phi(\vec{r}); \tag{2.10}$$
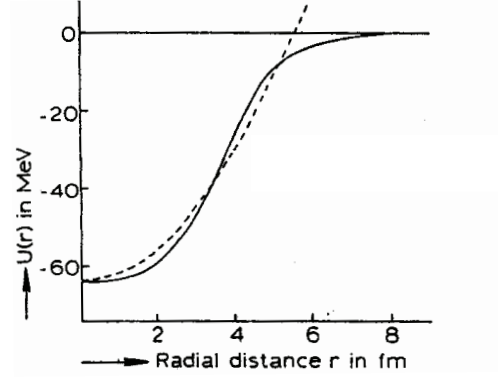
Figure 2.5: *The single-nucleon potential $U(r)$ for $A = 29$.*
The Woods-Saxon potential $U_{WS}(r)$ is shown by the solid line; whereas the dashed line is the harmonic oscillator potential $U_{HO}(r)$. Both potentials are calculated to produce the same depth at $r = 0$. Adapted from Ref. [63].

and the single-nucleon wave functions $\phi(r)$ (without considering intrinsic spin) can be written as a product of a radial wave function $R_{nl}(r)$ and a spherical harmonics $Y_{lm_l}(\theta, \varphi)$

$$\phi(\vec{r}) \equiv \phi_{nlm_l}(\vec{r}) = \frac{R_{nl}(r)}{r} Y_{lm_l}(\theta, \varphi), \tag{2.11}$$

where n is the number of nodes of the radial wave function, l is the orbital angular momentum and m_l is its projection on the z-axis. The spherical harmonics $Y_{lm_l}(\theta, \varphi)$ are normalized eigenfunctions of the squared orbital angular momentum operator $\vec{l}^2$ and its projection on the z-axis l_z

$$\vec{l}^2 Y_{lm_l}(\theta, \varphi) = l(l+1) Y_{lm_l}(\theta, \varphi),$$
$$l_z Y_{lm_l}(\theta, \varphi) = m_l Y_{lm_l}(\theta, \varphi). \tag{2.12}$$

The radial wave functions are the solutions of

$$\left(-\frac{\hbar^2}{2M_N} \frac{d^2}{dr^2} + \frac{\hbar^2}{2M_N r^2} l(l+1) + \frac{1}{2} M_N \omega^2 r^2 \right) R_{nl}(r) = \epsilon R_{nl}(r), \tag{2.13}$$

with the radial quantum number refering to the number of nodes $n = 0, 1, 2, 3, \ldots$, and have the form

$$R_{nl}(r) = \mathscr{N}_{nl} r^{l+1} \exp\left(-\frac{r^2}{2b^2} \right) L_n^{l+1/2} \left(\frac{r}{b} \right). \tag{2.14}$$

$\mathscr{N}_{nl}$ is the normalization factor which can be determined from the normalization condition

$$\int_0^\infty R_{nl}^2(r) dr = 1; \tag{2.15}$$

$b = \sqrt{\frac{\hbar}{M_N \omega}}$ is the harmonic oscillator length parameter and $L_n^{l+1/2} \left(\frac{r}{b} \right)$ are the generalized Laguerre polynomials.

The parity operator P transforms the space (r, θ, φ) spanned by single-nucleon wave functions as

$$(r, \theta, \varphi) \xrightarrow{P} (r, \pi - \theta, \pi + \varphi) \,,$$

$$P\phi_{nlm_l}(\vec{r}) = P \left(\frac{R_{nl}(r)}{r} Y_{lm_l}(\theta, \varphi) \right) = (-1)^l \phi_{nlm_l}(\vec{r}) \,. \tag{2.16}$$

All spherical harmonics have definite parity. The parity of single-nucleon wave functions is positive (negative), if l is even (odd). The eigen-energies corresponding to Eq.(2.10) are given by

$$\epsilon = \hbar\omega(2n + l + \frac{3}{2}) = \hbar\omega(N + \frac{3}{2}) \,, \tag{2.17}$$

where

$$N = 0, 1, 2, 3, \ldots ;$$
$$l = N, N - 2, \ldots, 1 \text{ or } 0 ;$$
$$n = \frac{N - l}{2} \,.$$

Each N number corresponds to a harmonic oscillator shell with definite eigen-energy. The distance between two consecutive oscillator shells is $\hbar\omega \approx 41A^{-1/3}$ MeV, and the lowest eigen-energy is $\frac{3}{2}\hbar\omega$. Using the notation from atomic spectroscopy, states with orbital angular momentum $l = 0, 1, 2, 3, 4, \ldots$, are labeled as $s, d, p, f, g, \ldots$. For each value of l, there are $(2l + 1)$ eigenstates of $\vec{l}^2$. Taking into account spin-$\frac{1}{2}$ of the nucleons, the total degeneracy of the Nth oscillator shell for identical nucleons is

$$\sum_{l=0 \text{ or } 1}^{N} 2(2l + 1) = (N + 1)(N + 2) \,. \tag{2.18}$$

Every oscillator shell possesses either even or odd l, therefore the parity of the shell is respectively either even or odd.

The number of nucleons in each shell predicted by Eq.(2.18) does not match with experimental magic numbers. Mayer [54] and Jensen *et al.* [55] introduced a spin-orbit coupling term

$$U_{ls}(r) = f(r) \left(\vec{l} \cdot \vec{s} \right) \,, \tag{2.19}$$

in Eq.(2.10). The orbital angular momentum operator is $\vec{l}$ and the spin operator of a nucleon is denoted as $\vec{s}$; and the radial function can be evaluated as [64]

$$f(r) = -V_{ls} \frac{\partial}{\partial r} V(r) \,. \tag{2.20}$$

V_{ls} is a strength constant, and $V(r)$ is the chosen mean potential. The spin-orbit term peaks at the nuclear surface because the nuclear density changes most rapidly at the surface.

The Hamiltonian h_0 can be rewritten in spherical coordinates with the added spin-orbit coupling term

$$h_0 = -\frac{\hbar^2}{2M_N}\frac{d^2}{dr^2} + \frac{\hbar^2}{2M_N r^2}l(l+1) + \frac{1}{2}M_N\omega^2 r^2 + f(r)\left(\vec{l}\cdot\vec{s}\right) . \tag{2.21}$$

Fig. 2.6 shows degeneracies of different orbits obtained from $U_{HO}(r)$, $U_{WS}(r)$, and $U_{WS}(r) + U_{ls}(r)$ potentials. Let us remark that adding a centrifugal term to the HO potential, $g(r)(\vec{l}\cdot\vec{l})$, results in a splitting of the harmonic oscillator orbitals according to different values of l, similar to that given by the WS potential.

In an orbital angular momentum and spin coupled form, the single-nucleon wave functions are

$$\begin{aligned}
\phi_{nlsjm}(\vec{r},\vec{s},\vec{t}) &= \frac{R_{nl}(r)}{r}\left[Y_l(\theta,\varphi)\otimes\chi_{\frac{1}{2}}(\vec{s})\right]_m^{(j)} \\
&= \frac{R_{nl}(r)}{r}\sum_{m_l m_s}\left(lm_l\frac{1}{2}m_s\,\middle|\,jm\right)Y_{lm_l}(\theta,\varphi)\chi_{\frac{1}{2}m_s} ,
\end{aligned}$$

$$\tag{2.22}$$

where s is the intrinsic spin $(s=\frac{1}{2})$, and m_s is its projection on the z-axis, $\chi_{\frac{1}{2}m_s}$ is the spin-$\frac{1}{2}$ spinor, the $\left(lm_l\frac{1}{2}m_s\,\middle|\,jm\right)$ are Clebsch-Gordan coefficients, and $\vec{j}=\vec{l}+\vec{s}$ is conserved.

The Pauli exclusion principle requires that only one nucleon can be in a specific quantum state. The quantized spherical mean potential enables us to label a nucleon state by quantum numbers n,l,j,m_j. We can differentiate those orbits by using the z component of j, namely m_j (or j_z); and for every j, it generates $2j+1$ magnetic substates. In other words, an orbit of j in a quantized spherical mean potential has $2j+1$ degenerate substates. However, in the absence of spin-orbit interaction, states with $j=l\pm\frac{1}{2}$ are degenerate.

The spin-orbit potential Eq.(2.19) removes the degeneracy inherent to the WS potential or HO plus centrifugal term potential, according to the values of the total angular momentum $j=l\pm\frac{1}{2}$. For example, for the orbit "$1f_{7/2}$" the integer "1" is the number of nodes plus one; the character "f" is the notation of l, here, $l=3$; and the half-integer "7/2" represents the value of j. The energy splitting caused by the spin-orbit potential is approximately proportional to l, c.f. Eq.(2.19). For larger l, the spin-orbit splitting effect is more pronounced.

The single-particle level structure shown in the right column in Fig. 2.6 represents groups of close lying states (orbits), called shells, separated by larger energy gaps.

The existence of shells and shell gaps gives rise to the magic numbers discussed above. A neutron (proton) *closed shell* is formed if all orbits in the given shell are fully occupied by neutrons (protons). The number of neutrons (protons) in each closed shell is given by the sum of occupations of individual orbital, comprising the shell. Magic numbers predicted by the right column in Fig. 2.6 perfectly agree with the experimental magic numbers, c.f. Fig. 2.7.
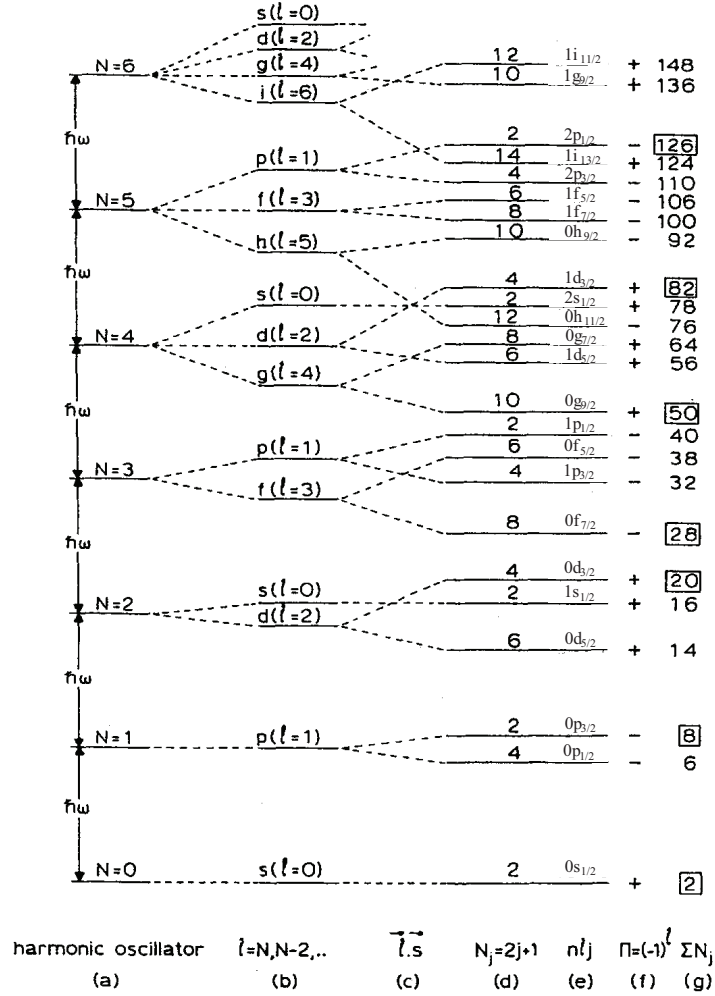
Figure 2.6: *Approximate sequence of single-nucleon states.*
(a) The single-nucleon energies described by $U_{HO}(r)$ as a function of the oscillator quantum number N;
(b) A schematic plot of the single-nucleon energies produced by a Woods-Saxon potential $U_{WS}(r)$;
(c) Level splittings caused by the spin-orbit coupling term are schematically shown;
(d) The degeneracies of the number $N_j = 2j + 1$ of identical nucleons in each shell;
(e) The spectroscopic notation of the single-nucleon quantum numbers n, l, and j;
(f) The parity of each shell;
(g) The magic numbers are shown to be equal to the subtotals of the number of nucleons at the energy gaps.
Adapted from Ref. [63].

Nuclei having closed proton and neutron shells are called *closed-shell nuclei*, e.g., $^{16}_{8}O_8$ and $^{40}_{20}Ca_{20}$. Nuclei with partially occupied shells are called *open-shell nuclei*. A partially occupied shell is called valence shell.

In a closed shell, a nucleon occupying one of the orbits cannot move to another orbit of the closed shell because of the Pauli exclusion principle since all orbits are fully occupied. However, nucleons from a closed shell can be excited to the next partially occupied shell, creating holes in the closed shell. These excitations are called *particle-hole excitations*.
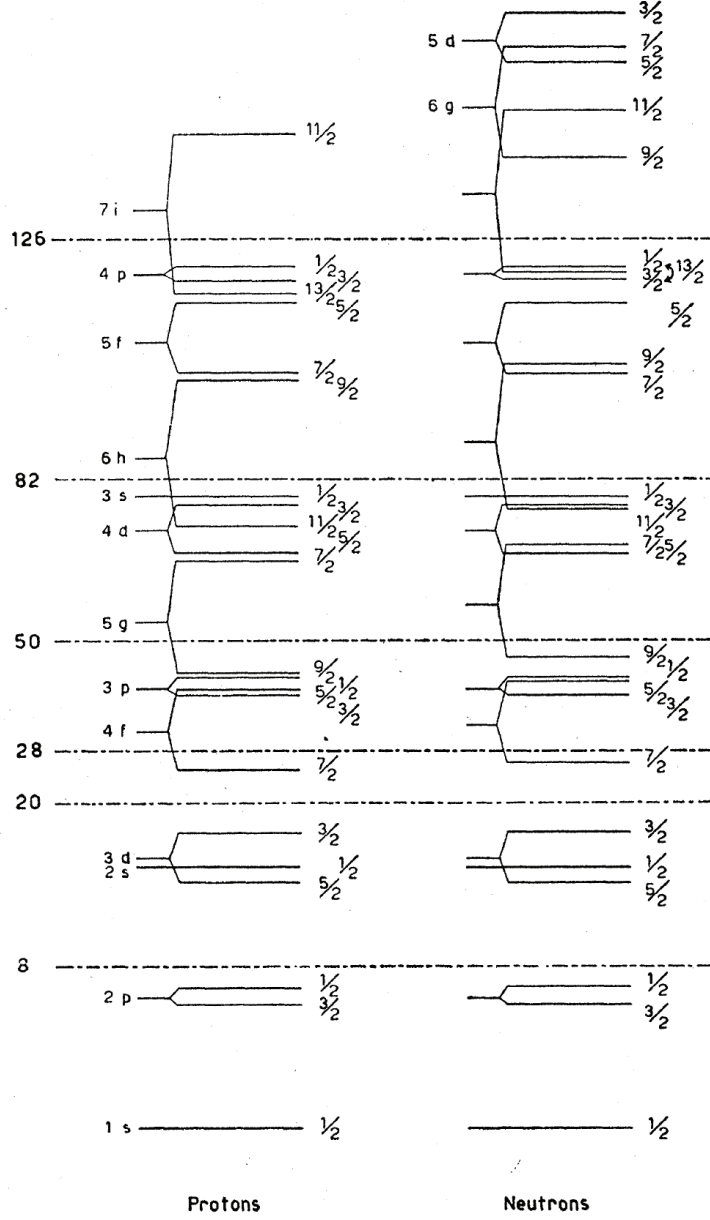
Figure 2.7: *The protons' and neutrons' single-nucleon spectra.*
Magic numbers are shown at the left side (first column). Splitting due to harmonic oscillator potential $U_{HO}(r)$ plus a centrifugal term is illustrated in the second column. Degeneracies due to the spin-orbit term $U_{ls}(r)$ are at the right side of each level scheme. Adapted from Ref. [65].

For heavy nuclei, a shell-model calculation assumes a closed shell that is inert, and looks for degrees of freedom in valence shells; or all shells are considered, and looks for degrees of freedom in all shells. The latter approach is named as *no-core shell model* [66].

However, for no-core shell model framework, only for very light nuclei shell model calculations can be performed for all A nucleons in little truncated model space (including many HO shells). At present, light nuclei, such as $^{13}_{6}C_7$ and $^{16}_{8}O_8$ are still calculated with important

truncation [66].

For many-nucleon systems, shell-model calculations are performed only for valence nucleons situated in a valence shell beyond the closed-shell core, which is assumed to be inert, and do not take into account higher-lying unoccupied orbitals (excluded space). Sometimes, in the calculations within two major oscillator shells, cross-shell particle-hole excitations can be taken into account.

In the present work, we focus on the sd-shell space which consists of the $0d_{5/2}$, $1s_{1/2}$, and $0d_{3/2}$ valence orbitals, and we assume that the $0s_{1/2}$, $0p_{3/2}$, and $0p_{1/2}$ shells are closed, so that there are no particle-hole excitations from the lower shells. Furthermore, we assume that the valence nucleons will not be promoted to the higher pf-shell space which consists of $0f_{7/2}$, $1p_{3/2}$, $0f_{5/2}$, and $1p_{1/2}$. The nucleons are confined to the sd-shell space, therefore, only positive-parity levels are considered in an sd-shell space calculation. The valence space defined in such a way is named as *model space*. The inert core is represented as a vacuum state, $|0\rangle$.

Including the spin-orbit term, c.f. Eq.(2.21), the radial wave functions are solutions of the following second-order differential equation

$$-\frac{\hbar^2}{2M_N}R''(r) + \frac{\hbar^2}{2M_N}\frac{l(l+1)}{r^2}R(r) + [U(r)R(r) + a_{ls}f(r)]\,R(r) = \epsilon R(r)\,, \qquad (2.23)$$

which contains dependence on j via a_{ls}, the expectation value of the $(\vec{l}\cdot\vec{s})$ operator in a state with definite l, s, and j quantum numbers:

$$a_{ls} = \frac{1}{2}\left[j(j+1) - l(l+1) - s(s+1)\right] = \begin{cases} \frac{1}{2}l\,, & \text{for } j = l + \frac{1}{2}\,, \\ -\frac{1}{2}(l+1)\,, & \text{for } j = l - \frac{1}{2}\,. \end{cases} \qquad (2.24)$$

Now, we explicitly give the full single-nucleon wave functions, including their isospin representation,

$$\begin{aligned} \phi_{nlsjm,tt_z}(\vec{r},\vec{s},\vec{t}) &= \frac{R_{nlj}(r)}{r}\left[Y_l(\theta,\varphi)\otimes\chi_{\frac{1}{2}}(\vec{s})\right]_m^{(j)}\Theta_{\frac{1}{2}t_z} \\ &= \frac{R_{nlj}(r)}{r}\sum_{m_l m_s}\left(lm_l\frac{1}{2}m_s\middle|jm\right)Y_{lm_l}(\theta,\varphi)\chi_{\frac{1}{2}m_s}\Theta_{\frac{1}{2}t_z}\,, \end{aligned}$$

$$(2.25)$$

where $\Theta_{\frac{1}{2}t_z}$ is the isospinor, and it resembles proton and neutron states in Eq.(1.2)

$$\Theta_{\frac{1}{2},-\frac{1}{2}} \equiv |p\rangle = \begin{pmatrix} 0 \\ 1 \end{pmatrix}\,, \qquad \Theta_{\frac{1}{2},\frac{1}{2}} \equiv |n\rangle = \begin{pmatrix} 1 \\ 0 \end{pmatrix}\,. \qquad (2.26)$$

2.1.1   The Eigenvalue Problem

Many-nucleon states, which form the basis to diagonalize the residual interaction H_{residual}, are constructed from the single-nucleon wave functions shown in Eq.(2.25). Two methods are used to construct basis states, namely the m-scheme and $J(T)$-coupled methods. In the present work, we employ the m-scheme. Its brief description is given below, whereas the explanation of $J(T)$-coupled method is provided in Refs. [57, 63].

The basis in the shell model is given by the many-body Slater determinants:

$$\Phi_\vartheta(\vec{r}_1, \vec{r}_2, \ldots, \vec{r}_A) = \Phi_{\vartheta 1, \vartheta 2, \ldots, \vartheta A}(\vec{r}_1, \vec{r}_2, \ldots, \vec{r}_A) = \frac{1}{\sqrt{A!}}
\begin{vmatrix}
\phi_{\vartheta 1}(\vec{r}_1) & \phi_{\vartheta 1}(\vec{r}_2) & \ldots & \phi_{\vartheta 1}(\vec{r}_A) \\
\phi_{\vartheta 2}(\vec{r}_1) & \phi_{\vartheta 2}(\vec{r}_2) & \ldots & \phi_{\vartheta 2}(\vec{r}_A) \\
\cdot & & & \cdot \\
\cdot & & & \cdot \\
\cdot & & & \cdot \\
\cdot & & & \cdot \\
\phi_{\vartheta A}(\vec{r}_1) & \phi_{\vartheta A}(\vec{r}_2) & \ldots & \phi_{\vartheta A}(\vec{r}_A)
\end{vmatrix}, \quad (2.27)$$

where ϑ_i represents the set of quantum numbers n_i, l_i, j_i, m_i, and ϑ denotes a set of single-nucleon configurations $\{\vartheta_1, \vartheta_2, \ldots, \vartheta_A\}$. Thus, the basis states are given by normalized and antisymmetrized products of A single-nucleon wave functions $\phi_{nlsjm,tt_z}(\vec{r}, \vec{s}, \vec{t})$. Slater determinants in Eq.(2.27) can be characterized by a definite value of M:

$$M = \sum_{i=1}^A m_i. \tag{2.28}$$

To solve the Schrödinger equation for $H = H_0 + H_{\text{residual}}$, we calculate the matrix elements of the Hamiltonian in the basis of many-body states, which are eigenfunctions of the eigen-equation for an independent-nucleon Hamiltonian H_0, and diagonalize it to get the eigenvalues and eigenvectors (coefficients of linear expansion of the eigenstates in terms of basis states). The Hamiltonian H_0 in Eq.(2.21) is rotationally invariant in space (and isospace). Therefore, the J_z and J are conserved for all eigenstates. In practice, it is preferable before the calculation of the Hamiltonian matrix to project all basis states onto states with good total angular momentum J (and isospin T). We will label the projected basis states as $[\Phi(\vec{r}_1, \vec{r}_2, \ldots, \vec{r}_A)]_{JT,k}$ where $k = 1, \ldots, d$; d is the number of different basis states with the same J and T (the dimension of the model space). $[\Phi]_{JT,k}$ is constructed from the Slater determinants where particles are distributed among a fixed set of single-particle orbitals n, l, j. $[\Phi]_{JT,k}$ is the eigenfunction of H_0 with eigenvalue $(E_0)_{JT,k}$ given by a sum of single-nucleon energies expressed as

$$(E_0)_{JT,k} = \sum_{i=1}^A \epsilon_i. \tag{2.29}$$

The eigen-energies $(E_0)_{JT,k}$ correspond to $[\Phi_\vartheta(\vec{r}_1, \vec{r}_2, \ldots, \vec{r}_A)]_{JT,k}$. To shorten the notation, we will omit J and T, and refer to the set of $[\Phi(\vec{r}_1, \vec{r}_2, \ldots, \vec{r}_A)]_{JT,k}$ as $|\Phi_k\rangle$. To find the set of

eigenstates of the complete Hamiltonian H, $|\Psi_p\rangle$,

$$H |\Psi_p\rangle = E_p |\Psi_p\rangle \,, \tag{2.30}$$

we express $|\Psi_p\rangle$ in terms of basis functions,

$$|\Psi_p\rangle = \sum_{k=1}^{d} a_{kp} |\Phi_k\rangle \,, \tag{2.31}$$

with the normalization condition

$$\sum_{k=1}^{d} a_{kp}^2 = 1 \,, \quad p = 1, \ldots, d \,. \tag{2.32}$$

Substituting Eq.(2.31) into equation Eq.(2.30), we get

$$(H_0 + H_{\text{residual}}) \sum_{k=1}^{d} a_{kp} |\Phi_k\rangle = E_p \sum_{k=1}^{d} a_{kp} |\Phi_k\rangle \,. \tag{2.33}$$

Multiplying this equation from the left-hand side by $|\Phi_{k'}\rangle$ and making use of the orthonormality of the basis functions $|\Phi_k\rangle$, we get a system of equations

$$\sum_{k=1}^{d} H_{k'k} a_{kp} = E_p a_{k'p} \,, \tag{2.34}$$

where the matrix elements of the Hamiltonian H are

$$H_{k'k} \equiv \langle \Phi_{k'}| H |\Phi_k\rangle = (E_0)_k \delta_{k'k} + \langle \Phi_{k'}| H_{\text{residual}} |\Phi_k\rangle \,. \tag{2.35}$$

The second term at the right-hand side of Eq.(2.35) are the matrix elements of the two-body interaction between many-body Slater determinants or two-body matrix elements (TBME's). They can be expressed in terms of the matrix elements between two-nucleon states.

To obtain the eigenvalues E_p and the coefficients a_{kp}, we have to diagonalize the matrix $H_{k'k}$. As the basis is orthogonal and normalized, the eigenvectors of different eigenvalues must be orthogonal and can be normalized in such a way that

$$\sum_{k=1}^{d} a_{kp} a_{kp'} = \delta_{pp'} \quad \text{for } E_p \neq E_{p'} \,. \tag{2.36}$$

If $E_p = E_{p'}$, but $p \neq p'$, the corresponding eigenvectors Ψ_p and $\Psi_{p'}$ can be made orthonormal by some orthogonalization procedure.

There are a number of different numerical algorithms for matrix diagonalization, e.g. the Jacobi method for small matrices ($d \leq 50$), the Householder method for matrices with $50 \leq d \leq 200$, the Lanczos method for dimensions $d \geq 200$ and for giant matrices [48].

The dimension of the configuration space in m-scheme is proportional to the product of two combinatorial numbers of N_p active protons in the model space of total occupation $\Omega_p = \sum_{j_p}(2j_p+1)$ and N_n active neutrons in the model space of total occupation $\Omega_n = \sum_{j_n}(2j_n+1)$,

$$\binom{\Omega_p}{N_p}\binom{\Omega_n}{N_n}. \tag{2.37}$$

Therefore, if the number of nucleons and the total occupation of a model space increase, the dimensions of the matrices drastically increase to a colossal size. This is the reason why, presently, with actual computing power, only light nuclei can be described by the no-core shell model [66]. For heavier nuclei, we assume that the closed shell is inert, and we take all allowed configurations of N_p valence protons and N_n valence neutrons in the valence space.

For the present work, we treat $^{16}_{8}\text{O}_8$ as an inert core and define $0d_{5/2}, 1s_{1/2}$, and $0d_{3/2}$ as valence shells, the orbits lying energetically higher than the valence space, i.e., $0f_{7/2}, 1p_{3/2}, 0f_{5/2}$, $1p_{1/2}$ and above, are always kept free, however, part of the low-lying excitations of valence nucleons to those free orbits, as well as core excitations, should be effectively incorporated in the residual interaction. Then, taking $^{29}_{14}\text{Si}_{15}$ as an example, the numbers of valence protons and neutrons are 6 and 7, respectively. The dimension of the configuration space for $^{29}_{14}\text{Si}_{15}$ is

$$\binom{12}{6}\binom{12}{7} = 924 \times 792 = 731808. \tag{2.38}$$

2.2 Large Scale Shell Model Calculations

A few very powerful computer programs which incorporate the m-scheme for large-scale shell-model calculations have been developed recently in the world. Among them are AN-TOINE by Caurier and Nowacki [67], OXBASH by Brown *et al.* [68], NuShell by Rae [69], MSHELL by Mizusaki [70], REDSTICK by Ormand and Johnson [71] for no-core shell model, the Oslo code [72], etc. The technical problem of SM is to diagonalize an enormous matrix with limited computer memory. Great efforts have been made to develop algorithms to improve the performance of SM codes. At present, only ANTOINE and MSHELL can handle giant matrices up to one billion dimension. The diagonalization is performed by the Lanczos algorithm.

We have used ANTOINE to carry out the diagonalization in this work. The description of ANTOINE is briefly given below.

ANTOINE was written based on the idea of Glasgow group [73]. Each Slater determinant is represented by a word of integers, every bit of the word corresponds to a given single-nucleon state $|nljm; tt_z\rangle$. Every bit has a binary value to indicate whether the state is occupied or empty. A two-body operator $a_\vartheta^\dagger a_\eta^\dagger a_\beta a_\alpha$ will search the word having the bits $\vartheta, \eta, \beta, \alpha$ in the configuration 0011 and change it to the new word of 1100. The generated new word will be placed in the lists of all the words by the bi-section method.

In ANTOINE, a further improvement on Glasgow code has been implemented as given below. We simplify the notation for Slater determinants for protons and neutrons in a given model space as

$$\left[\Phi_\vartheta^\pi\right]_{M_{p_i}} \equiv \left[\Phi_\vartheta^\pi(\vec{r}_1, \vec{r}_2, \ldots, \vec{r}_{N_p})\right]_{M_{p_i}},$$

$$\left[\Phi_\vartheta^\nu\right]_{M_{n_j}} \equiv \left[\Phi_\vartheta^\nu(\vec{r}_1, \vec{r}_2, \ldots, \vec{r}_{N_n})\right]_{M_{n_j}},$$

respectively. i is the running index for proton blocks of Slater determinants having the same M_p, and j is for neutron blocks of Slater determinants having the same M_n. In the m-scheme, the total M is

$$M = M_{p_i} + M_{n_j}. \tag{2.39}$$

Hence, $\left[\Phi_\vartheta^\pi\right]_{M_{p_i}}$ and $\left[\Phi_\vartheta^\nu\right]_{M_{n_j}}$ will only be selected if their respective M_p and M_n fulfill Eq.(2.39). Then, we obtain a basis state which is the product of the selected Slater determinants of protons and neutrons,

$$|I\rangle = \left[\Phi_\vartheta^\pi\right]_{M_{p_i}} \cdot \left[\Phi_\vartheta^\nu\right]_{M_{n_j}} \tag{2.40}$$

with $I = 1, 2, 3, \ldots$. We take the example shown in Fig. 2.8, and all proton and neutron Slater determinants are grouped according to their respective M_p and M_n. There are 7 proton Slater determinants in the "M_p" block, whereas the "M_n" block contains 2 neutron Slater determinants. If we run a loop on $\left[\Phi_\vartheta^\pi\right]_{M_{p_i}}$ in the M_p block, and then on $\left[\Phi_\vartheta^\nu\right]_{M_{n_j}}$ in the M_n block, the proton Slater determinant $i = 1$ is associated with the neutron Slater determinant $j = 1$ and $j = 2$ to form states labeled as $I = 1$ and $I = 2$. Next, the proton Slater determinant $i = 2$ is associated with the neutron Slater determinant $j = 1$ and $j = 2$ to form states labeled as $I = 3$ and $I = 4$. After the first loop finishes, we obtain $I = 1, 2, 3, 4, \ldots, 14$, for the first block (M_p, M_n). Then the second loop will run on the "$M_p + 1$" and "$M_n - 1$" blocks. States $I = 15, 16, 17, \ldots, 26$ will be generated for the second block $(M_p + 1, M_n - 1)$. After the third loop finishes, eventually, we obtain states $I = 1, 2, 3, \ldots, 38$, for blocks (M_p, M_n), $(M_p + 1, M_n - 1)$, and $(M_p + 2, M_n - 2)$.
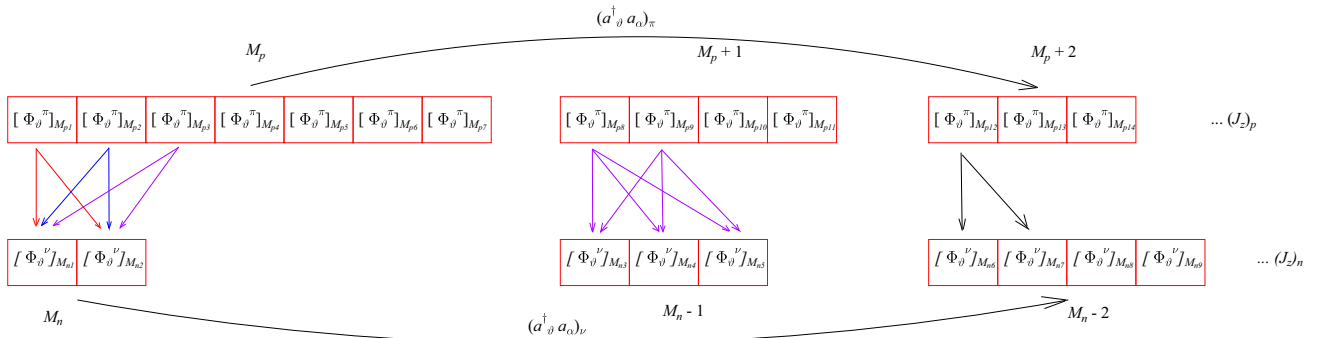
Figure 2.8: *Schematic representation of the shell-model basis of m-scheme.*

Then, we numerically construct an array $R(i)$ as

$$I = R(i) + j \,. \tag{2.41}$$

For the example shown in Fig. 2.8, we have

$$
\begin{aligned}
&\textbf{for the first block: } (M_p, M_n)\\
&\quad 1 = R(1) + 1 \,,\\
&\quad 2 = R(1) + 2 \,,\\
&\quad 3 = R(2) + 1 \,,\\
&\cdots,\\
&\cdots,\\
&\cdots,\\
&\quad 14 = R(7) + 2 \,,\\
&\textbf{for the second block: } (M_p + 1, M_n - 1)\\
&\quad 15 = R(8) + 3 \,,\\
&\quad 16 = R(8) + 4 \,,\\
&\quad 17 = R(8) + 5 \,,\\
&\quad 18 = R(9) + 3 \,,\\
&\cdots,\\
&\cdots,\\
&\cdots,\\
&\quad 26 = R(11) + 5 \,,\\
&\textbf{for the third block: } (M_p + 2, M_n - 2)\\
&\quad 27 = R(12) + 6 \,,\\
&\quad 28 = R(12) + 7 \,,\\
&\quad 29 = R(12) + 8 \,,\\
&\quad 30 = R(12) + 9 \,,\\
&\cdots,\\
&\cdots,\\
&\cdots,\\
&\quad 38 = R(14) + 9 \,,
\end{aligned}
\tag{2.42}
$$

With i, j, and $R(i)$, we obtain I. For proton-proton and neutron-neutron matrix elements, all $(R(i), R(i'), \langle i| H |i'\rangle)$ and $(j, j', \langle j| H |j'\rangle)$ are precalculated and stored. In the Lanczos algorithm, a loop on i and j will produce all the proton-proton and neutron-neutron matrix elements, $(I, I', \langle I| H |I'\rangle)$.

2.3 Second Quantization

We rewrite the Hamiltonian H of Eq.(2.33) in second quantization (occupation number) formalism. Suppose that a fermionic creation operator $a_\vartheta^\dagger$ and an annihilation operator a_ϑ, creates and annihilates a single-nucleon state $|\vartheta\rangle \equiv |n, l, j, m, tt_z\rangle$,

$$|\vartheta\rangle = a_\vartheta^\dagger |0\rangle \,, \tag{2.43}$$
$$|0\rangle = a_\vartheta |\vartheta\rangle \,, \tag{2.44}$$

respectively. Following the previous discussion, we treat closed shells as the vacuum states. a_ϑ is the Hermitian conjugate of $a_\vartheta^\dagger$, $a_\vartheta = \left(a_\vartheta^\dagger\right)^\dagger$. These creation and annihilation operators obey the anti-commutation relations,

$$\left\{a_\vartheta^\dagger, a_\eta\right\} = a_\vartheta^\dagger a_\eta + a_\eta a_\vartheta^\dagger = \delta_{\vartheta\eta} \,, \tag{2.45}$$

$$\left\{a_\vartheta^\dagger, a_\eta^\dagger\right\} = \{a_\vartheta, a_\eta\} = 0 \,. \tag{2.46}$$

The coordinate representation of the single-nucleon state ϑ is $\left\langle \vec{r}, \vec{s}, \vec{t}\, \middle|\, \vartheta \right\rangle \equiv \phi_\vartheta(\vec{r})$. Then an A-nucleon antisymmetric state is given by

$$|\vartheta_1, \vartheta_2, \dots, \vartheta_A\rangle = a_{\vartheta_A}^\dagger a_{\vartheta_{A-1}}^\dagger a_{\vartheta_{A-2}}^\dagger \dots a_{\vartheta_2}^\dagger a_{\vartheta_1}^\dagger |0\rangle \,. \tag{2.47}$$

Using the second quantization formalism, H_0 and the residual interaction H_{residual} in Eq.(2.33) (or Eq.(2.7)) are represented by a symmetric one-body operator

$$\hat{O} = \sum_{i=1}^A \hat{O}(\vec{r}_i) \,; \tag{2.48}$$

and a symmetric two-body operator

$$\hat{T} = \sum_{i<j}^A \hat{T}(\vec{r}_i, \vec{r}_j) \,, \tag{2.49}$$

respectively. These operators act on a system of A identical fermions. $\hat{O}$ is described by its matrix elements between one-body states

$$\langle\vartheta| \hat{O} |\eta\rangle = \int \phi_\vartheta^*(\vec{r})\hat{O}(\vec{r}_i)\phi_\eta(\vec{r})d\vec{r}; \tag{2.50}$$

whereas $\hat{T}$ is described by its matrix elements between normalized and anti-symmetric two-body states

$$\langle\vartheta\eta| \hat{T} |\alpha\beta\rangle = \int \phi_\vartheta^*(\vec{r}_1)\phi_\eta^*(\vec{r}_2)\hat{T}(\vec{r}_1, \vec{r}_2) \left(1 - \hat{P}_{12}\right) \phi_\alpha(\vec{r}_1)\phi_\beta(\vec{r}_2)d\vec{r}_1 d\vec{r}_2 \,, \tag{2.51}$$

with $\hat{P}_{12}$ an exchange operator. Then the one-body operator and the two-body operator can be written in the second-quantized form as

$$\hat{O} = \sum_{\vartheta\eta} \langle\vartheta|\,\hat{O}\,|\eta\rangle\, a_\vartheta^\dagger a_\eta\,, \text{ and} \tag{2.52}$$

$$\hat{T} = \frac{1}{4} \sum_{\vartheta\eta\alpha\beta} \langle\vartheta\eta|\,\hat{T}\,|\alpha\beta\rangle\, a_\vartheta^\dagger a_\eta^\dagger a_\beta a_\alpha\,, \tag{2.53}$$

respectively. The factor $\frac{1}{4}$ is inserted to avoid four-fold counting. The shell-model Hamiltonian in Eq.(2.33) is rewritten in the second-quantization formalism as

$$\hat{H} = \sum_{\vartheta\eta} \langle\vartheta|\,\hat{O}\,|\eta\rangle\, a_\vartheta^\dagger a_\eta + \frac{1}{4} \sum_{\vartheta\eta} \langle\vartheta\eta|\,\hat{V}\,|\alpha\beta\rangle\, a_\vartheta^\dagger a_\eta^\dagger a_\beta a_\alpha\,, \tag{2.54}$$

or compactly as

$$\hat{H} = \sum_{\vartheta} \epsilon_\vartheta a_\vartheta^\dagger a_\vartheta + \frac{1}{4} \sum_{\vartheta\eta\alpha\beta} V_{\vartheta\eta\alpha\beta} a_\vartheta^\dagger a_\eta^\dagger a_\beta a_\alpha\,. \tag{2.55}$$

2.4 Residual Interaction

The residual interaction is the NN interaction in the nuclear medium. The general assumptions on the nature of the NN potential include

- nucleons are non-relativistic particles and their substructure does not play the role in NN potential;

- nucleons interact through a potential;

- and only two-body effects are considered.

Generally, there are three approaches to obtain the effective shell-model interactions (residual interaction):

(a) schematic interactions with a few parameters fitted to experimental data, with a local descriptive power only;

(b) microscopic interactions derived from the NN experimental data via a renormalization procedure (G-matrix [74, 75, 76, 77, 78] or V_{low-k} plus corrections for the model-space restriction [79]);

(c) empirical interactions (fitted to the experimental data).

2.4.1 Schematic Interactions

Schematic interactions are parametrized functions of nucleon coordinates. These functions are used to calculate all TBME's in a given model space

$$V_{ijkl;JT} \equiv \langle ij; JT| \hat{V}(1,2) |kl; JT \rangle \,, \tag{2.56}$$

here $i \equiv n_i, l_i, j_i$ represents quantum numbers of a nucleon state. For instance, an interaction between two nucleons can be a zero-range (δ-type)

$$\hat{V}(1,2) = V_0 \delta(\vec{r}_1 - \vec{r}_2)(1 + \alpha \vec{\sigma}_1 \cdot \vec{\sigma}_2) \,, \tag{2.57}$$

where V_0 and α are the two parameters governing the schematic interaction. These two parameters are adjusted to reproduce low-energy spectra of a few given neighboring nuclei. These parameters may be different from one region of the nuclear chart to another.

Another example is the pairing interaction between alike nucleons. For a constant pairing force, it is defined as an extra attraction between pairs of nucleons coupled to $J = 0$, $T = 1$, which results in TBME's that are non-zero for

$$\langle ii; 01| \hat{V}_{\text{pairing}}(1,2) |kk; 01 \rangle = -(-1)^{l_i+l_k} \frac{1}{2} G \sqrt{(2j_i+1)(2j_k+1)} \,, \tag{2.58}$$

where G is the strength, and zero matrix elements otherwise.

The other example is the quadrupole-quadrupole interaction, which is necessary for the proton-neutron part, to describe rotation of deformed nuclei. This is a $\lambda = 2$ component of the general (proton-neutron) multipole-multipole interaction (a separable interaction) of the type

$$\hat{V}(1,2) = \sum_\lambda \chi_\lambda (Q_\lambda \cdot Q_\lambda) = \sum_\lambda \chi_\lambda r_\pi^\lambda r_\nu^\lambda Y_\lambda(\Omega_\pi) \cdot Y_\lambda(\Omega_\nu) \,, \tag{2.59}$$

Schematic interactions are simple to handle, but their predictions (parameters) are only valid for a small region in the nuclear chart.

2.4.2 Microscopic Interactions

For many years, microscopic interactions were based on the so-called G-matrix, which is a scattering matrix for two nucleons in a nuclear medium [74, 75, 76] . G-matrix appears as a solution of the Bethe-Goldstone equation [80]

$$\hat{G}(\omega) = \hat{V} + \hat{V} \frac{\hat{Q}_{2p}}{(\omega - \hat{H}_{(0)_{2p}})} \hat{G}(\omega) \,, \tag{2.60}$$

where $\hat{H}_{(0)_{2p}}$ is an unperturbed Hamiltonian of the intermediate two-particle system, the Pauli operator $\hat{Q}_{2p}$ produces a non-vanishing result only if it acts on a pair of particles, both of

which are above the Fermi level. The parameter ω represents the starting energy at which G-matrix is evaluated. It is considered as a softer interaction compared to the bare NN potential. Evaluations of the G-matrix for finite nuclei can be found in Refs. [76, 77]. As a second step, the G-matrix is used to calculate the effective interaction for the model space to be used in the shell-model calculations

$$\hat{V}_{eff} = \hat{G} + \hat{G}\frac{\hat{Q}'}{(E_v - \hat{H}_{(0)_v})}\hat{V}_{eff}$$
$$= \hat{G} + \hat{G}\frac{\hat{Q}'}{(E_v - \hat{H}_{(0)_v})}\hat{G} + \hat{G}\frac{\hat{Q}'}{(E_v - \hat{H}_{(0)_v})}\hat{G}\frac{\hat{Q}'}{(E_v - \hat{H}_{(0)_v})}\hat{G} + \ldots, \tag{2.61}$$

where the prime on the projection operator $\hat{Q}'$ indicates that the ladder diagrams are excluded. Thus the effective interaction is given as a perturbation expansion in orders of G. The leading-order term in this expression is given by the G-matrix itself. Calculations for finite nuclei in valence spaces show the necessity to go beyond leading order, taking into account higher-order terms, such as core polarization and so on, see Ref. [78]. More details and the current status can be found in Ref. [76]. In spite of much progress in the development of techniques to get V_{eff}, numerical evaluation of Eq.(2.61) is very complicated. In addition, it is not clear whether the series converges, i.e. whether a next-order term in the expansion is smaller than the previous one. It is very difficult to go beyond the second-order term in perturbation and it is hard to incorporate three-nucleon interactions.

Recently, a new approach to get a soft interaction has been developed. The high-momentum component of the bare NN-interaction is integrated out down to a given cut-off momentum Λ within the renormalization group approach, resulting in a so-called V_{low-k} [79]. For a cut-off $\Lambda \sim 2.1$ fm^{-1}, low-momentum interactions derived from different bare NN potentials are very similar to each other. The soft interaction brings promising results in studies of nuclear matter properties. It is possible to incorporate three-body forces provided by effective-field theory potentials [81, 82, 83, 84, 85], very important for application in nuclear spectroscopy within the shell-model approach.

To be applied in shell-model calculations for heavy nuclei in a given valence space, core-polarization and other diagrams should be added to V_{low-k}. For first applications within the shell model see [86] and references therein. Up to now, a microscopic interaction based on the G-matrix or on V_{low-k}, derived from the bare two-nucleon potential, leads to a reasonable description of nuclei with two or a few valence nucleons beyond a closed-shell core in a one-oscillator shell valence space. As soon as the model space increases, the agreement deteriorates. A possible reason is the absence of many-body forces, in particular, the lack of a three-body force. As shown in systematic analyses, it is always mainly the monopole part of the interaction which requires modification [87]. This is why, to arrive at a successful description, microscopically obtained TBME's are subjected to an adjustment to known experimental data in the model space. This can be performed either by minimal monopole changes [87, 88, 89], or by a least-square fit to all TBME's [90, 91] of which the fitting procedure is illustrated in the next section.

2.4.3 Empirical Interactions

The descriptive and predictive power of these interactions is very high (see [48] for numerous examples). Practically, empirical corrections can be imposed to the two-body matrix elements $V_{ijkl,JT}$ of H_{residual} in a given model space. All TBME's and single-particle energies (SPEs) are treated as free parameters. The diagonalization of $\langle \Phi_{k'} | H | \Phi_k \rangle$, c.f. Eq.(2.35), produces the eigen-energies which are represented by linear combinations of these parameters with the coefficients being scalar two-body transition densities and occupation numbers. Therefore, the TBME's can be iteratively fitted by a least-squares method to reproduce experimental low-energy spectra of nuclei from the model space. The iterations stop when convergence for the final set of $V_{ijkl,JT}$ and SPEs is reached. To reach convergence, we may employ the linear combination method [91, 92], which chooses the most important linear combinations of TBME's to be determined in a least-squares fit. Fig. 2.9 displays the iteration of this fitting procedure. The interactions obtained by this method describe the experimental data very accurately. The SPEs are typically taken from the experimental spectra of the closed-shell-core plus a valence nucleon. However, if the number of valence shells of the given model space increases, the number of free parameters grows drastically. Therefore, a microscopic effective interaction serves as a starting point to get a good empirical interaction.
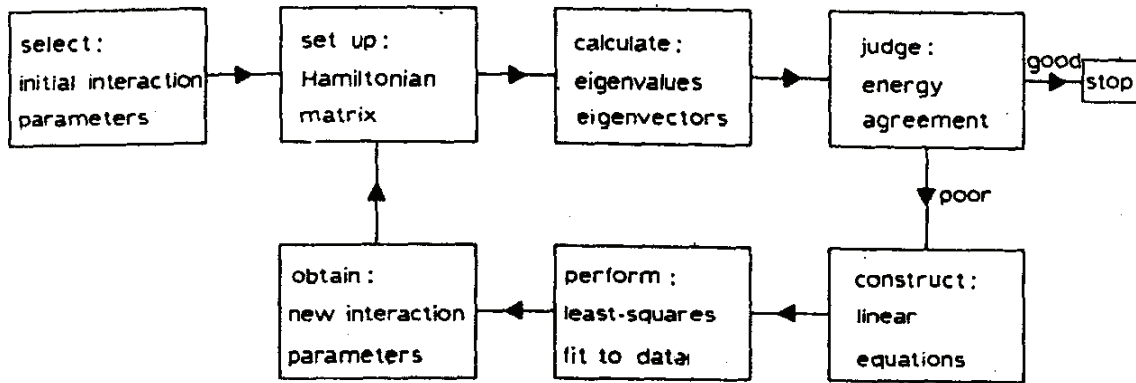
Figure 2.9: *The procedure to deduce the best set of TBME's $V_{ijkl,JT}$.*
$V_{ijkl,JT}$ are fitted to experimental excitation energies (and electromagnetic properties) in a given model space using an iterative least-squares fit. Adapted from Ref. [63].

The universal-(1s0d) interaction (USD) proposed by Wildenthal and Brown [92] for the *sd*-shell model space is a good example which accurately reproduces low-lying excited levels and transition probabilities. It consists of 63 TBMEs and 3 SPEs. The starting values of the TBME's are taken from those calculated by the G-matrix interaction of Kuo [93]. Other examples are the (0p)-shell interaction of Cohen and Kurath [94], which comprises 15 TBME's and 2 SPEs; and the (1p0f)-shell GXPF1 interaction [50, 90], which have 195 TBME's and 4 SPEs.

We use the USD interaction and its recent variations, i.e., USDA and USDB [49], for the present work.

2.5 Construction Formalism of Isospin Non-Conserving Hamiltonian

In this section we develop the formalism to construct realistic isospin-nonconserving (INC) Hamiltonians for the shell-model calculations of high precision.

As we introduced in the previous section, the shell-model Hamiltonian is given by SPEs ε_i, and TBME's of the residual interaction in the harmonic oscillator basis. We suppose that proton-proton, neutron-neutron and proton-neutron matrix elements may all be different. Similarly, proton and neutron SPEs are not the same. The goal is to find an interaction which describes well both nuclear structure and the splitting of isobaric multiplets of states.

In principle, charge-dependent effective interaction may be derived microscopically from the bare charge-dependent NN force (e.g., CD-Bonn potential) by applying a renormalization technique [76, 79]. However, such interactions, obtained from a two-body potential only, should still be adjusted, in particular, to get correct monopole properties [48, 87]. This is done by a least-squares fit of the monopole part of the Hamiltonian or of the whole set of TBME's to experimental data. Since the number of the matrix elements is huge, it is not feasible for the moment to get a realistic charge-dependent effective interaction in this way.

An alternative approach to the problem is first to get a reliable effective shell-model interaction in the isospin-symmetric formalism adjusted to describe experimental ground- and excited-state energies, and then to add a small charge-dependent part within the perturbation theory, and to constrain its parameters to experimental data. Diagonalization of the total INC Hamiltonian in the harmonic oscillator basis will lead to isospin mixing.

In the sd-shell model space (consisting of $0d_{5/2}$, $1s_{1/2}$, and $0d_{3/2}$ orbitals), the most precise isospin-conserving Hamiltonian, which is denoted below as $\mathscr{H}_0$, is either the USD interaction [92] or its two more recent versions — USDA or USDB [49]. First, we obtain its eigenvalues and eigenvectors:

$$\mathscr{H}_0|\alpha, T, T_z\rangle \equiv (H_0 + V_0)|\alpha, T, T_z\rangle = E(\alpha, T)|\alpha, T, T_z\rangle \,.$$

$E(\alpha, T)$ is independent from T_z. H_0 is the independent-particle harmonic oscillator Hamiltonian which defines the (isoscalar) single-particle energies $\varepsilon^{(0)} = (\varepsilon_i^p + \varepsilon_i^n)/2$, and V_0 are TBME's in sd shell.

Then, we construct a realistic isospin-symmetry violating term to get the total INC Hamiltonian. In general, we consider a charge-dependent interaction, which includes the Coulomb interaction acting between (valence) protons, and also charge-dependent forces of nuclear origin. The Coulomb interaction reads

$$V_{coul}(r) = \frac{e^2}{r} \,, \tag{2.62}$$

while the charge-dependent nuclear forces are represented in this work either by a scaled $T = 1$ component of the isospin-conserving interaction $V_0^{T=1}$ or by a linear combination of Yukawa-type potentials:

$$
\begin{aligned}
V_\pi(r) &= \frac{\exp(\mu_\pi r)}{\mu_\pi r}, \\
V_\rho(r) &= \frac{\exp(\mu_\rho r)}{\mu_\rho r},
\end{aligned}
\tag{2.63}
$$

where $\mu_\pi = 0.7$ fm^{-1} and $\mu_\rho = 3.9$ fm^{-1}, corresponding to the exchange of pion or ρ-meson, respectively, and r being the relative distance between two interacting nucleons. The Coulomb interaction contributes only to the proton-proton matrix elements, while the charge-dependent nuclear forces may contribute to all nucleon-nucleon channels. Thus, we can express the charge-dependent part of the two-body interaction as

$$
V = V^{pp} + V^{nn} + V^{np} = \lambda_{coul} V_{coul}(r) + \sum_{q=pp,nn,pn} \left(\lambda_\pi^q V_\pi^q(r) + \lambda_\rho^q V_\rho^q(r) + \lambda_0^q V_0^q \right),
\tag{2.64}
$$

where V_0 denotes $V_0^{T=1}$, while λ_{coul}, λ_π^q, λ_ρ^q, λ_0^q are strength parameters characterizing the contribution of charge-dependent forces. These parameters can be established by a fit to experimental data.

The two-body charge-dependent interaction V in Eq.(2.64) can alternatively be decomposed in terms of tensors of ranks 0, 1, and 2 in isospin space, i.e.

$$
V = V^{(0)} + V^{(1)} + V^{(2)},
$$

where the two-body matrix elements are related to those in proton-neutron formalism by the following relations:

$$
\begin{aligned}
V_{ijkl,J}^{(0)} &= \tfrac{1}{3} \left(V_{ijkl,J}^{pp} + V_{ijkl,J}^{nn} + V_{ijkl,J}^{pn(T=1)} \right), \\
V_{ijkl,J}^{(1)} &= V_{ijkl,J}^{pp} - V_{ijkl,J}^{nn}, \\
V_{ijkl,J}^{(2)} &= V_{ijkl,J}^{pp} + V_{ijkl,J}^{nn} - 2V_{ijkl,J}^{pn(T=1)}.
\end{aligned}
\tag{2.65}
$$

In addition, the charge-dependent Hamiltonian may contain a one-body term, H_{CD}^{1b}. We define it to have a pure isovector character and thus it gives rise to the isovector single-particle energies (ISPE's), defined as $\varepsilon_i^{(1)} = \varepsilon_i^p - \varepsilon_i^n$, to account for the Coulomb effects in the core nucleus. Thus, the most general charge-dependent part of the effective Hamiltonian reads

$$
H_{CD} = H_{CD}^{1b} + V.
$$

The charge-dependent part of the effective interaction is well known to be small and to be mainly of two-body type. The shift of isobaric multiplets due to the presence of charge-dependent Hamiltonian, H_{CD}, in the lowest order of the perturbation theory is given by its

expectation value in the states having good isospin: $\langle \alpha, T, T_z | H_{CD} | \alpha, T, T_z \rangle$. Application of the Wigner-Eckart theorem leads to the following expression similar to that discussed in the first chapter for the Coulomb interaction alone:

$$\langle \alpha, T, T_z | H_{CD} | \alpha, T, T_z \rangle = E^{(0)}(\alpha, T) + E^{(1)}(\alpha, T)T_z + E^{(2)}(\alpha, T)\left[3T_z^2 - T(T+1)\right] , \quad (2.66)$$

where the isoscalar part contributes only to the overall shifts of the multiplet, the isovector part and ISPE's ($\varepsilon_i^{(1)}$) results in $E^{(1)}(\alpha, T)$, while the isotensor part is the only contributor to $E^{(2)}(\alpha, T)$. The latter two terms lead to isospin-symmetry violation which includes the splitting of the isobaric multiplet and to the isospin mixing in the states.

Since only the isovector and isotensor part of H_{CD} could lead to isospin-symmetry violation, we will be interested in these two terms only. Futhermore, in the fit of nuclear TBME's in the isospin-symmetric formalism, part of the isoscalar Coulomb term has been taken into account by an empirical correction to the experimental binding energies (see [49] and references therein). Therefore, we add the isospin-conserving Hamiltonian with a charge-dependent Hamiltonian, which contains isovector (iv) and isotensor (it) terms only, namely,

$$H_{CD}^{iv+it} = \sum_{q=1,2} \left(\lambda_{coul}^{(q)} V_{coul}^{(q)}(r) + \lambda_{\pi}^{(q)} V_{\pi}^{(q)}(r) + \lambda_{\rho}^{(q)} V_{\rho}^{(q)}(r) + \lambda_0^{(q)} V_0^{(q)} \right) + \sum_i \varepsilon_i^{(1)}$$

$$= \sum_{\nu} \lambda_{\nu}^{(q)} V_{\nu}^{(q)} + \sum_i \varepsilon_i^{(1)} , \quad (2.67)$$

where q now denotes the isotensor rank of the operators and labels the corresponding strength parameter, while the indice ν is used to list all separate terms.

The isovector $E^{(1)}(\alpha, T)$ and isotensor $E^{(2)}(\alpha, T)$ contributions to the expectation value of H_{CD}^{iv+it} (or H_{CD}), can be either extracted from the energy shift due to the isovector $V^{(1)}$ (or H_{CD}^{1b}) and isotensor $V^{(2)}$ parts of the charge-dependent Hamiltonian, respectively, or from calculations of the energy shifts of all multiplet members. Following the latter method, we represent the TBME's of V_{ν} in terms of the proton-proton matrix elements only and then we calculate its expectation value in each state of the multiplet $E_{\nu}(\alpha, T, T_z) = \langle \alpha, T, T_z | V_{\nu} | \alpha, T, T_z \rangle$. Then, the isovector and isotensor contributions to a given multiplet of states are respectively expressed as

$$E_{\nu}^{(1)}(\alpha, T) = \frac{3}{T(T+1)(2T+1)} \sum_{T_z=-T}^{T} (-T_z) E_{\nu}(\alpha, T, T_z) ,$$

$$E_{\nu}^{(2)}(\alpha, T) = \frac{5}{T(T+1)(2T-1)(2T+1)(2T+3)} \sum_{T_z=-T}^{T} \left[3T_z^2 - T(T+1)\right] E_{\nu}(\alpha, T, T_z) .$$

$$(2.68)$$

Summing over all contributions to the H_{CD}, we get theoretical IMME b and c coefficients of the quadratic IMME Eq.(1.26) as

$$b^{th}(\alpha, T) = \sum_{\nu} \lambda_{\nu}^{(1)} E_{\nu}^{(1)}(\alpha, T) ,$$

$$c^{th}(\alpha, T) = 3 \sum_{\nu} \lambda_{\nu}^{(2)} E_{\nu}^{(2)}(\alpha, T) . \quad (2.69)$$

ISPE's are only included into the expression for b^{th} values. Fitted b and c coefficients are presented in Appendix B.

To find the best strengths $\lambda_\nu^{(q)}$, we have performed a least-squares fit of theoretical b^{th} and c^{th} coefficients to experimental IMME b and c coefficients : $b_i^{exp} \pm \sigma_i$ ($i = 1, \ldots, N_b$) and $c_j^{exp} \pm \sigma_j$ ($j = 1, \ldots, N_c$). Implying that they have a Gaussian distribution, we have minimised the χ^2 deviation (e.g., for b coefficients):

$$\chi^2 = \sum_{i=1}^{N_b} \frac{(b_i^{exp} - b_i^{th})^2}{\sigma_i^2} \, , \tag{2.70}$$

with respect to the parameters $\lambda_\nu^{(1)}$, i.e.

$$\frac{\partial \chi^2}{\partial \lambda_\nu^{(1)}} = \frac{\partial}{\partial \lambda_\nu^{(1)}} \sum_{i=1}^{N_b} \frac{(b_i^{exp} - b_i^{th})^2}{\sigma_i^2} = 0 \, , \tag{2.71}$$

which has lead us to a system of linear equations for $\lambda_\nu^{(1)}$:

$$\sum_{i=1}^{N_b} \left[\frac{E_{\mu i}^{(1)} b_i^{exp}}{\sigma_i^2} - \sum_\nu \frac{\lambda_\nu^{(1)} E_{\nu i}^{(1)} E_{\mu i}^{(1)}}{\sigma_i^2} \right] = 0. \tag{2.72}$$

In matrix form, this system looks like

$$\Lambda W = Q \quad \text{or} \quad \sum \Lambda_\nu W_{\nu\mu} = Q_\mu \, , \tag{2.73}$$

with

$$\Lambda_\nu = \lambda_\nu^{(1)} \, ,$$

$$W_{\nu\mu} = \sum_{i=1}^{N_b} \frac{E_{\nu i}^{(1)} E_{\mu i}^{(1)}}{\sigma_i^2} \, ,$$

$$Q_\mu = \sum_{i=1}^{N_b} \frac{E_{\mu i}^{(1)} b_i^{exp}}{\sigma_i^2} \, . \tag{2.74}$$

Since theoretical b and c coefficients are linear functions of unknown parameters $\lambda_\nu^{(q)}$ in Eq.(2.69), the fitting procedure is reduced to solving linear equations. Solution of these equations with respect to Λ results in the set of the most optimal strength parameters $\lambda_\nu^{(1)}$:

$$\Lambda = QW^{-1} \, . \tag{2.75}$$

To get uncertainties of the strength parameters found, we evaluate the root mean-square (rms) deviation from the error matrix W^{-1} as

$$\Delta \lambda_\nu^{(1)} = \sqrt{\langle (\lambda_\nu^{(1)} - \overline{\lambda_\nu^{(1)}})^2 \rangle} = \sqrt{(W^{-1})_{\nu\nu}} \, . \tag{2.76}$$

A similar procedure holds for the adjustment of c coefficients.

After adjusting the interaction, we solve the eigenproblem for a thus constructed INC Hamiltonian in the proton-neutron formalism: $[H_{INC}, T] \neq 0$:

$$H_{INC}|\alpha_p, \alpha_n\rangle \equiv (H + H_{CD}^{iv+it})|\alpha_p, \alpha_n\rangle = E|\alpha_p, \alpha_n\rangle \,.$$

As a result, the Hamiltonian eigenstates do not possess good isospin quantum number anymore and thus are mixtures of different T values.

2.5.1 TBME's of the Coulomb and Yukawa-type potentials

Harmonic oscillator parameter

The TBME's of the Coulomb and Yukawa-type potentials Eq.(2.62) and Eq.(2.63), used to calculate the energy shifts, were evaluated using the harmonic-oscillator wave functions for mass $A = 39$ and the subsequent scaling

$$S(A) = \left(\frac{\hbar\omega(A)}{\hbar\omega(A_0 = 39)} \right)^{1/2} . \tag{2.77}$$

The scaling factor incorporates the A-dependence of the TBME's. In Ref. [30], $\hbar\omega$ was taken in its most commonly used parameterization expressed by the Blomqvist-Molinari formula [95]:

$$\hbar\omega(A) = 45A^{-1/3} - 25A^{-2/3}; \tag{2.78}$$

For the sd shell, an additional scaling factor was imposed (see Eq.(3.7) in Ref. [30]) to improve the agreement with the data at the beginning and at the end of the sd shell.

However, recent empirical values of $\hbar\omega$, derived from updated experimental nuclear charge radii in Ref. [96], differ significantly from the values predicted by Ormand and Brown in Ref. [30], especially in the middle of the sd shell, not considered in Ref. [30]. The comparison is shown in Fig. 2.10. Some improvement is reached by a recent global parametrization of the Blomqvist-Molinari formula for the whole nuclear chart ($A = 1, \ldots, 248$) performed by Kirson [97].

However, none of these approaches resulted in sufficiently low root-mean-square (rms) deviation values in our fit for b and c coefficients. This may be due to the fact that all proposed parameterizations for $\hbar\omega$ values in the sd shell are not close to the values extracted from experimental nuclear charge radii. To overcome this difficulty, in this work we scaled the TBME's as given by Eq.(2.77), using however directly experimentally-based values for $\hbar\omega$ values in sd shell, mentioned above and shown in Fig. 2.10. The ISPE's were also evaluated for $A = 39$ and then scaled as given by Eq.(2.77).
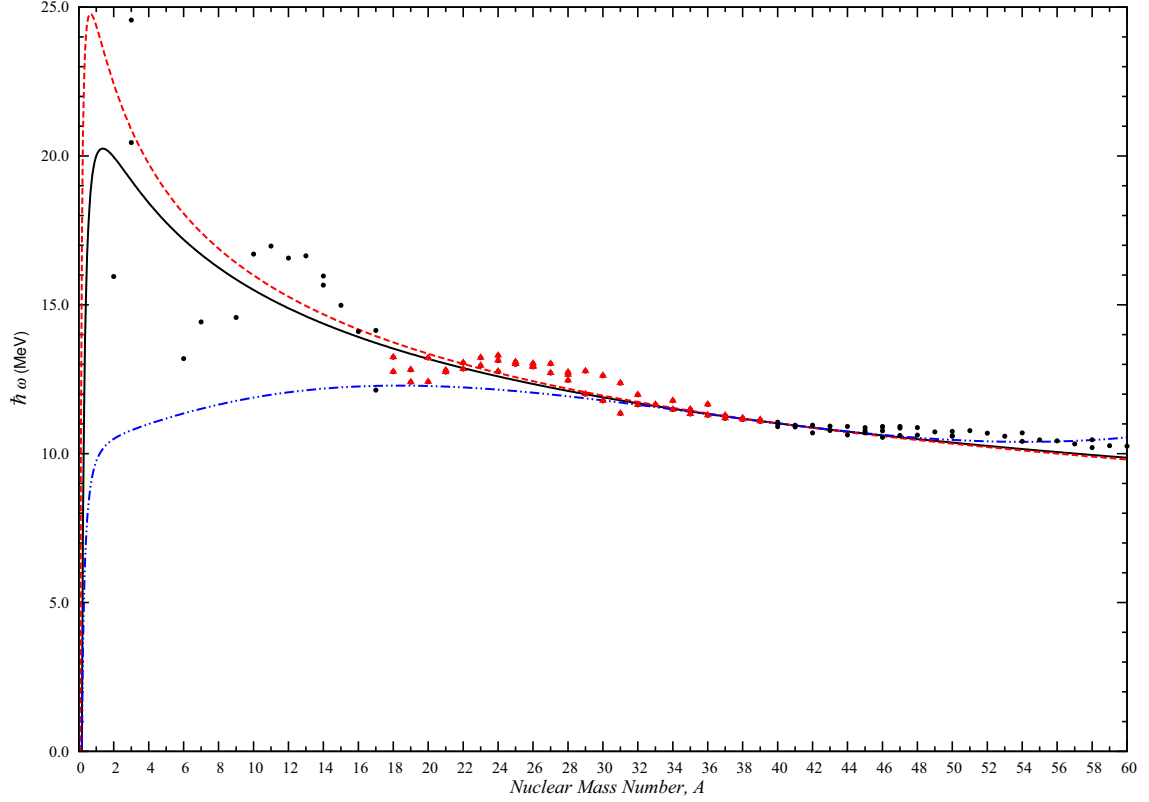
Figure 2.10: *Harmonic-oscillator energy spacing, $\hbar\omega$.*
Blomqvist-Molinari formula [95] (solid black line), Blomqvist-Molinari formula refitted by Kirson [97] (dashed red line), $\hbar\omega$ calculated by using $\hbar\omega = \hbar^2/(mb^2)$ and $\hbar^2/m = 41.458$ MeV fm^2 Ref. [97] and measured nuclear charge radii from [96] (black dots). In present work, we refitted $\hbar\omega$ from $A = 18, \ldots, 39$ based on the formalism of [97] (red triangles), and the refitted $\hbar\omega$ values are very close to [97] until they coincide with black dots. Obviously, parameterized $\hbar\omega$ with an additional factor from Eq. 3.7 in [30] deviates from the recently adopted experimental values (double-dot-dashed blue line).

Short-range correlations

Since the TBME's of Coulomb or meson-exchange potentials are calculated by using harmonic-oscillator wave functions in a restricted model space, it is important to account for the presence of SRC's. We have carefully studied this issue by two different methods. First, the Jastrow-type correlation function, which modifies the relative part of the harmonic oscillator basis, $\phi_{nl}(r)$, to

$$\phi'_{nl}(r) = [1 + f(r)]\,\phi_{nl}(r)\,, \tag{2.79}$$

with $f(r)$ being parametrized as

$$f(r) = -\gamma e^{-\alpha r^2}\left(1 - \beta r^2\right)\,. \tag{2.80}$$

Then the radial part of the TBME's of the Coulomb and of Yukawa type potentials between the modified harmonic-oscillator wave functions $\phi'_{nl}(r)$ and $\phi'_{n'l}(r)$ becomes

$$\int_0^\infty \phi'_{nl}(r)v(r)\phi'_{n'l}(r)dr = \int_0^\infty \phi_{nl}(r)v(r)\left[1 + f(r)\right]^2 \phi_{n'l}(r)dr. \tag{2.81}$$

We used three different sets of parameters α, β and γ in Eq.(2.80): those given by Miller and Spencer [98] and two alternative sets recently proposed on the basis of coupled-cluster studies with Argonne (AV18) and CD-Bonn potentials [53] (see Table 2.1). For brevity, we will refer to the two latter sets as CD-Bonn and AV18.

Table 2.1: *Parameters for Jastrow-type short-range correlation functions.*

	α	β	γ
Miller-Spencer	1.10	0.68	1.00
CD-Bonn	1.52	1.88	0.46
Argonne-V18	1.59	1.45	0.92

Besides, we have also used another renormalization scheme following the unitary correlation operator method (UCOM) [99]. Since we need to correct only central operators, the UCOM reduces to application of central correlators only, i.e. the radial matrix elements are of the form

$$\int_0^\infty \phi_{n'l}(r)v\left(R_+(r)\right)\phi_{nl}(r)dr, \tag{2.82}$$

where two different $R_+(r)$ functions have been used in $S = 0, T = 1$ and $S = 1, T = 1$ channels, namely,

$$R_+^{\mathrm{I}}(r) = r + \alpha\left(\frac{r}{\beta}\right)^\eta \exp\left[-\exp\left(\frac{r}{\beta}\right)\right], \tag{2.83}$$

with $\alpha = 1.3793$ fm, $\beta = 0.8853$ fm, $\eta = 0.3724$ in $S = 0, T = 1$ channel, and

$$R_+^{\mathrm{II}}(r) = r + \alpha\left(1 - \exp\left(-\frac{r}{\gamma}\right)\right)\exp\left[-\exp\left(\frac{r}{\beta}\right)\right], \tag{2.84}$$

with $\alpha = 0.5665$ fm, $\beta = 1.3888$ fm, $\gamma = 0.1786$ in $S = 1, T = 1$ channel [99].

The modifications of V_{coul} and V_ρ brought about by different approaches to the SRC issue are shown in Fig. 2.11 and Fig. 2.12, respectively.

Although UCOM renormalization scheme differs from the Jastrow-type correlation functions, we can easily notice that either of the $R_+(r)$ functions does not strongly affect the original potentials. Somewhat stronger modifications are brought about by the CD-Bonn based

parametrization. Miller-Spencer parameterization of the correlation function induces the highest suppression of the potentials at short distances and leads to the vanishing at $r = 0$. Similar conclusions are reported in Ref. [100] in the context of the double-beta decay studies. Strong modifications are clearly seen for AV18 as well.
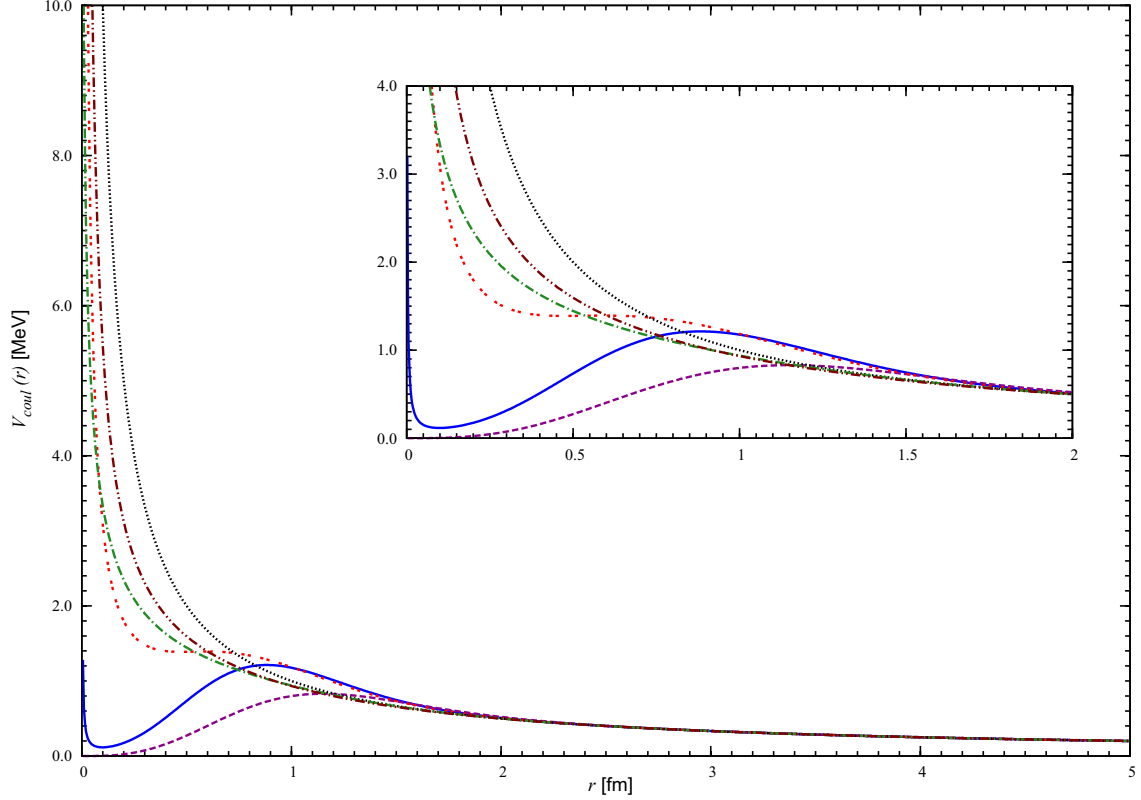
Figure 2.11: *$V_{coul}(r)$ adjusted by different SRC's.*
$V_{coul}(r)$ without SRC (dotted black line), $V_{coul}(r)$ with proposed parameters for Jastrow type SRC on the basis of coupled-cluster calculation with CD-Bonn (double-dashed red line) or with Argonne V18 [53] (solid blue line), $V_{coul}(r)$ with Miller-Spencer parameterized Jastrow type SRC [98] (dashed purple line); $V_{coul}(R_+^I(r))$ with UCOM SRC (dot-dashed green line), $V_{coul}(R_+^{II}(r))$ with UCOM SRC (double-dot-dashed brown line). The inset enlarges the left-hand part of this figure.

To illustrate the effect from different approaches to the SRC on later results, we present in Table 2.2 the ratios of the Coulomb expectation values in the ground and several low-lying excited states of a few selected nuclei from the bottom, top and the middle of the *sd* shell-model space, i.e. ^{18}Ne (2 valence protons), ^{38}K (2 proton holes), and ^{30}S and ^{26}Mg, respectively. The second column of Table 2.2 contains absolute expectation values of the bare Coulomb interaction, while the other columns show the ratios to it from Coulomb interaction expectation values which include SRC.

It is seen that the Miller-Spencer approach to SRC quenches Coulomb matrix element (as well as that of Yukawa ρ-exchange potential) and thus reduces Coulomb expectation values more compared to other SRC schemes. Interestingly, the CD-Bonn parametrization and in some cases the AV-18 parametrization show even a small increase of the Coulomb expectation value.
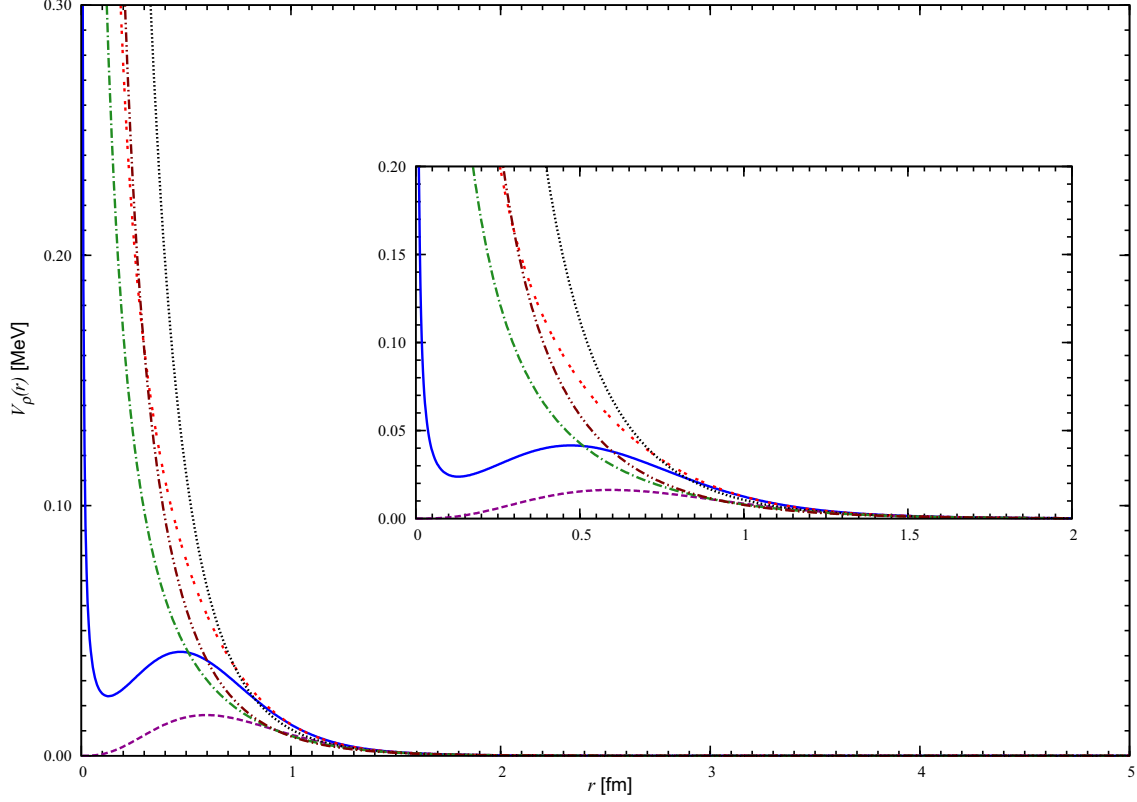
Figure 2.12: *$V_\rho(r)$ adjusted by different SRC's.*
$V_\rho(r)$ without SRC (dotted black line), $V_\rho(r)$ with proposed parameters for Jastrow type SRC on the basis of coupled-cluster calculation with CD-Bonn (double-dashed red line) or with Argonne V18 [53] (solid blue line), $V_\rho(r)$ with Miller-Spencer parameterized Jastrow type SRC [98] (dashed purple line); $V_\rho(R_+^I(r))$ with UCOM SRC (dot-dashed green line), $V_\rho(R_+^{II}(r))$ with UCOM SRC (double-dot-dashed brown line). The inset enlarges the left-hand part of this figure.

2.5.2 Remarks

The effect of quenching imposed by various SRC approaches on Coulomb matrix elements (and on matrix elements of Yukawa ρ-exchange potential) are not very close to one another, c.f. Fig. 2.11 and Fig. 2.12. However, the differences of the ratios of expectation values shown in Table 2.2 from unity for Miller-Spencer, CD-Bonn, Argonne V18, and UCOM, are indeed just 0.027, 0.008, 0.004, 0.014, respectively.

In order to verify the implication of various SRCs, we establish two methods in chapter 4. First, we compare the root mean square deviation values produced from a shell-model fit with or without an SRC approach. Besides, we also compare the average Coulomb strength parameters affected by different SRC approaches.

The third method is to compare physical observables calculated by INC Hamiltonian (with or without an SRC approach) with experimental ones. For example, the branching ratios of isospin-forbidden proton emission. However, this work is reserved in perspective.

Table 2.2: *Ratios of Coulomb expectation values of ^{18}Ne, ^{38}K, ^{30}S, ^{26}Mg, produced from various SRC approaches to Coulomb evaluation without SRC.*

| | $\langle\psi\|V_{coul\ \text{without SRC}}\|\psi\rangle$ (MeV) | $\langle\psi\|V_{coul\ \text{with SRC}}\|\psi\rangle/\langle\psi\|V_{coul\ \text{without SRC}}\|\psi\rangle$ | | | |
		Miller-Spencer	CD-Bonn	Argonne V18	UCOM
Mass 18, ^{18}Ne					
0^+ g.s.	0.531	0.900	1.008	0.978	0.958
2^+	0.449	0.961	1.010	0.997	0.981
4^+	0.389	0.984	1.007	1.001	0.991
0^+	0.412	0.952	1.005	0.990	0.979
2^+	0.380	0.993	1.006	1.003	0.994
0^+	0.425	0.980	1.011	1.004	0.987
Mass 38, ^{38}K					
0^+ g.s.	16.402	0.986	1.007	1.003	0.991
2^+	16.316	0.986	1.007	1.003	0.992
Mass 30, ^{30}S					
0^+ g.s.	10.721	0.984	1.007	1.002	0.990
2^+	10.696	0.985	1.007	1.002	0.991
2^+	10.704	0.985	1.007	1.002	0.991
1^+	10.632	0.987	1.007	1.003	0.992
Mass 26, ^{26}Mg					
0^+ g.s.	2.518	0.967	1.008	0.998	0.984
2^+	2.480	0.974	1.008	1.000	0.986
2^+	2.491	0.972	1.008	0.999	0.986
0^+	2.491	0.972	1.008	0.999	0.986

Chapter 3

Experimental Isobaric Multiplet Mass Equation Coefficients

Contents

We have compiled a new set of *isobaric multiplet mass equation* (IMME) b and c coefficients for 648 experimentally available $T = 1/2, 1, 3/2$, and 2 multiplets. Compared to the old compilation [101], 218 new data points have been added, most of them for nuclei in the pf-shell. The new compilation profits from the experimental advances in the spectroscopy of proton-rich nuclei around the $N = Z$ line, in particular those with very low production cross section. Moreover, the progress in atomic mass measurements [102] lead to a considerable improvement of the precision of ground state (g.s.) mass excess data for IMME multiplets. These improved and new experimental data may help us to analyze the exchange symmetry between neutrons and protons that is important for the nuclear structure at the vicinity of the $N = Z$ line. In this chapter, we present the fitting procedure and the resulting database of IMME coefficients for nuclei with $A = 1$, 3, 5, 6, 7, ..., 71, considering all experimentally identified multiplets. Based on this new compilation, we analyze the correlation of IMME b and c coefficients, with $A^{\frac{2}{3}}$ and $A^{-\frac{1}{3}}$, respectively. Plots of these correlations show discontinuities at closed shells. The b coefficients tend to increase with the average excitation energy $\overline{E}_{exc}$ of the multiplet.

3.1 IMME Fitting Procedure

Recently, more experimental data of higher precision on nuclear mass excess and level schemes have been accumulated for most of the $N \approx Z$ sd-shell nuclei. The recently extended experimental data enable us to revise the database of experimental IMME coefficients used to adjust the isovector and isotensor strength parameters in the H_{CD}, c.f. Eq.(2.67) of chapter 2.

As the latest evaluation of experimental isobaric mass multiplet splittings by Britz *et al.* [101] is already 13 years old, we have revised it and built up our own data base by incorporating all recent mass measurements from the evaluation [103] (or some particular references) and from experimental level schemes [104]. Some excited levels in Ref. [101] have been excluded from our compilation because they disappeared from Ref. [104]. Only data for nuclei with experimentally measured masses are adopted. This new set of compiled IMME a, b, c (and d, e) coefficients is described below and is listed in Appendix A. It includes recent pf-shell space experimental data points and will be published as Ref. [105]. The amount of newly added data points is shown in Table 3.1.

Table 3.1: *Comparison of the amount of old and new IMME multiplet data points*

Isospin, T	Number of data points	
	Present work	Previous work [101]
1/2 (doublet)	334	289
1 (triplet)	127	109
3/2 (quartet)	23	26
2 (quintet)	7	6

We perform an error-weighted least-squares fit to the IMME Eq.(1.26) by considering the experimental mass excesses and their error bars, $\mathscr{M}_i^{exp} \pm \sigma_i$, by assuming that they have a Gaussian distribution, and by minimising the χ^2 deviation, to find the best a, b, c; or a, b, c, d; or a, b, c, e coefficients,

$$\chi^2 = \sum_{i=1}^{N} \frac{(\mathscr{M}_i^{exp} - \mathscr{M}_i^{IMME})^2}{\sigma_i^2} \,, \tag{3.1}$$

with respect to IMME coefficients,

$$\frac{\partial \chi^2}{\partial \kappa_\nu} = \frac{\partial}{\partial \kappa_\nu} \sum_{i=1}^{N} \frac{(\mathscr{M}_i^{exp} - \mathscr{M}_i^{IMME})^2}{\sigma_i^2} = 0 \,, \quad \nu = 1, 2, \cdots, 5. \tag{3.2}$$

Here, $\kappa_1, \kappa_2, \ldots, \kappa_5$ correspond to the IMME coefficients a, b, c, d, and e; ν is the index of coefficients to be fitted, i.e., $\nu = 1, 2$, and 3 for quartets and quintets with a, b, and c coefficients; whereas $\nu = 1, 2, 3$, and 4 or 5 for quintets with a, b, c, d or e coefficients. The index i labels

the members of a multiplet; $N = 4$ for quartets and $N = 5$ for quintets. Eq.(3.2) leads to a system of linear equations for κ_ν:

$$\sum_{i=1}^{N} \left[\frac{T_{z_i} \mathscr{M}_i^{exp}}{\sigma_i^2} - \sum_\nu \frac{\kappa_\nu T_{z_i}^2}{\sigma_i^2} \right] = 0. \tag{3.3}$$

Putting the linear equations into matrix form, one obtains

$$KX = Y \quad \text{or} \quad \sum_\nu K_\nu X_{\nu\mu} = Y_\mu, \tag{3.4}$$

with

$$K_\nu = \kappa_\nu, \quad X_{\nu\mu} = \sum_{i=1}^{N} \frac{T_{z_i}^2}{\sigma_i^2}, \quad Y_\mu = \sum_{i=1}^{N} \frac{T_{z_i} \mathscr{M}_i^{exp}}{\sigma_i^2}. \tag{3.5}$$

As the IMME is a linear function of the unknown coefficients κ_ν (a, b, c, ...coefficients) in Eq.(1.26), the fitting procedure is reduced to solving linear equations. Solution of these equations with respect to K results in the set of the optimized coefficients κ_ν,

$$K = YX^{-1}. \tag{3.6}$$

Error Estimate for the mass excess of excited states. The uncertainty of the mass excess of excited states that appear in higher lying multiplets is obtained by combining the uncertainty of the ground-state mass excess $\sigma_{A,T_z,g.s.}$ and the uncertainty of excitation energy $\sigma_{A,T_z,J\pi}$ of the the excited state (e.s.)

$$\sigma_{A,T_z,J\pi} = \sqrt{\sigma_{A,T_z,g.s.}^2 + \sigma_{A,T_z,J\pi}^2}. \tag{3.7}$$

Uncertainties computed from Eq.(3.7) become the input to Eq.(3.1).

Error Estimate for Fitting Procedure. To get uncertainties of the fitted IMME coefficients, we evaluate the root mean-square deviation from the error matrix X^{-1} in Eq.(3.6) as

$$\Delta\kappa_\nu = \sqrt{\langle (\kappa_\nu - \overline{\kappa_\nu})^2 \rangle} = \sqrt{(X^{-1})_{\nu\nu}}. \tag{3.8}$$

The definition of average excitation energy. We may average the excitation energy, E_{exc}, of a multiplet by defining the E_{exc} relative to the lowest-lying multiplet of the same T treated as $E_{exc} = 0$. For example, the average excitation of the lowest-lying multiplet $\frac{5}{2}^+$ of the quartet $A = 21$ is set to zero. The average excitation of the next higher-lying multiplet, $\frac{1}{2}^+$, is

$$\begin{aligned}
\overline{E}_{\frac{1}{2}^+} &= \frac{E_{\left(\frac{1}{2}^+, T_z=3/2\right)} + E_{\left(\frac{1}{2}^+, T_z=1/2\right)} + E_{\left(\frac{1}{2}^+, T_z=-1/2\right)} + E_{\left(\frac{1}{2}^+, T_z=-3/2\right)}}{4} \\
&= \frac{279.93 + 289.7 + 241 + 200}{4} \\
&= 253 \, \text{keV}
\end{aligned}$$

3.2 IMME b and c Coefficients

The IMME is given in Eq.(1.26). We may rearrange the a, b, and c coefficients in Eq.(1.27) as

$$a = \mathscr{M}_0 + E_{coul}^{(0)} - T(T+1)E_{coul}^{(2)}\,, \qquad b = \Delta_{nH} - E_{coul}^{(1)}\,, \qquad c = 3E_{coul}^{(2)}\,, \tag{3.9}$$

where $E_{coul}^{(0)}$, $E_{coul}^{(1)}$, and $E_{coul}^{(2)}$ are respectively the expectation values of isoscalar, isovector, and isotensor parts of the Coulomb interaction. They replace $E_{coul}^{(q)}(\alpha, T)$ in Eq.(1.24) and Eq.(1.27). The ingredients of this expression are the charge-free nuclear mass

$$\mathscr{M}_0 = \frac{1}{2}(M_n + M_H)A + (M_n - M_H)T_z + \langle \alpha, T, T_z |\, \mathscr{H}_0 \, |\alpha, T, T_z \rangle \,.$$

If we assume that the Coulomb interaction is the only contribution shifting the IAS of an isobaric multiplet and treat a nucleus as a uniformly charged sphere of radius $R = r_0 A^{1/3}$, the total Coulomb energy of a nucleus is given by

$$E_{coul} = \frac{3e^2}{5R}Z(Z-1) = \frac{3e^2}{5r_0 A^{\frac{1}{3}}}\left[\frac{A}{4}(A-2) + (1-A)T_z + T_z^2\right]\,. \tag{3.10}$$

This extremely simplified expression, Eq.(3.10), when put into the IMME, provides an estimate of the IMME coefficients [22, 106]

$$a = \frac{3e^2}{20r_0}\frac{A(A-2)}{A^{\frac{1}{3}}}\,, \quad b = -\frac{3e^2}{5r_0}\frac{(A-1)}{A^{\frac{1}{3}}}\,, \quad c = \frac{3e^2}{5r_0}\frac{1}{A^{\frac{1}{3}}}\,. \tag{3.11}$$

A comparison of this crude estimation with experimental b and c coefficients is shown in Fig. 3.1 and Fig. 3.3, respectively.

Equation (3.9) shows that the expectation values of isovector and isotensor operators are related to IMME b and c coefficients, respectively. To extract these two expectation values, we need at least two *Coulomb energy differences* (CED)[1] of the same A and T. In other words, an extraction is still possible even when the nuclear mass excess data of the given multiplet are not complete. However, we impose a more stringent principle, i.e., an isobaric multiplet will only be adopted if every member's nuclear mass excess has been measured. Using the extended experimental data base, we have compiled more sets of complete isobaric multiplet, particularly in pf-shell nuclei, and also have updated sd-shell nuclei isobaric multiplets, which are used to deduce experimental expectation values of isovector and isotensor operators that will be used later on for our fit of strength parameters in Eq.(2.67).

---

[1] A Coulomb energy difference is the difference in excitation energy between excited IAS states. It is obtained by normalizing the absolute binding energies of the ground states of all members of a given isobaric multiplet.

3.2.1 IMME b Coefficients

Other than the relation of b with $A^{2/3}$ and $A^{-1/3}$ given in Eq.(3.11), we also consider the expression [107]

$$b = -\frac{3e^2}{5r_0}A^{2/3}\,. \tag{3.12}$$

The b coefficients in both Eq.(3.11) and Eq.(3.12) are deduced assuming a uniformly charged sphere. The only difference between Eq.(3.12) and the b in Eq.(3.11) is that Z is neglected in the term of $Z(Z-1)$ in Eq.(3.10) in comparison to Z^2, causing $Z(Z-1) \approx Z^2$. The plot of Eq.(3.12) is added to Fig. 3.1, which depicts $-b$ as a function of $A^{2/3}$ for 491 multiplets. The crude estimation of b coefficients from a uniformly charged sphere, Eq.(3.11) and Eq.(3.12), predicts correctly the overall trend of the b coefficients. However, it underestimates the magnitude of b by about ~1 MeV. Bethe and Bacher [106] proposed that the effect of antisymmetrisation should be considered instead of a purely classical estimation of the Coulomb energy in a nucleus. Based on this idea, Sengupta calculated the Coulomb energy of mirror nuclei with $A = 3, \cdots, 39$ using a statistical model [108]. Nolen and Schiffer wrote an extensive review on the calculation of Coulomb energies. In their comparison of theoretical models, which included Sengupta's calculation, with experimental results, they showed that there is a reduction between $5\% - 10\%$ in theoretical Coulomb energies of nuclei in p, sd and pf-shell spaces [109]. Therefore, instead of the Coulomb interaction, the energy from non-Coulomb charge-dependent forces may fill the gap between theoretical b coefficients and experimental ones.

The weighted fit (solid line) function of all b coefficients of all multiplets is $b = -691.39(\pm 90)A^{2/3} + 1473.44(\pm 95)$. Most of the lowest-lying multiplets' b coefficients have a lower error bar than the higher-lying multiplets' b. Hence, the weighted fit line is closer to the b coefficients of the lowest lying multiplets. However, the unweighted fit (dashed line) function, $b = -723.4A^{2/3} + 1927.9$, presents a more even description of b coefficients. The discrepancy between the weighted fit and the unweighted one shows that b coefficients tend to increase with excitation energy for higher lying multiplets. The unweighted fit is less influenced by the few low-A nuclei which have more precise measurements on nuclear mass and energy level schemes. A method of systematically analyzing the behavior of b coefficients of doublets (Coulomb energy difference) was given by Everling [110]. However, pursuing such analysis is beyond the scope of this thesis.

Figure 3.2 presents b coefficients of the lowest-lying doublets of $A = 1, \cdots, 71$, and the lowest-lying quartets of $A = 7, \cdots, 41$. We found that there are a few separately best fitted lines in Fig. 3.2. Discontinuities of these fitted lines occur at the closed (p, sd, pf) shells at $A = 4$, 16, and 40. These shell effects are not described by the uniformly charged sphere assumption. Such discontinuities were already noticed by Jänecke and were indicated in Fig. 2 of his Ref. [107]. In the present study, we find that there is a discontinuity at $A = 56$; it points toward $0f_{7/2}$ subshell gap which was not indicated in Ref. [107]. Jänecke did not show the discontinuity at $A = 12$, because his plot included the lowest-lying triplets in the fitted line, and he fitted from the region of mass $A = 5$ to $A = 15$. Furthermore, we also find that

there is a discontinuity for $T = 3/2$ quartets, which was not shown in Ref. [107] due to limited experimental data.

One can notice small-amplitude oscillations of b coefficients about the fitted lines which can be related to Coulomb pairing effects. The oscillatory behavior of b coefficients is explored in chapter 5.
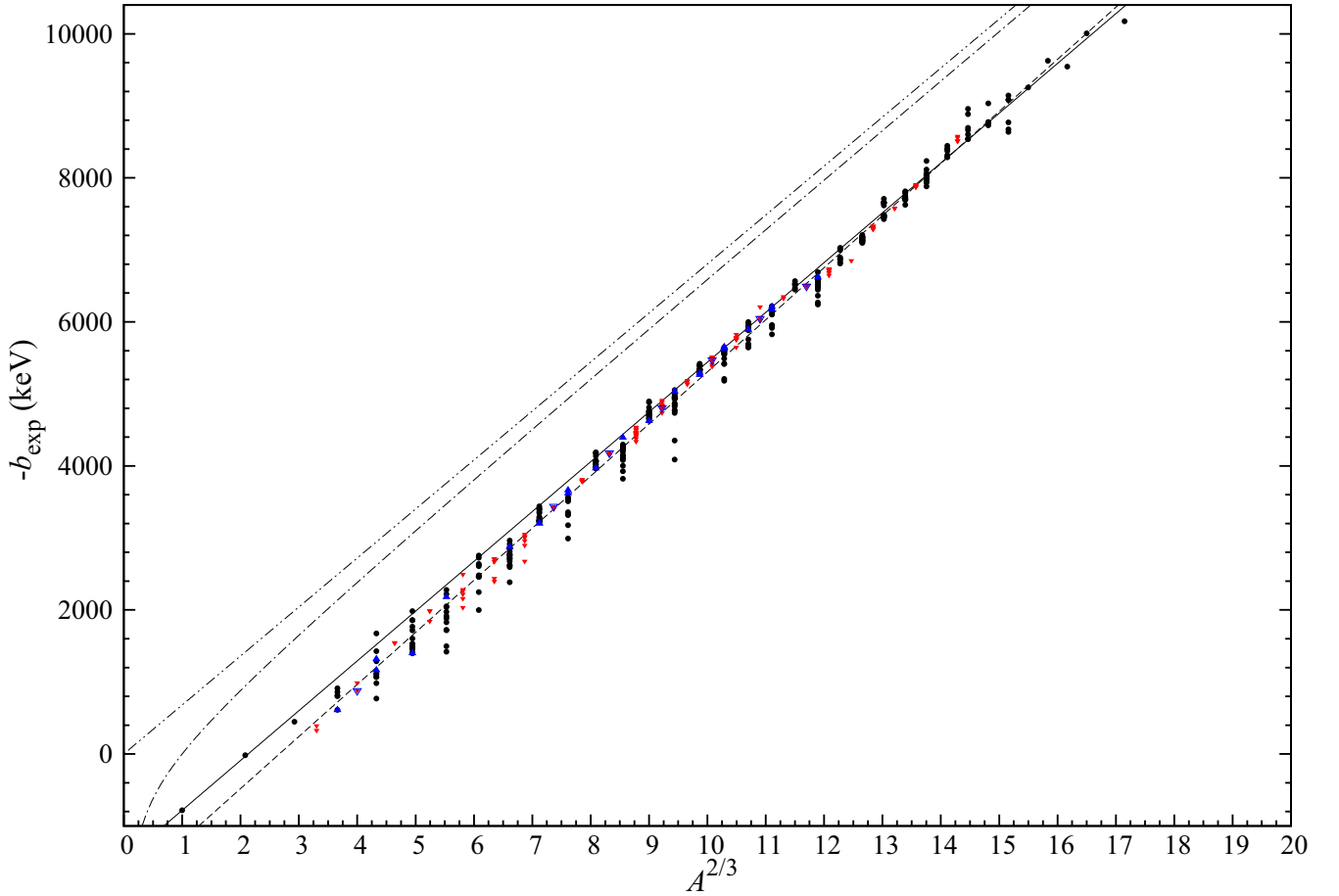
Figure 3.1:   *The b coefficients as a function of $A^{2/3}$ for all $T = 1/2, 1, 3/2, 2$ multiplets.*
These b coefficients are obtained by fitting a quadratic IMME, c.f. Table A.2, A.3, A.4, and A.5 in Appendix A.
(Black) circles are doublets. Triplets are represented by down (red) triangles, whereas up (blue) circles are quartets. Down (blue) triangles are quintets. A weighted fit to b coefficients, $b = -691.39(\pm90)A^{2/3} + 1473.44(\pm95)$ is displayed by solid line. Dashed line shows the unweighted fit to b coefficients, $b = -723.4A^{2/3} + 1927.9$. (Black) dotted-dash line is $b = \frac{3e^2(A-1)}{5r_0A^{1/3}}$. (Black) double-dotted-dash line is $b = \frac{3e^2}{5r_0}A^{2/3}$.
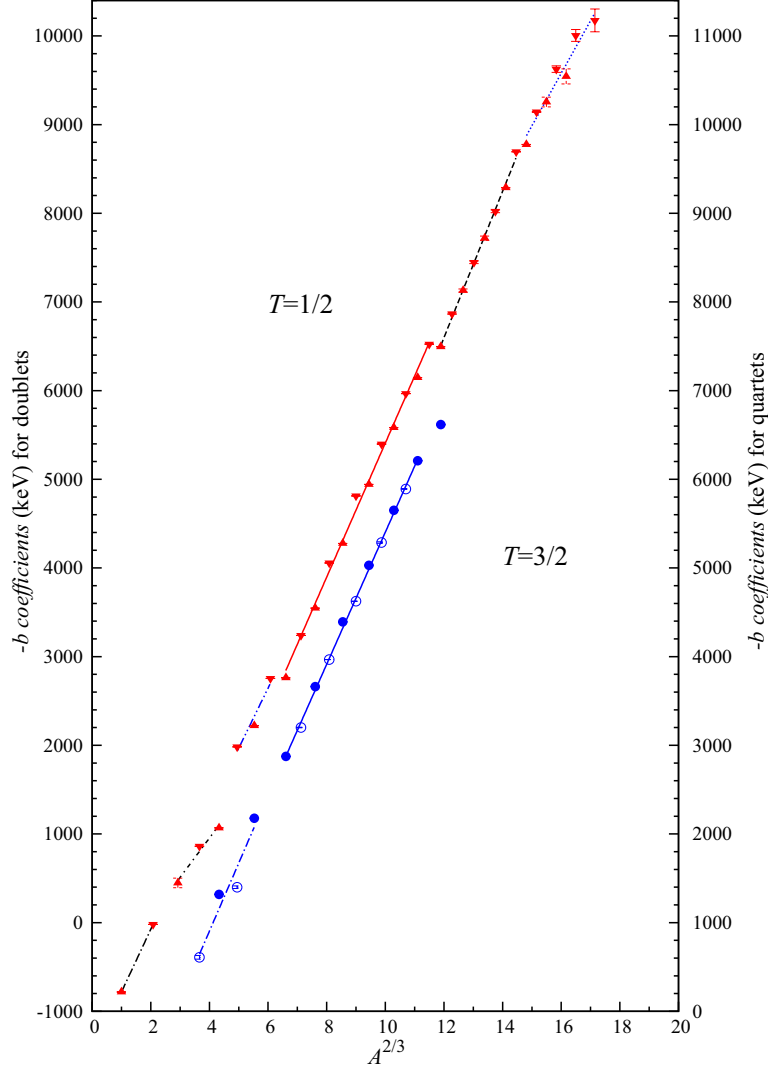
Figure 3.2: *Plot of the lowest-lying doublets and quartets of $-b$ coefficients as a function of $A^{2/3}$.*
These b coefficients are fitted according to the quadratic IMME. Up (red) triangles are doublets with $4n+3$; whereas down (red) triangles are doublets with $4n+1$. Quartets with $4n+1$ are represented by filled (blue) circles, and open (blue) circles are quartets with $4n+3$. ($T = 1/2$) doublets and ($T = 3/2$) quartets refer to the left y-axis, and to the right y-axis, respectively. Unweighted fit within various shell spaces are depicted by lines:

$T = 1/2$:
(Black) dotted-dash line, s shell space, $b = -707.12A^{2/3} + 1489.5$, $A = 1, 3$.
(Black) dotted-short-dash line, p shell space, $b = -444.31A^{2/3} + 823.29$, $A = 5, 7, 9$.
(Blue) double dotted-dash line, p shell space, $b = -676.9A^{2/3} + 1416.8$, $A = 11, 13, 15$.
(Red) solid lines, sd shell space, $b = -756.1A^{2/3} + 2152.3$, $A = 17, 19, \ldots, 39$.
(Black) dashed line, f shell space, $b = -824.51A^{2/3} + 3296.4$, $A = 41, 43, \ldots, 55$.
(Blue) dotted line, pf shell space, $b = -592.77A^{2/3} - 94.754$, $A = 57, 59, \ldots, 71$.

$T = 3/2$:
(Blue) dotted-dash line, p shell space, $b = -767.76A^{2/3} + 2167.6$, $A = 7, 9, 11, 13$.
(Blue) solid lines, sd shell space, $b = -744.76A^{2/3} + 2044.4$, $A = 17, 19, \ldots, 37$
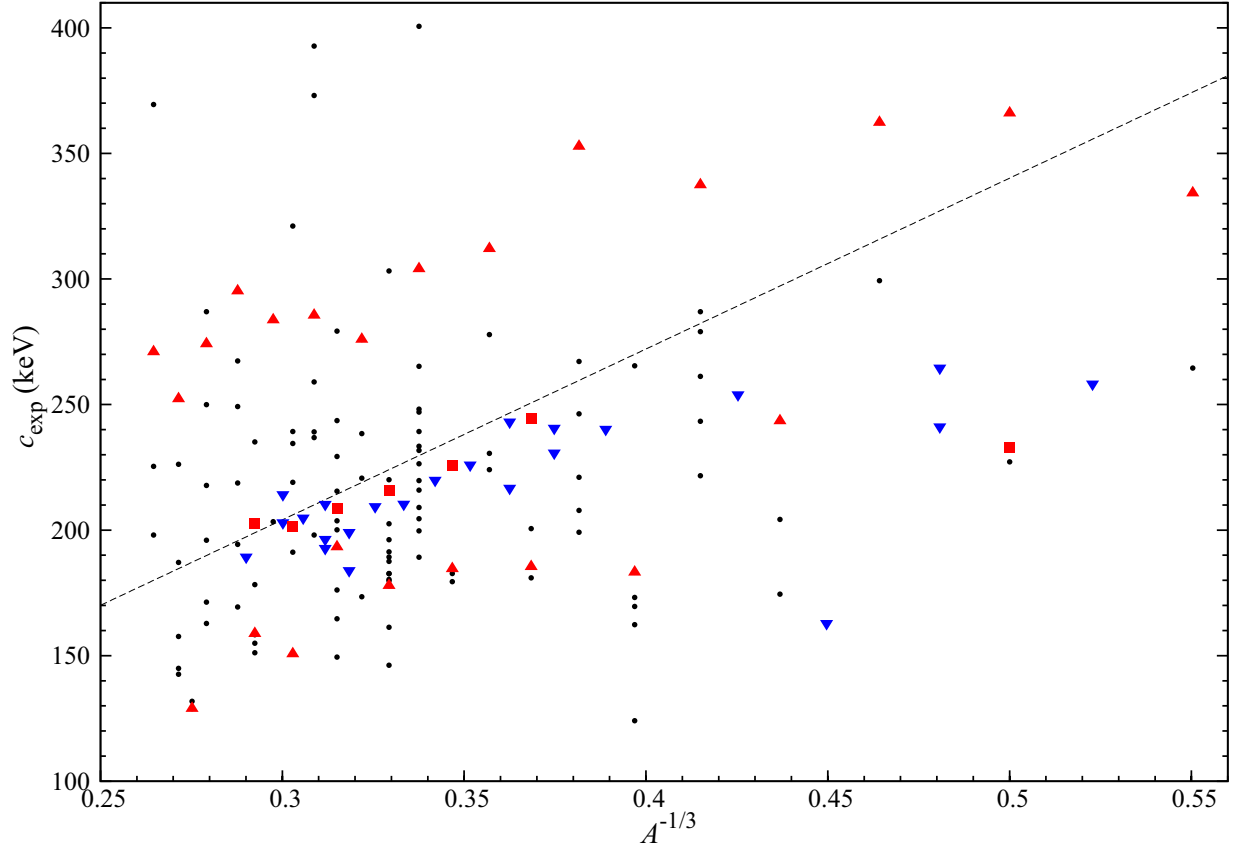
Figure 3.3: *The c coefficients as a function of $A^{-1/3}$ for all $T = 1, 3/2$, and 2 multiplets.*
These c coefficients are fitted according to the quadratic IMME. (Red) up triangles are the lowest-lying triplets, whereas (black) circles are higher-lying triplets. (Blue) down triangles are quartets, and (red) squares are quintets. The dashed line is $c = \frac{3e^2}{5r_0} A^{-\frac{1}{3}}$.

3.2.2   IMME c Coefficients

All experimental c coefficients are plotted in Fig. 3.3 as a function of $A^{-1/3}$ together with a straight line deduced from the idea of classical homogeneously charged sphere, Eq.(3.11). For the lowest-lying triplets' and quintets' c coefficients, indicated as red triangles and red squares, respectively, this classical assumption is roughly valid. However, higher-lying multiplets' c coefficients, mainly from triplets, do not show any trend related to $A^{-1/3}$, c.f. Fig. 3.3.

We separately replot the lowest-lying triplets, quartets, and quintets in Fig. 3.4 and Fig. 3.5 as a function of A and $A^{-1/3}$, respectively. The triplets' c coefficients form two families for $A = 4n$ and $A = 4n + 2$. A staggering effect between these two families of triplets is clearly visible. Quintets in the sd-shell space also show a small staggering behavior when they are plotted as a function of $A^{-1/3}$ in Fig. 3.5. However, this effect is not noticeably seen when quintets are plotted as a function of A in Fig. 3.4. Quartets' c coefficients do not exhibit any staggering effect. The details and theoretical description of these effects can be found in chapter 5.
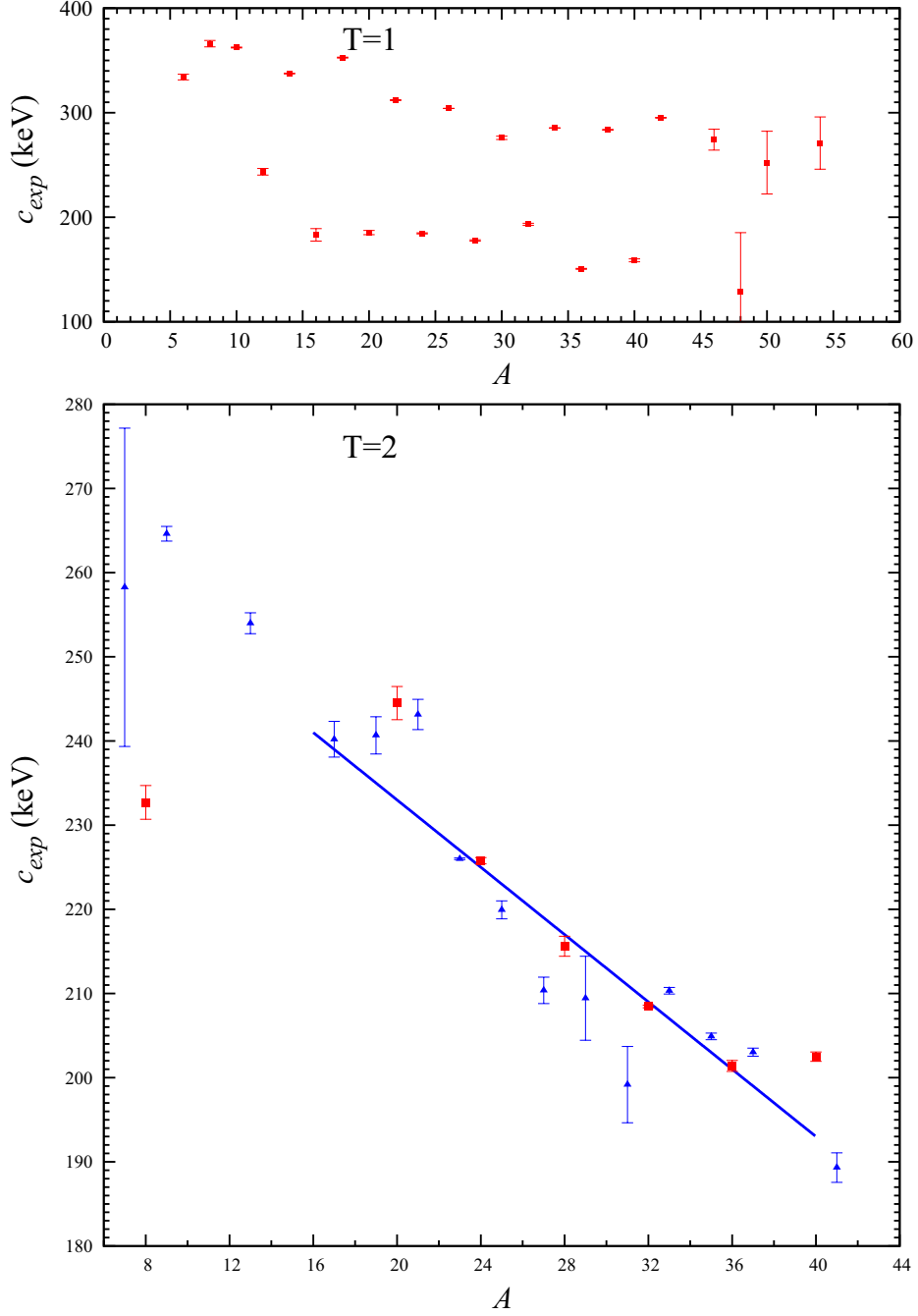
Figure 3.4: *The c coefficients as a function of A for the lowest lying triplets, quartets, and quintets.* These c coefficients are fitted according to the quadratic IMME. (Red) squares in the upper figure are the lowest-lying triplets, whereas (red) squares in the lower figure are the lowest-lying quintets. (Blue) triangles are quartets. The solid (blue) line is $c = -2A + 273$, which is an unweighted fit upon quintets of $A = 24, 28, 32$, and 36.
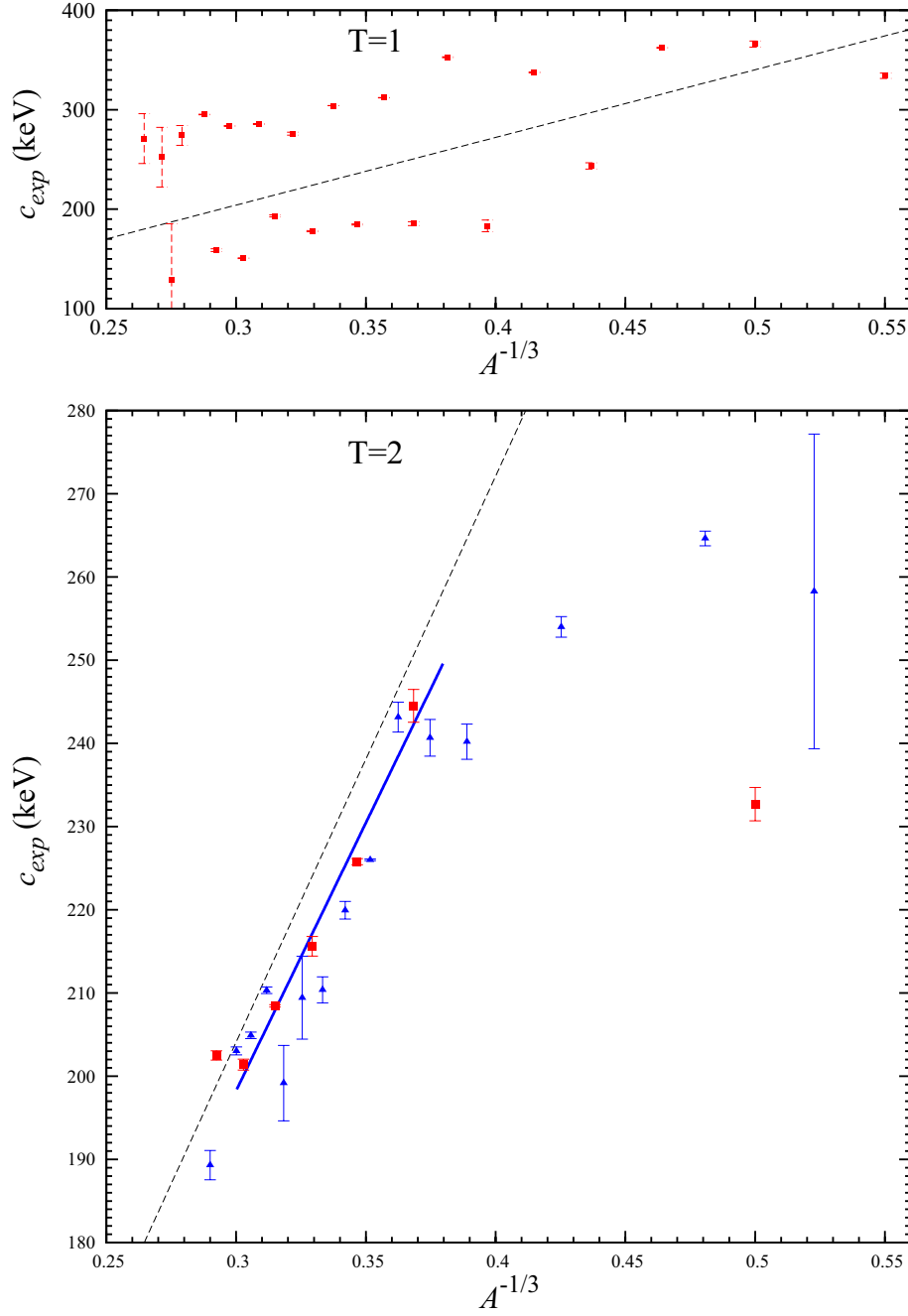
Figure 3.5: *The c coefficients as a function of $A^{-1/3}$ for the lowest-lying triplets, quartets, and quintets.* These c coefficients are fitted according to the quadratic IMME. (Red) squares in the upper figure are the lowest-lying $T = 1$ triplets, whereas (red) squares in the lower figure are the lowest-lying $T = 2$ quintets. (Blue) triangles are $T = 3/2$ quartets. The solid (blue) line is $c = 643.852A^{-1/3} + 5.097$, which is an unweighted fit to the quintets of $A = 20, 24, 28, 32,$ and 36. The dashed lines in the upper and the lower figures are $c = \frac{3e^2}{5r_0}A^{-\frac{1}{3}}$.

The sd-shell space quintet's c coefficients exhibit a more pronounced linear proportional relation to $A^{-1/3}$ than A, c.f. Fig. 3.4 and Fig. 3.5. It is because they are more aligned to the fitted line, $c = 643.9A^{-1/3} + 5.097$ in Fig. 3.5, and this fitted line is close to the dashed line, which is the expression of c in Eq.(3.11). Overall, this crude estimation fairly predicts the trend of c coefficients of the lowest-lying triplets and quintets.

The updated experimental data shows that the plot of $A = 8$ triplet in Fig. 3.4 and Fig. 3.5 is different from Fig. 3 in Ref. [107]. This anomaly of the $A = 8$ triplet in our plots is due to strong isospin mixing of $T = 0$ and $T = 1$ states in ^{8}Be.

3.3   Tabulation of the IMME Coefficients

All IMME coefficients are tabulated in Appendix A. Table A.2 lists the a and b coefficients for all $T = 1/2$ doublets in p, sd, and pf shells. There is no c coefficient for a doublet. Table A.3 presents the b and c coefficients for $T = 1$ triplets. The IMME least-squares fit indicates that the a coefficient is equal to the mass excess of the $T_z = 0$ nucleus, hence a coefficients are listed in column seven.

Table A.4 shows the a, b, and c coefficients deduced from the quadratic IMME fit to $T = 3/2$ quartets. A non-zero d coefficient plays a key role to indicate an IMME beyond the quadratic form, they are listed as well in the last column. If first-order perturbation theory is insufficient to account for the charge dependence of the interaction or if isospin mixing of nearby states causes the isospin impurity of quartets and quintets, a non-zero d of $\approx$1 keV [111] would be a signature. For instance, the lowest-lying d coefficient for the $A = 32$ quintet is 0.89 ± 0.22 keV. All masses of this $A = 32$ quintet were measured with high precision [112]. However, most of the d coefficients of quartets are larger than 1 keV (from ~2 keV to ~100 keV), c.f. Fig. 3.6. These values are one to two orders higher than the theoretical prediction. More precise measurements of the mass excess and of excited levels may be required to verify these high d coefficients.

Table A.5 lists the fitted IMME coefficients for experimentally available $T = 2$ quintets. The table include results of IMME fits where cubic and/or quartic terms are considered. From the normalized χ^2 value of quadratic IMME fit for $A = 8$ (quintet), there is a strong indication for the need of the cubic term. This quintet has the smallest A of all known quintets, but it has the highest d value. It may be due to non-perturbative effect which is caused by the less tightly bound nature and small Coulomb barriers of those states [113].
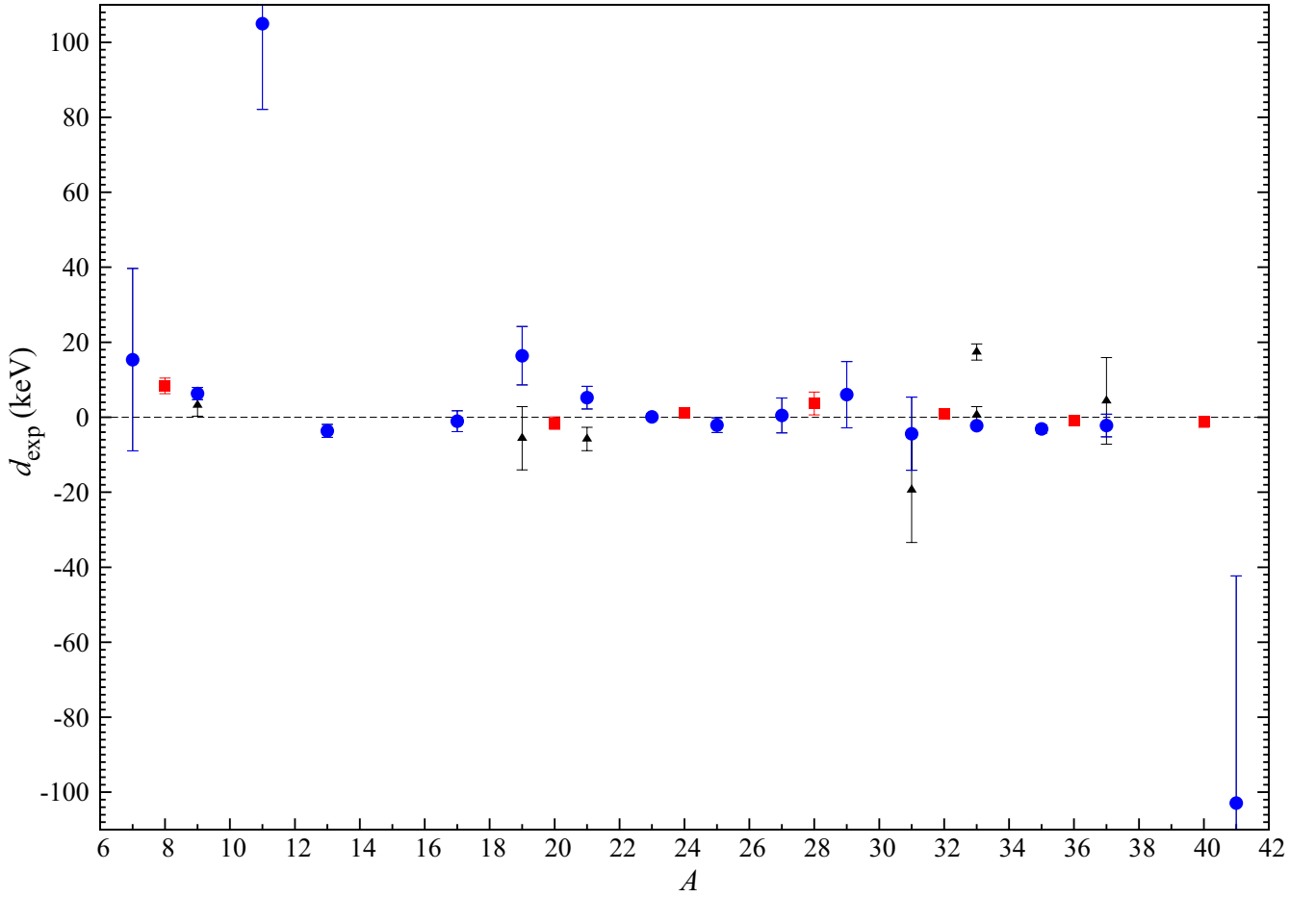
Figure 3.6: *The d coefficients as a function of A for all quartets and quintets.*
These d coefficients are fitted according to the cubic IMME. (Blue) circles and (red) squares are d coefficients of the lowest-lying quartets and quintets, respectively; whereas (blue) triangles are d of higher-lying quartets, c.f. Table A.4 and A.5 in Appendix A.

"To see a world in a grain of sand,
And a heaven in a wild flower,
Hold infinity in the palm of your hand,
And eternity in an hour."
《Auguries of Innocence》
William Blake (1757-1827).

Results

Chapter 4

Fit of INC Hamiltonian to Experimental b and c Coefficients

Contents

In this chapter we present the results of the fit of the theoretical b and c coefficients of the IMME to the experimentally deduced b and c coefficients for sd-shell nuclei, which allowed us to find the best set of the parameters Eq.(2.67) of the charge-dependent part of the shell-model Hamiltonian. We found that the parameters are quite sensitive to the isospin-invariant interaction, to the composition of the charge-dependent Hamiltonian and to the approach of SRC's, as well as to the number of data points selected.

In the first section we describe the fitting procedure and the experimental data selection. In the second section we discuss the results of the fit (the values of parameters) and explore their physical meaning.

4.1 Fitting procedure

We have followed the fitting strategy proposed in Ref. [30]. First, we construct theoretical b and c coefficients described in Eq.(2.69) by using properly obtained INC Hamiltonian, as described in the previous section (using experimentally based $\hbar\omega$ and accounting for the SRC by one of the approaches mentioned in chapter 2). Then, we separately fit theoretical b and c coefficients to newly compiled experimental b and c coefficients to get the most optimal values of $\lambda_\nu^{(1)}$ and $\lambda_\nu^{(2)}$, respectively. The isovector and isotensor Coulomb strengths obtained in both fits are averaged $(\overline{\lambda}_{coul} = (\lambda_{coul}^{(1)} + \lambda_{coul}^{(2)})/2)$ and are kept constant. We assume here that the isovector and isotensor Coulomb strengths are equal. Then the rest of the strength parameters are refitted with this fixed Coulomb strength.

In order to verify our method, we performed a direct comparison with the results of Ref. [30]. We have followed their setting exactly by adopting the experimental values from Table 5[1] of Ref. [30], the parameterization of the $\hbar\omega$ and the scaling factors (see Eqs. (3.5) –(3.7) of Ref. [30]) for TBME's of V and ISPE's, as well as the Jastrow-type function to account for the SRC effects of Miller and Spencer [98][2]. In Ref. [30], selected experimental data only consisted of the bottom $(A = 18 - 22)$ and the top $(A = 34 - 39)$ of sd-shell space and included 42 experimental b coefficients and 26 experimental c coefficients. We have also imposed certain truncations on calculations for $A = 22$ and $A = 34$, as was done in that work [30]. In this way, we have successfully reproduced the strength parameters given in TABLE 2 of Ref. [30].

For curiosity, besides the USD interaction, we have also tested USDA and USDB [49], keeping the setting of Ormand and Brown, but skipping their truncations for masses 22 and 34. The newly found strength parameters are summarized in Table 4.1. The uncertainties on the strength parameters have been deduced from Eq.(3.8). They are significantly smaller than the values published in Ref. [30] due to the fact that the authors used some folding with the rms deviation [114]. It is remarkable that there is not much difference between different nuclear interactions for the small data set and all strength parameters are in agreement with the range of values found by Ormand and Brown (uncertainties included).

4.1.1 Experimental data base of b and c coefficients

In the present study an extended and updated experimental data base is used where all the latest relevant experimental mass measurements and excited states have been taken into account in the fit. As we aim to have a global parameterization, we include all the newly compiled lowest-lying IMME multiplets and all available isobaric doublets $(T = 1/2)$, triplets $(T = 1)$, quartets $(T = 3/2)$ and quintets $(T = 2)$ for masses between $A = 18$ and $A = 39$, which are well described by the sd-shell model, c.f. chapter 3 and Appendix A.

---

[1] In Table 5 of Ref. [30], the experimental values of the b coefficients for $A = 18$ $(2^+, T = 1)$ and $A = 20$ $(3^+, T = 1)$ should be 3.785 MeV and 4.197 MeV, respectively. [2] In Ref. [30], however, a $[1 + f(r)]$ factor required in Eq.(2.81) was used without being squared.

Table 4.1: *Fitted strength parameters[a] to experimental values used in* Ref. [30].

	USD	USDA	USDB
rms (keV): b coefficients	23.3	30.0	27.3
rms (keV): c coefficients	6.9	8.9	8.9
$\overline{\lambda}_{coul}$	1.0109 (1)	1.0234 (2)	1.0210 (2)
$\lambda_0^{(1)} \times 100$	-1.5336 (60)	-1.3311 (64)	-1.5193 (64)
$\lambda_0^{(2)} \times 100$	-4.5291 (162)	-5.0809 (171)	-4.8639 (167)
$\varepsilon_{0d5/2}^{(1)}$	3.4028 (2)	3.4014 (2)	3.3983 (2)
$\varepsilon_{0d3/2}^{(1)}$	3.3118 (6)	3.2668 (6)	3.2736 (6)
$\varepsilon_{0s1/2}^{(1)}$	3.2622 (5)	3.2751 (5)	3.2703 (5)

[a] All strength parameters are given in the unit of MeV.

4.1.2 Selected Data Range for b and c coefficients

In this work we have used three different ranges of data in a full sd-shell model space.

- *Range I.* It includes all ground states (g.s.) and a few low-lying excited states throughout the sd-shell (note that the middle of sd-shell was not considered in Ref. [30]). This range consists of 81 b coefficients and 51 c coefficients. Only excited states with the discrepancy between the energy calculated by the isospin-symmetry invariant Hamiltonians (USD, USDA, and USDB) and experimental excitation energy below ~200 keV are included.

- *Range II.* It represents an extension of *Range I*, which includes more excited states. It contains 26 more $T = 1/2$ doublets, an additional triplet and an additional quartet of states resulting in 107 b coefficients and 53 c coefficients.

- *Range III.* The widest range, which tops up *Range II* with 32 more excited states from 25 doublets, 6 triplets, and an additional quartet, resulting altogether in 139 b coefficients and 60 c coefficients.

These three ranges of selected experimental data points are the same for each fit with either USD, or USDA, or USDB interactions. They are presented and discussed in the section below.

4.2 Results of the Fit of INC Hamiltonian to Experimental b and c Coefficients

All calculations have been performed in a full (untruncated and from $A = 18$ to $A = 39$) sd shell. The TBME's of schematic interactions (Coulomb and meson exchange) have been evaluated for $A = 39$ and scaled using experimentally obtained $\hbar\omega$. The fit procedure is stated in section 4.1.

4.2.1 INC Hamiltonian and Coulomb strength

We have tested five different combinations of INC forces: (i) V_{coul}, (ii) V_{coul} and V_π, (iii) V_{coul} and V_ρ, (iv) V_{coul} and V_0. The main criterium for the choice of the best Hamiltonian structure was the value of the rms and the value of the Coulomb strength. It turned out that almost all combinations gave similar rms values (within 2 keV). However, on the basis of the Coulomb strength parameter we could make a selection. We suppose here that the Coulomb strength should be close to unity. Indeed, higher-order Coulomb effects which are not taken into account here may be responsible for some deviations of the Coulomb strength from unity. However, we suppose that this may be within 1-2% and any stronger renormalization (5% or more) should be avoided.

The Coulomb strengths from various combinations of the INC Hamiltonians are summarized in Fig. 4.1, Fig. 4.2, and Fig. 4.3. The calculations correspond to the USD, USDA, and USDB interactions, respectively, and a fit to the data from *Range I*, *Range II*, and *Range III*, while all approaches to the SRC were taken into account. The figures show that USD, USDA, and USDB, with three data selections, produce similar trends and results.

First, using the Coulomb interaction as only source of the isospin-symmetry breaking force produces a reasonable value of the isovector strength (around 1.00), but the isotensor strength largerly deviates from unity (up to 1.19). This is the manifestation of the so-called Nolen-Schiffer anomaly first evidenced in $T = 1/2$ mirror energy shifts [109], and later also found in $T = 1$ displacement energies (c.f. Ref. [115] and references therein). We find that the Coulomb potential alone satisfactorily describes the mirror energy differences, possibly due to the fact that the Coulomb effects of the core are taken into account through empirical ISPE's (established by the fit as well). However, the Coulomb force alone does not reproduce experimental isotensor shifts. The average Coulomb strength, $\overline{\lambda}_{coul}$ is therefore larger than unity (around 1.10) and results in an rms deviation for b coefficients of between $65 - 85$ keV (after averaging $\lambda_{coul}^{(1)}$ and $\lambda_{coul}^{(2)}$) and an rms deviation for c coefficients of around 22 keV, c.f. Table 4.2. Since the sd-shell model wave functions include configuration mixing fully within $0\hbar\omega$ model space, this may be evidence of the necessity for the charge-dependent forces of nuclear origin.

Table 4.2: *Fitted strength parameters[a] for Coulomb as an only source of the ISB force.*

	without SRC	Miller-Spencer	USD CD-Bonn	Argonne V18	UCOM
rms (keV): b coefficients[b]	64.9	85.5	64.8	70.6	72.6
rms (keV): c coefficients	19.8	26.1	19.7	21.4	22.2
$\overline{\lambda}_{coul}$	1.077	1.116	1.070	1.082	1.095
$\varepsilon_{0d5/2}^{(1)}$	3.228	3.208	3.228	3.223	3.221
$\varepsilon_{0d3/2}^{(1)}$	3.047	2.941	3.044	3.014	3.008
$\varepsilon_{0s1/2}^{(1)}$	3.281	3.279	3.281	3.281	3.280

[a] All strength parameters are presented in 4 significant figures and in the unit of MeV.

[b] Before averaging $\lambda_{coul}^{(1)}$ and $\lambda_{coul}^{(1)}$, the rms deviations for b coefficients are around 36 keV.
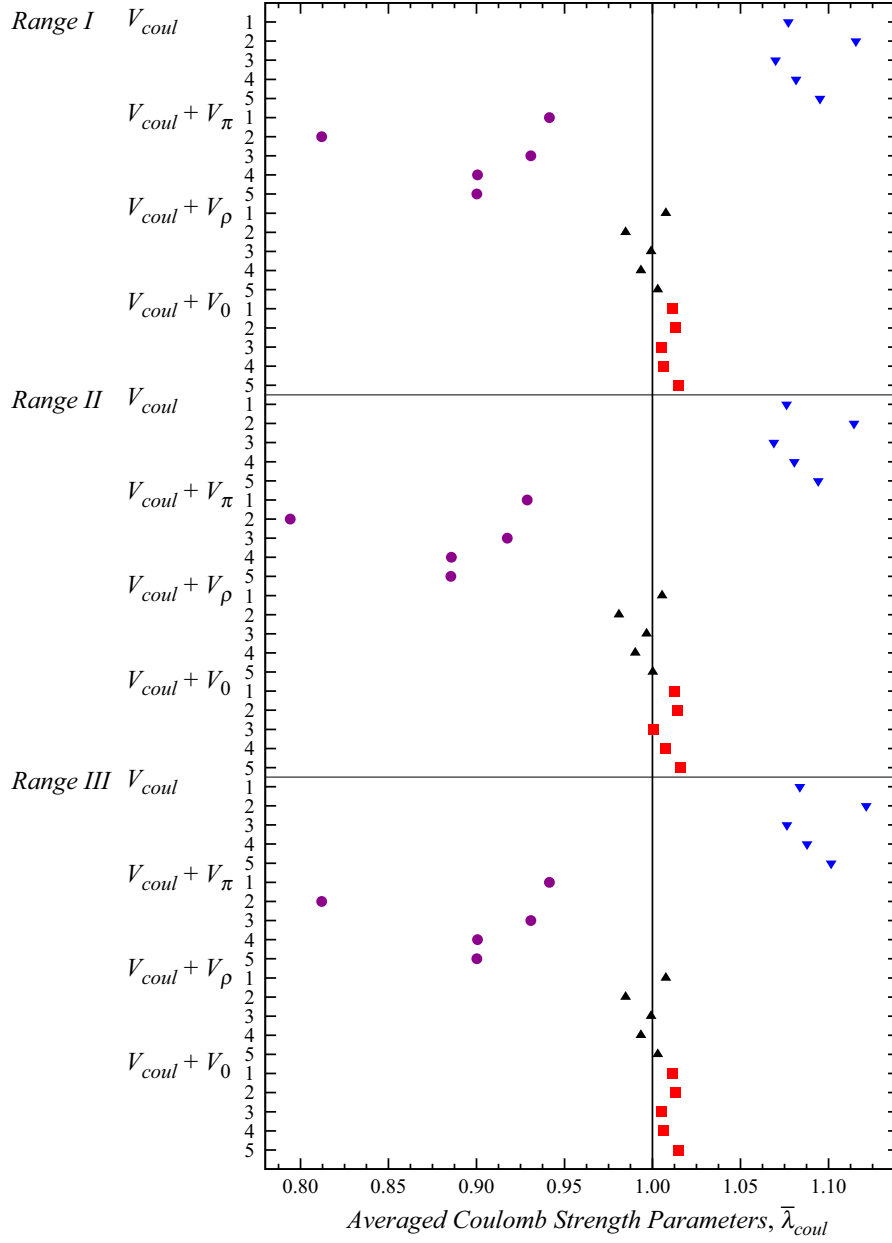
Figure 4.1: *Average Coulomb strength parameter, $\overline{\lambda}_{coul}$, obtained from the fit with the USD interaction to the Range I, Range II, and Range III data.*

(i) The $\overline{\lambda}_{coul}$ of the fit with V_{coul} alone are represented by down (blue) triangles.

(ii) The $\overline{\lambda}_{coul}$ obtained from the fit with V_{coul} and V_{π} combination are depicted by (purple) circles.

(iii) The $\overline{\lambda}_{coul}$ fitted from V_{coul} and V_{ρ} combination are shown by up (black) triangles.

(iv) The $\overline{\lambda}_{coul}$ of the fit with V_{coul} and V_0 combination are displayed as (red) squares.

The y-axis tic labels: 1, "without SRC"; 2, Miller-Spencer; 3, CD-Bonn; 4, AV-18; 5, UCOM.

Please see section 4.1.2 for the description of data range.
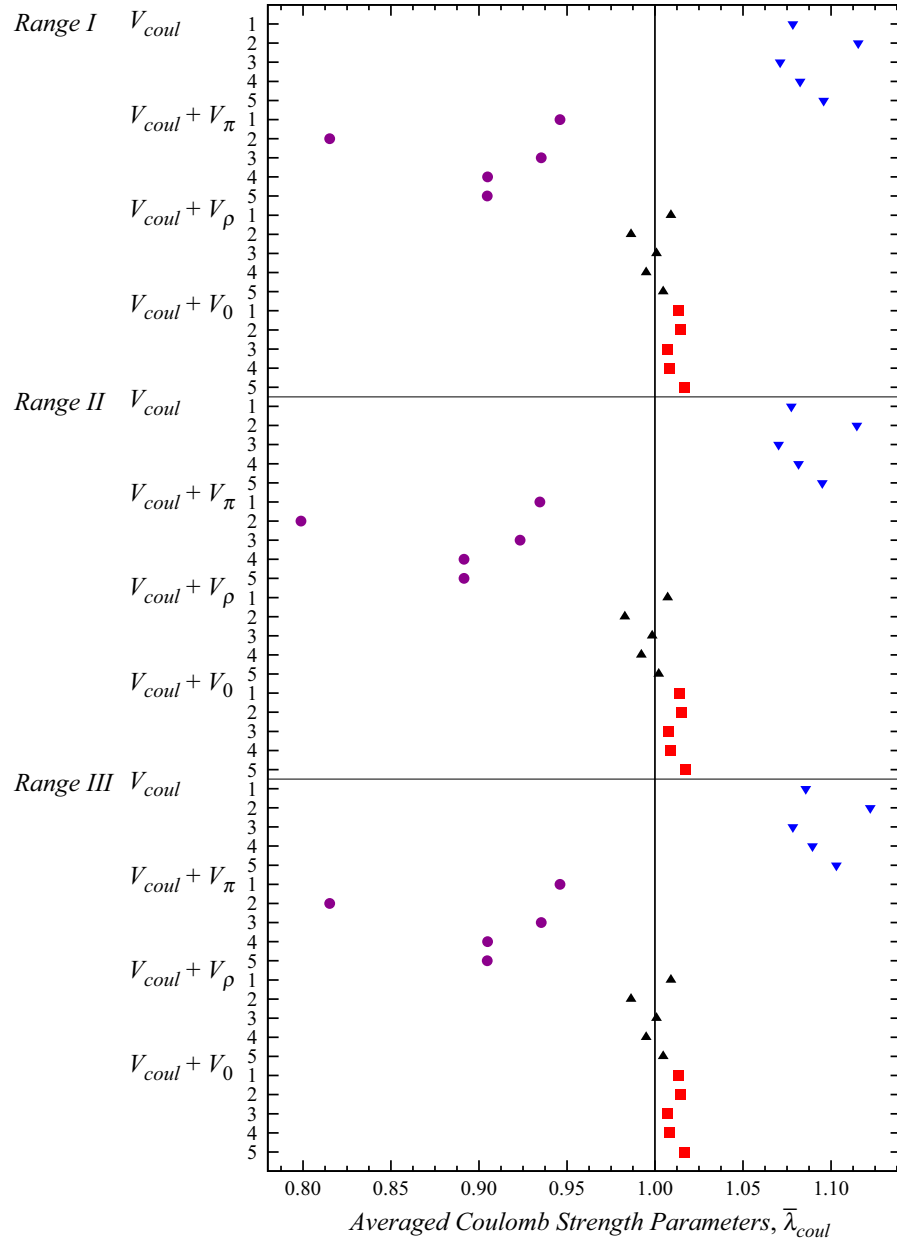
Figure 4.2: *Average Coulomb strength parameter, $\overline{\lambda}_{coul}$, obtained from the fit with the USDA interaction to the Range I, Range II, and Range III data.*

Please refer to Fig. 4.1 for further descriptions.
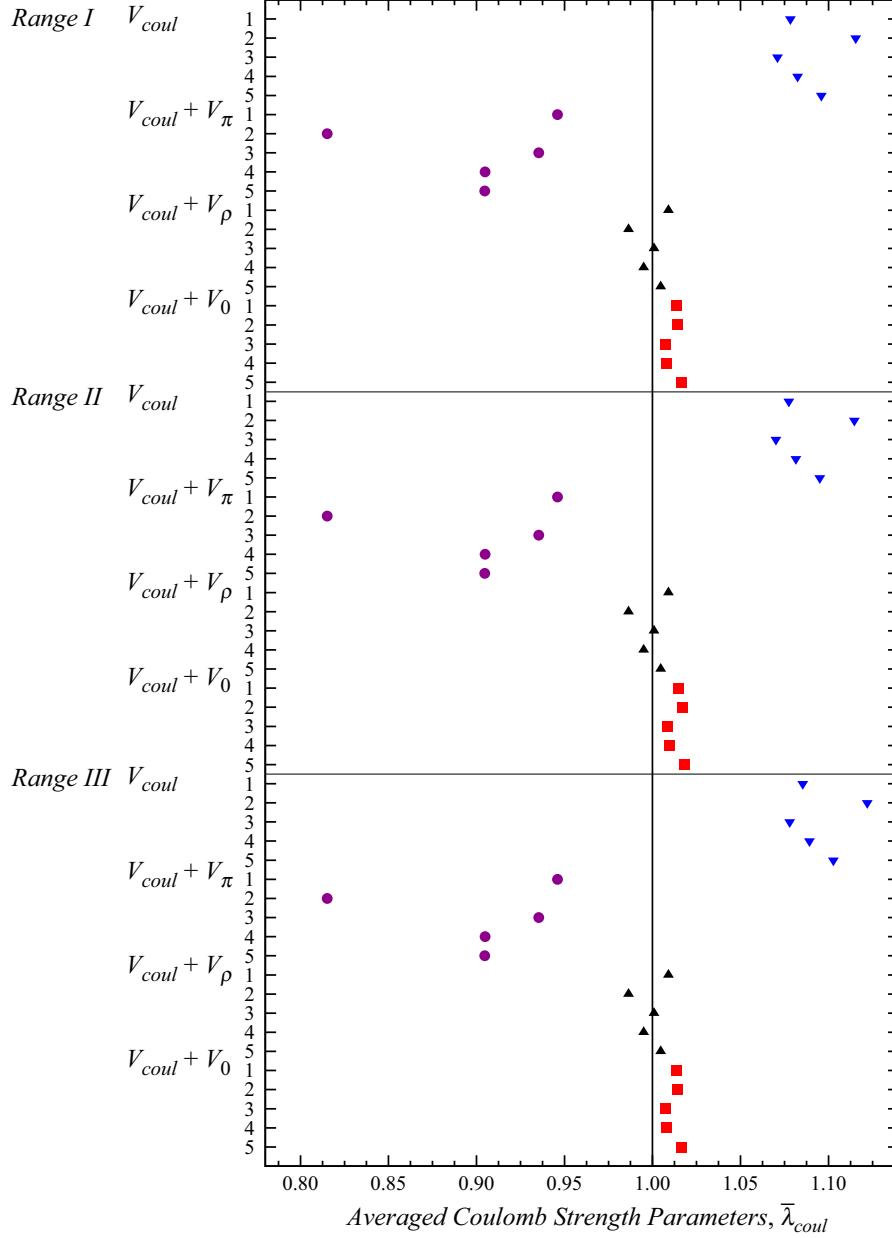
Figure 4.3: *Average Coulomb strength parameter, $\overline{\lambda}_{coul}$, obtained from the fit with the USDB interaction to the Range I, Range II, and Range III data.*
Please refer to Fig. 4.1 for further descriptions.

Next, it turns out that the Coulomb interaction combined with the pion-exchange potential V_π also requires a strong renormalization of the Coulomb strength. This was noticed already by Ormand and Brown in Ref. [30]. The Coulomb strength reduces to about 0.8 for Miller-Spencer parametrization of the Jastrow function and to around $0.9 - 0.95$ for other SRC approaches. Due to these reasons, we do not use pion exchange as an INC nuclear force model in this work.

A better fit is provided by the exchange of a more massive meson, e.g. ρ-meson. Following theoretical studies [116, 117, 118], we use in the present work an 85% reduction in the mass of ρ-meson. A better agreement with the exchange of a meson heavier than the pion meson may

signify a shorter range of a charge-dependent force of nuclear origin.

We confirm also the conclusion of Ref. [30] that a combination of the pion and ρ-meson exchange potential to model nuclear charge-dependent forces does not allow one to improve the value of the rms deviation. This is why we present here strength parameters only for two combinations of the ISB forces from the list above, namely, (iii) V_{coul} and V_ρ and (iv) V_{coul} and V_0. The resulting rms deviations based on these two combinations and the corresponding Coulomb strengths are indeed rather close, in agreement with the conclusion of Ref. [30]. We discuss both cases in the next section.

4.2.2   Root Mean Square Deviation Values and Strength Parameters

Table 4.3 gives an overview of strength parameters for two types of INC Hamiltonian: (iii) V_{coul} and V_ρ (columns 3,5,7) and (iv) V_{coul} and V_0 (columns 2,4,6). Calculations have been performed for the USD, USDA, and USDB nuclear Hamiltonians and for each of the three data ranges. All four approaches to SRC (Jastrow type function with three different parametrizations or UCOM) from section 2.5.1 have been tested and the intervals of parameter variations are indicated in the table.

As seen from Table 4.3, the rms deviation changes little for various types of the SRC (within 1 keV) and for both INC Hamiltonians.

The rms deviation turns out to depend mainly on the number of data point used in a fit. It is remarkable that although *Range I* contains almost twice the number of data points of Ref. [30], the rms deviation increases only by ~ 5 keV. Overall, the rms deviation of *Range II* is ~30% higher compared to *Range I*, while the rms deviation value for *Range III* is about twice as large as that of *Range I*. It should also be remembered that low-lying states calculated with the isospin-conserving USD/USDA/USDB interactions are in general in better agreement with experiment than high-lying states.

We notice that the USD interaction always produces slightly lower rms deviations than USDB and USDA. This happens even in the fits to *Range III* data, although the USD was adjusted to a smaller set of excited levels as compared to the later versions USDA and USDB.

Variations in the values of the parameters indicated in each entry of the table are due to the different SRC approaches. In general, a narrower range of values of a parameter corresponds to a higher strength of this parameter. The most crucial role is played by the Coulomb potential as it is the major contribution to isobaric mass splittings. The Coulomb strength can be slightly greater or less than unity for different combinations of ISB forces.

To reduce the discrepancy of the Coulomb strength from unity, the strengths of the charge-dependent forces of nuclear origin, $\lambda^{(q)}_{\nu \neq coul}$, are adjusted in the fit to patch up their contributions to theoretical isobaric mass splittings led to match with experimental isobaric mass splittings.

We keep the isovector and isotensor strengths of the charge-dependent forces of nuclear origin as two independent parameters.

V_{coul} and V_0 combination. These combinations almost always produce the lowest rms deviations for b and c coefficients. Fitted to the smallest range of data, the isovector and isotensor strengths of the nuclear isospin-violating contribution represent about 0.7–1.7% and 2.9 – 4.2%, respectively, of the original isospin-conserving sd interaction. We notice that the charge-asymmetric part of the interaction increases in a fit to the *Range III* data, amounting to 2.3–3.2% of the nuclear interaction.

The Miller-Spencer parameterization and UCOM SRC schemes quench the Coulomb expectation values more than the AV-18 and CD-Bonn parameterizations (see Table 2.2 as an example). This is why the highest values of $\overline{\lambda}_{coul}$ in columns 2, 4, and 6 belong to UCOM SRC and $\overline{\lambda}_{coul}$ of Miller-Spencer parameterization SRC are very close to them. At the same time, those parameterizations result in the most negative values of $\lambda_0^{(q)}$ in columns 2, 4, and 6 to compensate for the Coulomb effect.

V_{coul} and V_ρ combination. For the combination of the Coulomb and Yukawa ρ-exchange type potentials as the isospin-symmetry breaking forces, it should be noted that typical expectation values of V_ρ are about 3 to 4 orders of magnitude smaller than the expectation values of V_{coul}. Therefore, small variations in the Coulomb strength (of the order of 1-2%) require a factor of up to 20 variation in the corresponding strength $\lambda_\rho^{(q)}$ (e.g., ranging from 5 to 102 MeV for an isovector ρ-exchange strength with USD interaction in *Range I* of the data selection). So, the ρ-exchange potential strength is very sensitive to the SRC procedure. The lowest $\overline{\lambda}_{coul}$ and, therefore, the highest absolute $\lambda_\rho^{(q)}$ in columns 3, 5, and 7 belong to the Miller-Spencer parameterization SRC. The lowest absolute $\lambda_\rho^{(q)}$ in *Range III* are from SRC with the CD-Bonn parameterization. The highest values of the $\overline{\lambda}_{coul}$ and, thus, closest to unity, are for the CD-Bonn and UCOM SRC schemes for the three ranges of data (see also Fig. 4.1).

We also notice an increase of the isovector parameter $\lambda_\rho^{(1)}$ in a fit to the *Range III* data.

Regarding the ISPE's, their values stay consistent within certain intervals. Amazingly, the value of $\varepsilon_{0d5/2}^{(1)}$ stays almost constant, without showing any dependence on the particular SRC approach, because most probably, it is the orbital which is most constrained by the data. At the same time, the value of $\varepsilon_{0d3/2}^{(1)}$ depends somewhat on the SRC procedure. The highest value in column 2 always corresponds to the Miller-Spencer parameterization. The value of $\varepsilon_{0d3/2}^{(1)}$ stays constant for the V_{coul} and V_ρ combination, but changes slightly for the V_{coul} and V_0 combination. As a general trend we notice a reduction of the values of ISPE's when we increase a number of data points in a fit.

The values of parameters given in Table 4.3 lie outside the intervals obtained by Ormand and Brown who considered the V_{coul} and V_0 combination. In particular, we get systematically

lower values of the isotensor strength parameter $\lambda_0^{(2)}$, as well as a lower values of $\varepsilon_{0d5/2}^{(1)}$, even for the *Range I* of data. The inclusion of nuclei from the middle of the *sd*-shell space, combined with the latest experimental data and with the newly developed approaches to SRC allowed us to construct a set of high-precision isospin-violating Hamiltonians in the full *sd*-shell model space. The applications of this result will be discussed in the next chapters.

Table 4.3: *Various combinations of INC potential and their strength parameters[a].*

Data Range	USD		USDA		USDB	
	V_{coul} V_0	V_{coul} V_ρ	V_{coul} V_0	V_{coul} V_ρ	V_{coul} V_0	V_{coul} V_ρ
Range I[b]						
rms (keV): b coefficients	∼34.4	∼35.3	∼37.5	∼37.2	∼36.5	∼36.5
rms (keV): c coefficients	∼9.0	∼10.5	∼10.2	∼10.8	∼9.6	∼10.6
$\overline{\lambda}_{coul}$	1.005 - 1.015	0.9847 - 1.003	1.007 - 1.016	0.9864 - 1.005	1.008 - 1.017	0.9855 - 1.003
$\lambda_0^{(1)} \times 100$	-1.520 - -0.7174	—	-1.691 - -0.7714	—	-1.743 - -0.8625	—
$\lambda_0^{(2)} \times 100$	-3.871 - -2.631	—	-4.225 - -2.904	—	-4.126 - -2.847	—
$-\lambda_\rho^{(1)}$	—	7.536 - 102.1	—	1.258 - 81.81	—	3.546 - 90.25
$\lambda_\rho^{(2)}$	—	48.26 - 209.2	—	50.79 - 216.3	—	50.88 - 216.2
$\varepsilon_{0d5/2}^{(1)}$	3.277 - 3.278	3.288 - 3.290	3.269 - 3.272	3.290 - 3.293	3.264 - 3.269	3.287 - 3.290
$\varepsilon_{0d3/2}^{(1)}$	3.279 - 3.304	3.287 - 3.295	3.271 - 3.298	3.293 - 3.308	3.265 - 3.288	3.289 - 3.300
$\varepsilon_{0s1/2}^{(1)}$	3.356 - 3.377	3.369 - 3.372	3.359 - 3.368	3.386 - 3.395	3.356 - 3.378	3.383 - 3.388
Range II[b]						
rms (keV): b coefficients	∼45.3	∼46.9	∼47.7	∼48.7	∼46.7	∼48.2
rms (keV): c coefficients	∼9.1	∼10.4	∼10.2	∼10.8	∼9.6	∼10.5
$\overline{\lambda}_{coul}$	1.006 - 1.016	0.9902 - 1.005	1.008 - 1.017	0.9829 - 1.007	1.008 - 1.018	1.006 - 1.016
$\lambda_0^{(1)} \times 100$	-1.496 - -1.175	—	-2.083 - -1.158	—	-2.209 - -1.325	—
$\lambda_0^{(2)} \times 100$	-3.856 - -2.617	—	-4.220 - -2.900	—	-4.118 - -2.839	—
$-\lambda_\rho^{(1)}$	—	11.51 - 123.8	—	7.290 - 103.3	—	9.326 - 113.5
$\lambda_\rho^{(2)}$	—	33.70 - 212.2	—	35.38 - 219.0	—	35.58 - 219.3
$\varepsilon_{0d5/2}^{(1)}$	3.269 - 3.270	3.284 - 3.287	3.263 - 3.267	3.286 - 3.291	3.257 - 3.261	3.284 - 3.287
$\varepsilon_{0d3/2}^{(1)}$	3.278 - 3.301	3.278 - 3.286	3.273 - 3.300	3.286 - 3.300	3.266 - 3.288	3.280 - 3.290
$\varepsilon_{0s1/2}^{(1)}$	3.317 - 3.339	3.325 - 3.330	3.324 - 3.347	3.341 - 3.353	3.320 - 3.342	3.337 - 3.346
Range III[b]						
rms (keV): b coefficients	∼65.5	∼66.5	∼68.1	∼68.5	∼66.4	∼67.4
rms (keV): c coefficients	∼10.0	∼10.4	∼11.1	∼10.7	∼10.4	∼10.4
$\overline{\lambda}_{coul}$	1.015 - 1.025	0.9734 - 1.004	1.018 - 1.027	0.9772 - 1.008	1.018 - 1.028	0.9743 - 1.005
$\lambda_0^{(1)} \times 100$	-3.215 - -2.359	—	-3.515 - -2.540	—	-3.595 - -2.669	—
$\lambda_0^{(2)} \times 100$	-3.658 - -2.409	—	-4.014 - -2.684	—	-3.922 - -2.633	—
$-\lambda_\rho^{(1)}$	—	40.57 - 240.4	—	35.51 - 219.7	—	38.71 - 231.4
$\lambda_\rho^{(2)}$	—	33.52 - 215.6	—	34.98 - 211.7	—	35.44 - 223.0
$\varepsilon_{0d5/2}^{(1)}$	3.239 - 3.240	3.247 - 3.248	3.228 - 3.232	3.252	3.224 - 3.229	3.250
$\varepsilon_{0d3/2}^{(1)}$	3.232 - 3.257	3.161 - 3.178	3.228 - 3.255	3.174 - 3.185	3.221 - 3.245	3.167 - 3.179
$\varepsilon_{0s1/2}^{(1)}$	3.200 - 3.219	3.160	3.195 - 3.216	3.164 - 3.167	3.201 - 3.222	3.165 - 3.168

[a] All strength parameters are given in the unit of MeV.
[b] Please see section 4.1.2 for the data range.

4.3   Remarks

The rms deviations of the fit of V_{coul} alone without any other charge-dependent force, as well as the respective V_{coul} strengths (c.f. Table 4.2 and Table 4.3), show that V_{coul} should be coupled with another charge-dependent force in order to decrease rms deviations and to renormalize V_{coul} strengths near to unity. In addition, the V_{coul} and V_0 combination produces lower rms deviations and the respective V_{coul} strengths are closer to unity compared to other charge-dependent force combinations. In addition, the Yukawa ρ-meson exchange potential, which is used to model the nuclear origin charge-dependent force, produces rms deviations and V_{coul} strengths which are comparable with what had been produced by the V_{coul} and V_0 combination. In the following chapters, we present the applications of the INC Hamiltonian which is based on the V_{coul} and V_0 combination. We compare the effect of various SRC's in applications like isospin-mixing correction to superallowed β decay and isospin-forbidden proton emission discussed in chapter 7 and chapter 8, respectively.

Chapter 5

Staggering Effects in b and c Coefficients

Contents

Nowadays, there is a large amount of experimental data on isobaric doublets, triplets, and quartets in sd-shell nuclei. In addition, all the lowest-lying quintets are experimentally accessible. This amount of data in sd shell is the richest among p-, sd-, and pf-shell nuclei. Therefore, we devote this chapter to discuss b and c coefficients fitted with shell-model INC Hamiltonians and to present the extracted isovector and isotensor Coulomb and charge-dependent nuclear forces' contribution to the staggering effects in isobaric doublets and quartets, as well as triplets and quintets in sd-shell nuclei. These staggering effects are regular oscillatory deviations of the b and c coefficients from the prediction of the uniformly charged sphere model, see Eq.(3.11). A few systematic plots following Jänecke's schematic model [107] reveal these nuclear structure effects. Moreover, we will update the parameters of Jänecke's schematic model. Besides, we revisit Hecht's formalism in elucidating the staggering effects via Wigner's supermultiplet theory [119].
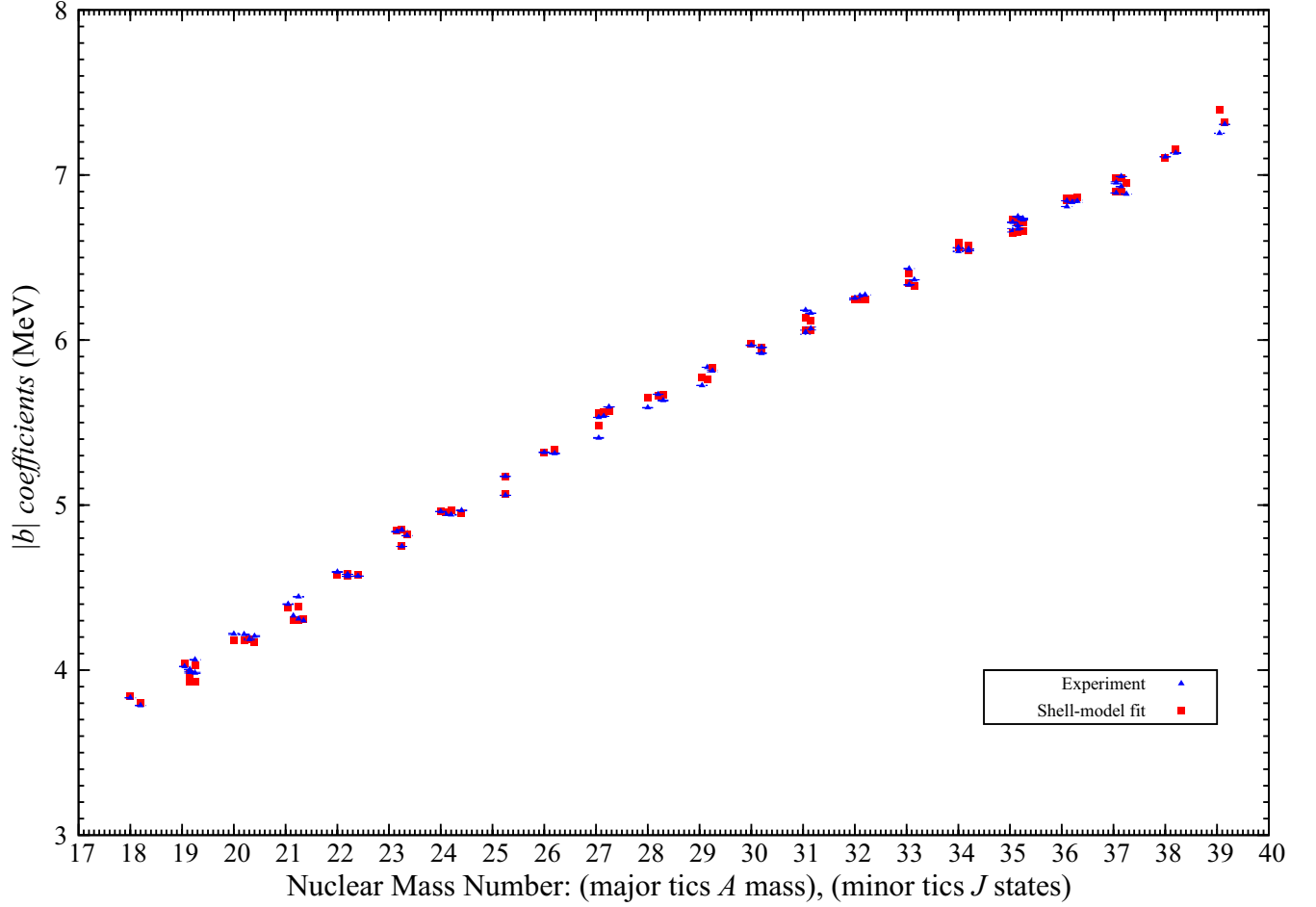
Figure 5.1: *Experimental |b| coefficients compared with their values obtained in a shell-model fit.*
All *b* coefficients are from *Range I* data in *sd*-shell space. Minor *x*-axis tics are *J* states, which are arranged in an increment of 0.05 for every $\frac{1}{2}$ step. The coefficients are plotted in accord with Table B.1, Table B.2, Table B.3 and Table B.4. The *b* coefficients of shell-model fit are produced from V_{coul} and V_0 (USD) combination, and the UCOM SRC scheme.

5.1   Fitted b and c coefficients

5.1.1   Fitted b coefficients

The newly constructed INC Hamiltonians, i.e., the V_{coul} and V_0 combination, and the V_{coul} and V_ρ combination, adjusted with various SRC approaches, reproduce the experimental b and c coefficients with very low rms deviations, c.f. Table 4.3. The ratios of the rms deviations of various SRCs, with USD, USDA, and USDB to the average $|b|$ coefficients in *sd*-shell space are less than ~0.01. Overall, the deviations of b coefficients obtained in a shell-model fit from the experimental ones are less at the top and the bottom of *sd*-shell space than the deviations in the middle shell, c.f. Table B.1, except for the $\frac{1}{2}^+$ of $A = 39$ doublet, c.f. Table B.1. However,

if we refit according to the smaller data range selected in Ref. [30], this deviation reduces from 142 keV to 47 keV. The big deviation may be due to the inclusion of data from the middle shell. On the other hand, if we refit with *Range II* data and with *Range III* data, this deviation reduces to 116 keV and to 49 keV, respectively. It is because the addition of more data points renormalizes the discrepancies of the fit. Although the inclusion of the b coefficient of $\frac{1}{2}^+$ of $A = 39$ doublet reduces the quality of the fit, we retain it in the data set to adjust the ISPEs' strengths, $\varepsilon_i^{(1)}$ in Eq.(2.67).

One of the factors causing the deviation is due to how accurate the USD interaction is capable to reproduce ground states and excited states for each nucleus in sd-shell space, like the low deviations of b coefficients of the doublets of mass $A = 35$, c.f. Table B.1. These low deviations may be related to the ability of the USD interaction to reproduce the low lying excited levels of $A = 35$, $T = 1/2$ with just a few tens keV different from the respective experimental values.

The other reason is due to the characteristic property of the error-weighted least-squares fit, and this reason plays the major role in renormalizing the fit. Experimental b coefficients with very low error bars are well described by shell model fitted b coefficients with very low deviations. This is the reason why most of the lowest-lying multiplets' b coefficients are very close to experimental values. For example, the deviation of the b coefficients of mass $A = 32$ quintet from the experimental value is the lowest among the five quintets. Therefore, advances in mass measurements and nuclear spectra determinations deducing data points with low error bars may influence the data, which are dominant in adjusting the fit of the strengths of charge-dependent forces in INC Hamiltonian; particularly, data from the top and from the bottom of sd-shell space, which are used to calibrate the ISPEs. Similar trends of deviations happen at other combinations of charge-dependent forces, as well as USDA and USDB. For USDA and USDB interactions (with either $V_{coul} + V_0$ or $V_{coul} + V_\rho$, and with different SRC schemes), the deviations are a few keV higher than USD.

In Fig. 5.2, the shell model fitted b coefficients follow the experimental data trend exactly, as well as b coefficients from the uniformly charged sphere model. However, the b coefficients calculated by the uniformly charged sphere model in the lower mass region deviate more than those in the higher mass region. The prediction of uniformly charged sphere model based on $Z(Z-1)$ (c.f. Eq.(3.10)) is about ~300 keV closer to experimental values as compared to the model based on the assumption $Z(Z-1) \approx Z^2$, which gives

$$b = \frac{3e^2}{5r_0} A^{2/3} . \tag{5.1}$$

The ratio $1/Z$ for sd-shell space is in the range from 5.3×10^{-2} ($Z = 19$) to 12.5×10^{-2} ($Z = 8$), that means Z is still comparable with Z^2 for nuclei at the bottom of sd-shell space. This reason causes the latter model produces higher deviation than the first one at the bottom of sd-shell space.

Although it is not seen in the scale of Fig. 5.2, in fact, the b coefficients of sd-shell space exhibit oscillating behavior around the linear line as a function of $A^{2/3}$, which is fitted to the
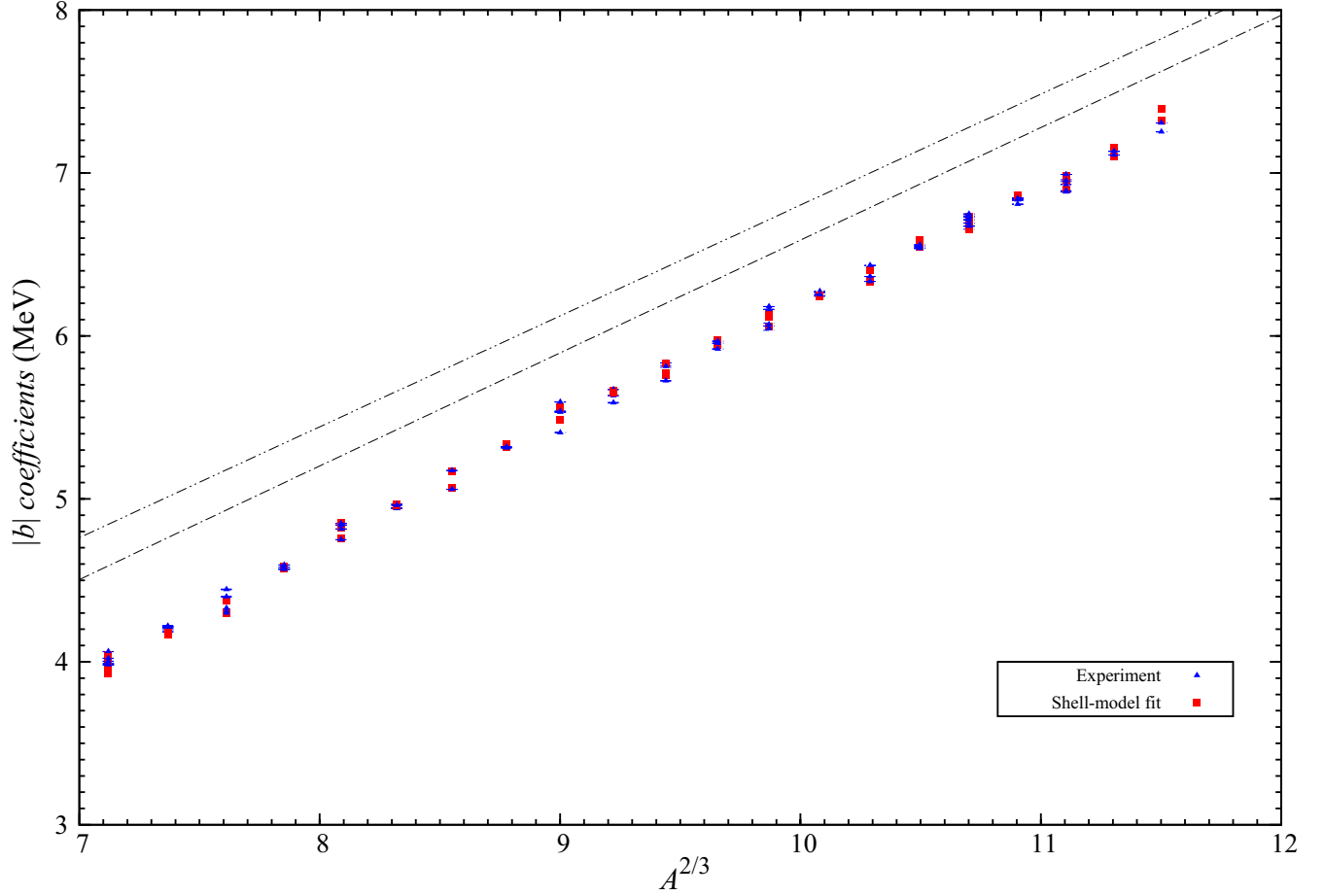
Figure 5.2: *The |b| coefficients in sd-shell space as a function of $A^{2/3}$.*
(Black) dotted-dash line is $b = \frac{3e^2(A-1)}{5r_0 A^{1/3}}$. (Black) double-dotted-dash line is $b = \frac{3e^2}{5r_0} A^{2/3}$. Please refer to Fig. 5.1 for further descriptions.

data points.

5.1.2 Fitted c coefficients

For c coefficients, overall, the rms deviation values are seen to be small, c.f. Table 4.3. It is because the ratio of these rms deviation values to c coefficients are around ~0.045. The deviations at the top and at the bottom of sd-shell space are higher than the deviations in the middle shell, c.f. Fig. 5.3. Possible reasons of such deviation are similar to the factors causing deviations between shell model fitted and experimental b coefficients. Based on the uniformly charged sphere assumption, c.f. Eq.(3.11), we replot c coefficients as a function of $A^{-1/3}$ in Fig. 5.4.

Both plots of c coefficients exhibit oscillatory patterns, c.f. Fig. 5.3, Fig. 5.4. We distinguish four groups of data in this plot.

- The first group consists of the lowest-lying triplets' points connected by the solid line in Fig. 5.4, which produce oscillations with the largest amplitude. These points are always the highest or the lowest c coefficients, except for $A = 20, 24, 28$, and 32, for which their higher-lying levels' c coefficients are smaller than the lowest-lying levels' c values.

- The second group consists of the first higher-lying triplets' c coefficients which have magnitudes different from the lowest-lying triplets' c coefficients about ~2 keV to ~90 keV.

- The third group is formed by all quartets and other higher-lying triplets which are distributed in between the maxima and minima points. The quartets' c coefficients do not display any staggering effect.

- All quintets form the last group. Their c coefficients are also more aligned with the dashed line, $c = \frac{3e^2}{5r_0} A^{-1/3}$, c.f. Eq.(3.11).
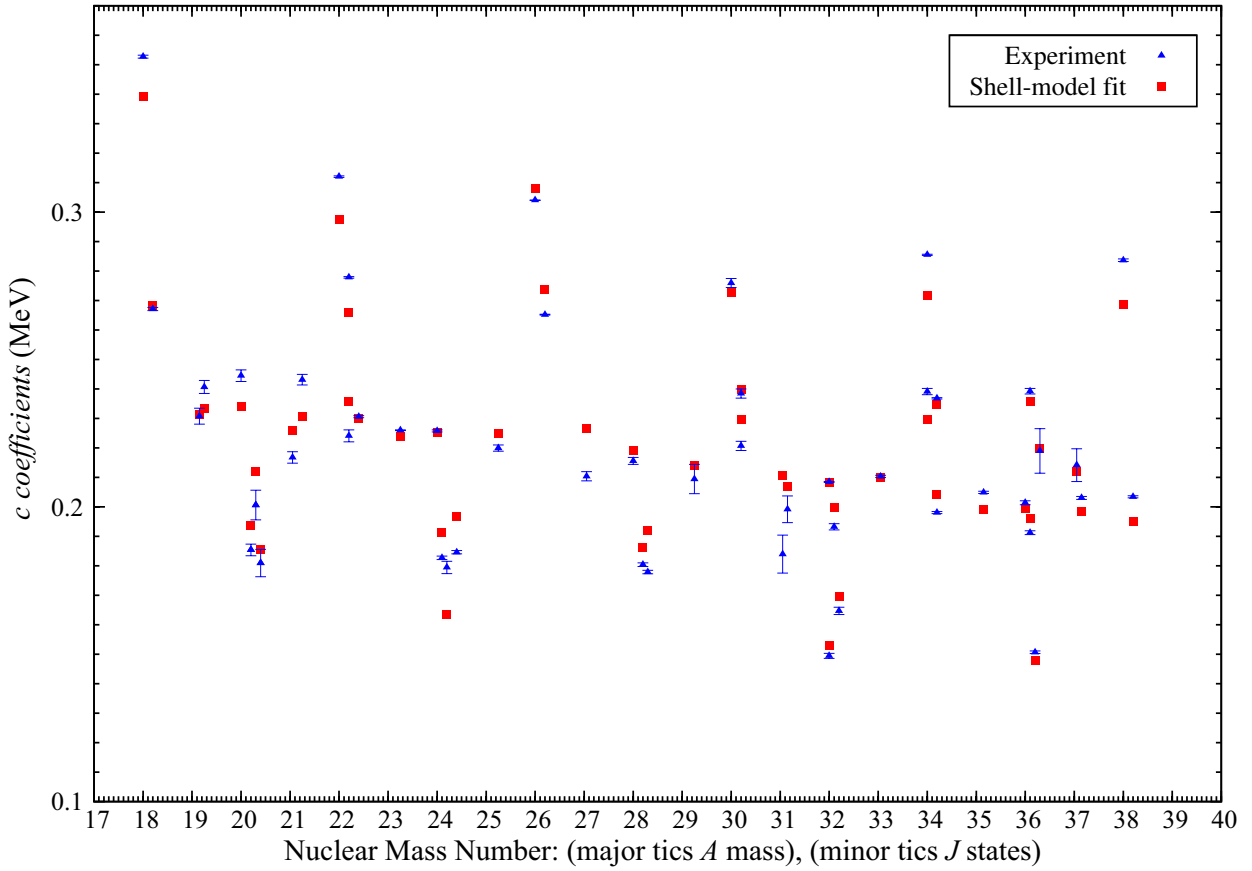
Figure 5.3: *Comparison of experimental and shell-model c coefficients.*
All c coefficients are from *Range I* data of *sd*-shell space. Minor x-axis tics are J states, which are arranged in an increment of 0.05 for every $\frac{1}{2}$ step. The c coefficients are plotted in accord with Table B.2, Table B.3 and Table B.4. The c coefficients obtained in a shell-model fit are produced from V_{coul} and V_0 (USD), and the UCOM SRC scheme.

The lowest-lying and the first higher-lying triplets' c coefficients exhibit pronounced oscillatory behaviors with similar trend, but of different amplitudes, c.f. Fig. 5.4. The uniformly charged sphere model, the black dashed line in Fig. 5.4, which nicely describes the overall trend of c coefficients, can not predict the oscillatory behavior of c coefficients.
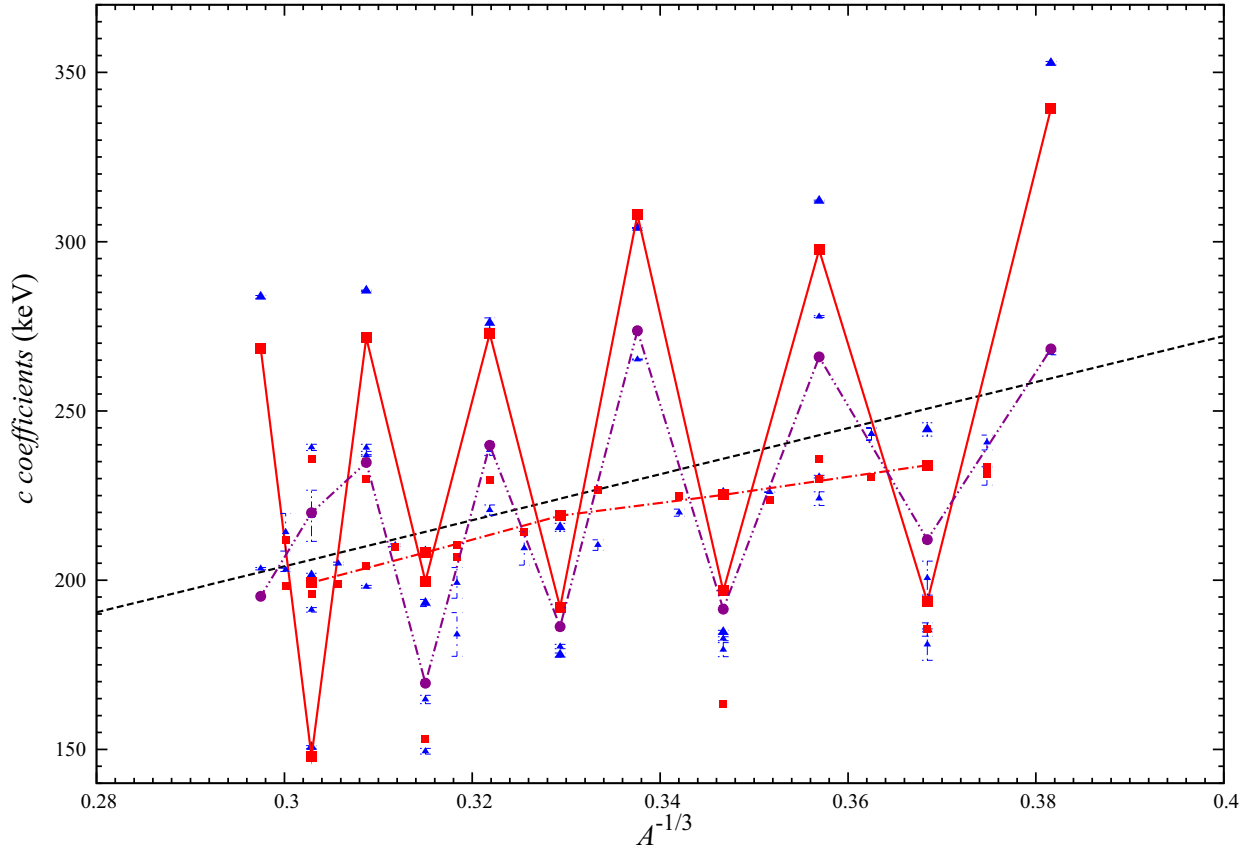
Figure 5.4: *Plot of c coefficients in sd-shell space as a function of $A^{-1/3}$.*
The solid (red) line connects all the lowest-lying triplets' c coefficients fitted by shell model; whereas the (red) dotted-dash line links all quintets' c coefficients fitted by shell model. The (purple) double-dotted-dash line links all (purple) dots which display the first higher-lying triplets' c coefficients fitted by shell model. The (black) dashed line is $c = \frac{3e^2}{5r_0}A^{-1/3}$. Please refer to Fig. 5.3 for further descriptions.

5.2 Staggering Effects of b and c Coefficients

The oscillatory effects in IMME b and c coefficients were noticed by Jänecke in the 1960's, c.f. Refs. [10, 107], and references therein. At that moment, the available experimental data was limited to $T \leq 1$ multiplets, and empirical interactions capable to accurately reproduce low-lying excited levels and transition probabilities, like USD, had not been developed yet. In addition, at that time it was not feasible to perform exact numerical calculation which requires computational power and also sophisticated coding. There were, however, a few analytical models proposed to explain the oscillatory effect. One of them was the Wigner's supermultiplet scheme suggested by Hecht [119]. The other explanation was given by the empirical approach based on a schematic model introduced by Jänecke [10, 107].

As now we have USD (and its variants USDA, and USDB) empirical interactions as input to the shell model, better computational codes, like ANTOINE, to diagonalize all matrices in the *sd*-shell space that were too large in the 1960's, and also updated experimental data, which

fully cover the lowest-lying doublets, triplets, quartets, and quintets, it would be interesting to revisit the staggering effect of the b and c coefficients of sd-shell nuclei with the empirical INC interactions. First, we present our numerical analysis, then we give updated parameters for the schematic model suggested by Jänecke, and finally we compare our results with the Wigner's supermultiplet scheme.

5.2.1 Perspective of Empirical INC Hamiltonians

The b coefficients obtained from experiment and from a shell-model fit for the lowest-lying doublets and quartets in sd-shell nuclei are presented in the main figure (a) in Fig. 5.5. Shell model calculation have been performed with the V_{coul} and V_0 combination. The oscillatory behavior of the b coefficients of doublets and quartets is clearly seen. The data points form two families for $A = 4n + 1$ and $A = 4n + 3$ multiplets. There is no staggering effect in the b coefficients of $T = 1$ triplets, c.f. small figure (d) in Fig. 5.5, and $T = 2$ quintets. These conclusions about the staggering effects in the b coefficients of doublets and quartets, and of triplets agree with what had been noticed by Jänecke [107] and by Hecht [119]. Jänecke's simple model showed that there was no staggering effect for the b coefficients of $T = 1$ triplets [107].

Figure 5.5 shows that the b coefficients obtained in a shell-model fit for doublets and quartets closely follow the experimental trend. The oscillations of doublet b coefficients has a higher amplitude compared to quartets' oscillatory amplitude. These amplitudes are shown in two small figures (b) and (c) in Fig. 5.5 as deviations from the experimental values from a fitted line. The staggering effects of doublets and quartets are in opposite direction. This opposite tendency is naturally manifested in Wigner's supermultiplet theory, which will be discussed in the last section of this chapter.

The charge-dependent term in the Hamiltonian was obtained by fitting combinations of V_{coul} and V_0 (or V_{coul} and V_ρ), and ISPEs ϵ_i. We sum over all contributions in V_{coul}, V_0 or V_{coul}, V_ρ and ISPEs to obtain the b (and c) coefficient of a given multiplet, c.f. Eq.(2.69). Therefore, we can break down various contributions from the components of charge-dependent Hamiltonian accordingly. Contributions of these terms to the b coefficients obtained in a shell-model fit for doublets and quartets are depicted in Fig. 5.6 and Fig. 5.7, respectively. The contribution to the b coefficient from V_0 is amplified by a factor of 20.

The isovector Coulomb force $V_{coul}^{(1)}$ is the main contribution to the staggering effects of the b coefficients of doublets and quartets, c.f. Fig. 5.6. However, ISPEs $\epsilon_i^{(1)}$ do not exhibit any oscillatory behavior. It is interesting to note that the isovector nuclear Hamiltonian $V_0^{(1)}$ follows the same oscillatory trend as $V_{coul}^{(1)}$, but with a smaller amplitude.
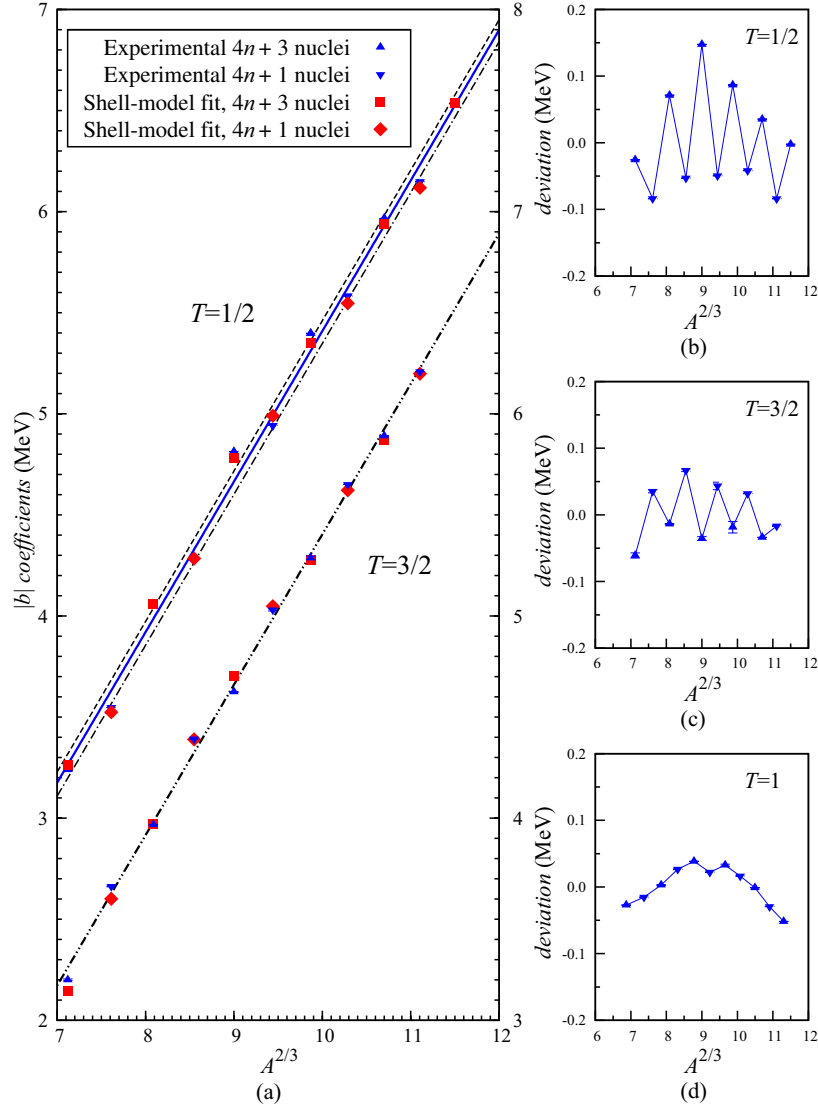
Figure 5.5: *Staggering effect of |b| coefficients of the lowest-lying doublets and quartets in sd-shell nuclei.*
Figure (a): the |b| coefficients of the lowest-lying doublets and quartets. The |b| coefficients obtained in a shell-model fit are produced with V_{coul} and V_0 (USD), and the UCOM SRC scheme. The presented b coefficients are plotted in accord with Table B.1 and Table B.3 – *Range I*. The linearly fitted upper solid (blue) line of $T = 1/2$ is $b = 0.7447A^{2/3} - 1.2552$, the dashed (black) line is $0.7442A^{2/3} - 1.1987$, and the dotted-dash (black) line is $0.7463A^{2/3} - 1.3329$. The linearly fitted lower double-dotted dash (black) line of $T = 3/2$ is $b = 0.7441A^{2/3} - 1.2547$. These linear fits are based on experimental lowest-lying multiplets. The doublet b coefficients are plotted with respect to the left y-axis, while the right y-axis is used for the quartet b coefficients.
Figure (b): the deviations of experimental b coefficients ($T = 1/2$) from the solid (blue) line.
Figure (c): the deviations of experimental b coefficients ($T = 3/2$) from the double-dotted dash (black) line.
Figure (d): the deviations of experimental b coefficients ($T = 1$) from the solid (blue) line.
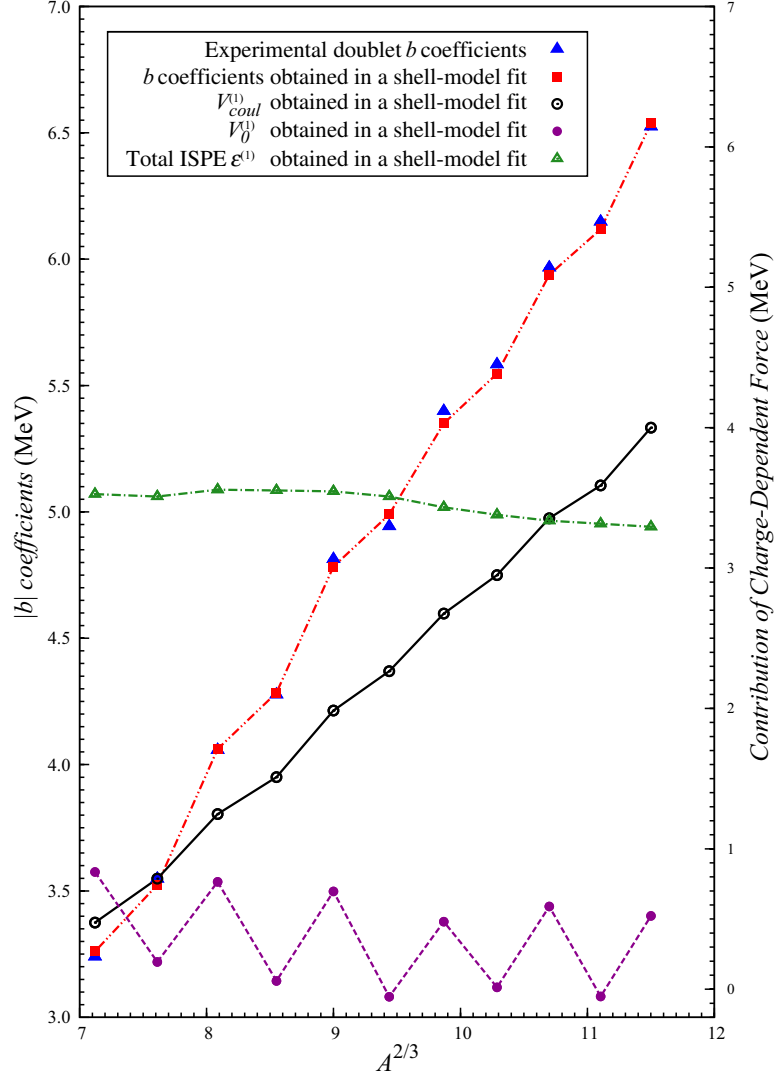
Figure 5.6: *Contributions of the various charge-dependent forces to doublet b coefficients.*
The $|b|$ coefficients of the g.s. of doublets in *sd*-shell nuclei (Table B.1 – *Range I* data). All charge-dependent
contributions obtained in a shell-model fit (V_{coul} and V_0 (USD), and the UCOM SRC scheme) are plotted as
a function of $A^{2/3}$. The $|b|$ values refer to the left y-axis. Plots of the total ISPE $\sum_i \epsilon_i^{(1)}$, $V_{coul}^{(1)}$, and $V_0^{(1)}$
contributions refer to the right y-axis. The V_0 contribution is multiplied with a factor of 20.
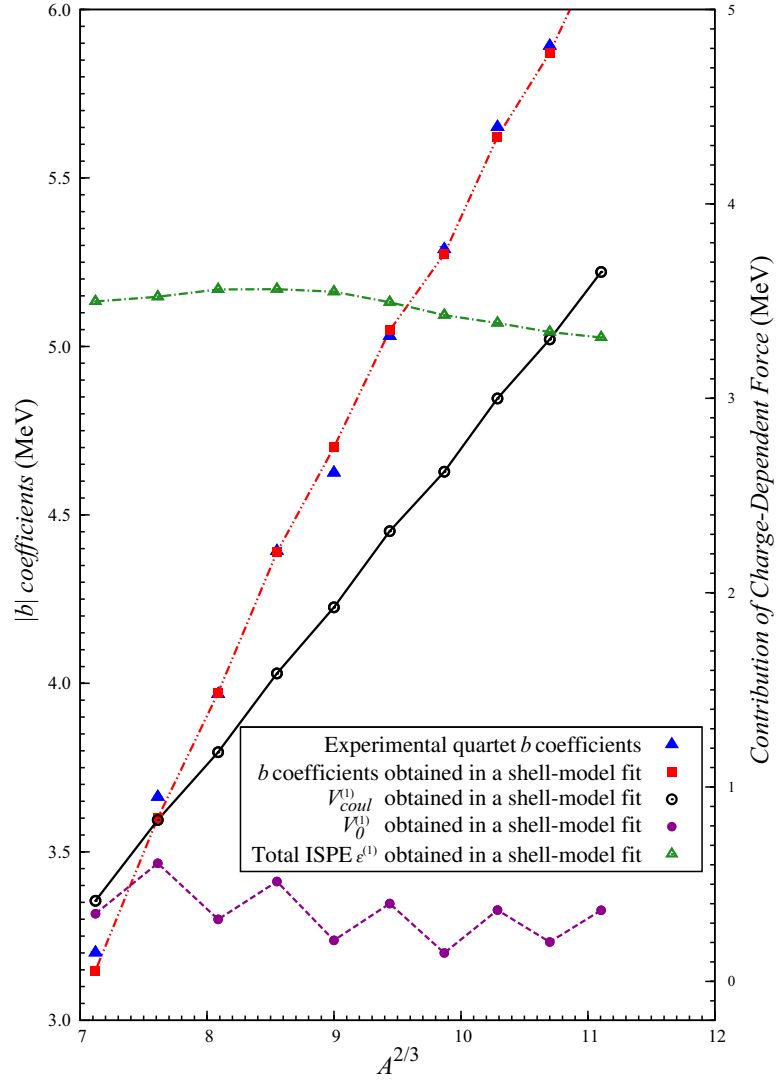
Figure 5.7: *Contributions of the various charge-dependent forces to quartet b coefficients.*
The $|b|$ coefficients of the lowest-lying quartets in *sd*-shell nuclei (Table B.3 – *Range I* data). Please refer to Fig. 5.6 for further descriptions.

The c coefficients of the lowest-lying triplets and quintets in sd-shell nuclei are presented in Fig. 5.8. The c coefficients obtained in a shell-model fit for triplets follow the experimental trend closely, whereas three fitted quintets are slightly off from the experimental values, i.e., $A = 20, 28$ and 36.

The experimental and shell model fitted c coefficients of triplets clearly form two different families of $A = 4n$ and $A = 4n + 2$ multiplets, respectively. However, this behavior is not obvious in the c coefficients of quintets. The oscillation of c values of the lowest-lying triplets has a higher amplitude compared to quintets' oscillatory amplitude (if quintets have oscillatory behavior).

Contributions of different terms of the charge-dependent Hamiltonian to c coefficients are shown in Fig. 5.9. One can see that the isotensor Coulomb force $V_{coul}^{(2)}$ is the main contributor. Furthermore, the plot also indicates that V_{coul} alone does not reproduce the experimental c coefficients. For the $4n + 2$ family, the deviation is about ~40 keV; whereas for the $4n$ family, it is around ~5 keV. This is the evidence showing that $V_{coul}^{(2)}$ should be supplemented by another two-body interaction of nuclear origin, which we model as $V_0^{(2)}$ (or $V_\rho^{(2)}$) in this thesis.

The contribution of the empirical isotensor nuclear Hamiltonian $V_0^{(2)}$ follow the same oscillatory trend as the contribution of $V_{coul}^{(2)}$, and $V_0^{(2)}$ contribution to c values is about ~40 keV for $A = 4n$ multiplets and ~5 keV for $A = 4n + 2$ multiplets. $V_0^{(2)}$ supplements a negative contribution to the c coefficient of triplet $A = 36$, c.f. Fig. 5.9.

Nonetheless, the $V_0^{(2)}$ contribution to quintets' c coefficients shows a noticeable oscillatory effect, c.f. Fig. 5.10. However, the V_{coul} contribution does not have staggering behavior and does not resemble a straight line either. The differences between the $V_0^{(2)}$ contributions and quintets' experimental c coefficients for $A = 20$ and 24 are about 25 keV and 20 keV, respectively.

If V_0 is replaced by V_ρ, or USD is supplemented by USDA or USDB, or the other SRC scheme is used to supersede UCOM, the staggering effects of the contributions from different components of the charge-dependent Hamiltonian H_{CD} to b and c coefficients have similar trends as what have been presented here.
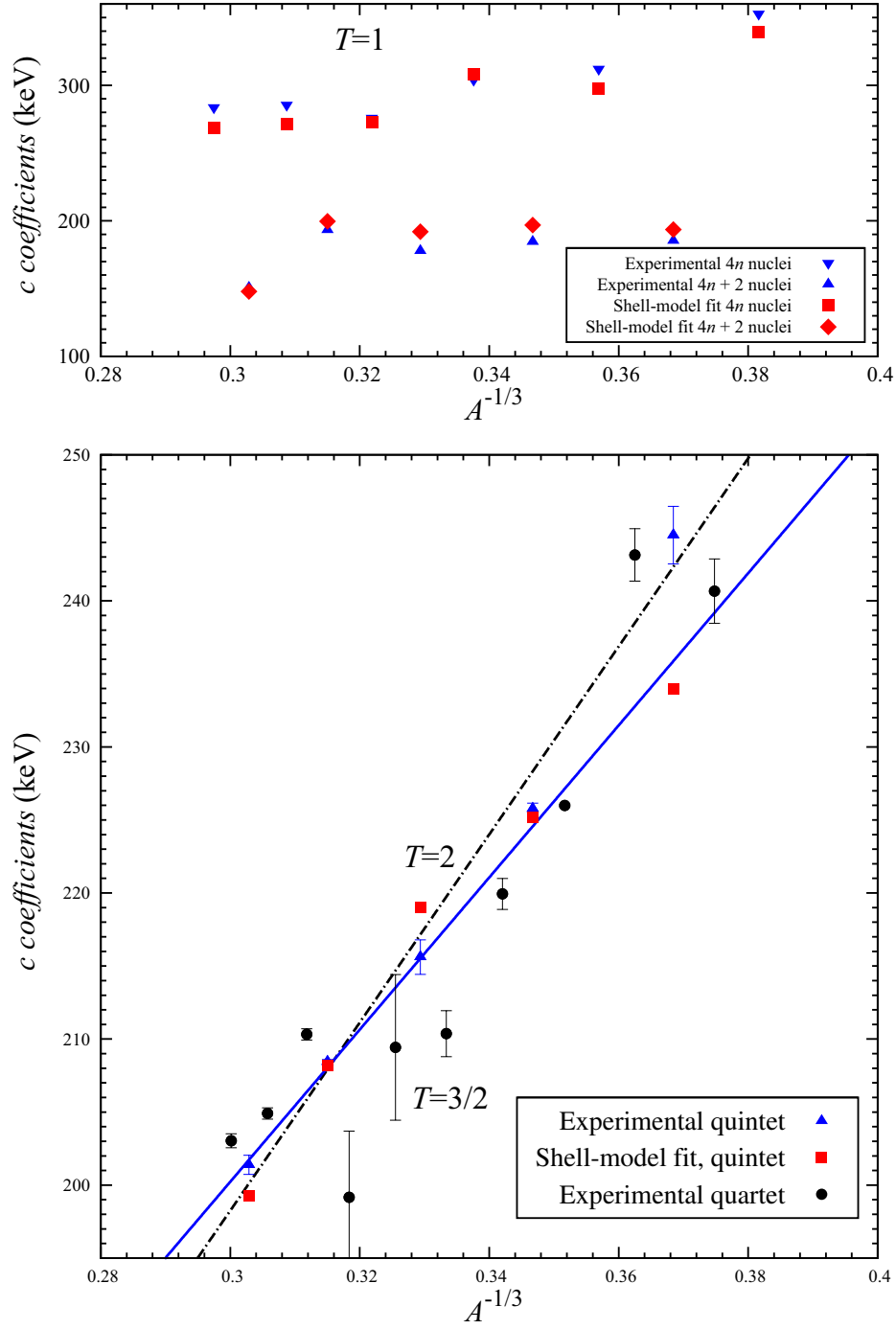
Figure 5.8: *Staggering effect of c coefficients of the lowest-lying triplets, quartets and quintets.*
The c coefficients are plotted as a function of $A^{-1/3}$ (Table B.2, Table B.3 and Table B.4 – *Range I* data).
The main figure shows c coefficients of the lowest-lying quartets and quintets. The c coefficients obtained
in a shell-model fit are produced from V_{coul} and V_0 (USD) combination, and the UCOM SRC scheme. The
dotted-dash (black) line, $c = 643.852A^{-1/3} + 5.097$, is an unweighted fit to experimental c values. The solid
(blue) line, $c = 520.846A^{-1/3} + 43.975$, is an unweighted fit to the c coefficients obtained in a shell-model
fit.
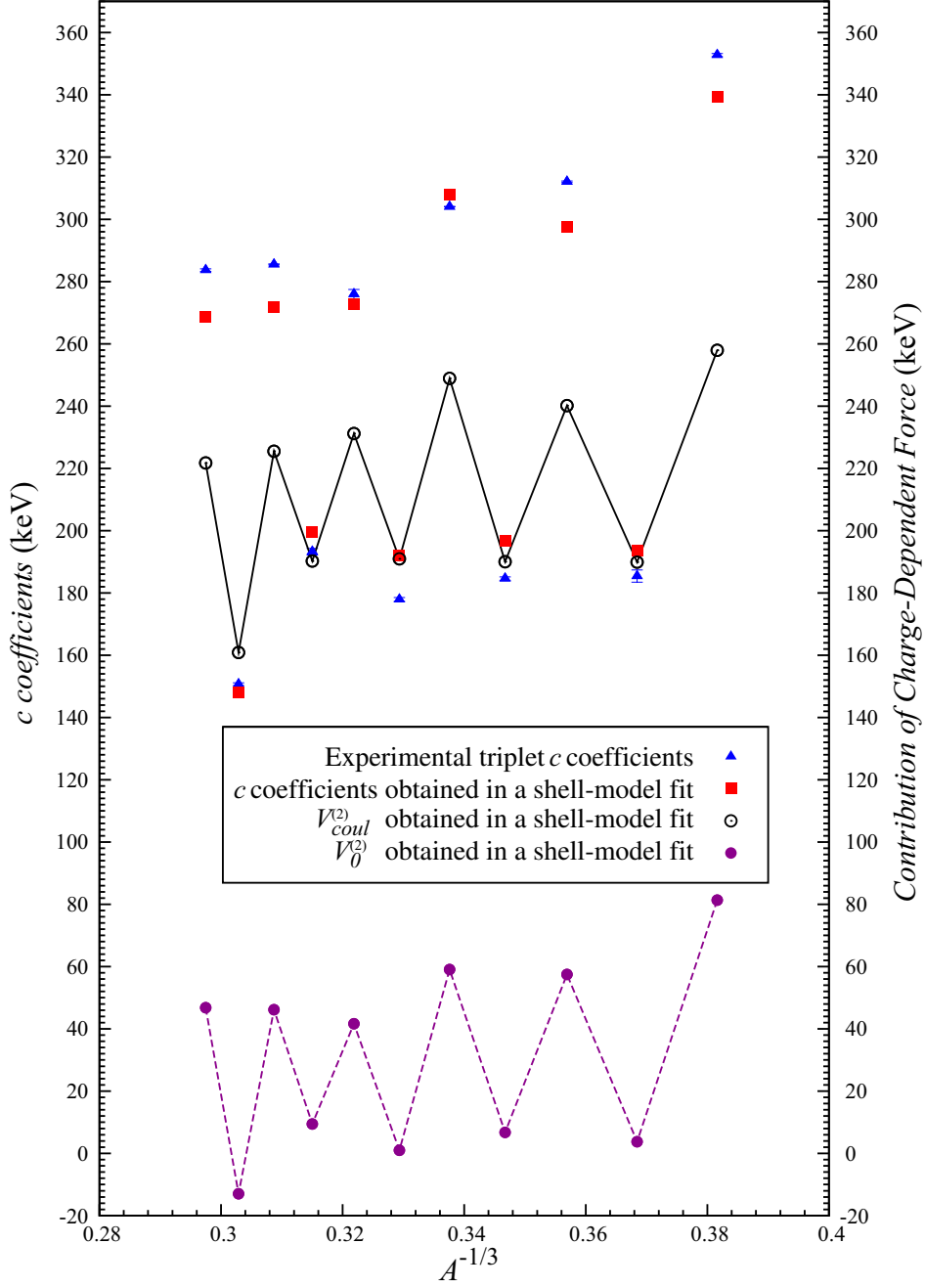
Figure 5.9: *Contributions of the various charge-dependent forces to the lowest-lying triplet c coefficients.*
The c coefficients of the lowest-lying triplets (Table B.2) and all charge-dependent contributions obtained in a shell-model fit (V_{coul} and V_0 (USD), and the UCOM SRC scheme) are plotted as a function of $A^{-1/3}$.
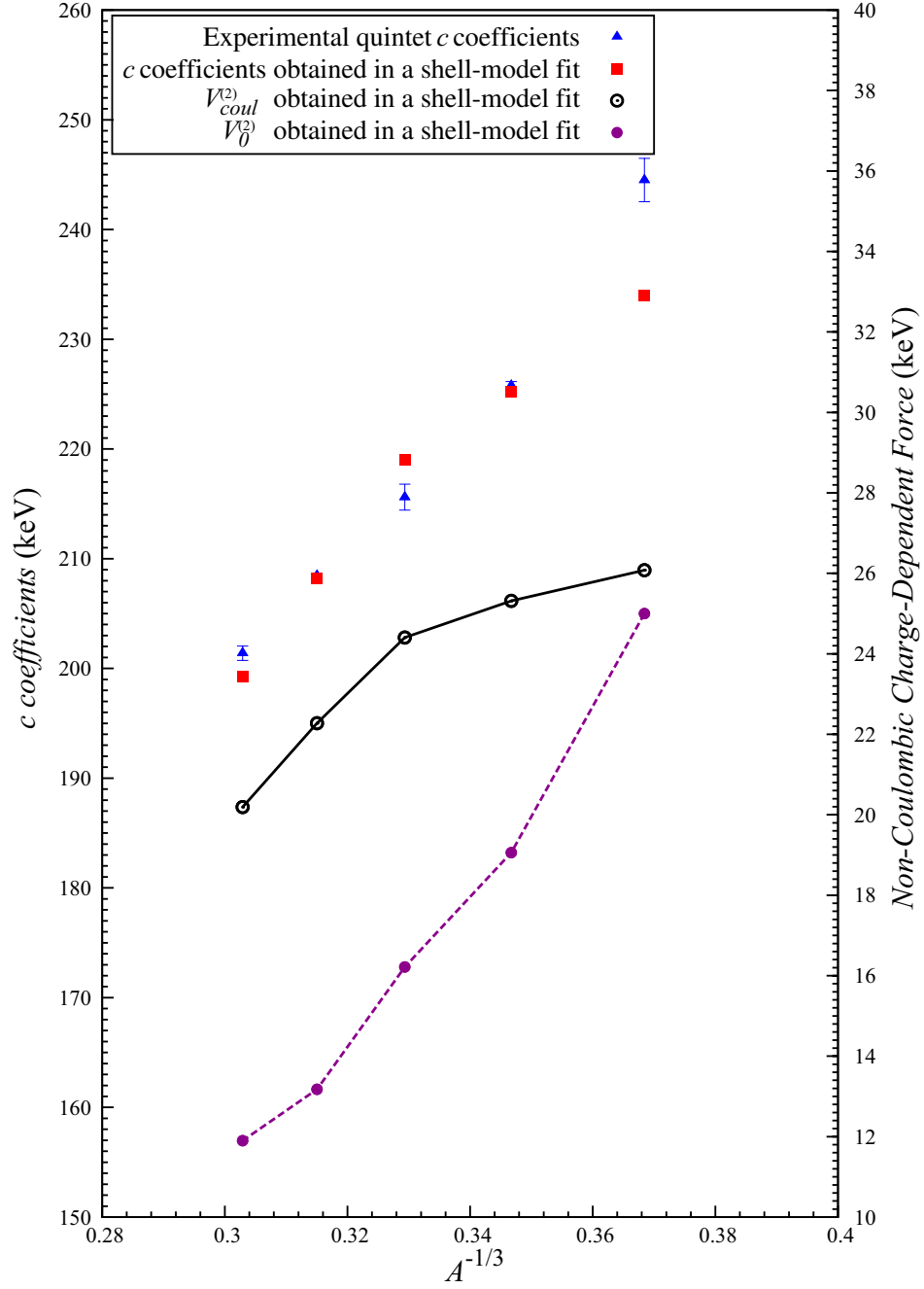
Figure 5.10: *Contributions of the various charge-dependent forces to the lowest-lying quintet c coefficients.* The presented c coefficients are quoted from Table B.4 – *Range I* data. Only plot of $V_0^{(2)}$ refer to the right y-axis. Please refer to Fig. 5.9 for further descriptions.

5.2.2 Jänecke's schematic Model

Jänecke's model is based on an approximate formula for the Coulomb energy proposed by Carlson and Talmi [120]. By considering effective two-body interaction between Z' valence proton(s) outside a closed shell, Carlson and Talmi derived that the total Coulomb energy of a nucleus is

$$E_{coul} = Z'\chi + \frac{1}{2}Z'(Z'-1)\alpha + \left\lfloor \frac{1}{2}Z' \right\rfloor \beta \,, \tag{5.2}$$

where $\left\lfloor \frac{1}{2}Z' \right\rfloor$ is the largest integer less than or equal to $\frac{1}{2}Z'$, α and β relate to the Coulomb interaction between two protons in the j shell, and χ defines the long-range Coulomb interaction of the inert core with a single proton. This expression is approximately valid when the j shell is occupied with protons only, but holds fairly well when both protons and neutrons are present in the j shell, or when protons occupy more than one shell. In order to match Eq.(5.2) with Eq.(1.26), Jänecke proposed to replace the pairing term $\left\lfloor \frac{1}{2}Z' \right\rfloor \beta$ by a quadratic term in T_z [107]. This quadratic term is itself a quadratic term of $Z = \frac{1}{2}A - T_z$, and is also a quadratic term of $Z' = Z - Z_{core}$. This modification yields

$$\left\lfloor \frac{1}{2}Z' \right\rfloor \to a + bT_z + cT_z^2 = (\mu - \nu\left[A - 2Z_{core}\right])Z' + \nu Z'^2 \,, \tag{5.3}$$

where the coefficients μ and ν are defined as

$$\mu = \begin{cases} \frac{1}{2}, & \text{for even-}A \text{ nuclei,} \\ \frac{1}{2}\left(1 - \frac{1}{2T}(-1)^{A/2-T}\right), & \text{for odd-}A \text{ nuclei,} \end{cases} \tag{5.4}$$

and

$$\nu = \begin{cases} \frac{1}{4T}\left(1 + \frac{1}{2T-1}(-1)^{A/2-T}\right), & \text{for even-}A \text{ nuclei,} \\ \frac{1}{4T}, & \text{for odd-}A \text{ nuclei,} T > 1/2 \,. \end{cases} \tag{5.5}$$

These two expressions for μ and ν are obtained within an independent-particle model assuming that the states under consideration are the lowest possible states for given A and T, and every single-particle level is fourfold degenerate with at most two protons and two neutrons in one level of a Nilsson-like model. The values of μ and ν coefficients for $T = 1/2, 1, 3/2,$ and 2 quoted from [107] are listed in Table 5.1.

By inserting Eq.(5.3) into Eq.(5.2), the total Coulomb energy of a nucleus reads

$$E_{coul} = Z'\chi + \frac{1}{2}Z'(Z'-1)\alpha + \left[(\mu - \nu\left[A - 2Z_{core}\right])Z' + \nu Z'^2\right]\beta \,. \tag{5.6}$$

Introducing $E_1 = \alpha$, $E_2 = \chi - \frac{1}{2}\alpha(2Z_{core}+1)$, $E_3 = \beta$, we get for isovector and isotensor contribution:

$$E_{coul}^{(1)} = \frac{1}{2}E_1 A + E_2 + \mu E_3 \,, \tag{5.7}$$

Table 5.1: *Magnitudes of μ and ν coefficients in* Eq.(5.3), *quoted from* Ref. [107]

| Isospin, T | μ | | | | ν | | | |
	$A = 4n$	$A = 4n+1$	$A = 4n+2$	$A = 4n+3$	$A = 4n$	$A = 4n+1$	$A = 4n+2$	$A = 4n+3$
$\frac{1}{2}$	–	0	–	1	–	0	–	0
1	$\frac{1}{2}$	–	$\frac{1}{2}$	–	0	–	$\frac{1}{2}$	–
$\frac{3}{2}$	–	$\frac{2}{3}$	–	$\frac{1}{3}$	–	$\frac{1}{6}$	–	$\frac{1}{6}$
2	$\frac{1}{2}$	–	$\frac{1}{2}$	–	$\frac{1}{6}$	–	$\frac{1}{12}$	–

and

$$E_{coul}^{(2)} = \frac{1}{6}E_1 A + 2\nu E_3 \,, \tag{5.8}$$

respectively. The coefficients E_i with $i = 1, 2$, and 3, are related to the expectation value of $1/R$, because the average distance between protons should increase with the nuclear volume [107]. Therefore, defining $E_1 = \hat{E}_1/A^{1/3}$, with $\hat{E}_1$ being constant values, which are different from shell to shell, the isovector Coulomb energy becomes a linear function of $A^{2/3}$.

Isovector Coulomb Energies

Using Eq.(5.4) and Eq.(5.7), we may derive the isovector Coulomb energies for $T = 1/2$ doublets, $T = 1$ triplets, $T = 3/2$ quartets, and $T = 2$ quintets

$$E_{coul\,(T=1/2)}^{(1)} = \frac{1}{2}E_1 A + E_2 + \frac{1}{2}E_3 + (-1)^{(A+1)/2}\frac{E_3}{2} \,, \tag{5.9}$$

$$E_{coul\,(T=1)}^{(1)} = \frac{1}{2}E_1 A + E_2 + \frac{1}{2}E_3 \,, \tag{5.10}$$

$$E_{coul\,(T=3/2)}^{(1)} = \frac{1}{2}E_1 A + E_2 + \frac{1}{2}E_3 + (-1)^{(A-1)/2}\frac{E_3}{6} \,, \tag{5.11}$$

$$E_{coul\,(T=2)}^{(1)} = \frac{1}{2}E_1 A + E_2 + \frac{1}{2}E_3 \,, \tag{5.12}$$

respectively. The last terms of Eq.(5.9) and Eq.(5.11) determine the amplitude of the oscillations of the b coefficients of doublets and quartets. Comparison of the last term of Eq.(5.9) and Eq.(5.11) shows that the amplitude of quartets is less than doublets' amplitude. Eq.(5.10) and Eq.(5.12) indicate that there is no oscillatory behavior in triplets' and quintets' isovector Coulomb energies (b coefficients).

Isotensor Coulomb Energies

Applying Eq.(5.5) and Eq.(5.8), we can obtain the isotensor Coulomb energies for $T = 1$ triplets, $T = 3/2$ quartets, and $T = 2$ quintets

$$E^{(2)}_{coul\,(T=1)} = \frac{1}{6}\left(E_1 + \frac{1}{2}\left[1 - (-1)^{A/2}E_3\right]\right),\tag{5.13}$$

$$E^{(2)}_{coul\,(T=3/2)} = \frac{1}{6}\left(E_1 + \frac{1}{3}E_3\right),\tag{5.14}$$

$$E^{(2)}_{coul\,(T=2)} = \frac{1}{6}\left(E_1 + \frac{1}{4}\left[1 - \frac{1}{3}(-1)^{(A-2)/2}E_3\right]\right),\tag{5.15}$$

respectively. Like the isovector Coulomb energy, the last term of Eq.(5.13) and Eq.(5.15) shows that the amplitude of the oscillations of the triplets' c coefficients is greater than the quintets' amplitude. Eq.(5.14) shows that the quartet isotensor Coulomb energy $E^{(2)}_{coul\,(T=3/2)}$ is merely a constant which is different from shell to shell. Hence, an oscillatory behavior is not predicted for quartet c coefficients ($c = 3E^{(2)}_{coul}$, see Eq.(2.69)).

Table 5.2: *Magnitudes of fitted E_1, E_2, and E_3 in Eq.(5.7) to Eq.(5.15), c.f. Fig. 3.2.*

Shell Space	E_1 (keV)	E_2 (keV)	E_3 (keV)
$0p_{3/2}$	467	799	46
$0p_{1/2}$	577	1377	79
$1s_{1/2}0d_{5/2}0d_{3/2}$	487	1199	134
$0f_{7/2}$	454	3089	254
$1p_{3/2}$	298	858	398

The E_i values have been refitted from the presently compiled experimental lowest-lying multiplet b coefficients in chapter 3. We deduce the E_i values using linear equations given in the description of Fig. 3.2 and Eq.(5.7). The E_i coefficients are listed in Table 5.2. The value of E_3 deduced from the fit to b coefficients predicts the $\frac{1}{2}E_3$ amplitude for c coefficients in $T = 1$, which is in very good agreement with the experimental amplitude, see Fig. 5.9 or Fig. 5.12.

5.2.3 Hecht's formalism: Wigner's supermultiplet

Hecht proposed two approaches to calculate the Coulomb interaction energy for nuclei with protons and neutrons in the valence space [119, 121, 122, 123, 124]. One approach is based on Wigner's supermultiplet scheme [5, 119, 121], whereas the other exploits the low-seniority limit of the jj-coupling scheme [122, 123, 124]. The latter formalism may give poor results for nuclei having both protons and neutrons in the same shell, while the former one may not be valid in heavier nuclei. Here, we discuss the first algebraic approach.

In this approach, Wigner's supermultiplet quantum numbers – the total spin S and the isospin T – are assumed to be good quantum numbers. We need to establish the favoured spin-isospin U(4) representation, which is consistent with a given isospin of a nuclear state. This isospin T corresponds to the favoured ground-state U(4) representation of the $T_z = \pm T$ members of a given isobaric multiplet. A U(4) representation is described by a four-rowed Young tableau $\left[\tilde{f}_1, \tilde{f}_2, \tilde{f}_3, \tilde{f}_4\right]$ and it has a conjugate Young tableau $[f_1, f_2, f_3, f_4]$, which determines the spatial symmetry of all the members of a given isobaric multiplet. Generally, a U(4) representation contains many states that are all degenerate.

Using first-order perturbation theory and assuming that the Coulomb energies are independent of the spatial quantum numbers, Hecht showed that the dominant part consists of the matrix elements of that part of the Coulomb interaction which is a full space scalar. Moreover, other than S and T, these matrix elements depend also on the supermultiplet labels $\left[\tilde{f}_1, \tilde{f}_2, \tilde{f}_3, \tilde{f}_4\right]$. Only this part of the Coulomb matrix element is considered [119].

The results given by Hecht for isospin doublets ($T = 1/2$), triplets ($T = 1$) and quartets ($T = 3/2$) are listed below.

Isospin Doublets

For isospin doublets the number of valence nucleons $\mathcal{N}$ must be odd. There are two cases, namely $\mathcal{N} = 4k + 1$ and $\mathcal{N} = 4k + 3$, with $k = 0, 1, 2, \ldots$, which correspond to $4n + 1$ and $4n + 3$ nuclei, respectively. The isovector coefficients for isovector Coulomb energy are

Case (A): $\mathcal{N} = 4k + 1$:
The favoured supermultiplet is $[k + 1, k, k, k]$ in U(4) or $(100)^1$ in SU(4). This supermultiplet has $(S, T) = (1/2, 1/2)$. The isovector coefficients is

$$E_{(100)T=1/2}^{(1)} = 3a'_c + 3(\mathcal{N} - 1)b' . \tag{5.16}$$

---

[1] We use here the notation $(\lambda\mu\nu)$ for SU(4) irreducible representations defined as $(\lambda = f_1 - f_2 \quad \mu = f_2 - f_3 \quad \nu = f_3 - f_4)$.
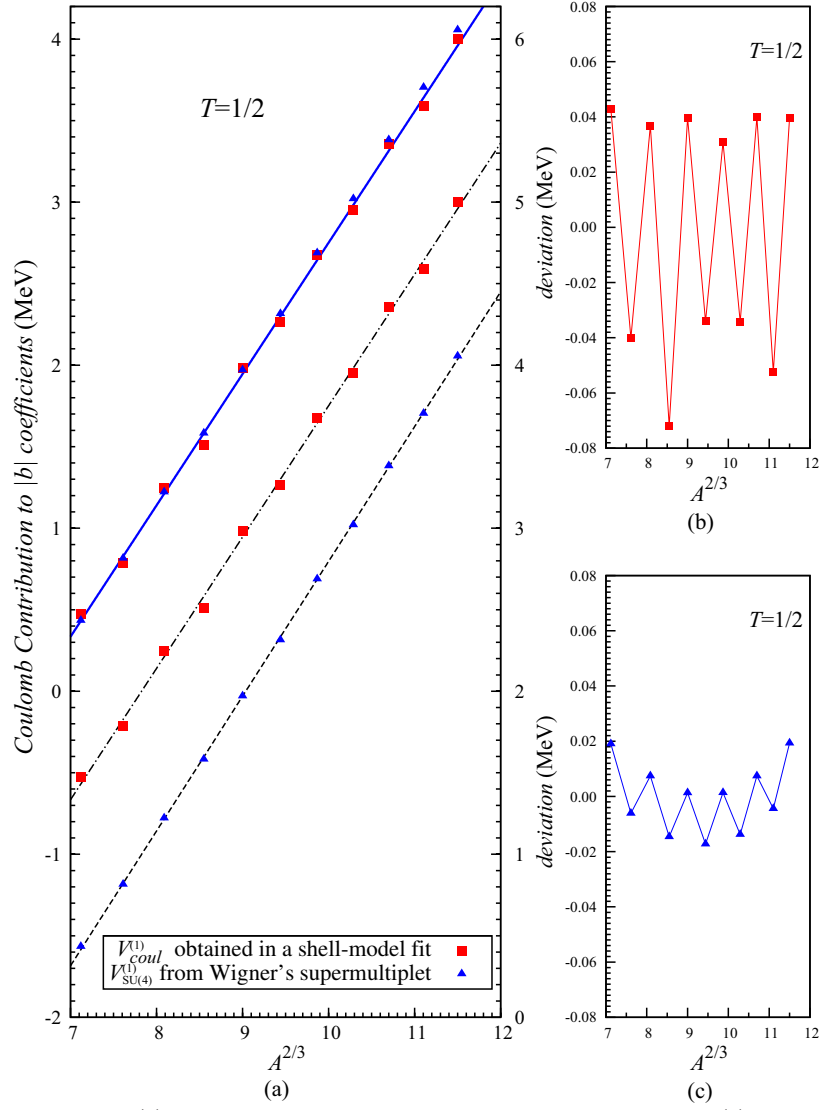
Figure 5.11: *Comparison of $V_{coul}^{(1)}$ contribution obtained in a shell-model fit with $V_{SU(4)}^{(1)}$ contribution calculated by Wigner's supermultiplet formalism, to $|b|$ coefficients for the lowest-lying $T = 1/2$ doublets in sd-shell nuclei.*
Figure (a): The $V_{coul}^{(1)}$ contribution is produced from V_{coul} and V_0 (USD), and the UCOM SRC scheme. Both linearly fitted upper solid (blue) line and (black) dotted-dash line are $b = 0.8056A^{2/3} - 5.3049$. These lines are fitted according to the $V_{coul}^{(1)}$ obtained in a shell-model fit. (Black) dashed line is $b = 0.8268A^{2/3} - 5.4717$, and is fitted according to the $V_{SU(4)}^{(1)}$ contribution calculated by Wigner's supermultiplet formalism. (Red) squares and (blue) triangles at the vicinity of solid (blue) lines are plotted with respect to the left y-axis, but the right y-axis is used for (red) squares and (blue) triangles at the vicinity of dotted-dash and dashed line. Although (red) square values refer to the right y-axis, they should be shifted down 1 MeV.
Figure (b): the deviations of $V_{coul}^{(1)}$ contribution obtained in a shell-model fit from the solid (blue) line.
Figure (c): the deviations of $V_{SU(4)}^{(1)}$ contribution calculated by Wigner's supermultiplet formalism from the double-dotted dash (black) line.
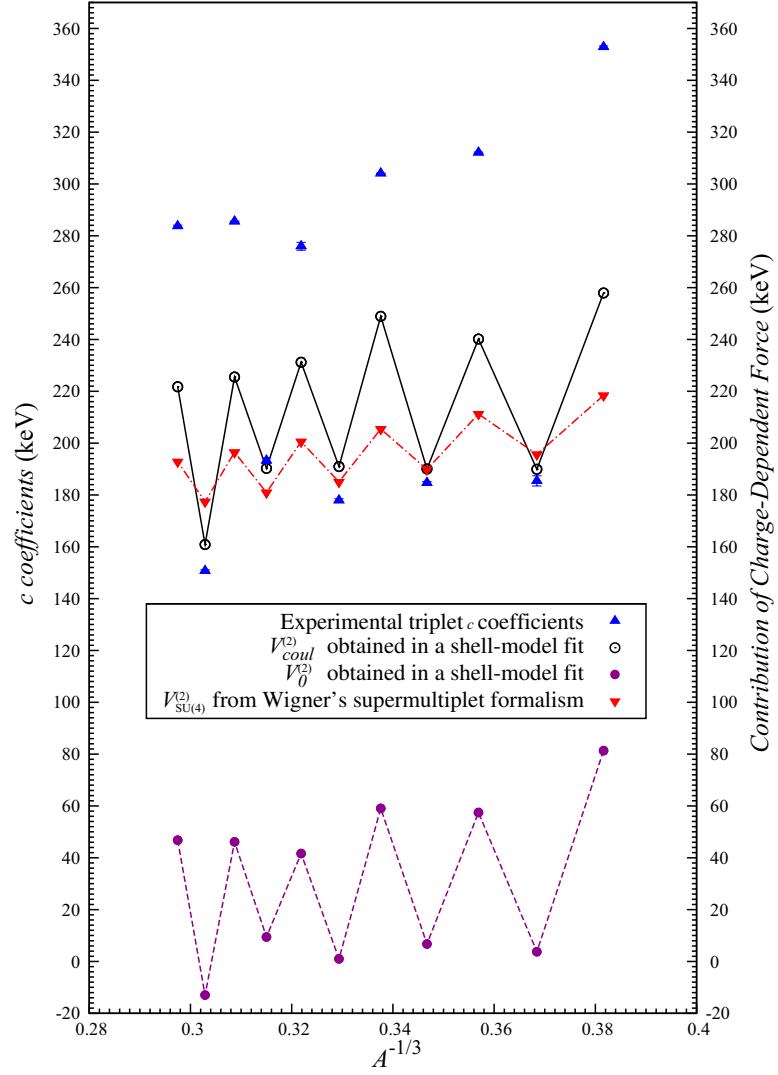
Figure 5.12: *Comparison of $V_{coul}^{(2)}$ contribution obtained in a shell-model fit with $V_{\mathrm{SU}(4)}^{(2)}$ contribution calculated by Wigner's supermultiplet formalism, to c coefficients for the lowest-lying $T = 1$ triplets in sd-shell nuclei.* All experimental c coefficients are from *Range I* data in *sd*-shell nuclei, c.f. Table B.2 in Appendix B.

Case (B): $\mathcal{N} = 4k + 3$:
The favoured supermultiplet is $[k+1, k+1, k+1, k]$ in U(4) or (001) in SU(4), and it also has $(S, T) = (1/2, 1/2)$. The isovector coefficient is

$$E^{(1)}_{(001)T=1/2} = 3a'_c + 3(\mathcal{N} - 1)b' + 36c' \,. \tag{5.17}$$

The coefficients a'_c, b' and c' are given by Ref. [119] as

$$a'_c = \sum_{J, j_c} \frac{(2J+1)}{(2j+1)} \langle (jj_c)J| \frac{e^2}{3r_{ij}} |(jj_c)J\rangle = \begin{cases} \frac{1}{192}c^2\sqrt{\frac{M_N\omega}{2\pi\hbar}}, & \text{for } p\text{-shell multiplets,} \\ \frac{7}{4608}c^2\sqrt{\frac{M_N\omega}{2\pi\hbar}}, & \text{for } sd\text{-shell multiplets,} \end{cases}$$

$$b' = \frac{1}{24}(\alpha + 3\beta) \,,$$

$$c' = \frac{1}{48}(\alpha - \beta) \,, \tag{5.18}$$

respectively, where,

$$\alpha = \frac{19}{12}, \quad \beta = \frac{4}{3}, \text{ for } p\text{-shell multiplets, and} \tag{5.19}$$

$$\alpha = \frac{119}{96}, \quad \beta = \frac{7}{6}, \text{ for } sd\text{-shell multiplets.} \tag{5.20}$$

The staggering behavior of the b coefficients from $\mathcal{N} = 4k + 1$ to $\mathcal{N} = 4k + 3$ is $36c'$, which is also the amplitude of the oscillatory effect. Eq.(5.16) and Eq.(5.17) do not determine the c coefficient, since $3T_z^2 - T(T+1) = 0$ for $T = 1/2$ doublets.

We compare the prediction from Wigner's supermultiplet formalism with our current shell model fitted b coefficients in Fig. 5.11.

Isospin Triplets

For isospin triplets the number of valence nucleons $\mathcal{N}$ must be even. There are two cases, i.e., $\mathcal{N} = 4k + 4$ and $\mathcal{N} = 4k + 2$, with $k = 0, 1, 2, \ldots$, which correspond to $4n$ and $4n + 2$ nuclei, respectively.

Case (C): $\mathcal{N} = 4k + 4$:
The favoured supermultiplet is $[k+2, k+1, k+1, k]$ in U(4) or (101) in SU(4). The supermultiplet contains $(S, T) = (0, 1), (1, 0)$ and $(1, 1)$. The isovector and the isotensor coefficients are

$$E^{(1)}_{(101)T=1} = 3a'_c + 3(\mathcal{N} - 1)b' + 18c' \,, \tag{5.21}$$

and

$$E^{(2)}_{(101)T=1} = b' - c' - [5 - 4S(S+1)]c' \,, \tag{5.22}$$

respectively.

Case (D): $\mathcal{N} = 4k + 2$:
The favoured supermultiplet is $[k+1, k+1, k, k]$ in U(4) or (010) in SU(4). The supermultiplet contains only $(S, T) = (0, 1)$ and $(1, 0)$. The isovector and the isotensor coefficients are

$$E_{(010)T=1}^{(1)} = 3a_c' + 3(\mathcal{N} - 1)b' + 18c', \tag{5.23}$$

and

$$E_{(010)T=1}^{(2)} = b' + 6c', \tag{5.24}$$

respectively.

We remark that the (101) representation of SU(4) contains both $(S, T) = (0, 1)$ and $(1, 1)$, hence S can be either 0 or 1, whereas the (010) representation with $T = 1$ must have $S = 0$. Eq.(5.21) and Eq.(5.23) indicate that $T = 1$ triplets do not show any staggering effect in the b coefficient, whereas oscillation from $\mathcal{N} = 4k + 4$ and $\mathcal{N} = 4k + 2$ happens in the c coefficient, and its amplitude is given as $12c'$ (if we assume $S = 0$), c.f. Fig. 5.12.

Isospin Quartets

For isospin quartets the number of valence nucleons $\mathcal{N}$ must be odd. There are two cases, i.e., $\mathcal{N} = 4k + 5$ and $\mathcal{N} = 4k + 3$, with $k = 0, 1, 2, \ldots$, which correspond to $4n + 1$ and $4n + 3$ nuclei, respectively.

Case (E): $\mathcal{N} = 4k + 5$:
The favoured supermultiplet is $[k+2, k+2, k+1, k]$ in U(4) or (011) in SU(4). The supermultiplet contains $(S, T) = (1/2, 1/2), (1/2, 3/2)$ and $(3/2, 1/2)$. The isovector and the isotensor coefficients are

$$E_{(011)T=3/2}^{(1)} = 3a_c' + 3(\mathcal{N} - 1)b' + 24c', \tag{5.25}$$

and

$$E_{(011)T=3/2}^{(2)} = b' + 2c', \tag{5.26}$$

respectively.
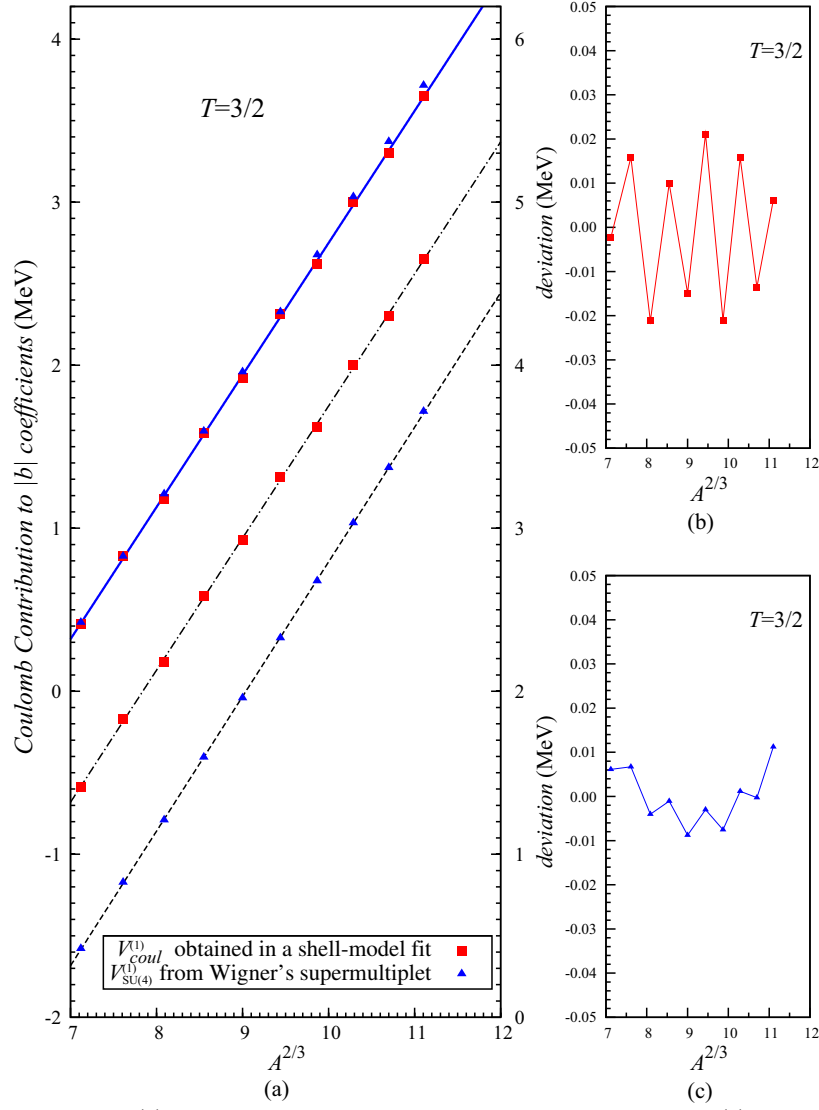
Figure 5.13: *Comparison of $V_{coul}^{(1)}$ contribution obtained in a shell-model fit with $V_{SU(4)}^{(1)}$ contribution calculated by Wigner's supermultiplet formalism, to $|b|$ coefficients for the lowest-lying $T = 3/2$ quartets in sd-shell nuclei. Figure (a): Both linearly fitted upper solid (blue) line and (black) dotted-dash line are $b = 0.8101A^{2/3} - 5.3514$. These lines are fitted according to the $V_{coul}^{(1)}$ contribution to the $|b|$ coefficients obtained in a shell-model fit. (Black) dashed line is $b = 0.82568A^{2/3} - 5.4635$, and is fitted according to the $V_{SU(4)}^{(1)}$ contribution calculated by Wigner's supermultiplet formalism. Please refer to Fig. 5.11 for further descriptions.*
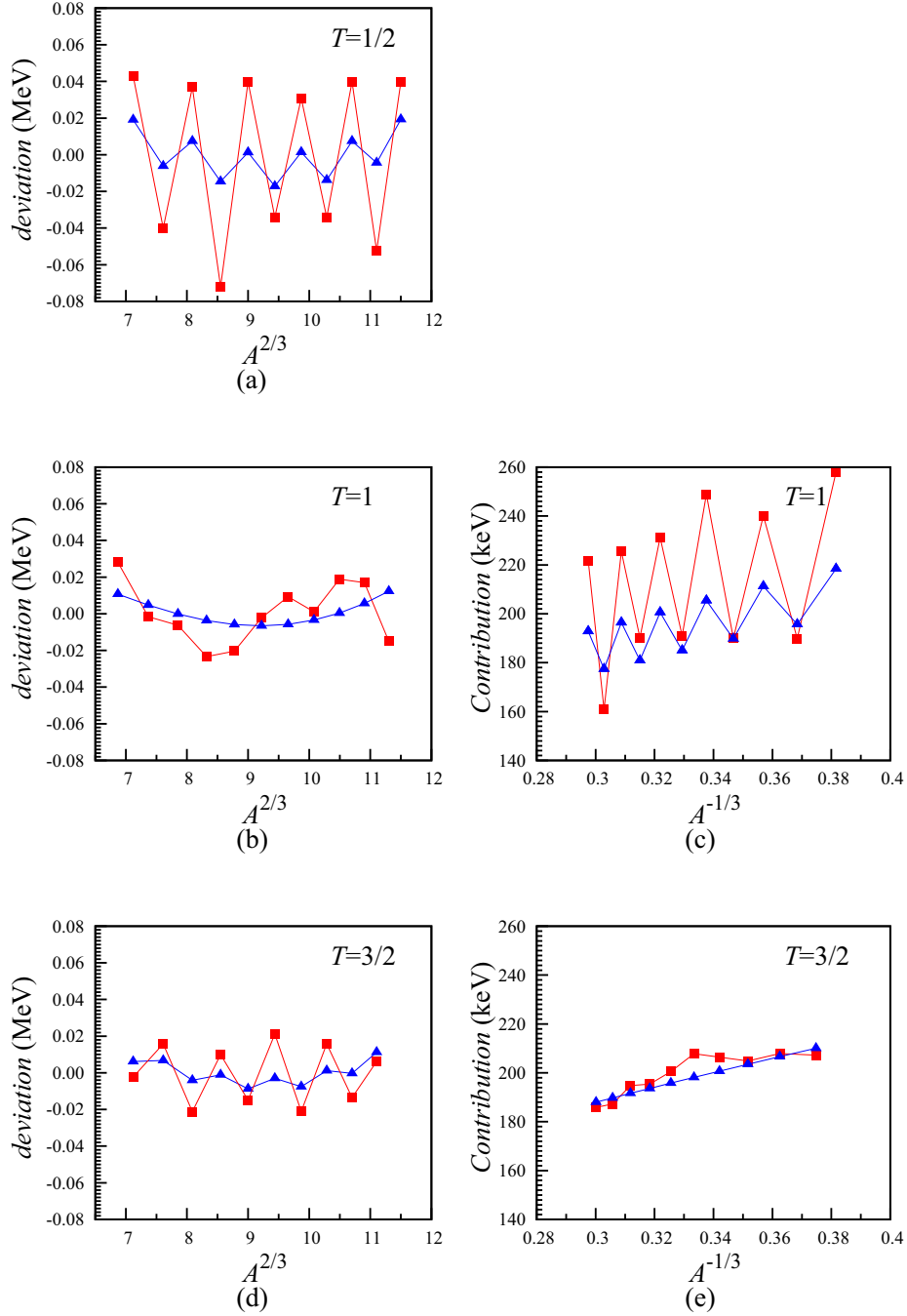
Figure 5.14: *Comparison of V_{coul} from a shell-model fit and $V_{SU(4)}$ from Wigner's supermultiplet.* The V_{coul} values are represented by (red) squares, whereas the $V_{SU(4)}$ are displayed as (blue) triangles. Figures (a), (b), and (d) are the deviations of $V_{coul}^{(1)}$ and $V_{SU(4)}^{(1)}$ contributions. Figures (c) and (e) are $V_{coul}^{(2)}$ and $V_{SU(4)}^{(2)}$ contributions to the c coefficients.

Case (F): $\mathscr{N} = 4k + 3$:

The favoured supermultiplet is $[k+2, k+1, k, k]$ in U(4) or (110) in SU(4). The supermultiplet contains $(S, T) = (1/2, 1/2), (1/2, 3/2)$ and $(3/2, 1/2)$. The isovector and the isotensor coefficients are

$$E^{(1)}_{(110)T=3/2} = 3a'_c + 3(\mathscr{N} - 1)b' + 12c' \,, \tag{5.27}$$

and

$$E^{(2)}_{(110)T=3/2} = b' + 2c' \,, \tag{5.28}$$

respectively.

Eq.(5.25) and Eq.(5.27) show that $T = 3/2$ quartets do show staggering in the b coefficient. Oscillation between $\mathscr{N} = 4k+5$ and $\mathscr{N} = 4k+3$ happens in the b coefficient, and its amplitude is given as $12c'$. This amplitude is smaller than the amplitude of oscillation in $T = 1/2$ doublets. Comparing Eq.(5.25) and Eq.(5.27) with Eq.(5.16) and Eq.(5.17), the differences in the amplitudes of multiplets of $\mathscr{N} = 4k+1$ and $\mathscr{N} = 4k+3$, and $\mathscr{N} = 4k+5$ and $\mathscr{N} = 4k+3$ shows that the oscillations of $T = 1/2$ doublets and $T = 3/2$ quartets progress in the opposite direction. However, Eq.(5.26) and Eq.(5.28) indicate that $T = 3/2$ quartets have no staggering effect in the c coefficient.

We conclude that staggering in b and c coefficients are naturally manifested in Wigner's supermultiplet theory [5]. The trend is correctly predicted by Wigner's supermultiplet scheme, although the amplitudes are smaller than the Coulomb contribution $V^{(q)}_{coul}$ obtained in a shell-model fit, c.f. Fig. 5.11, Fig. 5.13, and Fig. 5.12. We summarize of the comparisons of the $V^{(q)}_{coul}$ and $V^{(q)}_{SU(4)}$ oscillatory trends in Fig. 5.14.

5.3 Remarks

This chapter has presented a detailed study of the staggering behavior of the b and c coefficients. For the first time, we provide a true microscopic description of these subtle effects within the shell model. Moreover, we could even successfully separate the contributions from various charge-dependent forces to the respective mirror energy difference and tensor energy difference in terms of the isovector and isotensor energies, c.f. Fig. 5.6, Fig. 5.7, Fig. 5.9, and Fig. 5.10. Two additional models explaining the staggering effect have been revised: (i) Jänecke's schematic model and (ii) Coulomb energy contributions within the SU(4) Wigner supermultiplet theory, which was developed by Hecht. The quintet staggering effect is not as pronounced as triplet's one, c.f. Fig. 5.8. Experimental mass measurements with high precision may shed light on proving the existence of quintet staggering effect.

Applications of the INC Hamiltonian

Chapter 6

Masses and extension of the IMME beyond the quadratic form

Contents

The fit and analysis in the previous chapters were based on the assumption of the quadratic form of the IMME. Indeed, it is a very good approximation, valid at present for the majority of experimentally measured isobaric multiplets. However, in a few cases there is experimental evidence of the breaking of the quadratic IMME. In this chapter, we go beyond the perturbation analysis of the isospin-symmetry breaking effect. We exploit the results of the exact diagonalization of the INC Hamiltonian to get theoretical mass differences in the isobaric multiplets and to test the validity of the quadratic IMME for the sd-shell $T = 2$ quintets. As an example, we choose the mass $A = 32$, $T = 2$ quintet, which has recently been measured with high precision, with the purpose to quantitatively probe our new parametrization of H_{INC} (described in chapter 4). We calculate nuclear mass excesses of all five members of this quintet and fit b, c, d, and e coefficients (in different combinations) from these theoretical mass excesses to look for the best description. Comparison of our results with the recent analysis of Signoracci and Brown [125], who used the strength parameters of Ref. [30] to calculate the mass excesses, is presented as well.

6.1 Introduction

Recent experimental advances in producing and in transporting nuclei with very short half-lives, and in ion-trapping techniques enable experimentalists to determine atomic masses with unprecedented high precision, c.f. [102]. Consequently, many more mass excesses of isobaric quartets and quintets can be accessed to test the IMME of Eq.(1.26). The main question is whether the IMME should remain in its quadratic form or whether the IMME should be extended to a cubic or a quartic form.

The cubic and quartic IMME are given as

$$M(\alpha, T, T_z) = a(\alpha, T) + b(\alpha, T)T_z + c(\alpha, T)T_z^2 + d(\alpha, T)T_z^3 \,, \tag{6.1}$$

and

$$M(\alpha, T, T_z) = a(\alpha, T) + b(\alpha, T)T_z + c(\alpha, T)T_z^2 + d(\alpha, T)T_z^3 + e(\alpha, T)T_z^4 \,, \tag{6.2}$$

respectively. A non-zero d (and/or e) coefficient can be due to the presence of ISB three- (or four-body) interactions among the nucleons [9], and/or may arise due to the isospin mixing in excited states of isobaric multiplets with nearby state(s) of the same J^π, but different T value. Theoretical estimations of d coefficients from isospin mixing predict values around ≈ 1 keV [111]. To probe such low values, recent experimental improvements become crucial in providing precise mass measurements of quartets and quintets. Various measurements of the mass $A = 32$ quintet (ground-state masses and excitation energies of the multiplet members) have been undertaken by different experimental groups [112, 113, 126]. These measurements indicate rigorous improvements in reducing relative mass uncertainties from as low as 10^{-8} further to 3×10^{-9} [102, 112, 113, 126]. These results point toward the presence of a non-zero d coefficient (see Table 6.4).

In the shell model the direct evaluation of absolute binding energies is possible with the isospin-conserving Hamiltonian, provided a certain algorithm is followed in the subtraction of empirical Coulomb energies from experimental binding energies used in the fit. Then the subtracted Coulomb energy should simply be added to the shell-model binding energy to get the full theoretical binding energy of a nucleus. In fitting the USD interaction, the subtraction of the Coulomb energy has been done in a kind of average way [127, 128].

In particular, an unknown amount of residual isoscalar Coulomb energy may remain in the charge independent nuclear Hamiltonian [127, 128]. Adding an INC term in the Hamiltonian requires the precise knowledge of the isoscalar Coulomb contribution and this prohibits the evaluation of the binding energies [34]. In spite of this fact, we can well describe theoretical mass differences of isobaric multiplets, which is sufficient to study the b, c, d, and e coefficients of the IMME, as is shown in the present chapter. The a coefficient however remains undetermined.

6.2 Extended IMME for quintets: case of $A = 32$

Using Eq.(6.2), we can express the mass excess for each member of a given $T = 2$ quintet in terms of a, b, c, d, and e coefficients as

$$
\begin{aligned}
M(\alpha, 2, T_z = 2) &= a(\alpha, 2) + 2b(\alpha, 2) + 4c(\alpha, 2) + 8d(\alpha, 2) + 16e(\alpha, 2)\,, \\
M(\alpha, 2, T_z = 1) &= a(\alpha, 2) + b(\alpha, 2) + c(\alpha, 2) + d(\alpha, 2) + e(\alpha, 2)\,, \\
M(\alpha, 2, T_z = 0) &= a(\alpha, 2)\,, \\
M(\alpha, 2, T_z = -1) &= a(\alpha, 2) - b(\alpha, 2) + c(\alpha, 2) - d(\alpha, 2) + e(\alpha, 2)\,, \\
M(\alpha, 2, T_z = -2) &= a(\alpha, 2) - 2b(\alpha, 2) + 4c(\alpha, 2) - 8d(\alpha, 2) + 16e(\alpha, 2)\,.
\end{aligned}
\tag{6.3}
$$

Then, the IMME a, b, c, d, and e coefficients are given as

$$
a = M_{T_z=0}\,,
\tag{6.4}
$$

$$
b = \frac{1}{12}\left[(M_{T_z=-2} - M_{T_z=2}) + 8(M_{T_z=1} - M_{T_z=-1})\right]\,,
\tag{6.5}
$$

$$
c = \frac{1}{24}\left[16(M_{T_z=1} + M_{T_z=-1}) - (M_{T_z=2} + M_{T_z=-2}) - 30M_{T_z=0}\right]\,,
\tag{6.6}
$$

$$
d = \frac{1}{12}\left[(M_{T_z=2} - M_{T_z=-2}) + 2(M_{T_z=1} - M_{T_z=-1})\right]\,,
\tag{6.7}
$$

$$
e = \frac{1}{24}\left[-4(M_{T_z=1} + M_{T_z=-1}) + (M_{T_z=2} + M_{T_z=-2}) + 6M_{T_z=0}\right]\,.
\tag{6.8}
$$

Here, we have shortened the notation for a, b, c, d, and e coefficients and the notation for mass excess of each member. Eq.(6.5) and Eq.(6.7) show that b and d are related to the difference between $M_{T_z=-2}$ and $M_{T_z=2}$ and to the difference between $M_{T_z=1}$ and $M_{T_z=-1}$ Note that b and d are not linked to a (or $M_{T_z=0}$). Meanwhile, c and e are defined by the sum of $M_{T_z=2}$ and $M_{T_z=-2}$ and the sum of $M_{T_z=1}$ and $M_{T_z=-1}$. These coefficients are independent of a, if the parametrization Eq.(6.3) is used (then a enters in each mass member and cancels in the expressions Eq.(6.6)-Eq.(6.8)). This set of relations is kept for least-squares fits on the cubic IMME, or on the quartic (without d) IMME, or on the quartic IMME, as long as every input mass excess has the same uncertainty, e.g., ± 1 keV.

In this section we consider in detail the $A = 32$ quintet of 0^+ states. If we assumed all uncertainties on the experimental mass excesses of $A = 32$ in Table A.5 were 1 keV, the a, b, c, d, and e coefficients would be as listed in Table 6.1. The b coefficients in the first and the third column are the same, when d is not considered in the fit presented in these two columns, whereas the b coefficients in the second column and the last column are the same, when d is included in both fits. In short, the presence of the d coefficient adjusts the respective b coefficient in the fit. The c and e resemble the similar situation as b and d. However, the inclusion of e only influences c about 0.0096544×10^{-2} compared to the inclusion of d, which adjust b about 0.0557596×10^{-2}. c.f. Table 6.1.

Mass excesses calculated in the shell model do not have uncertainties. To obtain a theoretically fitted b coefficient, which is close to the experimental one, the theoretical values of $(M_{T_z=-2} - M_{T_z=2})$ and $(M_{T_z=1} - M_{T_z=-1})$ should be close to the experimental mass differences.

Similarly, c and e coefficients are determined by the a-removed sum of the mass excesses of $T_z = \pm 1$ and $T_z = \pm 2$ isobaric members of the multiplet.

Table 6.1: *The experimental $a, b, c, d,$ and e coefficients[a] of the $A = 32$, $J^\pi = 0^+$, $T = 2$ quintet.*

	Quadratic Fit (keV)	Cubic Fit (keV)	Quartic Fit (without d) (keV)	Quartic Fit (keV)
a	-13967.56	-13967.56	-13967.58	-13967.58
b	-5469.91	-5472.96	-5469.91	-5472.96
c	207.16	207.16	207.18	207.18
d	—	0.90	—	0.90
e	—	—	-0.01	-0.01

[a] The least-squares fit of IMME coefficients assumes every mass excess has similar uncertainty, ± 1 keV.

Table 6.2: *Mass differences and mass summations of M_{-2} and M_2; and M_1, M_{-1}, and M_0.*

	$M_{-2} - M_2$ (keV)	$M_1 - M_{-1}$ (keV)	$M_1 + M_{-1} - 2M_0$ (keV)	$M_2 + M_{-2} - 2M_0$ (keV)
Exp. values quoted in Ref. [125]	-21877.48	-10944.24	414.22	1657.26
Theoretical values in Ref. [125]:				
USD	-21669.83	-10837.25	418.11	1673.09
USDA	-21669.62	-10836.63	404.98	1653.43
USDB	-24802.19	-12402.79	417.24	1667.38
Deduced from Table A.5	-21877.48	-10944.12	414.34	1657.26
Present work[a]:				
USD	-21857.65	-10927.76	415.00	1661.46
USDA	-21858.35	-10927.30	404.55	1649.76
USDB	-21856.66	-10927.93	416.24	1664.32

[a] Present calculations use V_{coul} (UCOM) and V_0 combination.
[b] Shorthand notations for $M_{T_z=i} \equiv M_i$, $i = -2, -1, 0, 1, 2$.

Table 6.3: *Comparison of $b, c, d,$ and e coefficients of the $A = 32$, $J^\pi = 0^+, T = 2$ quintet.*

		b, c (keV)	b, c, d (keV)	b, c, e (keV)	b, c, d, e (keV)
Exp. values	b	$-5471.9\ (3)$	$-5473.1\ (3)$	$-5471.1\ (3)$	$-5473.0\ (5)$
quoted in Ref. [125]	c	$208.6\ (2)$	$207.2\ (3)$	$205.5\ (5)$	$207.1\ (6)$
	d	—	$0.93\ (12)$	—	$0.92\ (19)$
	e	—	—	$0.61\ (10)$	$0.02\ (16)$
	χ^2/n	64.282	0.005	4.525	
Theoretical values in Ref. [125]:					
USD	b	-5417.7	-5419.0	-5417.7	-5419.0
	c	209.1	209.1	209.0	209.0
	d	—	0.39	—	0.39
	e	—	—	0.03	0.03
USDA	b	-5417.6	-5418.6	-5417.7	-5418.6
	c	207.3	207.3	201.1	201.1
	d	—	0.30	—	0.30
	e	—	—	1.40	1.40
USDB	b	-6200.7	-6201.7	-6200.7	-6201.8
	c	208.4	208.4	208.7	208.7
	d	—	0.28	—	0.28
	e	—	—	-0.07	-0.07
Present work[a]:					
Exp. values	b	$-5471.7\ (3)$	$-5472.9\ (3)$	$-5471.0\ (3)$	$-5473.0\ (5)$
taken from Table A.5	c	$208.5\ (2)$	$207.2\ (3)$	$205.7\ (5)$	$207.2\ (6)$
	d	—	$0.89\ (22)$	—	$0.90\ (19)$
	e	—	—	$0.57\ (10)$	$-0.01\ (16)$
	χ^2/n	27.617	0.001	21.602	
USD	b	-5464.3	-5463.7	-5464.3	-5463.7
	c	207.7	207.7	207.4	207.4
	d	—	-0.18	—	-0.18
	e	—	—	0.06	0.06
USDA	b	-5464.4	-5463.3	-5464.4	-5463.3
	c	206.8	206.8	201.0	201.0
	d	—	-0.31	—	-0.31
	e	—	—	1.31	1.31
USDB	b	-5464.1	-5463.9	-5464.1	-5463.9
	c	208.0	208.0	208.1	208.1
	d	—	-0.07	—	-0.07
	e	—	—	-0.03	-0.03

[a] Present calculations use V_{coul} (UCOM) and V_0 combination.

Table 6.2 summarizes mass differences (or sums) of $\pm T_z$ multiplet members as obtained from experimental or theoretical mass excesses. Table 6.3 shows the values of the IMME coefficients obtained for each set of mass excesses by a least-squares fitting procedure, c.f. section 3.1. Two sets of experimental values are taken as evaluated in Ref. [125] (first entry of the tables) and from Table A.5 (fifth entry of the tables). Theoretical results correspond to two sets of calculations. In the upper parts of the tables (entries 2-4), we show the results from Ref. [125], who performed their calculations based on the parameters from Ref. [30], which used an old data set and did not include $A = 32$, on top of the USD, USDA or USDB interaction. The second set of theoretical results is our work (entries 6-8 in the lower parts of these tables). The mass differences have been obtained from the diagonalization of the presently constructed INC Hamiltonian H_{INC} using the combination of V_{coul} (with UCOM) and V_0, c.f. section 2.5.

The isobaric multiplet consists of 0^+ ground state for ^{32}Ar and ^{32}Si, the third 0^+ for ^{32}P and ^{32}Cl, and the 10th 0^+ for ^{32}S (for USDA, it is the 11th 0^+). To identify the IAS's in $T_z = 0, \pm 1$ nuclei, we calculated the corresponding Fermi matrix elements and compared it to the model independent value

$$M_{f0} = \sqrt{T(T+1) - T_z(T_z \pm 1)}\,. \tag{6.9}$$

The mass differences $(M_{T_z=-2} - M_{T_z=2})$ obtained by Ref. [125] for USD, USDA, and USDB deviate from experimental values by 207.65 keV, 207.86 keV, and 2924.71 keV, respectively. Meanwhile, the mass differences $(M_{T_z=1} - M_{T_z=-1})$ for USD, USDA, and USDB are different from experimental value by 106.99 keV, 107.57 keV, and 1458.55 keV, respectively. Consequently, the produced b coefficients deviate about ~50 keV to ~730 keV, c.f. Table 6.3. This discrepancy should be kept in mind when comparing the values of the predicted d coefficient with the experimental value.

At the same time, theoretical mass differences $(M_{T_z=-2} - M_{T_z=2})$ and $(M_{T_z=1} - M_{T_z=-1})$ obtained in the present work, are much closer to experimental values. The deviations are at most ~20 keV only. These mass differences result in a very accurate set of theoretical b coefficients, which are about ~10 keV different from the experimental b values, c.f. Table 6.3. Note that the theoretical b coefficients almost coincide with the b coefficient listed in Table B.4, which is calculated during fitting procedure (within the perturbation theory). That means, the perturbation theory used in section 2.5 provides a very good approximation to the b coefficients.

Overall the c coefficients are close to experimental values, with only an offset of ~2 keV.

Our theoretically deduced ratio of $(M_{T_z=-2} - M_{T_z=2})$ to $(M_{T_z=1} - M_{T_z=-1})$ is higher than 2, leading to a negative value of the d coefficient (see Eq.(6.7)).

Deviations of nuclear mass excesses from the best IMME fit values (with coefficients from Table 6.3) are plotted in Fig. 6.1 and Fig. 6.2, assuming a quadratic and cubic form of the IMME, respectively. These figures include different experimental data sets and two different theoretical calculations of mass excesses (Ref. [125] and present work). It is obvious that the best fit is produced by a cubic form of the IMME (Fig. 6.2). The values of d coefficients from

various experimental results and theoretical calculations are listed in Table 6.4. Both theoretical d coefficients have been calculated without error-weighted fit (which is equivalent to assuming 1 keV error on each mass excess). As is seen from Table 6.3 and the figures, the quartic IMME provides the best description of the isobaric mass quintet for $A = 32$ nuclei. The quartic IMME with $d = 0$ is worse than the cubic one.

Our empirical approach cannot identify uniquely the reason for a non-zero d. The empirical effective interaction is of a two-body type, so three- or four-body interactions are not considered explicitly in our work. Certainly, the value of d coefficient relates to the degree of the isospin-mixing in the nuclear states. The detailed study can be found in Ref. [125].

However, the uncertainty of mass measurement of ^{32}Ar may affect both experimental results and theoretical description. So, direct re-measurement of ^{32}Ar mass would shed light on the issue.
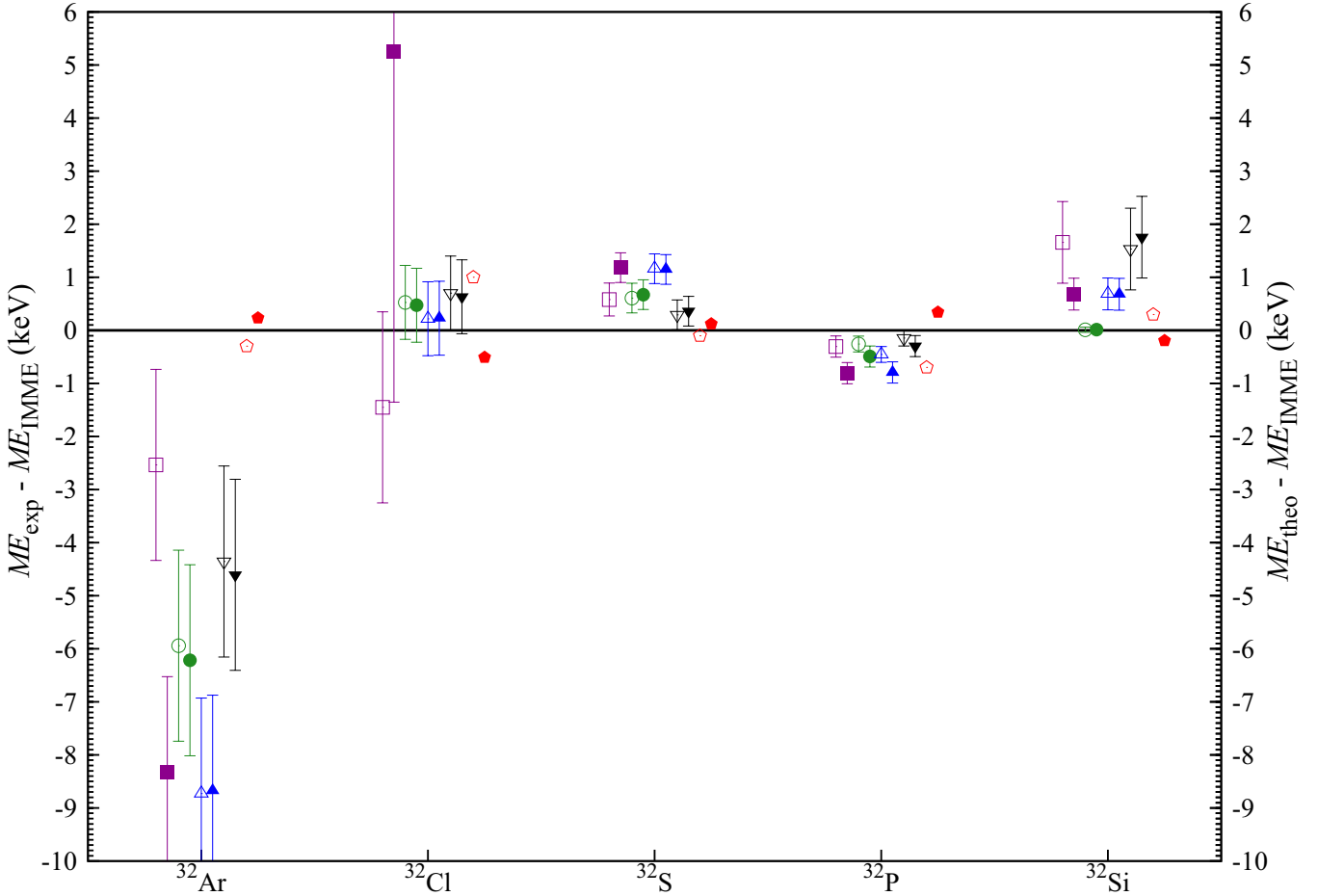
Figure 6.1: *Quadratic fit of quintet mass 32.*
(Purple) open and filled squares are quoted from Ref. [113] and Ref. [126], respectively. (Green) circles are quoted from Ref. [112], TABLE I, set A; (green) filled circles are from set B; up (blue) open and filled triangles are from set C and set D, respectively; down (black) triangles are from set E; down (black) filled triangles are from set F. The theoretical work of Signoracci and Brown [125] is presented as (red) pentagons; whereas (red) filled pentagons are present calculation. The experimental error bars are the respective mass excess error bars.
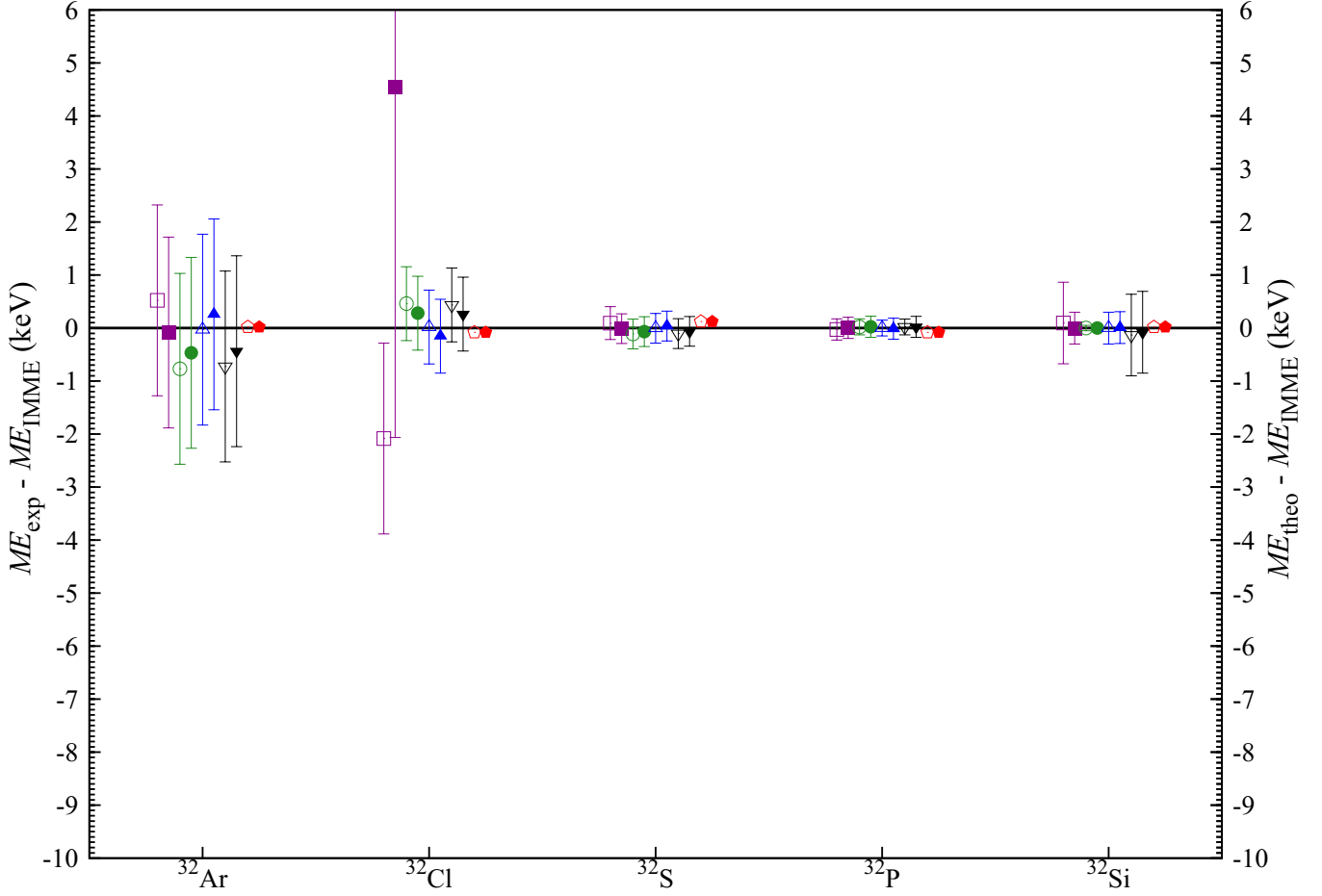
Figure 6.2: *Cubic fit of quintet mass 32.*
Please refer to Fig. 6.1 for further description.

6.3 Analysis of other sd-shell quintets

Besides the mass $A = 32$ quintets, there are four other quintets known experimentally in sd-shell nuclei, e.g. mass 20, 24, 28, and 36 listed in Table A.5. The $A = 20$ and $A = 36$ quintets must be taken with caution, because of cross shell effect. So, we concentrate our analysis on the $A = 24$ and $A = 28$ quintets. Although experimental mass excesses have a large error bar, we can still explore the predictions given by the theory.

The experimentally deduced and theoretically calculated IMME parameters are shown in Table 6.5. We notice that our calculated b and c coefficients deviate from the experimentally deduced values for $A = 28$ quintet. For this reason, we do not discuss possible d and/or e coefficients.

However, the description is very good for $A = 24$ quintet. Theoretical b and c coefficients are in very good agreement with the experimental values. The description of experimental or theoretical mass excesses with a cubic or quartic (with $d = 0$) IMME shows an unambiguous

Table 6.4: *Comparison of theoretical d coefficients with experimental values for $A = 32$ quintet.*

Experimental and Theoretical Works	d (keV)	$\frac{\chi^2}{n_{quadr.}}$	$\frac{\chi^2}{n_{cubic}}$
Triambak S. *et. al.* [113]	0.54 (16)	13.1	0.77
Kwiatkowski S. *et. al.* [126]	1.00 (9)	31	0.48
Set A from Kankainen A. *et. al.* [112]	0.52 (12)	9.9	0.86
Set B *Ibid.*	0.60 (13)	12.3	0.31
Set C *Ibid.*	0.90 (12)	28.3	0.002
Set D *Ibid.*	1.00 (13)	30.8	0.09
Set E *Ibid.*	0.51 (15)	6.5	0.74
Set F *Ibid.*	0.62 (16)	8.3	0.28
Signoracci A. & Brown B. A. [125] (USD)[a]	0.39	2.18	0.003
Present work[a]	−0.18	0.485	0.016

[a] $\frac{\chi^2}{n_{quadr.}}$ and $\frac{\chi^2}{n_{cubic}}$ for theoretical works are calculated by assuming uncertainty ±1 keV for every mass excess.

Table 6.5: *Theoretical b, c, d, and e coefficients of $T = 2$ quintets in two sd-shell nuclei.*

		b, c (keV)	b, c, d (keV)	b, c, e (keV)	b, c, d, e (keV)
$A = 24$	b	−4179.00	−4178.95	−4179.00	−4178.95
	c	224.31	224.31	219.71	219.71
	d	—	−0.02	—	−0.02
	e	—	—	1.039	1.039
		$\chi^2/n = 8.882$	$\chi^2/n = 4.439$	$\chi^2/n = 0.00076$	
$A = 28$	b	−4869.74	−4869.57	−4869.74	−4869.57
	c	216.84	216.84	204.53	204.53
	d	—	−0.05	—	−0.05
	e	—	—	2.78	2.78
		$\chi^2/n = 63.570$	$\chi^2/n = 31.767$	$\chi^2/n = 0.0070$	

[a] Present calculations use V_{coul} (UCOM) and V_0 combination.

[b] All $\frac{\chi^2}{n}$ are calculated by assuming uncertainty ±1 keV for every mass excess.

evidence for the presence of a non-zero *e*-value. The quality of the corresponding fit is much better. To check these predictions, a more precise measurement of $A = 24$ mass excesses is of high interest.

6.4 Remarks

The relationship between b and d coefficients is presented, c.f. Eq.(6.5) and Eq.(6.7). The magnitude of the d coefficient is sensitive to the INC Hamiltonian, which can be constructed from different isospin-conserving Hamiltonian e.g. USD, USDA, USDB. The existence of a non-zero d coefficient is confirmed. Most probably, the degree of isospin-mixing in nuclear states is related to the existence of d coefficient. In addition, our theoretical study shows that the e coefficient may exist in $A = 24$ and 28 quintets. More experimental proofs are needed to affirm the existence of the e coefficient. We plan to pursue the analysis of the non-diagonal Coulomb matrix elements and level splittings to explain the existence of d and e coefficients.

Chapter 7

Corrections to Superallowed $0^+ \rightarrow 0^+$ beta Decay

Contents

With the INC Hamiltonian, we perform theoretical calculations of isospin-mixing corrections to the experimental ft values for $0^+ \rightarrow 0^+$ β-transitions. Although the isospin-mixing corrections are just around ~0.01% to ~0.1%, after summing up all corrections, we see noticeable changes to the absolute $\mathscr{F}t$ values compared to the previous results. The determination of the Cabibbo-Kobayashi-Maskawa (CKM) matrix element V_{ud} is reviewed with this new isospin-mixing correction.

7.1 CKM Quark-Mixing Matrix

In the Standard Model, the leptons and quarks are grouped in generations. The charge-0 and charge--1 lepton fields and charge-$\frac{2}{3}$ and charge-$-\frac{1}{3}$ quark fields are written as

$$
\begin{aligned}
\nu_h &= (\nu_h^i) = \left(\nu_{e,h}\ \nu_{\mu,h}\ \nu_{\tau,h}\ \ldots\right), \\
l_h &= (l_h^i) = \left(e_h\ \mu_h\ \tau_h \ldots\right), \\
u_h &= (u_h^i) = \left(u_h\ c_h\ t_h\ \ldots\right), \\
d_h &= (d_h^i) = \left(d_h\ s_h\ b_h\ \ldots\right).
\end{aligned}
\tag{7.1}
$$

The subscript h is the helicity (L or R) and the superscript i is the generation. For instance, the helicity-projected electron states are $e_R = \frac{1}{2}(1 + \gamma^5)$ and $e_L = \frac{1}{2}(1 - \gamma^5)$. However, in the Standard Model, neutrinos are assumed as massless and only left-handed neutrinos exist.

The quark states in Eq.(7.1) are physically observed mass eigenstates of the Hamiltonian. However, in the charge-changing weak interaction, the other set of basis states called weak eigenstates (indicated with a prime) operates in the interaction. The mass eigenstates are a linear combination of weak eigenstates via a unitary transformation

$$
\begin{aligned}
u_h^j &= \sum_k (\mathbf{U}_h^u)_{jk} u_h'^k, \\
d_h^j &= \sum_k (\mathbf{U}_h^d)_{jk} d_h'^k.
\end{aligned}
\tag{7.2}
$$

The unitary matrices $\mathbf{U}_h^u$ and $\mathbf{U}_h^d$ have dimension $n \times n$, and n denotes the number of generations. The charge-changing weak interaction is mediated by the W gauge bosons, $W_\pm^\mu$, $+$ and $-$ show charge-raising and charge-lowering fields, respectively; and they are conjugate to each other, $(W_-^\mu)^\dagger = W_+^\mu$. The charge-changing Lagrangian of the Standard Model is given as

$$
\mathscr{L}_{cc} = -\frac{g}{\sqrt{2}} \sum_j \left(\overline{u}_L'^j \gamma_\mu d_L'^j + \overline{\nu}_L^j \gamma_\mu l_L^j \right) W_+^\mu +\ \text{h.c.}\ ,
\tag{7.3}
$$

where g is the coupling constant, and the charge-lowering field is implicitly contained in the hermitian conjugate (h.c.). Eq.(7.4) can be rewritten in terms of mass eigenstates

$$
\mathscr{L}_{cc} = -\frac{g}{\sqrt{2}} \sum_{jkm} \left(\overline{u}_L^k \gamma_\mu (\mathbf{U}_L^u)_{kj} (\mathbf{U}_L^d)_{jm}^\dagger d_L^m + \overline{\nu}_L^j \gamma_\mu l_L^j \right) W_+^\mu +\ \text{h.c.}\ .
\tag{7.4}
$$

Defining

$$
\begin{aligned}
V &= \mathbf{U}_L^u (\mathbf{U}_L^d)^\dagger\ , \text{ and} \\
V_{km} &= \sum_j (\mathbf{U}_L^u)_{kj} (\mathbf{U}_L^d)_{jm}^\dagger,
\end{aligned}
\tag{7.5}
$$

the matrix V is an $n \times n$ unitary matrix, and n denotes the number of families of quarks. It is characterized by n^2 independent real parameters. Due to orthogonal properties, $n \times n$ matrix will have $n(n-1)/2$ independent rotation angles and $\frac{1}{2}(n-1)(n-2)$ independent phases.

If there were only two families of quarks, there would be only one independent rotation angle (Cabibbo angle θ_c) describing the quark-mixing, and all phases of the mixing matrix can be absorbed through field redefinition, thus, no independent phase survives. The matrix V is real. Inserting V into Eq.(7.4), the $\mathscr{L}_{cc}$ is

$$\mathscr{L}_{cc} = -\frac{g}{\sqrt{2}} \left(\overline{u}_L \ \overline{c}_L \right) \gamma_\mu \begin{pmatrix} \cos\theta_c & \sin\theta_c \\ \text{-}\sin\theta_c & \cos\theta_c \end{pmatrix} \begin{pmatrix} d_L \\ s_L \end{pmatrix} W_+^\mu + \text{ h.c. .} \qquad (7.6)$$

and it is invariant under CP transformations [129].

Kobayashi and Maskawa proposed the existence of the third generation of quarks [130]. Hence, three independent rotation angles and six independent phases are expected in V. As in the Lagrangian, V resides between the u-type quark fields and d-type quark fields, five of the six independent phases can be absorbed. Thus six quarks will carry five physically relevant phases. After absorbing that five phases, the matrix V contains only one complex phase as the CP violating complex phase of the electroweak sector. The Lagrangian $\mathscr{L}_{cc}$ can be rewritten as

$$\mathscr{L}_{cc} = -\frac{g}{\sqrt{2}} \left(\overline{u}_L \ \overline{c}_L \ \overline{t}_L \right) \gamma_\mu \begin{pmatrix} V_{ud} & V_{us} & V_{ub} \\ V_{cd} & V_{cs} & V_{cb} \\ V_{td} & V_{ts} & V_{tb} \end{pmatrix} \begin{pmatrix} d_L \\ s_L \\ b_L \end{pmatrix} W_+^\mu + \text{ h.c. .} \qquad (7.7)$$

The matrix V is the renowned Cabibbo-Kobayashi-Maskawa matrix, which is the three generations quark-mixing matrix. In Kobayashi's and Maskawa's original article [130], V was written in terms of three angles, $\theta_1, \theta_2, \theta_3$, and the phase, δ as below,

$$V = \begin{pmatrix} \cos\theta_1 & -\sin\theta_1\cos\theta_3 & -\sin\theta_1\sin\theta_3 \\ \sin\theta_1\cos\theta_2 & \cos\theta_1\cos\theta_2\cos\theta_3 - \sin\theta_2\sin\theta_3 e^{i\delta} & \cos\theta_1\cos\theta_2\sin\theta_3 + \sin\theta_2\cos\theta_3 e^{i\delta} \\ \sin\theta_1\sin\theta_2 & \cos\theta_1\sin\theta_2\cos\theta_3 + \cos\theta_2\sin\theta_3 e^{i\delta} & \cos\theta_1\sin\theta_2\sin\theta_3 - \cos\theta_2\cos\theta_3 e^{i\delta} \end{pmatrix} . \quad (7.8)$$

However, the matrix V can also be written as

$$V_{CKM} = \begin{pmatrix} V_{ud} & V_{us} & V_{ub} \\ V_{cd} & V_{cs} & V_{cb} \\ V_{td} & V_{ts} & V_{tb} \end{pmatrix} , \qquad (7.9)$$

or

$$V = \begin{pmatrix} c_{12}c_{13} & s_{12}c_{13} & s_{13}e^{-i\delta_{13}} \\ -s_{12}c_{23} - c_{12}s_{23}s_{13}e^{i\delta_{13}} & c_{12}c_{23} - s_{12}s_{23}s_{13}e^{i\delta_{13}} & s_{23}c_{13} \\ s_{12}s_{23} - c_{12}c_{23}s_{13}e^{i\delta_{13}} & -c_{12}s_{23} - s_{12}c_{23}s_{13}e^{i\delta_{13}} & c_{23}c_{13} \end{pmatrix} , \qquad (7.10)$$

with $V_{us} \approx \sin\theta_c \approx 0.22$, θ_c is the Cabibbo angle, and $V_{ud} \approx 0.97$ [1]; whereas $s_{ij} = \sin\theta_{ij}$ and $c_{ij} = \cos\theta_{ij}$ with Euler angles θ_{ij} (i and j label quark families). These three forms are physically equivalent, as well as the other form proposed by Wolfenstein which parameterizes the relative magnitudes of the different elements [131, 132],

$$V = \begin{pmatrix} 1 - \frac{\lambda^2}{2} - \frac{\lambda^4}{8} & \lambda & A\lambda^3(\rho - i\eta) \\ -\lambda + \frac{A^2\lambda^5}{2}\left[1 - 2(\rho + i\eta)\right] & 1 - \frac{\lambda^2}{2} - \frac{\lambda^4}{8}(1 + 4A^2) & A\lambda^2 \\ A\lambda^3 \left\{ 1 - \left[1 - \frac{\lambda^2}{2}\right](\rho + i\eta) \right\} & -A\lambda^2 + \frac{A\lambda^4}{2}\left[1 - 2(\rho + i\eta)\right] & 1 - \frac{A\lambda^4}{2} \end{pmatrix} , \qquad (7.11)$$

with neglecting terms of $O(\lambda^6)$, $V_{us} = s_{12}c_{13} = \lambda \approx \sin\theta_c$, $V_{ub} = s_{13}e^{-i\gamma} = A\lambda^3(\rho - i\eta)$, $V_{cb} = s_{23}c_{13} = A\lambda^2$. The unitarity of the CKM matrix in the form proposed by Wolfenstein is evident to the order λ^3. Despite different forms of the CKM matrix, the mixing between the first two families is approximated by the Cabibbo angle, whereas that between the second and third, and the first and third families is of the order of the square and cube of the angle respectively. In addition, the phase may be represented and may exist in different elements of those matrices. However, those matrices are physically equivalent as interference of CP conserving amplitude and CP violating amplitude will reveal all physically observable measurements. Those amplitudes of any process will consist of more than one term involving various CKM elements, whereby the phase, even though located differently in different conventions, will show up identically through interference terms.

The CKM matrix can be tested either on its orthogonality or on its normalization of rows and columns. The description of the first testing approach can be found in Ref. [129]. We use the latter approach to test the CKM matrix.

7.2 Unitarity Test on CKM Matrix – Test the Normalization of rows and columns

Although the Standard Model does not specify the values of the CKM matrix elements, it dictates that the CKM matrix must be unitary. The normalization test of the CKM matrix does not verify the CP violating phase, however, the test is less complicated than orthogonality one. Six constraints read as

$$\sum_j V_{ij}V_{ji}^\dagger = \sum_j |V_{ij}|^2 = 1\,,$$
$$\sum_i V_{ji}V_{ij}^\dagger = \sum_i |V_{ij}|^2 = 1\,, \tag{7.12}$$

and these constraints seek for either a row or a column of the measured CKM matrix elements. As the contribution from the third quark family to $|V_{ub}|^2$ is insignificant, of the order of λ^6, c.f. Eq.(7.11), the first column or the first row of CKM matrix is the easiest to be tested. Nowadays, the consequence of experimental advances in measuring mass excess and decay rates allow us to have the best precision for the top row of CKM matrix,

$$|V_{ud}|^2 + |V_{us}|^2 + |V_{ub}|^2 = 1\,. \tag{7.13}$$

7.3 Corrected ft Values

The nuclear β-decay is one of the examples of a baryon decaying into another baryon in a nuclear medium, with the emission of two leptons. The β-decay rate, Γ [17], can be expressed as

$$\Gamma = \frac{1}{\tau} = \frac{\ln 2}{t} = \frac{G_F^2 g_V^2 m_e^5}{2\pi^3} V_{ud}^2 \left(f_V |M_F^0|^2 + f_A \lambda^2 |M_{GT}^0|^2 \right) , \qquad (7.14)$$

where τ is the mean life time, G_F is the fundamental weak interaction coupling constant, g_V is the vector coupling constant, m_e is the electron mass, V_{ud} is the upper-left CKM matrix elements, f_V is the phase-space integral for Fermi transitions, f_A is the phase-space integral for Gamow-Teller transitions, M_F and M_{GT} are the Fermi and Gamow-Teller matrix elements, respectively. The superallowed $0^+ \to 0^+$ β-decay is purely vector, therefore, the decay rate is characterized by the Fermi matrix element only $\left(|M_{GT}^0|^2 = 0 \right)$. If the isospin symmetry holds, the Fermi matrix element has a model-independent value

$$\left| M_F^0 \right|^2 = T(T+1) - T_z(T_z \pm 1) . \qquad (7.15)$$

This value should be corrected for possible ISB in nuclear states. Then, formally, we can express the corrected Fermi matrix element as

$$|M_F|^2 = \left| M_F^0 \right|^2 (1 - \delta_C) , \qquad (7.16)$$

where δ_C is the correction.

Besides δ_C, a decay process should be corrected for radiative effects. The radiative correction is usually divided into two parts, a nucleus-dependent part, δ_R, and a nucleus-independent part, Δ_R^V. δ_R can be in turn separated into two terms: δ_{NS}, which needs a detailed nuclear structure calculation, and δ'_R, which depends on Z and the maximum total electron energy of the transition only.

In practice, the β-decay is characterized by ft-values. From the measured half-lives, branching ratio and Q-values, one can extract an ft-value of a given transition. Starting from Eq.(7.14) and imposing nuclear structure and radiative corrections, one can extract the absolute $\mathcal{F}t$ value for a superallowed $0^+ \to 0^+$ beta decay as [17]

$$\mathcal{F}t = ft(1 + \delta'_R)(1 + \delta_{NS} - \delta_C) = \frac{K}{G_F^2 g_V^2} \times \frac{1}{V_{ud}^2} \times \frac{1}{|M_F^0|^2(1 + \Delta_R^V)} , \qquad (7.17)$$

where

$$K = \frac{2\pi^3 \ln 2}{m_e^5} , \quad \frac{K}{(\hbar c)^6} = \frac{2\pi^3 \hbar \ln 2}{(m_e c^2)^5} = 8120.2787(11) \times 10^{-10} \mathrm{GeV}^{-4}\mathrm{s} . \qquad (7.18)$$

The subscript V at the phase-space integral for Fermi transitions is dropped.

The constancy of the absolute $\mathscr{F}t$ value of superallowed $0^+ \to 0^+$ β transitions would validate the conserved vector current (CVC) hypothesis. Provided the CVC holds, the V_{ud} CKM matrix element can be extracted and used to test the unitarity of the CKM matrix. The nuclear structure correction (δ_C) due to the ISB in nuclear states is the one which provides the largest uncertainty to the unitarity test.

7.4   Isospin-Mixing Correction and Fermi β-decay

The common feature of the shell-model approaches is that the transition matrix elements calculated within the isospin-symmetry breaking scheme is divided into two parts. First, there is a contribution from the ISB effects in the configuration mixing of the spherical harmonic-oscillator basis functions. This is obtained via the diagonalization of an effective Hamiltonian which does not conserve the isospin. The parameters can be adjusted to describe experimental splittings of isobaric multiplets. Second, in the calculation of transition rates one has to change the harmonic-oscillator single-particle wave functions to realistic spherically-symmetric wave functions obtained from a better suited finite-well plus Coulomb potential (to account for the isospin nonconservation outside the model space).

Within the shell model, the Fermi matrix element for the transition between the initial state $|i\rangle$ and the final state $|f\rangle$ has a form

$$M_F = \langle f| \, T_+ \, |i\rangle = \sum_\alpha \langle f| \, a_\alpha^\dagger b_\alpha \, |i\rangle = \sum_{\alpha\theta} \langle f| \, a_\alpha^\dagger \, |\theta\rangle \, \langle\theta| \, b_\alpha \, |i\rangle \;, \tag{7.19}$$

where $a_\alpha^\dagger$ creates a neutron (b_α annihilates a proton) in a state with quantum numbers α, and $|\theta\rangle$ represents the complete set of states in $(A-1)$ nucleus. If a Hamiltonian obeys Eq.(1.15), then

$$\langle f| \, a_\alpha^\dagger \, |\theta\rangle^* = \langle\theta| \, b_\alpha \, |i\rangle \;, \tag{7.20}$$

states $|i\rangle$ and $|f\rangle$ are isospin analogues, and the Fermi matrix element is

$$M_F^0 = \sum_{\alpha\theta} | \, \langle f| \, a_\alpha^\dagger \, |\theta\rangle \, |^2 \,. \tag{7.21}$$

As the INC Hamiltonian does not commute with the isospin operators, then $|i\rangle$ and $|f\rangle$ are not isospin analogue, and a correction for M_F^0 in Eq.(7.16) is proposed. Besides, the δ_C can be represented as a sum of (i) the isospin-mixing correction δ_{IM}, and (ii) the radial overlap correction δ_{RO} [17],

$$\delta_C = \delta_{IM} + \delta_{RO} \,. \tag{7.22}$$

The δ_{IM} does not include corrections from nodal mixing

$$\sum_{\alpha\beta\theta} \langle \overline{f}| \, a_\alpha^\dagger \, |\theta\rangle \, \langle\theta| \, a_\beta \, |\overline{i}\rangle = M_F^0 \sqrt{1 - \delta_{IM}} \,, \tag{7.23}$$

where $|\bar{i}\rangle$ and $|\bar{f}\rangle$ are not the exact eigenstates in Eq.(7.21). They are the shell-model eigenstates of INC Hamiltonian. Meanwhile, the δ_{RO} include corrections from nodal mixing for M_F^0

$$\sum_{\alpha\theta} \left| \langle \bar{f} | a_\alpha^\dagger | \theta \rangle \right|^2 r_\alpha^\theta = M_F^0 \sqrt{1 - \delta_{RO}} \,, \tag{7.24}$$

where every r_α^θ is a radial overlap integral of proton and neutron radial functions. If the proton and neutron radial functions are similar, $r_\alpha^\theta = 1$ and $\delta_{RO} = 0$. Contrary, non-identical radial functions of both nucleons yield proton radial functions $\psi^p(r)$ expanded in terms of a complete set of neutron radial functions $\psi^n(r)$

$$\psi^p(r) = \sum_N a_N \psi_N^n(r) \,, \tag{7.25}$$

where N are all possible radial nodes, and a_N describes the ISB correction δ_{RO}.

We have calculated the contribution to δ_C from configuration mixing of the shell-model basis states, referred as δ_{C1} in [32] or δ_{IM} in [133], see Table 7.1. Discrepancies between the present results and those from the previous work [32, 133] may be ascribed to different fitting strategies and updated values of experimental IMME b and c coefficients. The difference between our method and that of Ref. [133] was already noted before. The authors of Ref. [32] adjusted strength parameters locally for each multiplet under consideration (case by case).

7.5 The Determination of V_{ud}

According to the CVC, $g_V = 1$, and the experimental ft value of superallowed β-decay can be directly related to the fundamental weak-interaction coupling constant, G_F. The best experimentally studied cases incorporate only $T = 1$ emitters, for which the model independent Fermi matrix element equals to $\sqrt{2}$. Then Eq.(7.17) can be further simplified to

$$\mathscr{F}t = ft(1 + \delta_R')(1 + \delta_{NS} - [\delta_{IM} + \delta_{RO}]) = \frac{K}{G_F^2 V_{ud}^2} \times \frac{1}{2(1 + \Delta_R^V)} \,. \tag{7.26}$$

From δ_{IM} values calculated with different parametrizations of the INC Hamiltonian for sd-shell nuclei (Table 7.1), we have calculated the average values with error bars corresponding to the standard deviations (see Table 7.2). Using these new average δ_{IM} corrections and the other corrections from Ref. [17], we propose new $\mathscr{F}t$ values for four well known emitters from sd-shell. These values are given in Table 7.2 in comparison with the values obtained by Towner and Hardy [17]. We notice non-negligible changes of the $\mathscr{F}t$ values of ^{34}Cl and ^{34}Ar. Experimental ft-values of the best emitters and theoretically corrected $\mathscr{F}t$ values (for sd shell nuclei we have implemented the results of the present work) are shown in Fig. 7.1.

Table 7.1: δ_{IM} *calculated from INC nuclear Hamiltonian of combination with* $V_{coul} + V_0$.

Nuclear Hamiltonian	Parent Nucleus	Present Work				Previous Work	
		UCOM[a]	Jastrow type SRC function			Ormand & Brown[b]	Towner & Hardy[c]
			Argonne V18[a]	CD-Bonn[a]	Miller Spencer[a]		
USD							
	^{22}Mg	0.025	0.024	0.024	0.026	0.017[d]	0.010 (10)
	^{26m}Al	0.016	0.016	0.015	0.017	0.01[b]	0.025 (10)
	^{26}Si	0.053	0.053	0.052	0.053	0.028[d]	0.022 (10)
	^{30}S	0.024	0.023	0.022	0.026	0.056[d]	0.137 (20)
	^{34}Cl	0.031	0.030	0.030	0.030	0.06[b]	0.091 (10)
	^{34}Ar	0.007	0.007	0.007	0.008	0.008[d]	0.023 (10)
USDA							
	^{22}Mg	0.025	0.024	0.023	0.027		
	^{26m}Al	0.016	0.016	0.015	0.019		
	^{26}Si	0.047	0.047	0.046	0.049		
	^{30}S	0.019	0.018	0.017	0.021		
	^{34}Cl	0.028	0.027	0.027	0.028		
	^{34}Ar	0.007	0.007	0.007	0.008		
USDB							
	^{22}Mg	0.025	0.025	0.024	0.027		
	^{26m}Al	0.017	0.017	0.016	0.019		
	^{26}Si	0.051	0.050	0.050	0.053		
	^{30}S	0.023	0.022	0.021	0.025		
	^{34}Cl	0.031	0.030	0.030	0.030		
	^{34}Ar	0.006	0.007	0.006	0.007		

[a] Strength parameters are implemented from Table 4.3, *Range I* (full *sd*-shell).
[b] δ_{IM} in TABLE I. of Ref. [133].
[c] Unscaled δ_{C1} in TABLE III. of Ref. [32].
[d] In present work, we calculated without truncation, with Miller-Spencer parameterized Jastrow type SRC function, $[1 + f(r)]^2$, and with strength parameters from [30].

Table 7.2: δ_{IM} *calculated with strength parameters fitted from full sd-shell space.*

Parent Nucleus	Exp. ft^c	Corrections (%)				$\mathscr{F}t$ values	
		$\delta_{IM}{}^a$	$\delta_{RO}{}^b$	$\delta'_R{}^b$	$\delta_{NS}{}^b$	Present work[a]	Towner & Hardy[c]
^{22}Mg	3052 (7)	0.0244 (11)	0.370 (20)	1.466 (17)	−0.225 (20)	3077.6 (72)	3078.0 (74)
^{26}Al^m	3036.9 (9)	0.0148 (10)	0.280 (15)	1.478 (20)	0.005 (20)	3072.9 (14)	3072.4 (14)
^{34}Cl	3049.4 (12)	0.0313 (3)	0.550 (45)	1.443 (32)	−0.085 (15)	3072.8 (22)	3070.6 (21)
^{34}Ar	3053 (8)	0.0070 (4)	0.635 (55)	1.412 (35)	−0.180 (15)	3070.7 (84)	3069.6 (85)

[a] Present calculations with V_{coul} and V_0 (USD). The error bars are provided from the standard deviation based on different SRC schemes.
[b] Table II, V, VI in Ref. [32].
[c] Table 4 in Ref. [17].
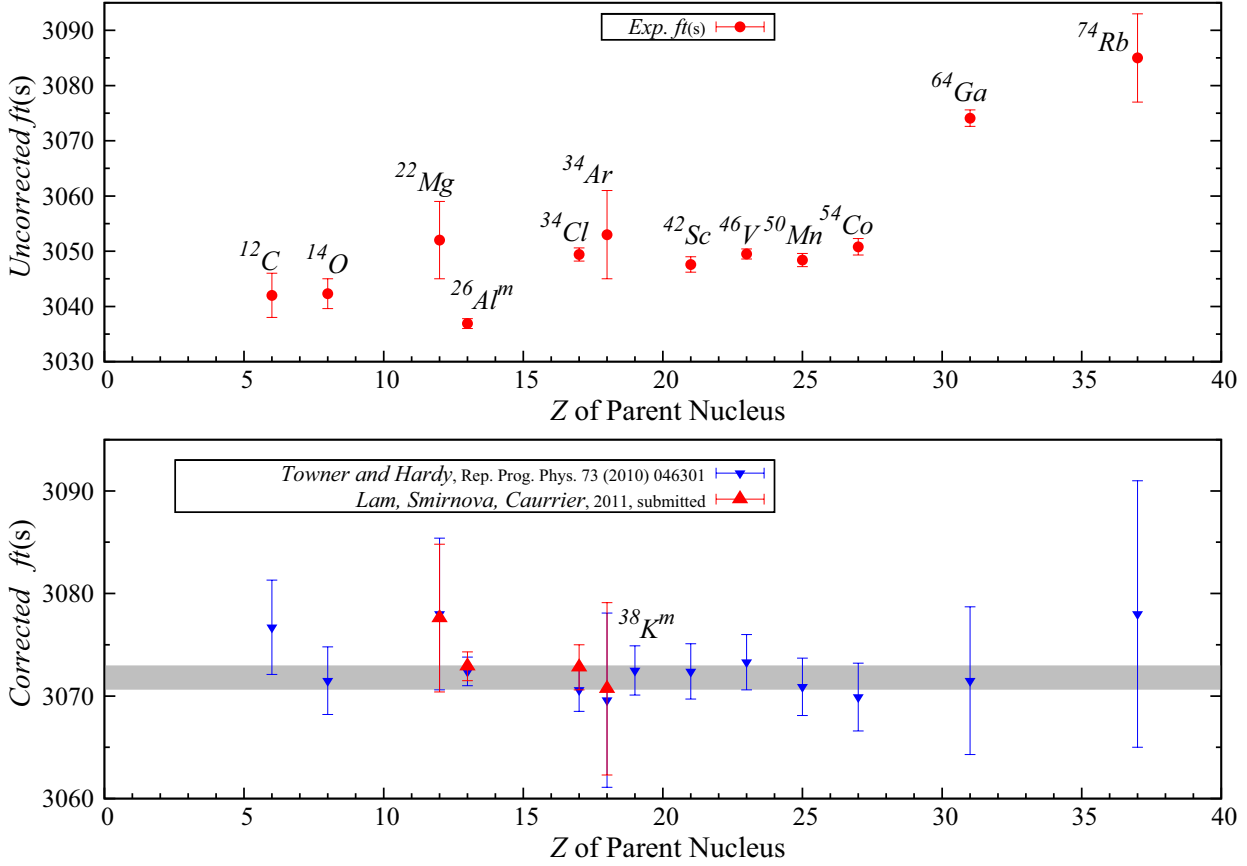
Figure 7.1: *Experimental ft values, and comparison of corrected ft values (or $\mathscr{F}t$ values).*
The upper figure depicts experimental ft values, but the ft value of $^{38}K^m$, 5051.9($\pm$0.1)s, is not feasible to be shown. The lower figure shows $\mathscr{F}t$ values. Up (red) triangles are $\mathscr{F}t$ values with present calculated δ_{IM}. Down (blue) triangles are $\mathscr{F}t$ values from Ref. [17]. Horizontal (grey) strip is 1 standard deviation value.

As a result, we obtain a new averaged $\overline{\mathscr{F}t}$ value

$$\overline{\mathscr{F}t} = 3073.12\,(63)\ \text{s}$$

and a new value of the corresponding $|V_{ud}|$ matrix element:

$$|V_{ud}|^2 = \frac{K}{2G_F^2(1+\Delta_R^V)\overline{\mathscr{F}t}} = \frac{2915.64 \pm 1.08}{\overline{\mathscr{F}t}}\,,$$

$$\frac{G_F}{(\hbar c)^3} = (1.16637 \pm 0.00001) \times 10^{-5}\ \text{GeV}^{-2}\ [1]\ ,$$

$$|V_{ud}|^2 = 0.94875 \pm 0.00041\,,$$

$$|V_{ud}| = 0.97404 \pm 0.00021\,. \tag{7.27}$$

The value of $|V_{us}|$ is 0.22521 ± 0.00094, and the value of $|V_{ub}|$ is $(3.93 \pm 0.36) \times 10^{-3}$ [17]. Finally, the unitarity of the first row of the CKM matrix,

$$|V_{ud}|^2 + |V_{us}|^2 + |V_{ub}|^2 = 0.99949 \pm 0.00059\,, \tag{7.28}$$

which shows the satisfactory of the unitarity test with a precision of 0.06%.

133

7.6 Remarks

Towner's and Hardy's unitary test has the result $|V_{ud}|^2 + |V_{us}|^2 + |V_{ub}|^2 = 0.99999 \pm 0.00060$. The present δ_{IM} calculation is not based on case by case treatment of strength parameters $\lambda_\nu^{(q)}$ and the theoretical values are not scaled by a factor of $(\Delta E)^2_{theo}/(\Delta E)^2_{exp}$, where ΔE denotes the energy separation of the analogue and non-analogue states [32]. However, the quantitative implication of the present INC Hamiltonian to the unitary test of CKM quark-mixing matrix is noticeable. Besides, various SRC approaches lead to very close values of δ_{IM}, c.f. Table 7.1. We keep the calculation of radial overlap correction δ_{RO} in perspective.

Chapter 8

Isospin-Forbidden Proton Emission

Contents

A β-delayed proton is emitted from the IAS populated in a β-decay of a parent nucleus (precursor). The process goes via the isospin-symmetry breaking and thus, to describe the proton branching ratios, we need an INC Hamiltonian. This is also one of the applications, as well as also a test for the newly constructed INC Hamiltonians. The decay of ^{22}Al to ^{22}Mg, then to ^{21}Na is our example in this thesis. Comparison between presently calculated spectroscopic factors of the decay of ^{22}Mg to ^{21}Na with Brown's results [33] is presented.

8.1 Introduction

Proton-rich nuclei manifest exotic decay modes, such as direct proton or di-proton emission, as well as β-delayed multi-particle emission. In a β-delayed process, a precursor experiences the superallowed β-decay to the IAS in a daugther nucleus, followed by (typically isospin-forbidden) multi-particle decay of the IAS. However, the topic of multi-particle decay is beyond the scope of the thesis. In this chapter we focus only on the discussion of the isospin-forbidden proton emission.

A partial decay scheme of ^{22}Al is given in Fig. 8.1. The β^+-decay of the parent nucleus $^{22}_{13}$Al with isospin $T = 2$ populates the states of the daughter nucleus $^{22}_{12}$Mg lying in the Q-window. Among those mainly Gamow-Teller transitions, there is a superallowed decay (Fermi/Gamow-Teller mixed) to the 4^+ $(T = 2)$ state (the analogue state of the ^{22}Al ground state). This state lies at about 14.04 MeV excitation energy in $^{22}_{12}$Mg and it is unbound to many decay channels — proton emission, di-proton emission, α-emission (the latter decays are not shown in the figure). The IAS can be easily identified experimentally.

8.2 Spectroscopic Factors

The (multi)-particle emission from the IAS turns out to be isospin forbidden (e.g. of ^{22}Al). In this work we consider the emission of a proton from a $T = 2$ IAS which populates $(A-1, Z-2, T-\frac{3}{2})$ states. Since $\Delta T = 3/2$, the decay proceeds via the isospin symmetry breaking in the initial and/or final states. To describe the decay modes of the IAS, we need isospin-mixed nuclear wave functions obtained from an INC Hamiltonian.

A probability for a nucleon emission is characterized by the so-called spectroscopic factors defined for a nucleon removal as

$$\theta_{if}^2(nlj) = \frac{1}{2J+1}\langle\Psi_f^{A-1}(J')||a_{nlj}||\Psi_i^A(J)\rangle^2\,, \tag{8.1}$$

where $|\Psi_i^A(J)\rangle$ is an initial state in mass-A nucleus, characterized by the total angular momentum J, where $|\Psi_f^{A-1}(J')\rangle$ is a final state in mass-$(A - 1)$ nucleus, characterized by the total angular momentum J', a_{nlj} is the nucleon annihilation operator. From the angular momentum selection rule, $\vec{J'} = \vec{j} + \vec{J}$.

The initial state in ^{22}Mg and the final states in ^{21}Na have been calculated from the INC Hamiltonian developed in this thesis (the USD interaction supplemented by the V_{coul} with different types of the SRC and without SRC as well and V_0 as charge-dependent terms). The spectroscopic factors, θ^2, calculated for a proton emission from the 4^+ IAS of ^{22}Mg to the low-lying states in ^{21}Na are summarized in Table 8.1. The results for $d_{5/2}$ and $d_{3/2}$ are summed together to produce a spectroscopic factor for an $l = 2$-transfer.

We can notice an overall enhancement of the θ^2 obtained in this work compared to the previous results [33], especially, for the transitions to the lowest $7/2^+$, $9/2^+$ and $11/2^+$ states. This is due to a slightly higher degree of impurity of the IAS predicted by the new Hamiltonian. The values of the spectroscopic factors come out to be very sensitive to subtle details of the ISB part of the Hamiltonian. As a next step of this study, we plan to calculate the branching ratios for the proton emission to compare with the experimental results. The case of the proton emission may serve as a stringent test for the INC parametrization. More results will be published in Ref. [134].

Table 8.1: *Calculated spectroscopic factors θ^2 for isospin-forbidden proton decay from 4^+, T=2, IAS state in ^{22}Mg to states in ^{21}Na.*

J^π	$10^4\theta^2$												
	Present Work[a]										Previous Work	
	UCOM		Jastrow type SRC function						w/o SRC		Brown [33]	
			Argonne V18		CD-Bonn		Miller-Spencer					
	$l=0$	$l=2$	$l=0$	$l=2$	$l=0$	$l=2$	$l=0$	$l=2$	$l=0$	$l=2$	$l=0$	$l=2$
$\frac{3}{2}^+$		0.08		0.08		0.08		0.08		0.08		0.13
$\frac{5}{2}^+$		0.38		0.37		0.35		0.47		0.35		0.18
$\frac{7}{2}^+$	0.00	7.30	0.00	7.01	0.01	6.22	0.00	9.88	0.01	6.20	0.04	1.71
$\frac{9}{2}^+$	0.00	6.31	0.00	5.76	0.00	4.77	0.00	9.93	0.00	4.85	0.09	0.56
$\frac{13}{2}^+$		1.03		0.98		0.85		1.48		0.84		0.03
$\frac{5}{2}^+$		0.92		0.82		0.52		2.16		0.50		0.24
$\frac{11}{2}^+$		6.12		5.49		4.21		10.67		4.27		1.22
$\frac{5}{2}^+$		1.43		1.18		0.84		3.04		0.89		1.34
$\frac{3}{2}^+$		0.17		0.20		0.22		0.12		0.21		0.49
$\frac{7}{2}^+$	0.34	1.18	0.31	1.06	0.30	0.66	0.40	2.51	0.32	0.65	0.00	0.11
$\frac{3}{2}^+$		0.27		0.25		0.22		0.40		0.23		0.07
$\frac{13}{2}^+$		1.66		1.60		1.42		2.17		1.42		0.78
$\frac{9}{2}^+$	1.28	0.35	1.27	0.32	1.13	0.27	1.62	0.47	1.11	0.27	0.10	0.07
$\frac{9}{2}^+$	0.76	7.99	0.84	7.96	0.82	7.33	0.79	10.02	0.76	7.17	2.29	5.69
$\frac{7}{2}^+$	1.49	16.41	1.43	16.50	1.20	15.24	2.22	20.27	1.18	14.81	0.40	11.90

[a] Present calculations use V_{coul} (UCOM) and V_0 combination.
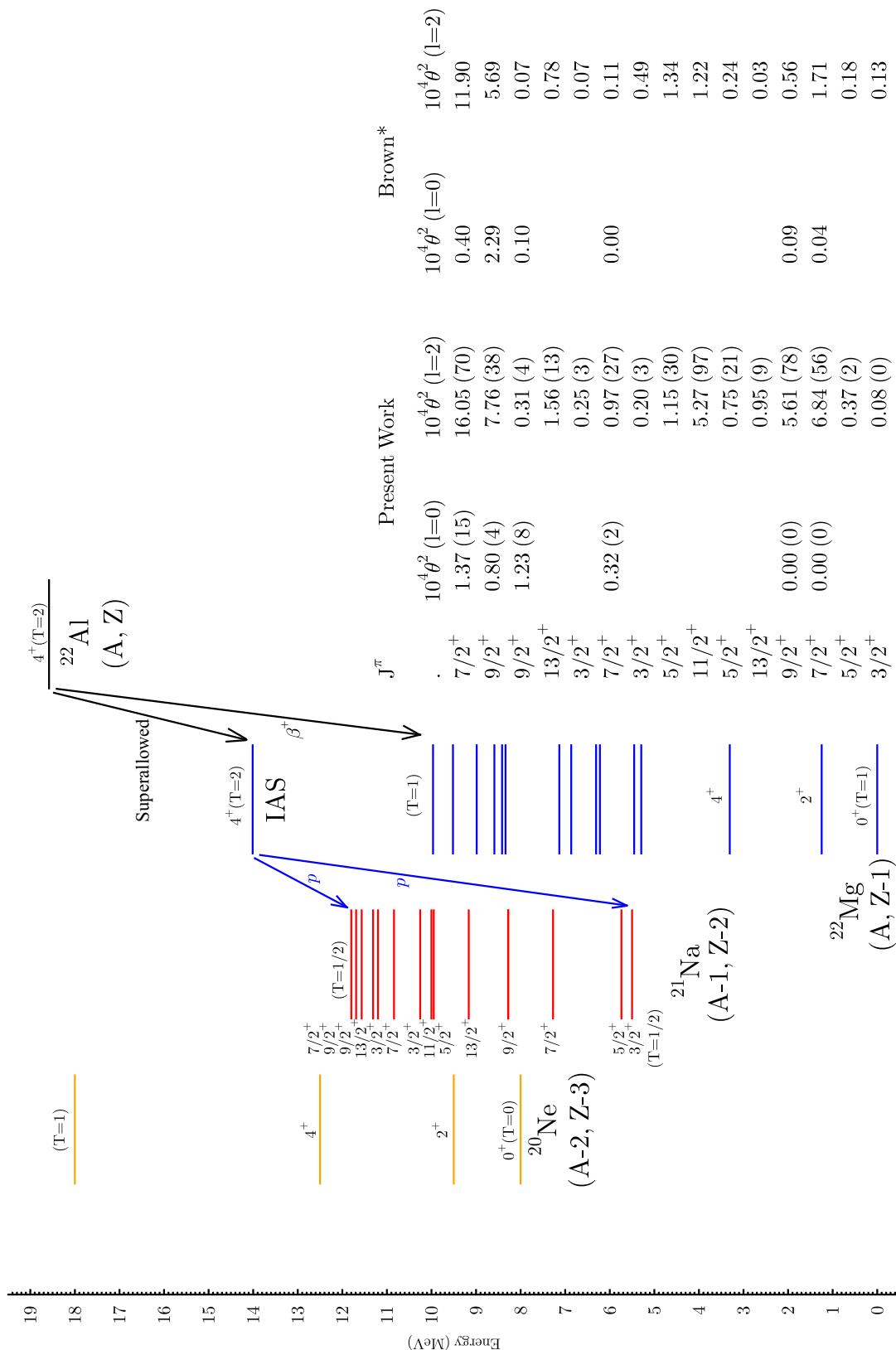
Figure 8.1: *Partial decay scheme of ^{22}Al. Comparison of present calculation with* Ref. [33].

The isospin-forbidden proton spectroscopic factors are calculated with INC Hamiltonian fitted from various SRCs. The θ^2 are averaged values calculated from each SRC, i.e., UCOM, CD-Bonn and AV18.

Appendices

Appendices

Appendix A

Coefficients of the Isobaric Multiplet Mass Equation

A.1 Notation

Readers may refer to Table A.1 to improve the readability of the following tables in this Appendix.

Table A.1: *Notations for* Tables A.2, A.3, A.4, A.5.

Notations	Description
T	Isobaric spin, or isospin, or isotopic spin.
T_z	Isospin projection, $\frac{N-Z}{2}$, where N is the number of neutrons, and Z is the number of protons for the nucleus (or the multiplet member).
A	Mass number of the nucleus, $A = N + Z$
$2J$	Two times total angular momentum, J.
π	Parity of the isobaric multiplet.
Nucl.	Element symbol for the nucleus.
Mass Excess	Nuclear mass excess in keV, all nuclear mass excess data are quoted from Ref. [103], unless specified. The mass excess of an excited level is the sum of the mass excess of the ground state (g.s.) plus the excitation energy.
$\overline{E}_{exc}$	The average excitation energy of the higher lying multiplet members above the members of the lowest lying multiplet, taken as having $E_{exc} = 0$. All multiplets in Table A.5 is the lowest lying states having $\overline{E}_{exc} = 0$.
a, b, c, d, e	IMME coefficients respectively corresponding to $\kappa_1, \kappa_2, \ldots, \kappa_5$ in Eq.(3.2) Chapter 3.
χ^2/n	Normalised chi-square value expressing the quality of the least-squares fit, where n is the number of degrees of freedom, i.e., the number of fitted multiplet members subtracts the number of fit parameters (coefficients), for example, $n = 2$ for only fitting a, b, c coefficients in column six of Table A.5; and $n = 1$ for only fitting a, b, c, d coefficients in column seven of the same Table.
( )	The number in the parenthesis is the uncertainty in the rightmost digits, for instance, the b coefficient of the first $\frac{1}{2}^+$ of $A = 23$ doublet, $-4024.9(14) = (-4024.9 \pm 1.4)$ keV
For Table A.4 and A.5:	
a, b, c	a, b, c coefficients of quadratic fit on IMME, these coefficients are respectively arranged in consecutive rows, followed by χ^2/n value.
For Table A.5:	
a, b, c, d	a, b, c, d coefficients of cubic fit on IMME, these coefficients and χ^2/n value are arranged as above.
a, b, c, e	a, b, c, e coefficients of quartic fit on IMME, these coefficients and χ^2/n value are arranged as above.

A.2 Experimental Data Base

A.2.1 Properties of $T = 1/2$ Doublets

Table A.2: *Properties of $T = 1/2$ Doublets*

A	J^π	Nucl.	Mass Excess	Nucl.	Mass Excess	$\overline{E}_{exc}$ (keV)	a (keV)	b (keV)	References
1									
	$\frac{1}{2}^+$	n	8071.317 (1)	H	7288.971 (1)	0	7680.144 (1)	782.347 (1)	
3									
	$\frac{1}{2}^+$	H	14949.81 (1)	He	14931.22 (1)	0	14940.51 (1)	18.59 (1)	[135]
5									
	$\frac{3}{2}^-$	He	11231 (20)	Li	11679 (50)	0	11455 (27)	-448 (54)	[136]
7									
	$\frac{3}{2}^-$	Li	14907.10 (1)	Be	15768.99 (7)	0	15338.04 (4)	-861.89 (7)	[136]
	$\frac{1}{2}^-$	Li	15384.71 (1)	Be	16198.07 (13)	454	15791.39 (6)	-813.36 (13)	[136]
	$\frac{7}{2}^-$	Li	19537 (9)	Be	20339 (50)	4601	19938 (26)	-802 (51)	[136]
	$\frac{5}{2}^-$	Li	21587 (50)	Be	22499 (10)	6706	22043 (26)	-912 (51)	[136]
	$\frac{3}{2}^-$	Li	22367 (1)	Be	22979 (60)	7335	22673 (30)	-612 (60)	[136]
9									
	$\frac{3}{2}^-$	Be	11348.44 (8)	B	12416.47 (91)	0	11882.46 (46)	-1068.03 (91)	[137]
	$\frac{5}{2}^-$	Be	13777.8 (13)	B	14761 (11)	2388	14270 (6)	-984 (12)	[137]
	$\frac{5}{2}^+$	Be	14397 (9)	B	15167 (25)	2900	14782 (14)	-770 (27)	[137]
	$\frac{1}{2}^-$	Be	14128 (12)	B	15196 (16)	2780	14662 (10)	-1068 (20)	[137]
	$\frac{7}{2}^-$	Be	17728 (60)	B	19401 (50)	6683	18565 (39)	-1673 (78)	[137]
	$\frac{7}{2}^-$	Be	22630 (22)	B	24056 (50)	11461	23343 (27)	-1426 (55)	[137]
	$\frac{5}{2}^-$	Be	25828 (9)	B	27116 (18)	14590	26472 (10)	-1288 (21)	[137]
	$\frac{3}{2}^+$	Be	28019 (8)	B	29126 (10)	16691	28573 (7)	-1107 (13)	[137]
	$\frac{7}{2}^+$	Be	28843 (5)	B	29956 (10)	17518	29400 (6)	-1113 (12)	[137]
11									
	$\frac{3}{2}^-$	B	8667.93 (42)	C	10650.34 (95)	0	9659.14 (52)	-1982.41 (104)	[138]
	$\frac{1}{2}^-$	B	10792.62 (42)	C	12650.3 (11)	2063	11721.5 (6)	-1857.7 (12)	[138]
	$\frac{5}{2}^-$	B	13112.82 (65)	C	14969.1 (16)	4382	14041.0 (8)	-1856.3 (17)	[138]
	$\frac{3}{2}^-$	B	13688.24 (52)	C	15454.5 (16)	4913	14571.4 (8)	-1766.3 (16)	[138]
	$\frac{7}{2}^-$	B	15410.8 (19)	C	17128.5 (16)	6611	16269.7 (13)	-1717.7 (25)	[138]
	$\frac{1}{2}^+$	B	15459.73 (52)	C	16989.5 (17)	6566	16224.6 (9)	-1529.8 (18)	[138]
	$\frac{5}{2}^+$	B	15953.44 (60)	C	17555.1 (17)	7096	16754.3 (9)	-1601.7 (18)	[138]
	$\frac{3}{2}^+$	B	16645.77 (59)	C	18150.0 (18)	7739	17397.9 (9)	-1504.3 (19)	[138]
	$\frac{3}{2}^-$	B	17228.2 (19)	C	18754.8 (20)	8333	17991.5 (14)	-1526.6 (27)	[138]
	$\frac{5}{2}^-$	B	17588.1 (21)	C	19070 (3)	8671	18329 (2)	-1482 (3)	[138]
	$\frac{7}{2}^+$	B	17852.9 (21)	C	19305 (8)	8920	18579 (4)	-1452 (8)	[138]
	$\frac{5}{2}^+$	B	17942.3 (21)	C	19349 (10)	8987	18646 (5)	-1407 (11)	[138]
	$\frac{7}{2}^+$	B	19265 (9)	C	20733 (5)	10340	19999 (5)	-1468 (11)	[138]
	$\frac{3}{2}^+$	B	19933 (17)	C	21329 (5)	10972	20631 (9)	-1396 (18)	[138]
13									
	$\frac{1}{2}^-$	C	3125.01 (1)	N	5345.48 (27)	0	4235.24 (14)	-2220.47 (27)	[139]
	$\frac{1}{2}^+$	C	6214.45 (2)	N	7710.4 (7)	2728	6962.4 (4)	-1495.9 (7)	[139]
	$\frac{3}{2}^-$	C	6809.52 (2)	N	8847 (2)	3594	7828 (1)	-2038 (2)	[139]
	$\frac{5}{2}^+$	C	6978.82 (2)	N	8892 (4)	3701	7936 (2)	-1914 (4)	[139]
	$\frac{5}{2}^+$	C	9989 (3)	N	11709 (9)	6614	10849 (5)	-1720 (10)	[139]
	$\frac{3}{2}^+$	C	10811 (6)	N	12231 (8)	7286	11521 (5)	-1420 (10)	[139]
	$\frac{7}{2}^+$	C	10617 (10)	N	12500 (5)	7324	11559 (6)	-1883 (12)	[139]
	$\frac{5}{2}^-$	C	10672 (3)	N	12721 (9)	7462	11697 (5)	-2049 (10)	[139]
	$\frac{1}{2}^-$	C	11985 (20)	N	14263 (11)	8889	13124 (12)	-2278 (23)	[139]
	$\frac{9}{2}^+$	C	12624.8 (1)	N	14345 (10)	9250	13485 (5)	-1721 (10)	[139]
	$\frac{7}{2}^-$	C	13878 (4)	N	15705 (10)	10557	14792 (6)	-1827 (11)	[139]
	$\frac{1}{2}^-$	C	14205 (5)	N	16178 (9)	10957	15192 (5)	-1973 (11)	[139]

continued from Table A.2   Properties of $T = 1/2$ Doublets

A	J^π	Nucl.	Mass Excess	Nucl.	Mass Excess	$\overline{E}_{exc}$ (keV)	a (keV)	b (keV)	References
15									
	$\frac{1}{2}^-$	N	101.44 (1)	O	2855.61 (49)	0	1478.52 (25)	-2754.17 (49)	[139]
	$\frac{5}{2}^+$	N	5371.59 (2)	O	8096.5 (6)	5256	6734.0 (3)	-2724.9 (6)	[139]
	$\frac{1}{2}^+$	N	5400.26 (2)	O	8039 (2)	5241	6719 (1)	-2638 (2)	[139]
	$\frac{3}{2}^-$	N	6425.22 (2)	O	9031.9 (18)	6251	7728.6 (9)	-2606.7 (18)	[139]
	$\frac{5}{2}^+$	N	7256.49 (2)	O	9715.0 (11)	7008	8485.7 (5)	-2458.5 (11)	[139]
	$\frac{3}{2}^+$	N	7402.27 (2)	O	9648.7 (18)	7047	8525.5 (9)	-2246.4 (18)	[139]
	$\frac{7}{2}^+$	N	7669 (1)	O	10131.5 (8)	7422	8900 (1)	-2463 (2)	[139]
	$\frac{1}{2}^+$	N	8414.06 (3)	O	10412.1 (7)	7935	9413.1 (4)	-1998.0 (7)	[139]
	$\frac{3}{2}^+$	N	8672.84 (12)	O	11139.6 (7)	8428	9906.2 (4)	-2466.8 (7)	[139]
	$\frac{1}{2}^+$	N	9151.15 (7)	O	11778 (2)	8986	10464 (1)	-2626 (2)	[139]
	$\frac{5}{2}^-$	N	9861 (1)	O	12344 (3)	9624	11103 (2)	-2482 (4)	[139]
17									
	$\frac{5}{2}^+$	O	-808.76 (1)	F	1951.70 (25)	0	571.47 (13)	-2760.46 (25)	[140]
	$\frac{1}{2}^+$	O	61.97 (10)	F	2447.03 (27)	684	1254.50 (15)	-2385.06 (29)	[140]
	$\frac{1}{2}^-$	O	2246.60 (16)	F	5056 (3)	3080	3651 (2)	-2809 (3)	[140]
	$\frac{5}{2}^-$	O	3034.0 (4)	F	5809 (4)	3850	4421 (2)	-2775 (4)	[140]
	$\frac{3}{2}^-$	O	3745.0 (16)	F	6592 (20)	4597	5168 (10)	-2847 (20)	[140]
	$\frac{3}{2}^+$	O	4276.0 (9)	F	6952 (20)	5043	5614 (10)	-2676 (20)	[140]
	$\frac{9}{2}^-$	O	4407.0 (5)	F	7172 (10)	5218	5789 (5)	-2765 (10)	[140]
	$\frac{3}{2}^-$	O	4570.4 (14)	F	7440 (11)	5434	6005 (6)	-2869 (11)	[140]
	$\frac{7}{2}^-$	O	4888.5 (4)	F	7624 (20)	5685	6256 (10)	-2735 (20)	[140]
	$\frac{5}{2}^-$	O	4924.0 (5)	F	7634 (20)	5708	6279 (10)	-2710 (20)	[140]
	$\frac{3}{2}^+$	O	5060.3 (6)	F	7772 (20)	5845	6416 (10)	-2711 (20)	[140]
	$\frac{1}{2}^-$	O	5130 (4)	F	7989 (9)	5988	6559 (5)	-2858 (10)	[140]
	$\frac{1}{2}^+$	O	5547 (8)	F	8512 (20)	6458	7029 (11)	-2964 (22)	[140]
	$\frac{5}{2}^+$	O	6053 (2)	F	8649 (7)	6780	7351 (4)	-2595 (7)	[140]
	$\frac{5}{2}^+$	O	6356.9 (8)	F	8979 (20)	7097	7668 (10)	-2622 (20)	[140]
	$\frac{3}{2}^+$	O	6393 (10)	F	9308 (20)	7279	7850 (12)	-2914 (23)	[140]
	$\frac{7}{2}^-$	O	6879.4 (9)	F	9498 (20)	7618	8189 (10)	-2618 (20)	[140]
19									
	$\frac{1}{2}^+$	F	-1487.44 (1)	Ne	1752.05 (16)	0	132.30 (8)	-3239.50 (16)	[141]
	$\frac{1}{2}^-$	F	-1377.55 (1)	Ne	2027.14 (21)	193	324.80 (10)	-3404.69 (21)	[141]
	$\frac{5}{2}^+$	F	-1290.30 (1)	Ne	1990.32 (19)	218	350.01 (10)	-3280.63 (19)	[141]
	$\frac{5}{2}^-$	F	-141.77 (13)	Ne	3259.61 (34)	1427	1558.92 (18)	-3401.39 (37)	[141]
	$\frac{1}{2}^-$	F	-28.7 (3)	Ne	3367.65 (53)	1538	1669.5 (3)	-3396.4 (6)	[141]
	$\frac{3}{2}^+$	F	66.59 (1)	Ne	3288.05 (43)	1546	1677.3 (3)	-3221.5 (5)	[141]
	$\frac{9}{2}^+$	F	1292.40 (1)	Ne	4546.75 (62)	2788	2919.6 (3)	-3254.4 (6)	[141]
	$\frac{3}{2}^+$	F	2420.73 (20)	Ne	5785.0 (24)	3971	4102.8 (2)	-3364.2 (3)	[141]
	$\frac{7}{2}^-$	F	2511.3 (7)	Ne	5949.2 (24)	4098	4230.2 (2)	-3437.9 (3)	[141]
	$\frac{9}{2}^-$	F	2545.1 (12)	Ne	5892 (4)	4087	4219 (2)	-3347 (4)	[141]
	$\frac{7}{2}^+$	F	2890.26 (5)	Ne	6131.2 (22)	4379	4510.7 (11)	-3240.9 (3)	[141]
	$\frac{5}{2}^+$	F	3062.5 (8)	Ne	6352 (4)	4575	4707 (2)	-3290 (4)	[141]
	$\frac{3}{2}^-$	F	3068.7 (5)	Ne	6301 (4)	4553	4685 (2)	-3232 (4)	[141]
	$\frac{13}{2}^+$	F	3161 (1)	Ne	6387 (4)	4642	4774 (2)	-3226 (4)	[141]
	$\frac{5}{2}^+$	F	3619.2 (9)	Ne	6844 (6)	5100	5232 (3)	-3225 (6)	[141]
	$\frac{1}{2}^+$	F	3850 (2)	Ne	7103 (10)	5344	5476 (5)	-3253 (10)	[141]
21									
	$\frac{3}{2}^+$	Ne	-5731.78 (4)	Na	-2184.64 (28)	0	-3958.21 (14)	-3547.14 (28)	[142]
	$\frac{5}{2}^+$	Ne	-5381.05 (4)	Na	-1852.74 (29)	342	-3616.89 (15)	-3528.31 (30)	[142]
	$\frac{7}{2}^+$	Ne	-3985.86 (5)	Na	-468.5 (4)	1732	-2227.2 (3)	-3517.3 (4)	[142]
	$\frac{1}{2}^-$	Ne	-2943.55 (10)	Na	613.26 (6)	2794	-1165.14 (29)	-3556.81 (58)	[142]
	$\frac{1}{2}^+$	Ne	-2937.62 (6)	Na	239.2 (5)	2609	-1349.2 (3)	-3176.8 (5)	[142]
	$\frac{9}{2}^+$	Ne	-2865.18 (16)	Na	644.5 (6)	2848	-1110.4 (4)	-3509.6 (8)	[142]
	$\frac{3}{2}^-$	Ne	-2069.14 (21)	Na	1494.3 (5)	3671	-287.4 (3)	-3563.4 (6)	[142]
	$\frac{5}{2}^+$	Ne	-1996.19 (15)	Na	1359.7 (5)	3640	-318.3 (3)	-3355.9 (5)	[142]
	$\frac{5}{2}^-$	Ne	-1847.82 (22)	Na	1677.6 (6)	3874	-85.1 (3)	-3525.4 (6)	[142]
	$\frac{11}{2}^+$	Ne	-1299.98 (51)	Na	2234 (2)	4426	467 (1)	-3534 (2)	[142]
	$\frac{5}{2}^+$	Ne	-1205.92 (17)	Na	2109.7 (7)	4411	451.9 (4)	-3315.6 (7)	[142]
	$\frac{3}{2}^+$	Ne	-1047.22 (16)	Na	2283.3 (8)	4577	618.0 (4)	-3330.5 (8)	[142]
	$\frac{3}{2}^-$	Ne	-1006.44 (7)	Na	1985.0 (8)	4448	489.3 (4)	-2991.4 (8)	[142]
23									

Appendix A. Coefficients of the Isobaric Multiplet Mass Equation

Properties of $T = 1/2$ Doublets

A	J^π	Nucl.	Mass Excess	Nucl.	Mass Excess	$\overline{E}_{exc}$ (keV)	a (keV)	b (keV)	References
	$\frac{3}{2}^+$	Na	-9529.85 (1)	Mg	-5473.26 (69)	0	-7501.56 (35)	-4056.59 (69)	[143]
	$\frac{5}{2}^+$	Na	-9089.86 (1)	Mg	-5022.55 (71)	446	-7056.21 (35)	-4067.31 (70)	[143]
	$\frac{7}{2}^+$	Na	-7453.84 (3)	Mg	-3421.1 (12)	2065	-5437.5 (6)	-4032.8 (12)	[143]
	$\frac{1}{2}^+$	Na	-7139.12 (2)	Mg	-3114.3 (16)	2375	-5126.7 (8)	-4024.9 (16)	[143]
	$\frac{1}{2}^-$	Na	-6890.00 (4)	Mg	-2702 (3)	2706	-4796 (2)	-4188 (3)	[143]
	$\frac{9}{2}^+$	Na	-6826.35 (3)	Mg	-2758.6 (13)	2710	-4792.5 (6)	-4067.8 (13)	[143]
	$\frac{3}{2}^+$	Na	-6547.79 (2)	Mg	-2565.2 (22)	2946	-4556.5 (11)	-3982.6 (22)	[143]
	$\frac{3}{2}^-$	Na	-5852.25 (4)	Mg	-1675 (5)	3738	-3764 (3)	-4177 (5)	[143]
	$\frac{5}{2}^-$	Na	-5681.78 (3)	Mg	-1500 (5)	3911	-3591 (3)	-4182 (5)	[143]
	$\frac{5}{2}^+$	Na	-5615.61 (2)	Mg	-1609 (5)	3890	-3612 (3)	-4006 (5)	[143]
	$\frac{1}{2}^+$	Na	-5100.21 (8)	Mg	-1120 (6)	4392	-3110 (3)	-3980 (6)	[143]
	$\frac{7}{2}^+$	Na	-4755.24 (5)	Mg	-788 (6)	4730	-2772 (3)	-3967 (6)	[143]
	$\frac{5}{2}^+$	Na	-4151.28 (11)	Mg	-186 (6)	5333	-2169 (3)	-3965 (6)	[143]
	$\frac{11}{2}^+$	Na	-3995.9 (3)	Mg	-20 (2)	5494	-2008 (1)	-3976 (18)	[143]
	$\frac{5}{2}^+$	Na	-3788.10 (10)	Mg	183 (7)	5699	-1803 (4)	-3971 (7)	[143]
	$\frac{3}{2}^+$	Na	-3763.82 (7)	Mg	218 (8)	5729	-1773 (4)	-3982 (8)	[143]
	$\frac{7}{2}^+$	Na	-3603.04 (12)	Mg	458.7 (61)	5930	-1572.2 (31)	-4061.8 (6)	[143]
	$\frac{3}{2}^-$	Na	-3565.43 (12)	Mg	511 (6)	5975	-1527 (3)	-4076 (6)	[143]
	$\frac{7}{2}^-$	Na	-3487.66 (4)	Mg	652 (6)	6084	-1418 (3)	-4139 (6)	[143]
25	$\frac{5}{2}^+$	Mg	-13192.77 (5)	Al	-8916.17 (48)	0	-11054.47 (24)	-4276.60 (48)	[144]
	$\frac{1}{2}^+$	Mg	-12607.73 (5)	Al	-8464.5 (7)	519	-10536.1 (4)	-4143.3 (7)	[144]
	$\frac{3}{2}^+$	Mg	-12218.02 (5)	Al	-7971.3 (7)	960	-10094.6 (4)	-4246.7 (7)	[144]
	$\frac{7}{2}^+$	Mg	-11581.00 (5)	Al	-7303.7 (7)	1613	-9442.3 (4)	-4277.3 (7)	[144]
	$\frac{5}{2}^+$	Mg	-11228.15 (5)	Al	-7126.7 (7)	1878	-9177.4 (4)	-4101.5 (7)	[144]
	$\frac{1}{2}^+$	Mg	-10629.41 (7)	Al	-6430.9 (11)	2525	-8530.1 (5)	-4198.5 (11)	[144]
	$\frac{3}{2}^+$	Mg	-10391.31 (6)	Al	-6242.9 (8)	2738	-8317.1 (4)	-4148.4 (8)	[144]
	$\frac{7}{2}^+$	Mg	-10455.0 (3)	Al	-6196.0 (7)	2729	-8325.5 (4)	-4259.0 (8)	[144]
	$\frac{3}{2}^-$	Mg	-9779.40 (5)	Al	-5854.2 (9)	3238	-7816.8 (5)	-3925.2 (9)	[144]
	$\frac{9}{2}^+$	Mg	-9787.71 (18)	Al	-5492.0 (9)	3415	-7639.8 (5)	-4295.7 (9)	[144]
	$\frac{7}{2}^-$	Mg	-9222.04 (20)	Al	-5220.7 (9)	3834	-7221.4 (5)	-4001.4 (9)	[144]
	$\frac{5}{2}^+$	Mg	-9284.9 (4)	Al	-5057.1 (9)	3884	-7171.0 (5)	-4227.8 (11)	[144]
	$\frac{9}{2}^+$	Mg	-9133.2 (3)	Al	-4890 (2)	4043	-7012 (1)	-4243 (2)	[144]
	$\frac{1}{2}^-$	Mg	-8915.7 (4)	Al	-5093 (2)	4051	-7004 (1)	-3822 (2)	[144]
	$\frac{3}{2}^+$	Mg	-8833.16 (15)	Al	-4724 (4)	4276	-6779 (2)	-4109 (4)	[144]
	$\frac{9}{2}^+$	Mg	-8481.2 (4)	Al	-4400 (5)	4614	-6441 (3)	-4081 (5)	[144]
27	$\frac{5}{2}^+$	Al	-17196.70 (11)	Si	-12384.35 (15)	0	-14790.52 (8)	-4812.36 (18)	[145]
	$\frac{1}{2}^+$	Al	-16352.94 (11)	Si	-11603.5 (3)	813	-13978.2 (2)	-4749.5 (3)	[145]
	$\frac{3}{2}^+$	Al	-16182.25 (11)	Si	-11427.0 (3)	986	-13804.6 (2)	-4755.3 (3)	[145]
	$\frac{7}{2}^+$	Al	-14984.69 (15)	Si	-10220.8 (3)	2188	-12602.7 (2)	-4764.0 (3)	[145]
	$\frac{5}{2}^+$	Al	-14461.8 (7)	Si	-9736.8 (4)	2692	-12099.3 (4)	-4725.1 (8)	[145]
	$\frac{3}{2}^+$	Al	-14214.7 (2)	Si	-9518.1 (4)	2925	-11866.4 (2)	-4696.7 (4)	[145]
	$\frac{9}{2}^+$	Al	-14192.5 (8)	Si	-9474.5 (3)	2958	-11833.5 (5)	-4718.1 (9)	[145]
	$\frac{1}{2}^+$	Al	-13516.3 (9)	Si	-8844.1 (2)	3611	-11180.2 (7)	-4672.2 (2)	[145]
	$\frac{3}{2}^+$	Al	-13239.9 (5)	Si	-8580.7 (2)	3881	-10910.3 (6)	-4659.2 (2)	[145]
	$\frac{1}{2}^-$	Al	-13142.1 (5)	Si	-8246.2 (2)	4097	-10694.2 (8)	-4895.9 (2)	[145]
	$\frac{5}{2}^+$	Al	-12786.5 (5)	Si	-8095.2 (9)	4350	-10440.8 (5)	-4691.4 (10)	[145]
	$\frac{11}{2}^+$	Al	-12686.4 (5)	Si	-7937.1 (5)	4479	-10311.7 (4)	-4749.4 (7)	[145]
	$\frac{7}{2}^+$	Al	-12616.7 (8)	Si	-7909.6 (7)	4528	-10263.1 (6)	-4707.2 (11)	[145]
	$\frac{5}{2}^+$	Al	-12385.1 (5)	Si	-7680.6 (2)	4758	-10032.8 (6)	-4704.6 (13)	[145]
	$\frac{5}{2}^+$	Al	-11948.7 (6)	Si	-7322 (2)	5155	-9636 (1)	-4626 (2)	[145]
	$\frac{3}{2}^-$	Al	-12041.1 (8)	Si	-7157 (5)	5192	-9599 (3)	-4884 (5)	[145]
	$\frac{9}{2}^+$	Al	-11776.8 (9)	Si	-7122.3 (5)	5341	-9449.6 (5)	-4654.5 (10)	[145]

continued from Table A.2   Properties of $T = 1/2$ Doublets

A	J^π	Nucl.	Mass Excess	Nucl.	Mass Excess	$\overline{E}_{exc}$ (keV)	a (keV)	b (keV)	References
29									
	$\frac{1}{2}^+$	Si	-21895.08 (1)	P	-16952.62 (60)	0	-19423.85 (30)	-4942.45 (60)	[145]
	$\frac{3}{2}^+$	Si	-20621.68 (2)	P	-15569.07 (60)	1329	-18095.38 (31)	-5052.61 (61)	[145]
	$\frac{5}{2}^+$	Si	-19866.93 (4)	P	-14998.71 (63)	1992	-17432.82 (32)	-4868.21 (63)	[145]
	$\frac{3}{2}^+$	Si	-19469.06 (2)	P	-14529.9 (7)	2425	-16999.5 (4)	-4939.1 (7)	[145]
	$\frac{5}{2}^+$	Si	-18828.05 (4)	P	-13846.7 (7)	3087	-16337.4 (4)	-4981.3 (7)	[145]
	$\frac{7}{2}^-$	Si	-18270.93 (15)	P	-13505.0 (7)	3536	-15888.0 (4)	-4765.9 (8)	[145]
	$\frac{7}{2}^+$	Si	-17814.9 (9)	P	-12872.1 (7)	4081	-15343.5 (6)	-4942.8 (2)	[145]
	$\frac{9}{2}^+$	Si	-17154.1 (7)	P	-12310.6 (9)	4692	-14732.4 (6)	-4843.5 (2)	[145]
	$\frac{1}{2}^+$	Si	-17054.73 (6)	P	-12194 (3)	4800	-14624 (2)	-4861 (3)	[145]
	$\frac{5}{2}^+$	Si	-16999.7 (6)	P	-11998.5 (8)	4925	-14499.1 (5)	-5001.2 (10)	[145]
	$\frac{3}{2}^-$	Si	-16960.52 (2)	P	-12610 (2)	4639	-14785 (1)	-4351 (2)	[145]
	$\frac{9}{2}^-$	Si	-16640.5 (5)	P	-11906 (3)	5151	-14273 (2)	-4735 (3)	[145]
	$\frac{7}{2}^+$	Si	-16082.2 (9)	P	-11127 (4)	5820	-13604 (2)	-4956 (4)	[145]
	$\frac{3}{2}^+$	Si	-15946.0 (2)	P	-10985 (3)	5959	-13465 (2)	-4961 (3)	[145]
	$\frac{1}{2}^-$	Si	-15514.2 (2)	P	-11426 (20)	5954	-13470 (10)	-4089 (20)	[145]
	$\frac{3}{2}^+$	Si	-15398.9 (2)	P	-10625 (5)	6413	-13012 (3)	-4774 (5)	[145]
	$\frac{5}{2}^+$	Si	-15373 (1)	P	-10448 (15)	6514	-12910 (8)	-4925 (15)	[145]
	$\frac{1}{2}^+$	Si	-15199.15 (14)	P	-10376 (5)	6637	-12787 (3)	-4824 (5)	[145]
31[1]									
	$\frac{1}{2}^+$	P	-24440.54 (1)	S	-19042.55 (24)	0	-21741.55 (12)	-5397.99 (24)	[145]
	$\frac{3}{2}^+$	P	-23174.39 (10)	S	-17793.7 (3)	1258	-20484.0 (2)	-5380.7 (4)	[145]
	$\frac{5}{2}^+$	P	-22206.8 (2)	S	-16807.0 (5)	2235	-19506.9 (3)	-5399.9 (5)	[145]
	$\frac{1}{2}^+$	P	-21306.4 (3)	S	-15963.55 (27)	3107	-18635.00 (20)	-5342.89 (40)	[145]
	$\frac{5}{2}^+$	P	-21145.5 (3)	S	-15757.1 (6)	3291	-18451.3 (3)	-5388.5 (6)	[145]
	$\frac{7}{2}^+$	P	-21025.9 (3)	S	-15691.5 (7)	3383	-18358.7 (4)	-5334.5 (7)	[145]
	$\frac{3}{2}^+$	P	-20934.7 (5)	S	-15606 (7)	3472	-18270 (4)	-5329 (7)	[145]
	$\frac{5}{2}^+$	P	-20250.2 (4)	S	-14963 (8)	4136	-17606 (4)	-5288 (8)	[145]
	$\frac{3}{2}^+$	P	-20179.8 (7)	S	-14839 (7)	4233	-17509 (4)	-5341 (7)	[145]
	$\frac{7}{2}^-$	P	-20009.6 (3)	S	-14591 (6)	4442	-17300 (3)	-5419 (6)	[145]
	$\frac{3}{2}^+$	P	-19846.9 (8)	S	-14518 (8)	4560	-17182 (4)	-5329 (8)	[145]
	$\frac{7}{2}^+$	P	-19806.7 (5)	S	-14463 (6)	4607	-17135 (3)	-5344 (6)	[145]
	$\frac{5}{2}^+$	P	-19657.4 (5)	S	-14325 (6)	4751	-16991 (3)	-5333 (6)	[145]
	$\frac{5}{2}^+$	P	-19325 (6)	S	-14021 (12)	5069	-16673 (7)	-5305 (14)	[145]
	$\frac{1}{2}^+$	P	-19184.4 (14)	S	-13892 (6)	5204	-16538 (3)	-5293 (6)	[145]
33									
	$\frac{3}{2}^+$	S	-26585.85 (1)	Cl	-21003.27 (44)	0	-23794.56 (22)	-5582.59 (44)	[145]
	$\frac{1}{2}^+$	S	-25744.85 (2)	Cl	-20192.75 (47)	826	-22968.80 (24)	-5552.10 (47)	[145]
	$\frac{5}{2}^+$	S	-24618.67 (4)	Cl	-19016.8 (6)	1977	-21817.7 (3)	-5601.9 (6)	[145]
	$\frac{3}{2}^+$	S	-24272.41 (2)	Cl	-18651.5 (6)	2333	-21461.9 (3)	-5620.9 (6)	[145]
	$\frac{5}{2}^+$	S	-23718.22 (2)	Cl	-18164.3 (6)	2854	-20941.2 (3)	-5554.0 (6)	[145]
	$\frac{7}{2}^+$	S	-23617.3 (1)	Cl	-18027.9 (6)	2972	-20822.6 (3)	-5589.4 (6)	[145]
	$\frac{3}{2}^-$	S	-23365.16 (2)	Cl	-18157.0 (6)	3034	-20761.1 (3)	-5208.2 (6)	[145]
	$\frac{5}{2}^+$	S	-22754.3 (2)	Cl	-17187.2 (6)	3824	-19970.7 (3)	-5567.1 (7)	[145]
	$\frac{3}{2}^+$	S	-22651.12 (6)	Cl	-17032.1 (5)	3953	-19841.6 (3)	-5619.1 (5)	[145]
	$\frac{5}{2}^-$	S	-22441.53 (6)	Cl	-17023.97 (48)	4062	-19732.75 (24)	-5417.57 (48)	[145]
	$\frac{1}{2}^+$	S	-22530.50 (11)	Cl	-16903.9 (7)	4078	-19717.2 (4)	-5626.6 (7)	[145]
	$\frac{3}{2}^-$	S	-22375.01 (2)	Cl	-16885.8 (8)	4165	-19630.4 (4)	-5489.2 (8)	[145]
	$\frac{1}{2}^+$	S	-22210.5 (3)	Cl	-16564.3 (5)	4408	-19387.4 (3)	-5646.2 (6)	[145]
	$\frac{3}{2}^+$	S	-22162.12 (5)	Cl	-16539.6 (6)	4444	-19350.6 (3)	-5623.1 (6)	[145]
	$\frac{1}{2}^-$	S	-21667.98 (4)	Cl	-16486 (4)	4718	-19077 (2)	-5182 (4)	[145]
	$\frac{5}{2}^+$	S	-21838.6 (7)	Cl	-16257.1 (6)	4747	-19047.8 (5)	-5581.5 (9)	[145]
	$\frac{7}{2}^-$	S	-21644.1 (10)	Cl	-16227.9 (11)	4859	-18936.0 (8)	-5416.2 (15)	[145]

continued from Table A.2   Properties of $T = 1/2$ Doublets

A	J^π	Nucl.	Mass Excess	Nucl.	Mass Excess	$\overline{E}_{exc}$ (keV)	a (keV)	b (keV)	References
35									
	$\frac{3}{2}^+$	Cl	-29013.52 (4)	Ar	-23047.39 (75)	0	-26030.45 (37)	-5966.13 (75)	[145]
	$\frac{1}{2}^+$	Cl	-27794.08 (8)	Ar	-21863.4 (8)	1202	-24828.7 (4)	-5930.7 (8)	[145]
	$\frac{5}{2}^+$	Cl	-27250.37 (8)	Ar	-21296.8 (8)	1757	-24273.6 (4)	-5953.6 (8)	[145]
	$\frac{7}{2}^+$	Cl	-26367.9 (2)	Ar	-20446.6 (17)	2624	-23407.3 (9)	-5921.3 (17)	[145]
	$\frac{3}{2}^+$	Cl	-26319.9 (1)	Ar	-20409.5 (8)	2666	-23364.7 (4)	-5910.4 (8)	[145]
	$\frac{5}{2}^+$	Cl	-26010.78 (9)	Ar	-20064.58 (76)	2993	-23037.67 (38)	-5946.20 (76)	[145]
	$\frac{7}{2}^-$	Cl	-25850.7 (2)	Ar	-19854 (10)	3178	-22853 (5)	-5996 (10)	[145]
	$\frac{1}{2}^+$	Cl	-25046.0 (6)	Ar	-19163 (10)	3926	-22105 (5)	-5883 (10)	[145]
	$\frac{3}{2}^-$	Cl	-24954.3 (3)	Ar	-19035 (10)	4036	-21995 (5)	-5919 (10)	[145]
	$\frac{3}{2}^-$	Cl	-24835.6 (2)	Ar	-18905 (10)	4160	-21871 (5)	-5930 (10)	[145]
	$\frac{9}{2}^-$	Cl	-24666 (2)	Ar	-18688 (3)	4354	-21677 (2)	-5977 (3)	[146]
	$\frac{11}{2}^-$	Cl	-23607 (2)	Ar	-17663 (3)	5396	-20635 (2)	-5943 (3)	[146]
	$\frac{11}{2}^-$	Cl	-23087 (2)	Ar	-17433 (3)	5771	-20260 (2)	-5653 (3)	[146]
	$\frac{13}{2}^-$	Cl	-22927 (2)	Ar	-17281 (3)	5927	-20104 (2)	-5645 (3)	[146]
	$\frac{15}{2}^-$	Cl	-20695 (2)	Ar	-14938 (3)	8214	-17816 (2)	-5756 (3)	[146]
	$\frac{15}{2}^-$	Cl	-20527 (2)	Ar	-14835 (3)	8350	-17681 (2)	-5691 (3)	[146]
	$\frac{19}{2}^-$	Cl	-18834 (2)	Ar	-13142 (3)	10043	-15988 (2)	-5691 (3)	[146]
	$\frac{23}{2}^-$	Cl	-16443 (2)	Ar	-10771 (3)	12424	-13607 (2)	-5671 (3)	[146]
37									
	$\frac{3}{2}^+$	Ar	-30947.67 (21)	K	-24800.20 (9)	0	-27873.94 (12)	-6147.48 (23)	[145]
	$\frac{1}{2}^+$	Ar	-29537.85 (23)	K	-23429.35 (10)	1391	-26483.60 (13)	-6108.51 (25)	[145]
	$\frac{7}{2}^-$	Ar	-29336.40 (22)	K	-23419.95 (10)	1496	-26378.18 (12)	-5916.46 (24)	[145]
	$\frac{5}{2}^+$	Ar	-28730.6 (3)	K	-22514.96 (15)	2252	-25622.8 (4)	-6215.6 (4)	[145]
	$\frac{3}{2}^-$	Ar	-28457.1 (4)	K	-22630.02 (16)	2331	-25543.5 (2)	-5827.1 (4)	[145]
	$\frac{5}{2}^+$	Ar	-28151.6 (4)	K	-22049.93 (12)	2774	-25100.8 (2)	-6101.6 (4)	[145]
	$\frac{5}{2}^-$	Ar	-27673.8 (3)	K	-21718.21 (13)	3178	-24696.0 (2)	-5955.6 (3)	[145]
	$\frac{5}{2}^+$	Ar	-27776.4 (14)	K	-21560.9 (3)	3206	-24668.6 (7)	-6215.5 (15)	[145]
	$\frac{3}{2}^-$	Ar	-27429.4 (4)	K	-21486 (2)	3417	-24458 (1)	-5943 (2)	[145]
	$\frac{3}{2}^+$	Ar	-27345.7 (7)	K	-21178 (3)	3612	-24262 (2)	-6167 (3)	[145]
39									
	$\frac{3}{2}^+$	K	-33807.19 (1)	Ca	-27282.70 (60)	0	-30544.95 (30)	-6524.49 (60)	[147]
	$\frac{1}{2}^+$	K	-31284.7 (2)	Ca	-24814.2 (11)	2496	-28049.4 (6)	-6470.5 (11)	[147]
	$\frac{7}{2}^-$	K	-30992.9 (2)	Ca	-24485.9 (9)	2806	-27739.4 (5)	-6507.0 (9)	[147]
	$\frac{3}{2}^-$	K	-30788.0 (2)	Ca	-24257 (3)	3023	-27522 (2)	-6531 (3)	[147]
	$\frac{9}{2}^-$	K	-30209.7 (2)	Ca	-23643.1 (10)	3619	-26926.4 (5)	-6566.6 (11)	[147]
	$\frac{1}{2}^+$	K	-29711.9 (3)	Ca	-23262.0 (18)	4058	-26486.9 (9)	-6449.9 (18)	[147]
41									
	$\frac{7}{2}^-$	Ca	-35137.92 (14)	Sc	-28642.41 (8)	0	-31890.17 (8)	-6495.51 (16)	[148]
	$\frac{3}{2}^-$	Ca	-33195.16 (21)	Sc	-26925.96 (12)	1830	-30060.56 (12)	-6269.20 (24)	[148]
	$\frac{3}{2}^+$	Ca	-33128.0 (3)	Sc	-26546.5 (5)	2053	-29837.3 (3)	-6581.5 (6)	[148]
	$\frac{3}{2}^-$	Ca	-32675.6 (4)	Sc	-26227.6 (5)	2439	-29451.6 (3)	-6448.0 (4)	[148]
	$\frac{5}{2}^-$	Ca	-32561.4 (6)	Sc	-26054.31 (11)	2583	-29307.9 (3)	-6507.1 (6)	[148]
	$\frac{5}{2}^+$	Ca	-32532.3 (4)	Sc	-25975.77 (11)	2637	-29254.0 (2)	-6556.5 (4)	[148]
	$\frac{1}{2}^+$	Ca	-32467.4 (2)	Sc	-25923.24 (13)	2695	-29195.3 (6)	-6544.2 (13)	[148]
	$\frac{7}{2}^+$	Ca	-32254.0 (7)	Sc	-25759.94 (11)	2884	-29007.0 (4)	-6494.1 (7)	[148]
	$\frac{7}{2}^-$	Ca	-32178.6 (6)	Sc	-25670.3 (3)	2966	-28924.5 (4)	-6508.3 (7)	[148]
	$\frac{3}{2}^+$	Ca	-31936.6 (7)	Sc	-25457.3 (3)	3194	-28697.0 (4)	-6479.3 (8)	[148]
	$\frac{11}{2}^+$	Ca	-31768.33 (20)	Sc	-25284.3 (7)	3364	-28526.3 (4)	-6484.0 (7)	[148]
	$\frac{1}{2}^+$	Ca	-31737.9 (4)	Sc	-25230.9 (4)	3406	-28484.4 (3)	-6507.0 (5)	[148]
	$\frac{3}{2}^+$	Ca	-31610.6 (9)	Sc	-25079.7 (3)	3545	-28345.2 (5)	-6530.9 (10)	[148]
	$\frac{1}{2}^-$	Ca	-31524.4 (3)	Sc	-25162 (5)	3547	-28343 (3)	-6362 (5)	[148]
	$\frac{5}{2}^+$	Ca	-31643.0 (5)	Sc	-24952 (13)	3593	-28298 (7)	-6691 (13)	[148]
	$\frac{7}{2}^-$	Ca	-31523.5 (8)	Sc	-24945.7 (3)	3656	-28234.6 (5)	-6577.8 (9)	[148]
	$\frac{3}{2}^-$	Ca	-31407.3 (4)	Sc	-24868.4 (3)	3753	-28137.9 (15)	-6538.9 (31)	[148]
	$\frac{5}{2}^+$	Ca	-31397.5 (5)	Sc	-24861.7 (3)	3761	-28129.6 (4)	-6535.8 (6)	[148]
	$\frac{1}{2}^+$	Ca	-31292.0 (6)	Sc	-24674 (5)	3907	-27983 (3)	-6618 (5)	[148]
	$\frac{7}{2}^-$	Ca	-30860.6 (10)	Sc	-24619.6 (4)	4151	-27740.1 (6)	-6241.0 (11)	[148]
	$\frac{7}{2}^-$	Ca	-29989.8 (16)	Sc	-24612.2 (6)	4590	-27301.0 (9)	-5377.6 (17)	[148]
43									
	$\frac{7}{2}^-$	Sc	-36188.14 (187)	Ti	-29321.2 (69)	0	-32754.7 (36)	-6866.9 (72)	[149]
	$\frac{3}{2}^+$	Sc	-36036.7 (19)	Ti	-29008.2 (70)	233	-32522.5 (36)	-7028.5 (73)	[149]
	$\frac{3}{2}^-$	Sc	-35715.8 (19)	Ti	-28846 (13)	474	-32281 (6)	-6870 (13)	[149]
	$\frac{7}{2}^+$	Sc	-34851.3 (19)	Ti	-27837.7 (70)	1411	-31344.5 (36)	-7013.6 (73)	[149]
	$\frac{11}{2}^-$	Sc	-34358.2 (19)	Ti	-27463.5 (70)	1844	-30910.9 (36)	-6894.7 (73)	[149]
	$\frac{9}{2}^+$	Sc	-34256.7 (19)	Ti	-27258.8 (70)	1997	-30757.8 (36)	-6997.9 (73)	[149]
	$\frac{15}{2}^-$	Sc	-33200.7 (19)	Ti	-26369.5 (70)	2970	-29785.1 (36)	-6831.2 (73)	[149]
	$\frac{19}{2}^-$	Sc	-33064.9 (19)	Ti	-26254.8 (70)	3095	-29659.9 (36)	-6810.1 (73)	[149]

continued from Table A.2   Properties of $T = 1/2$ Doublets

A	J^π	Nucl.	Mass Excess	Nucl.	Mass Excess	$\overline{E}_{exc}$ (keV)	a (keV)	b (keV)	References
45									
	$\frac{7}{2}-$	Ti	-39008.31 (81)	V	-31880 (17)	0	-35444 (9)	-7129 (17)	[150]
	$\frac{3}{2}-$	Ti	-38971.78 (83)	V	-31823 (17)	47	-35397 (9)	-7149 (17)	[151]
	$\frac{5}{2}-$	Ti	-38968.92 (84)	V	-31823 (17)	49	-35396 (9)	-7149 (17)	[151]
	$\frac{3}{2}+$	Ti	-38679.8 (9)	V	-31494 (17)	358	-35087 (9)	-7186 (17)	[150]
	$\frac{5}{2}+$	Ti	-38265.7 (9)	V	-31083 (17)	770	-34674 (9)	-7183 (17)	[150]
	$\frac{7}{2}+$	Ti	-37783.0 (9)	V	-30608 (17)	1249	-34196 (9)	-7175 (17)	[150]
	$\frac{9}{2}-$	Ti	-37654.7 (8)	V	-30556 (17)	1339	-34105 (9)	-7099 (17)	[150]
	$\frac{11}{2}-$	Ti	-37540.1 (8)	V	-30418 (17)	1466	-33979 (9)	-7122 (17)	[150]
	$\frac{9}{2}+$	Ti	-37127.8 (9)	V	-29963 (17)	1899	-33546 (9)	-7165 (17)	[150]
	$\frac{11}{2}+$	Ti	-36535.1 (10)	V	-29391 (17)	2482	-32963 (9)	-7144 (17)	[150]
	$\frac{13}{2}-$	Ti	-36352.1 (9)	V	-29254 (17)	2642	-32803 (9)	-7098 (17)	[150]
	$\frac{15}{2}-$	Ti	-35993.3 (9)	V	-28875 (17)	3010	-32434 (9)	-7118 (17)	[150]
	$\frac{13}{2}+$	Ti	-35562.3 (10)	V	-28436 (17)	3446	-31999 (9)	-7127 (17)	[150]
	$\frac{17}{2}-$	Ti	-35407.2 (9)	V	-28275 (17)	3603	-31841 (9)	-7132 (17)	[150]
	$\frac{15}{2}+$	Ti	-35087.2 (10)	V	-27970 (17)	3916	-31528 (9)	-7117 (17)	[150]
	$\frac{19}{2}-$	Ti	-34664.4 (10)	V	-27488 (17)	4368	-31076 (9)	-7176 (17)	[150]
	$\frac{7}{2}-$	Ti	-34285 (7)	V	-27080 (56)	4762	-30683 (28)	-7206 (56)	[151]
	$\frac{19}{2}+$	Ti	-33368.9 (11)	V	-26194 (17)	5663	-29782 (9)	-7175 (17)	[150]
	$\frac{23}{2}-$	Ti	-32846.4 (11)	V	-25673 (17)	6185	-29260 (9)	-7173 (17)	[150]
	$\frac{27}{2}-$	Ti	-31866.0 (12)	V	-24720 (17)	7151	-28293 (9)	-7146 (17)	[150]
47									
	$\frac{3}{2}-$	V	-42005.61 (32)	Cr	-34559 (14)	0	-38282 (7)	-7447 (14)	[152]
	$\frac{5}{2}-$	V	-41918.09 (32)	Cr	-34459 (14)	94	-38189 (7)	-7459 (14)	[152]
	$\frac{7}{2}-$	V	-41859.79 (32)	Cr	-34384 (14)	161	-38122 (7)	-7475 (14)	[152]
	$\frac{3}{2}+$	V	-41746.13 (32)	Cr	-34087 (14)	366	-37916 (7)	-7659 (14)	[152]
	$\frac{5}{2}+$	V	-41345.26 (32)	Cr	-33688 (14)	766	-37517 (7)	-7657 (14)	[152]
	$\frac{11}{2}-$	V	-40710.65 (33)	Cr	-33226 (14)	1314	-36969 (7)	-7484 (14)	[152]
	$\frac{7}{2}+$	V	-40867.06 (32)	Cr	-33213 (14)	1243	-37040 (7)	-7654 (14)	[152]
	$\frac{1}{2}+$	V	-40344.99 (34)	Cr	-32728 (16)	1746	-36536 (8)	-7617 (16)	[152]
	$\frac{9}{2}+$	V	-40258.65 (32)	Cr	-32602 (14)	1852	-36430 (7)	-7656 (14)	[152]
	$\frac{11}{2}+$	V	-39590.6 (5)	Cr	-31940 (14)	2517	-35765 (7)	-7650 (14)	[152]
	$\frac{15}{2}-$	V	-39390.6 (6)	Cr	-31905 (14)	2635	-35648 (7)	-7486 (14)	[152]
	$\frac{13}{2}+$	V	-38735.3 (6)	Cr	-31088 (14)	3371	-34912 (7)	-7647 (14)	[152]
	$\frac{19}{2}-$	V	-37872.6 (8)	Cr	-30420 (14)	4136	-34146 (7)	-7453 (14)	[152]
	$\frac{15}{2}+$	V	-38051.3 (7)	Cr	-30344 (14)	4085	-34197 (7)	-7708 (14)	[152]
	$\frac{23}{2}-$	V	-36102.6 (10)	Cr	-28654 (14)	5904	-32378 (7)	-7449 (14)	[152]
	$\frac{25}{2}-$	V	-34606.7 (11)	Cr	-27180 (14)	7389	-30893 (7)	-7427 (14)	[152]
	$\frac{27}{2}-$	V	-34122.2 (11)	Cr	-26648 (14)	7898	-30385 (7)	-7475 (14)	[152]
	$\frac{31}{2}+$	V	-32001.0 (13)	Cr	-24537 (14)	10014	-28269 (7)	-7464 (14)	[152]
49									
	$\frac{5}{2}-$	Cr	-45332.92 (237)	Mn	-37614.6670 (24)	0	-41474 (12)	-7718 (24)	[153]
	$\frac{7}{2}-$	Cr	-45061.20 (238)	Mn	-37353.2870 (24)	267	-41207 (12)	-7708 (24)	[153]
	$\frac{9}{2}-$	Cr	-44249.3 (24)	Mn	-36555.4870 (24)	1072	-40402 (12)	-7694 (24)	[153]
	$\frac{11}{2}-$	Cr	-43770.8 (24)	Mn	-36073.3570 (24)	1552	-39922 (12)	-7697 (24)	[153]
	$\frac{13}{2}-$	Cr	-42832.8 (24)	Mn	-35133.3670 (24)	2491	-38983 (12)	-7699 (24)	[153]
	$\frac{15}{2}-$	Cr	-42142.8 (24)	Mn	-34425.3670 (24)	3190	-38284 (12)	-7717 (24)	[153]
	$\frac{5}{2}-$	Cr	-41281 (6)	Mn	-33655.6670 (56)	4006	-37468 (28)	-7625 (56)	[153]
	$\frac{17}{2}-$	Cr	-41114.8 (25)	Mn	-33364.3670 (24)	4235	-37240 (12)	-7750 (24)	[153]
	$\frac{19}{2}-$	Cr	-40966.9 (25)	Mn	-33168.3670 (24)	4407	-37068 (12)	-7799 (24)	[153]
	$\frac{23}{2}-$	Cr	-39370.5 (25)	Mn	-31558.2670 (24)	6010	-35464 (12)	-7812 (24)	[153]
	$\frac{27}{2}-$	Cr	-37325.5 (27)	Mn	-29534.2670 (24)	8044	-33430 (13)	-7791 (25)	[153]
	$\frac{31}{2}+$	Cr	-34632.6 (28)	Mn	-26890.1670 (24)	10713	-30761 (13)	-7742 (25)	[153]

						continued from Table A.2	Properties of $T=1/2$ Doublets		
A	J^π	Nucl.	Mass Excess	Nucl.	Mass Excess	$\overline{E}_{exc}$ (keV)	a (keV)	b (keV)	References
51									
	$\frac{5}{2}^-$	Mn	-48243.71 (89)	Fe	-40221 (15)	0	-44233 (8)	-8022 (15)	[154]
	$\frac{7}{2}^-$	Mn	-48006.4 (9)	Fe	-39968 (15)	246	-43987 (8)	-8038 (15)	[154]
	$\frac{9}{2}^-$	Mn	-47103.9 (9)	Fe	-39075 (15)	1144	-43089 (8)	-8029 (15)	[154]
	$\frac{11}{2}^-$	Mn	-46755.2 (10)	Fe	-38705 (15)	1503	-42730 (8)	-8050 (15)	[154]
	$\frac{1}{2}^+$	Mn	-45967.8 (9)	Fe	-37732 (17)	2383	-41850 (9)	-8235 (17)	[154]
	$\frac{13}{2}^-$	Mn	-45286.4 (11)	Fe	-37268 (15)	2956	-41277 (8)	-8018 (15)	[154]
	$\frac{15}{2}^-$	Mn	-44992.9 (11)	Fe	-36946 (15)	3264	-40969 (8)	-8047 (15)	[154]
	$\frac{17}{2}^-$	Mn	-44563.1 (12)	Fe	-36632 (15)	3636	-40597 (8)	-7931 (15)	[154]
	$\frac{19}{2}^-$	Mn	-44104.0 (12)	Fe	-36124 (15)	4119	-40114 (8)	-7980 (16)	[154]
	$\frac{21}{2}^-$	Mn	-42603.9 (12)	Fe	-34613 (16)	5624	-38609 (8)	-7990 (16)	[154]
	$\frac{23}{2}^-$	Mn	-41772.2 (12)	Fe	-33729 (16)	6482	-37751 (8)	-8043 (16)	[154]
	$\frac{27}{2}^-$	Mn	-41068.1 (12)	Fe	-32952 (16)	7223	-37010 (8)	-8116 (16)	[154]
	$\frac{25}{2}^-$	Mn	-40351.6 (12)	Fe	-32288 (16)	7913	-36320 (8)	-8063 (16)	[154]
	$\frac{29}{2}^-$	Mn	-36733.3 (14)	Fe	-28753 (17)	11490	-32743 (8)	-7980 (17)	[154]
	$\frac{29}{2}^-$	Mn	-36462.2 (14)	Fe	-28509 (21)	11747	-32486 (11)	-7953 (21)	[154]
	$\frac{31}{2}^+$	Mn	-35451.9 (14)	Fe	-27571 (19)	12721	-31512 (9)	-7880 (19)	[154]
53									
	$\frac{7}{2}^-$	Fe	-50946.71 (171)	Co	-42658.60 (177)	0	-46802.65 (123)	-8288.11 (246)	[155]
	$\frac{9}{2}^-$	Fe	-49618.70 (173)	Co	-41331.6 (20)	1328	-45475.1 (13)	-8287.1 (26)	[155]
	$\frac{11}{2}^-$	Fe	-48607.47 (173)	Co	-40291.6 (20)	2354	-44449.5 (13)	-8315.9 (26)	[155]
	$\frac{19}{2}^-$	Fe	-47906.3 (17)	Co	-39462 (29)	3119	-43684 (15)	-8445 (29)	[155]
	$\frac{13}{2}^-$	Fe	-47770.8 (18)	Co	-39397.5 (22)	3219	-43584.2 (14)	-8373.3 (28)	[155]
	$\frac{15}{2}^-$	Fe	-47484.0 (18)	Co	-39077.5 (25)	3522	-43280.8 (15)	-8406.5 (31)	[155]
	$\frac{17}{2}^-$	Fe	-46941.3 (18)	Co	-38543.5 (27)	4061	-42742.4 (16)	-8397.8 (32)	[155]
55									
	$\frac{7}{2}^-$	Co	-54029.23 (54)	Ni	-45335.20 (79)	0	-49682.21 (48)	-8694.03 (95)	[156]
	$\frac{11}{2}^-$	Co	-51055.76 (57)	Ni	-42453.1 (22)	2928	-46754.4 (12)	-8602.7 (2.3)	[156]
	$\frac{1}{2}^+$	Co	-51106.98 (55)	Ni	-42150 (6)	3054	-46629 (3)	-8957 (6)	[156]
	$\frac{13}{2}^-$	Co	-50292.69 (58)	Ni	-41752.1 (25)	3660	-46022.4 (13)	-8540.6 (25)	[156]
	$\frac{15}{2}^-$	Co	-50254.62 (58)	Ni	-41718.1 (25)	3696	-45986.4 (13)	-8536.5 (25)	[156]
	$\frac{3}{2}^+$	Co	-50466.25 (54)	Ni	-41583 (7)	3658	-46025 (4)	-8883 (7)	[156]
	$\frac{17}{2}^-$	Co	-49515.45 (59)	Ni	-40852.1 (26)	4499	-45183.8 (14)	-8663.4 (27)	[156]
57									
	$\frac{3}{2}^-$	Ni	-56083.19 (67)	Cu	-47308.22 (62)	0	-51695.71 (45)	-8774.96 (91)	[157]
	$\frac{5}{2}^-$	Ni	-55314.7 (8)	Cu	-46280 (4)	899	-50797 (2)	-9034 (4)	[157]
	$\frac{1}{2}^-$	Ni	-54970.6 (8)	Cu	-46202 (4)	1110	-50586 (2)	-8768 (4)	[157]
	$\frac{5}{2}^-$	Ni	-53639.9 (8)	Cu	-44910 (10)	2421	-49275 (5)	-8730 (10)	[157]
59									
	$\frac{3}{2}^-$	Cu	-56357.70 (63)	Zn	-47214.92 (83)	0	-51786.31 (52)	-9142.78 (104)	[158]
	$\frac{5}{2}^-$	Cu	-55443.69 (64)	Zn	-46675 (50)	728	-51059 (25)	-8769 (50)	[158]
	$\frac{7}{2}^-$	Cu	-54959.14 (64)	Zn	-46321 (2)	1147	-50640 (1)	-8638 (2)	[158]
	$\frac{7}{2}^-$	Cu	-54492.48 (64)	Zn	-45818 (2)	1632	-50155 (1)	-8675 (3)	[158]
	$\frac{9}{2}^-$	Cu	-53966.78 (65)	Zn	-44882 (3)	2363	-49424 (2)	-9085 (3)	[158]
	$\frac{13}{2}^-$	Cu	-52909.92 (65)	Zn	-43829 (3)	3417	-48369 (2)	-9081 (3)	[158]
61									
	$\frac{3}{2}^-$	Zn	-56343 (16)	Ga	-47088 (53)	0	-51716 (28)	-9255 (55)	
63									
	$\frac{3}{2}^-$	Ga	-56547.1 (13)	Ge	-46921 (37)	0	-51734 (19)	-9626 (37)	
65									
	$\frac{3}{2}^-$	Ge	-56480.61 (257)	As	-46937 (85)	0	-51709 (43)	-9544 (85)	
67									
	$\frac{5}{2}^-$	As	-56585.98 (137)	Se	-46580 (67)	0	-51583 (34)	-10006 (67)	
71									
	$\frac{5}{2}^-$	Br	-56502.4 (54)	Kr	-46327 (128)	0	-51414 (65)	-10175 (129)	

[1] All g.s. mass excess data are quoted from Ref. [112, 159].

A.2.2 Properties of $T=1$ Triplets

Table A.3: *Properties of $T=1$ Triplets*

A	J^π	$T_z=1$ Nucl.	Mass Excess (keV)	$T_z=0$ Nucl.	Mass Excess (keV)	$T_z=-1$ Nucl.	Mass Excess (keV)	$\overline{E}_{exc}$ (keV)	b (keV)	c (keV)	References
6											
	0^+	He	17592.80 (42)	Li	17649.76 (10)	Be	18375.03 (545)	0	-391.12 (274)	334.16 (274)	[136]
	2^+	He	19390 (25)	Li	19453 (15)	Be	20045 (51)	1757	-328 (28)	265 (32)	[136]
8											
	2^+	Li	20945.80 (5)	Be	21568 (3)	B	22921.58 (100)	0	-988 (1)	366 (3)	[137]
	1^+	Li	21926.60 (11)	Be	22581.7 (10)	B	23691.1 (27)	922	-882.2 (14)	227.2 (17)	[137]
10											
	0^+	Be	12607.47 (8)	B	13790.78 (39)	C	15698.68 (41)	0	-1545.61 (21)	362.30 (44)	[137]
	2^+	Be	15975.50 (9)	B	17214.6 (7)	C	19052.4 (7)	3382	-1538.4 (4)	299.3 (8)	[137]
12											
	1^+	B	13368.9 (14)	C	15110 (3)	N	17338 (10)	0	-1984.6 (9)	243.5 (32)	[137]
	2^+	B	14322.0 (15)	C	16105.8 (7)	N	18298 (12)	970	-1988 (6)	204 (6)	[137]
	0^+	B	16092 (11)	C	17760 (20)	N	19777 (9)	2604	-1843 (7)	174 (22)	[137]
14											
	0^+	C	3019.89 (1)	N	5176.22 (2)	O	8007.46 (11)	0	-2493.78 (6)	337.46 (6)	[139]
	1^-	C	9113.7 (2)	N	10925.4 (1)	O	13180 (10)	5673	-2033 (5)	222 (5)	[139]
	0^+	C	9609.3 (2)	N	11481 (2)	O	13927 (10)	6272	-2159 (5)	287 (6)	[139]
	3^-	C	9748.1 (13)	N	11770 (3)	O	14279 (10)	6532	-2266 (5)	243 (6)	[139]
	2^+	C	10032 (4)	N	12035.67 (12)	O	14597 (10)	6821	-2283 (4)	279 (6)	[139]
	2^+	C	11337.8 (8)	N	13295 (7)	O	15775 (10)	8069	-2219 (5)	261 (9)	[139]
16											
	0^-	N	5804.1 (26)	O	8059 (4)	F	10680.3 (84)	41	-2438 (5)	183 (6)	[140]
	2^-	N	5683.7 (26)	O	8231.6 (4)	F	11104 (10)	199	-2710 (5)	162 (5)	[140]
	1^-	N	6080.9 (26)	O	8353 (8)	F	10873 (10)	295	-2396 (5)	124 (10)	[140]
	3^-	N	5981.9 (26)	O	8522 (2)	F	11401 (9)	495	-2710 (5)	170 (5)	[140]
	1^+	N	9037 (4)	O	11472 (2)	F	14438 (10)	3508	-2701 (6)	265 (6)	[140]
	2^+	N	9207 (4)	O	11705.3 (16)	F	14550 (10)	3680	-2672 (5)	173 (6)	[140]
18											
	0^+	O	-782.816 (1)	F	1914.66 (47)	Ne	5317.624 (364)	0	-3050.22 (18)	352.74 (51)	[141]
	2^+	O	1199.25 (9)	F	3934.95 (50)	Ne	7204.9 (4)	1964	-3002.8 (3)	267.1 (6)	[141]
	4^+	O	2772.02 (40)	F	5525 (2)	Ne	8693.8 (6)	3514	-2961 (1)	208 (2)	[141]
	0^+	O	2850.94 (11)	F	5626 (3)	Ne	8893.9 (7)	3641	-3021 (1)	246 (4)	[141]
	2^+	O	3137.62 (14)	F	5836.7 (9)	Ne	8934.0 (7)	3820	-2898.2 (4)	199 (1)	[141]
	0^+	O	4553.6 (6)	F	7009.58 (57)	Ne	9908 (8)	5008	-2677 (4)	221 (4)	[141]
20^1											
	2^+	F	-17.46 (3)	Ne	3231.3 (19)	Na	6850.2 (11)	0	-3433.8 (5)	185.1 (20)	[160]
	3^+	F	638.56 (5)	Ne	3842.1 (30)	Na	7447 (8)	621	-3404 (4)	200 (5)	[160]
	4^+	F	805.27 (5)	Ne	4048.1 (30)	Na	7652 (7)	814	-3423 (4)	181 (5)	[160]
22											
	0^+	Ne	-8024.714 (18)	Na	-4524.36 (21)	Mg	-399.94 (32)	0	-3812.39 (16)	312.03 (26)	[161]
	2^+	Ne	-6750.137 (19)	Na	-3229.39 (23)	Mg	847.08 (32)	1273	-3798.61 (16)	277.86 (28)	[161]
	4^+	Ne	-4667.0 (3)	Na	-1109.96 (30)	Mg	2908.28 (32)	3361	-3787.6 (3)	230.6 (4)	[161]
	2^+	Ne	-3568.9 (3)	Na	-8 (2)	Mg	4002.1 (5)	4459	-3785 (1)	224 (2)	[161]
24^2											
	4^+	Na	-8417.96 (4)	Mg	-4417.29 (5)	Al	-48.9 (10)	0	-4184.5 (5)	183.9 (5)	[143]
	1^+	Na	-7945.75 (4)	Mg	-3966.38 (22)	Al	376.9 (10)	450	-4161.3 (5)	182.0 (6)	[143]
	2^+	Na	-7854.76 (4)	Mg	-3875.03 (16)	Al	462 (4)	539	-4158 (2)	179 (2)	[143]
26											
	0^+	Mg	-16214.55 (3)	Al	-11981.81 (7)	Si	-7140.98 (11)	0	-4536.78 (6)	304.05 (9)	[145]
	2^+	Mg	-14405.82 (5)	Al	-10140.64 (7)	Si	-5345.1 (3)	1816	-4530.4 (2)	265.2 (2)	[145]
	2^+	Mg	-13276.21 (5)	Al	-9050.223 (65)	Si	-4357.5 (4)	2885	-4459.4 (2)	233.4 (3)	[145]
	0^+	Mg	-12625.99 (10)	Al	-8456.48 (15)	Si	-3808.5 (3)	3483	-4408.8 (2)	239.3 (3)	[145]
	3^+	Mg	-12273.00 (5)	Al	-8018.19 (15)	Si	-3385 (2)	3888	-4444 (1)	189 (1)	[145]
	2^+	Mg	-11881.98 (6)	Al	-7662.19 (9)	Si	-3003 (1)	4264	-4439 (1)	220 (1)	[145]
	3^+	Mg	-11864.47 (6)	Al	-7610.94 (8)	Si	-2958 (11)	4302	-4453 (6)	200 (6)	[145]
	0^+	Mg	-11242.26 (13)	Al	-7015.00 (14)	Si	-2335 (2)	4916	-4454 (1)	226 (1)	[145]
	2^+	Mg	-10922.81 (6)	Al	-6665.55 (10)	Si	-1912 (12)	5279	-4505 (6)	248 (6)	[145]
	4^+	Mg	-10738.44 (8)	Al	-6483.73 (8)	Si	-1811 (20)	5435	-4464 (10)	209 (10)	[145]
	4^+	Mg	-10498.95 (11)	Al	-6285.92 (10)	Si	-1579 (28)	5658	-4460 (14)	247 (14)	[145]
	0^+	Mg	-9959 (1)	Al	-5795.65 (12)	Si	-1201 (25)	6128	-4379 (13)	216 (13)	[145]
	2^+	Mg	-9468.79 (17)	Al	-5334.38 (9)	Si	-791 (25)	6582	-4339 (13)	205 (13)	[145]
	3^-	Mg	-9338.13 (5)	Al	-5245.63 (11)	Si	-352 (17)	6801	-4493 (9)	401 (9)	[145]
	2^+	Mg	-8843.3 (2)	Al	-4648.9 (3)	Si	9 (13)	7285	-4426 (7)	232 (7)	[145]

Appendix A. Coefficients of the Isobaric Multiplet Mass Equation

continued from Table A.3   Properties of $T = 1$ Triplets

A	J^π	$T_z = 1$ Nucl.	Mass Excess (keV)	$T_z = 0$ Nucl.	Mass Excess (keV)	$T_z = -1$ Nucl.	Mass Excess (keV)	$\overline{E}_{exc}$ (keV)	b (keV)	c (keV)	References
28^3											
	3^+	Al	-16850.49 (13)	Si	-12176.87 (10)	P	-7149.1 (11)	0	-4850.7 (6)	177.1 (6)	[145]
	2^+	Al	-16819.85 (13)	Si	-12111.24 (12)	P	-7043.4 (11)	68	-4888.2 (6)	179.6 (6)	[145]
	0^+	Al	-15878.11 (13)	Si	-11220.5 (8)	P	-6272 (3)	936	-4803 (2)	145 (2)	[145]
	3^+	Al	-15836.86 (13)	Si	-11116.55 (12)	P	-6015.1 (12)	1070	-4910.9 (6)	190.6 (6)	[145]
	2^+	Al	-15227.57 (13)	Si	-10609.34 (14)	P	-5633 (3)	1569	-4797 (2)	179 (2)	[145]
	1^+	Al	-15230.17 (13)	Si	-10592.37 (15)	P	-5581 (3)	1591	-4824 (2)	187 (2)	[145]
	2^+	Al	-14711.57 (13)	Si	-10060.16 (18)	P	-5045 (2)	2120	-4833 (1)	182 (1)	[145]
	1^+	Al	-14649.03 (13)	Si	-10046.79 (16)	P	-5006 (5)	2159	-4821 (3)	219 (3)	[145]
	4^+	Al	-14578.72 (13)	Si	-10058.29 (22)	P	-4933 (5)	2203	-4823 (3)	302 (3)	[145]
	2^+	Al	-14364.31 (13)	Si	-9714.2 (7)	P	-4743 (5)	2452	-4811 (3)	161 (3)	[145]
	3^+	Al	-13862.96 (18)	Si	-9253.4 (3)	P	-4253 (5)	2936	-4805 (3)	195 (3)	[145]
	1^+	Al	-13745 (1)	Si	-9162.5 (3)	P	-4176 (5)	3031	-4785 (3)	202 (3)	[145]
	3^+	Al	-13554.10 (13)	Si	-8951.48 (14)	P	-3985 (5)	3229	-4785 (3)	182 (3)	[145]
	6^-	Al	-11685 (2)	Si	-7136 (2)	P	-2209 (10)	5049	-4738 (5)	189 (6)	[145]
30											
	0^+	Si	-24432.96 (3)	P	-19523.60 (32)	S	-14062 (3)	0	-5185 (2)	276 (2)	[162]
	2^+	Si	-22197.639 (28)	P	-17263.15 (32)	S	-11851.8 (31)	2236	-5172.9 (15)	238.4 (16)	[162]
	2^+	Si	-20934.47 (4)	P	-16017.80 (32)	S	-10659.8 (31)	3469	-5137.4 (15)	220.7 (16)	[162]
	1^+	Si	-20663.48 (5)	P	-15698.40 (33)	S	-10386 (5)	3757	-5139 (3)	173 (3)	[162]
32^4											
	1^+	P	-24304.94 (12)	S	-19013.0 (10)	Cl	-13334.64 (57)	0	-5485.1 (3)	193.2 (11)	[145]
	2^+	P	-24226.88 (13)	S	-18900.5 (12)	Cl	-13244.7 (6)	94	-5491.1 (3)	164.7 (13)	[145]
	0^+	P	-23792.24 (13)	S	-18479.8 (8)	Cl	-12868.5 (6)	505	-5461.8 (3)	149.4 (9)	[145]
	1^+	P	-23155.55 (13)	S	-17890.1 (2)	Cl	-12166.1 (6)	1147	-5494.7 (3)	229.3 (4)	[145]
	2^+	P	-22982.10 (13)	S	-17672 (3)	Cl	-12009 (5)	1331	-5487 (3)	176 (4)	[145]
	3^+	P	-22549.94 (16)	S	-17286.2 (6)	Cl	-11615 (4)	1734	-5467 (2)	204 (3)	[145]
	1^+	P	-22075.24 (14)	S	-16808.0 (7)	Cl	-11141 (7)	2210	-5467 (4)	200 (4)	[145]
	2^+	P	-22087.15 (17)	S	-16820 (2)	Cl	-11065 (5)	2228	-5511 (3)	244 (4)	[145]
	2^-	P	-21040.95 (13)	S	-15939.0 (8)	Cl	-10279 (5)	3132	-5381 (3)	279 (3)	[145]
	3^-	P	-20985.0 (14)	S	-15792 (1)	Cl	-10169 (10)	3236	-5408 (5)	215 (5)	[145]
34											
	0^+	S	-29931.66 (6)	Cl	-24440.03 (7)	Ar	-18377.39 (34)	0	-5777.14 (17)	285.50 (18)	[145]
	2^+	S	-27804.10 (6)	Cl	-22282.13 (11)	Ar	-16286.5 (5)	2126	-5758.8 (3)	236.8 (3)	[145]
	2^+	S	-26627.45 (6)	Cl	-21056.7 (3)	Ar	-15089.9 (6)	3326	-5768.8 (3)	198.1 (4)	[145]
	0^+	S	-26015.25 (6)	Cl	-20499.9 (3)	Ar	-14506 (2)	3910	-5754 (1)	239 (1)	[145]
	2^+	S	-25816.85 (6)	Cl	-20292.2 (3)	Ar	-14249.6 (11)	4131	-5783.6 (5)	259 (1)	[145]
	0^+	S	-24703.48 (6)	Cl	-19430 (13)	Ar	-13410 (4)	5069	-5647 (2)	373 (13)	[145]
	2^+	S	-23503.54 (10)	Cl	-18070.7 (3)	Ar	-11852 (9)	6441	-5826 (5)	393 (5)	[145]
36											
	2^+	Cl	-29521.99 (4)	Ar	-23620.3 (4)	K	-17417.33 (35)	0	-6052.3 (2)	150.7 (5)	[145]
	3^+	Cl	-28733.55 (4)	Ar	-22894.4 (9)	K	-16617 (15)	772	-6058 (8)	219 (8)	[145]
	1^+	Cl	-28357.10 (4)	Ar	-22522.0 (6)	K	-16304.5 (5)	1126	-6026.3 (3)	191.2 (7)	[145]
	1^+	Cl	-27920.88 (4)	Ar	-22098.8 (9)	K	-15798.3 (4)	1581	-6061.3 (2)	239.2 (9)	[145]
	2^-	Cl	-27570.79 (4)	Ar	-21784 (10)	K	-15527 (20)	1893	-6022 (10)	234 (14)	[145]
	2^+	Cl	-27562.58 (4)	Ar	-21676.0 (6)	K	-15147 (30)	2058	-6208 (15)	321 (15)	[145]
38											
	0^+	Ar	-34714.74 (25)	K	-28670.3 (4)	Ca	-22058.47 (25)	0	-6328.1 (2)	283.7 (5)	[163]
	2^+	Ar	-32547.10 (25)	K	-26399.61 (30)	Ca	-19845.34 (27)	2218	-6350.88 (19)	203.39 (35)	[163]
40											
	4^-	K	-33535.49 (6)	Ca	-27188.16 (6)	Sc	-20523.3 (28)	0	-6506.1 (14)	158.7 (14)	[164]
	3^-	K	-33505.66 (6)	Ca	-27152.31 (5)	Sc	-20489.0 (32)	34	-6508.3 (16)	155.0 (16)	[164]
	2^-	K	-32735.35 (6)	Ca	-26421.58 (12)	Sc	-19751.2 (33)	780	-6492.1 (16)	178.3 (16)	[164]
	5^-	K	-32644.09 (6)	Ca	-26295.3 (7)	Sc	-19629.8 (35)	893	-6507.1 (17)	158.3 (19)	[164]
	1^+	K	-31245.62 (6)	Ca	-24977.1 (4)	Sc	-18238 (9)	2262	-6504 (5)	235 (5)	[164]
	4^-	K	-31138.33 (6)	Ca	-24797.01 (7)	Sc	-18153 (5)	2387	-6492 (3)	151 (3)	[164]
42											
	0^+	Ca	-38547.28 (15)	Sc	-32121.18 (17)	Ti	-25104.70 (28)	0	-6721.29 (16)	295.19 (23)	[165]
	2^+	Ca	-37022.58 (15)	Sc	-30534.87 (17)	Ti	-23548.7 (9)	1556	-6736.9 (5)	249.2 (5)	[165]
	0^+	Ca	-36710.0 (4)	Sc	-30247.6 (8)	Ti	-23250.5 (13)	1856	-6729.7 (7)	267.3 (13)	[165]
	2^+	Ca	-36123.11 (16)	Sc	-29634.59 (22)	Ti	-22708.6 (11)	2436	-6707.3 (5)	218.7 (6)	[165]
	4^+	Ca	-35794.87 (16)	Sc	-29305.81 (18)	Ti	-22428.1 (9)	2749	-6683.4 (5)	194.3 (5)	[165]
	6^+	Ca	-35357.84 (17)	Sc	-28879 (4)	Ti	-22061.7 (15)	3159	-6648 (1)	169 (4)	[165]
46^5											
	0^+	Ti	-44127.01 (32)	V	-37074.41 (34)	Cr	-29474 (20)	0	-7327 (10)	274 (10)	[166]
	2^+	Ti	-43237.72 (32)	V	-36159.48 (35)	Cr	-28581 (20)	899	-7328 (10)	250 (10)	[166]
	4^+	Ti	-42117.16 (32)	V	-35019.6 (5)	Cr	-27486 (20)	2018	-7315 (10)	218 (10)	[166]
	6^+	Ti	-40828.15 (35)	V	-33708.7 (9)	Cr	-26247 (20)	3298	-7291 (10)	171 (10)	[166]
	8^+	Ti	-39230.1 (5)	V	-32230.1 (12)	Cr	-24656 (20)	4853	-7287 (10)	287 (10)	[166]
	10^+	Ti	-37885.1 (5)	V	-30752 (1)	Cr	-23294 (20)	6248	-7296 (10)	163 (10)	[166, 167]
	12^+	Ti	-35909.5 (5)	V	-28806.2 (14)	Cr	-21311 (20)	8217	-7299 (10)	196 (10)	[166]
48											
	4^+	V	-44476.4 (11)	Cr	-37028.9 (74)	Mn	-29323 (112)	0	-7577 (56)	129 (57)	[168]
	2^+	V	-44168.2 (11)	Cr	-36722 (13)	Mn	-29011 (112)	310	-7578 (56)	132 (57)	[168]

A	J^π	$T_z = 1$ Nucl.	Mass Excess (keV)	$T_z = 0$ Nucl.	Mass Excess (keV)	$T_z = -1$ Nucl.	Mass Excess (keV)	$\overline{E}_{exc}$ (keV)	b (keV)	c (keV)	References
50											
	0^+	Cr	-50261.94 (89)	Mn	-42627.46 (89)	Fe	-34489 (60)	0	-7887 (30)	252 (30)	[169]
	2^+	Cr	-49478.62 (89)	Mn	-41827.30 (89)	Fe	-33724 (60)	783	-7878 (30)	226 (30)	[169]
	4^+	Cr	-48380.63 (89)	Mn	-40695.96 (90)	Fe	-32637 (60)	1889	-7872 (30)	187 (30)	[169]
	6^+	Cr	-47098.22 (90)	Mn	-39371.4 (14)	Fe	-31329 (60)	3194	-7885 (30)	158 (30)	[169]
	8^+	Cr	-45517.41 (92)	Mn	-37752.4 (14)	Fe	-29702 (60)	4803	-7908 (30)	143 (30)	[169]
	10^+	Cr	-43921.7 (9)	Mn	-36166.4 (18)	Fe	-28121 (60)	6390	-7900 (30)	145 (30)	[169]
54											
	0^+	Fe	-56253.84 (49)	Co	-48009.29 (51)	Ni	-39223 (50)	0	-8516 (25)	271 (25)	[170]
	2^+	Fe	-54845.65 (53)	Co	-46563.63 (53)	Ni	-37831 (50)	1416	-8507 (25)	225 (25)	[170]
	4^+	Fe	-53715.7 (6)	Co	-45357.32 (56)	Ni	-36603 (50)	2604	-8556 (25)	198 (25)	[170]
	6^+	Fe	-53304.6 (7)	Co	-45097.7 (7)	Ni	-36152 (50)	2978	-8576 (25)	369 (25)	[170]
58											
	0^+	Ni	-60226.96 (35)	Cu	-51462.70 (57)	Zn	-42298 (50)	0	-8964 (25)	200 (25)	[171]

[1] The mass excess of ^{20}Na is quoted from TABLE IV, column 4 of Ref. [172].
[2] The mass excess of ^{24}Al is quoted from TABLE IV, column 4 of Ref. [172].
[3] The mass excess of ^{28}P is quoted from TABLE IV, column 4 of Ref. [172].
[4] All g.s. mass excess data are quoted from Ref. [112, 159, 173].
[5] The 10^+ was only observed in Ref. [167]. Further cross check is needed.

A.2.3 Properties of $T = 3/2$ Quartets

Table A.4: *Properties of $T = 3/2$ Quartets*

A	J^π	Nucl.	T_z	Mass Excess (keV)	$\overline{E}_{\rm esc}$ (keV)	$a, b, c, \chi^2/n$ (keV)	a, b, c, d (keV)	References
7								
	$\frac{3}{2}^-$	He	$\frac{3}{2}$	26067 (8)	0	26398 (24)	26400 (25)	[136]
		Li	$\frac{1}{2}$	26147 (30)		−608 (21)	−636 (48)	
		Be	$-\frac{1}{2}$	26778 (30)		258 (19)	253 (21)	
		B	$-\frac{3}{2}$	27871 (71)		0.3993	15 (25)	
9								
	$\frac{3}{2}^-$	Li	$\frac{3}{2}$	24954.91 (9)	0	26337.7 (17)	26340.3 (18)	[137]
		Be	$\frac{1}{2}$	25740.6 (18)		−1318.8 (7)	−1332.4 (36)	
		B	$-\frac{1}{2}$	27071.5 (27)		264.6 (9)	263.1 (10)	
		C	$-\frac{3}{2}$	28909.45 (214)		14.81	6.33 (165)	
	$\frac{1}{2}^-$	Li	$\frac{3}{2}$	27646 (5)	2479	28847 (2)	28849 (3)	[137]
		Be	$\frac{1}{2}$	28325.5 (5)		−1164 (3)	−1168 (5)	
		B	$-\frac{1}{2}$	29492 (4)		241 (3)	239 (4)	
		C	$-\frac{3}{2}$	31127 (12)		1.221	3.2 (29)	
11								
	$\frac{1}{2}^+$	Be	$\frac{3}{2}$	20177.17 (24)	0	21909 (17)	21990 (25)	[138]
		B	$\frac{1}{2}$	21225 (16)		−1399 (15)	−1612 (49)	
		C	$-\frac{1}{2}$	22810 (40)		163 (11)	111 (16)	
		N	$-\frac{3}{2}$	24304 (46)		21.05	105 (23)	
13								
	$\frac{3}{2}^-$	B	$\frac{3}{2}$	16562.2 (11)	0	19257.8 (9)	19257.0 (9)	[139]
		C	$\frac{1}{2}$	18233.2 (12)		−2177.9 (12)	−2176.0 (15)	
		N	$-\frac{1}{2}$	20410.1 (5)		254.0 (13)	258.4 (24)	
		O	$-\frac{3}{2}$	23114.73 (953)		4.503	−3.66 (173)	
17								
	$\frac{1}{2}^-$	N	$\frac{3}{2}$	7870 (15)	0	11647.4 (17)	11647.5 (17)	[137]
		O	$\frac{1}{2}$	10269.9 (9)		−2875.1 (23)	−2874.4 (29)	
		F	$-\frac{1}{2}$	13144.6 (23)		240.2 (22)	239.0 (38)	
		Ne	$-\frac{3}{2}$	16500.45 (36)		0.1452	−1.06 (279)	
19								
	$\frac{5}{2}^+$	O	$\frac{3}{2}$	3333.58 (276)	0	7592.3 (19)	7609.7 (85)	[141]
		F	$\frac{1}{2}$	6052.2 (9)		−3200.4 (40)	−3235.0 (169)	
		Ne	$-\frac{1}{2}$	9283 (15)		240.7 (22)	231.6 (49)	
		Na	$-\frac{3}{2}$	12928 (12)		4.436	16.41 (779)	
	$\frac{3}{2}^+$	O	$\frac{3}{2}$	3429.6 (28)	106	7717.9 (22)	7712.1 (91)	[141]
		F	$\frac{1}{2}$	6173.2 (9)		−3205.0 (51)	−3193.5 (181)	
		Ne	$-\frac{1}{2}$	9368 (16)		230.8 (27)	234.1 (57)	
		Na	$-\frac{3}{2}$	13047.8 (156)		0.4397	−5.60 (844)	

continued from Table A.4   Properties of $T = 3/2$ Quartets

A	J^π	Nucl.	T_z	Mass Excess (keV)	$\overline{E}_{\text{esc}}$ (keV)	$a, b, c, \chi^2/n$ (keV)	a, b, c, d (keV)	References
21								
	$\frac{5}{2}^+$	F	$\frac{3}{2}$	−47.6 (18)	0	4898.3 (13)	4900.2 (17)	[142]
		Ne	$\frac{1}{2}$	3127.4 (14)		−3662.2 (23)	−3665.2 (29)	
		Na	$-\frac{1}{2}$	6791 (2)		243.1 (18)	236.6 (42)	
		Mg	$-\frac{3}{2}$	10913 (17)		3.016	5.23 (302)	
	$\frac{1}{2}^+$	F	$\frac{3}{2}$	232.32 (181)	253	5170.8 (15)	5168.8 (18)	[142]
		Ne	$\frac{1}{2}$	3417.1 (16)		−3617.2 (24)	−3613.8 (30)	
		Na	$-\frac{1}{2}$	7032 (2)		216.8 (19)	223.9 (43)	
		Mg	$-\frac{3}{2}$	11113 (17)		3.469	−5.79 (312)	
23								
	$\frac{5}{2}^+$	Ne	$\frac{3}{2}$	−5154.04 (11)	0	288.5 (2)	288.7 (9)	[143]
		Na	$\frac{1}{2}$	−1638.66 (15)		−3967.4 (2)	−3967.6 (18)	
		Mg	$-\frac{1}{2}$	2328.9 (16)		226.0 (1)	225.9 (4)	
		Al	$-\frac{3}{2}$	6748.07 (35)		0.02091	0.11 (79)	
25								
	$\frac{5}{2}^+$	Na	$\frac{3}{2}$	−9357.8 (12)	0	−3264.9 (7)	−3266.1 (14)	[144]
		Mg	$\frac{1}{2}$	−5405.8 (3)		−4391.8 (18)	−4390.1 (24)	
		Al	$-\frac{1}{2}$	−1015 (2)		219.9 (11)	222.4 (26)	
		Si	$-\frac{3}{2}$	3827 (10)		1.140	−2.11 (198)	
27								
	$\frac{1}{2}^+$	Mg	$\frac{3}{2}$	−14586.61 (5)	0	−8123.3 (12)	−8123.1 (24)	[145]
		Al	$\frac{1}{2}$	−10382.9 (7)		−4624.5 (29)	−4624.7 (37)	
		Si	$-\frac{1}{2}$	−5758 (3)		210.4 (16)	209.7 (67)	
		P	$-\frac{3}{2}$	−716 (27)		0.01071	0.48 (466)	
29								
	$\frac{5}{2}^+$	Al	$\frac{3}{2}$	−18215.4 (12)	0	−11141 (4)	−11140 (5)	[145]
		Si	$\frac{1}{2}$	−13605 (5)		−5030 (6)	−5033 (7)	
		P	$-\frac{1}{2}$	−8574 (3)		209 (5)	202 (13)	
		S	$-\frac{3}{2}$	−3157 (50)		0.4641	6.02 (9)	
31[1]								
	$\frac{3}{2}^+$	Si	$\frac{3}{2}$	−22949.04 (5)	0	−15465.8 (35)	−15468.3 (65)	[145]
		P	$\frac{1}{2}$	−18059.7 (17)		−5287.6 (87)	−5284.1 (116)	
		S	$-\frac{1}{2}$	−12775 (10)		199.2 (46)	204.5 (128)	
		Cl	$-\frac{3}{2}$	−7067 (50)		0.2025	−4.39 (976)	
	$\frac{1}{2}^+$	Si	$\frac{3}{2}$	−22196.81 (5)	747	−14713.7 (49)	−14725.1 (96)	[145]
		P	$\frac{1}{2}$	−17299.9 (15)		−5264.7 (127)	−5248.5 (173)	
		S	$-\frac{1}{2}$	−12047 (15)		184.0 (65)	207.4 (181)	
		Cl	$-\frac{3}{2}$	−6320 (71)		1.927	−19.42 (1399)	

						continued from Table A.4	Properties of $T = 3/2$ Quartets	
A	J^π	Nucl.	T_z	Mass Excess (keV)	$\overline{E}_\mathrm{esc}$ (keV)	$a, b, c, \chi^2/n$ (keV)	a, b, c, d (keV)	References
33								
	$\frac{1}{2}^+$	P	$\frac{3}{2}$	-26337.3 (11)	0	-18333.5 (5)	-18335.2 (7)	[145]
		S	$\frac{1}{2}$	-21105.8 (4)		-5650.6 (4)	-5645.9 (13)	
		Cl	$-\frac{1}{2}$	-15459 (1)		210.3 (4)	210.8 (4)	
		Ar	$-\frac{3}{2}$	-9384.31 (41)		13.66	-2.26 (62)	
	$\frac{3}{2}^+$	P	$\frac{3}{2}$	-24905.7 (11)	1414	-16898 (3)	-16898 (3)	[145]
		S	$\frac{1}{2}$	-19681 (3)		-5628 (1)	-5666 (6)	
		Cl	$-\frac{1}{2}$	-14019 (3)		193 (2)	192 (3)	
		Ar	$-\frac{3}{2}$	-8025 (2)		64.35	17.39 (217)	
	$\frac{5}{2}^+$	P	$\frac{3}{2}$	-24489.75 (110)	1838	-16480 (2)	-16480 (3)	[145]
		S	$\frac{1}{2}$	-19249 (4)		-5635 (1)	-5636 (5)	
		Cl	$-\frac{1}{2}$	-13613 (2)		196 (2)	197 (2)	
		Ar	$-\frac{3}{2}$	-7586 (2)		0.05883	0.55 (228)	
35								
	$\frac{3}{2}^+$	S	$\frac{3}{2}$	-28846.18 (5)	0	-20470.6 (8)	-20468.0 (12)	[145]
		Cl	$\frac{1}{2}$	-23360 (2)		-5891.1 (2)	-5884.1 (24)	
		Ar	$-\frac{1}{2}$	-17474.68 (77)		204.9 (4)	203.8 (6)	
		K	$-\frac{3}{2}$	-11172.90 (52)		8.471	-3.13 (108)	
37								
	$\frac{3}{2}^+$	Cl	$\frac{3}{2}$	-31761.55 (5)	0	-22905.5 (9)	-22903.1 (34)	[145]
		Ar	$\frac{1}{2}$	-25955 (6)		-6208.6 (3)	-6203.6 (68)	
		K	$-\frac{1}{2}$	-19750.5 (8)		203.0 (5)	202.0 (15)	
		Ca	$-\frac{3}{2}$	-13135.73 (79)		0.5335	-2.21 (303)	
	$\frac{1}{2}^+$	Cl	$\frac{3}{2}$	-30034.97 (7)	1660	-21260 (10)	-21257 (13)	[145]
		Ar	$\frac{1}{2}$	-24294 (10)		-6171 (6)	-6181 (25)	
		K	$-\frac{1}{2}$	-18114 (20)		214 (6)	213 (7)	
		Ca	$-\frac{3}{2}$	-11523 (17)		0.1432	4.37 (1154)	
41								
	$\frac{3}{2}^+$	K	$\frac{3}{2}$	-35559.54 (1)	0	-26059 (2)	-26098 (23)	[148]
		Ca	$\frac{1}{2}$	-29320.7 (9)		-6617 (3)	-6592 (16)	
		Sc	$-\frac{1}{2}$	-22703 (3)		189 (2)	344 (91)	
		Ti	$-\frac{3}{2}$	-15090 (364)		2.887	-102.90 (6057)	

[1] The mass excess of ^{31}S is quoted from Ref. [112].

A.2.4 Properties of $T = 2$ Quintets

Table A.5: *Properties of $T = 2$ Quintets.*

A	J^π	Nucl.	T_z	Mass Excess (keV)	$a, b, c, \chi^2/n$ (keV)	$a, b, c, d, \chi^2/n$ (keV)	$a, b, c, e, \chi^2/n$ (keV)	a, b, c, d, e (keV)	References
8	0^+	He	2	31609.61 (18)	32434.0 (17)	32435.2 (18)	32435.8 (18)	32435.8 (18)	[137]
		Li	1	31768.0 (55)	-877.6 (39)	-897.7 (64)	-878.0 (39)	-892.3 (74)	
		Be	0	32435.8 (18)	232.7 (20)	225.7 (27)	208.8 (69)	215.5 (75)	
		B	-1	33541 (9)	9.25	8.4 (21)	0.0	6.03 (261)	
		C	-2	35082 (23)		2.14	5.9 (17)	3.02 (206)	
							5.33		
20^1	0^+	O	2	3796.17 (89)	9692.2 (24)	9691.1 (26)	9691.0 (27)	9691.0 (27)	[160]
		F	1	6501.5 (30)	-3437.0 (41)	-3434.9 (47)	-3438.7 (46)	-3436.0 (86)	
		Ne	0	9691.0 (27)	244.5 (20)	246.8 (32)	250.3 (69)	248.1 (91)	
		Na	-1	13376 (12)	0.45	-1.5 (17)	0.0	-1.2 (31)	
		Mg	-2	17559 (27)		0.02	-1.1 (14)	-0.4 (25)	
							0.15		
24^2	0^+	Ne	2	-5951.64 (52)	1502.2 (6)	1502.7 (6)	1502.8 (6)	1502.8 (6)	[143]
		Na	1	-2451 (1)	-4178.6 (9)	-4177.3 (11)	-4175.3 (17)	-4174.6 (29)	
		Mg	0	1502.8 (6)	225.8 (4)	222.8 (15)	221.1 (22)	220.7 (27)	
		Al	-1	5900 (4)	2.45	1.1 (6)	0.0	-0.49 (174)	
		Si	-2	10755 (19)		0.94	0.72 (33)	1.00 (103)	
							0.08		
28^3	0^+	Mg	2	-15019 (2)	-6266.0 (10)	-6265.8 (10)	-6265.8 (10)	-6265.8 (10)	[145]
		Al	1	-10858.1 (4)	-4807.7 (20)	-4800.8 (61)	-4797.3 (97)	-4807.4 (189)	
		Si	0	-6266 (1)	215.6 (12)	204.8 (90)	203.2 (114)	209.2 (150)	
		P	-1	-1261 (20)	0.80	3.7 (31)	0.0	8.61 (1375)	
		S	-2	4073 (160)		0.14	1.81 (165)	-2.75 (746)	
							0.39		
32^4	0^+	Si	2	-24077.68 (30)	-13968.7 (2)	-13967.6 (3)	-13967.6 (3)	-13967.6 (3)	[112]
		P	1	-19232.46 (15)	-5471.7 (3)	-5472.9 (3)	-5471.0 (3)	-5473.0 (5)	
		S	0	-13967.57 (28)	208.5 (2)	207.2 (3)	205.7 (5)	207.2 (6)	
		Cl	-1	-8288.3 (7)	27.617	0.89 (22)	0.0	0.90 (19)	
		Ar	-2	-2200.2 (18)		0.001	0.57 (10)	-0.01 (16)	
							21.602		
36	0^+	S	2	-30664.13 (2)	-19377.7 (13)	-19378.2 (15)	-19378.1 (15)	-19378.1 (15)	[145]
		Cl	1	-25222.29 (9)	-6046.0 (19)	-6047.0 (24)	-6047.8 (37)	-6044.9 (63)	
		Ar	0	-19378.1 (15)	201.4 (7)	203.8 (33)	204.1 (47)	202.1 (59)	
		K	-1	-13128 (8)	0.34	-0.89 (120)	0.0	-2.09 (366)	
		Ca	-2	-6451 (40)		0.13	-0.42 (73)	0.77 (217)	
							0.34		
40	0^+	Ar	2	-35039.895 (2)	-22858.2 (9)	-22858.4 (10)	-22858.4 (10)	-22858.4 (10)	[164]
		K	1	-29151.5 (3)	-6495.9 (15)	-6497.8 (28)	-6498.6 (43)	-6481.6 (145)	
		Ca	0	-22858 (1)	202.5 (6)	206.0 (43)	206.0 (51)	197.2 (88)	
		Sc	-1	-16155 (9)	1.00	-1.23 (148)	0.0	-16.43 (1341)	
		Ti	-2	-8850 (160)		1.30	-0.53 (75)	7.78 (682)	
							1.50		

[1] The mass excess of ^{20}Na is quoted from TABLE IV, column 4 of Ref. [172].
[2] The mass excess of ^{24}Al is quoted from TABLE IV, column 4 of Ref. [172].
[3] The mass excess of ^{28}P is quoted from TABLE IV, column 4 of Ref. [172].
[4] The mass excess data and excited states are quoted from TABLE I, set C of Ref. [112]

Appendix A. Coefficients of the Isobaric Multiplet Mass Equation

Appendix B

Fitted IMME b and c Coefficients

Remarks: All experimental b and c coefficients in this appendix are quoted from Appendix A. The experimental b coefficients in Table B.1, B.2, B.3, and B.4 are added with neutron-hydrogen mass difference, Δ_{nH}=782.354 keV [101], c.f. Eq.(1.27). All theoretical b and c coefficients obtained in a shell-model fit are based on Eq.(2.69).

B.1   Fitted b Coefficients of $T = 1/2$ Doublets

Table B.1: *Fitted $T = 1/2$ Doublets*

mass, A	$2J^\pi$	b (exp) (keV)	b (fit) (keV)
19^2	1^+	4021.85 (16)	4042.91
	5^+	4062.98 (20)	4027.08
	3^+	4003.8 (4)	3976.6
21^3	3^+	4329.49 (28)	4306.43
	5^+	4310.67 (30)	4300.32
	7^+	4299.7 (4)	4307.5
23^3	3^+	4838.94 (69)	4844.20
	5^+	4849.66 (70)	4851.46
	7^+	4815.1 (11)	4825.0
25^3	5^+	5058.95 (48)	5066.56
27^4	5^+	5594.71 (18)	5566.08
	1^+	5531.9 (3)	5558.2
	3^+	5537.7 (3)	5563.8
29^4	1^+	5724.81 (60)	5772.33
	3^+	5834.96 (60)	5758.73
31^4	1^+	6180.35 (24)	6132.49
	3^+	6163.1 (3)	6120.2
33^4	3^+	6364.94 (44)	6329.27
	1^+	6334.46 (47)	6342.87
35^4	3^+	6748.48 (75)	6720.92
	1^+	6713.0 (8)	6732.2
	5^+	6735.9 (8)	6710.9
	3^+	6692.8 (8)	6727.1
	5^+	6728.55 (76)	6659.10
	1^+	6665 (10)	6652

		continued from Table B.1	Fitted $T = 1/2$ Doublets
mass, A	$2J^\pi$	b (exp) (keV)	b (fit) (keV)
37^4	3^+	6929.83 (23)	6900.61
	1^+	6890.86 (25)	6901.43
	5^+	6884.0 (3)	6950.6
39^5	3^+	7306.84 (60)	7319.56
	1^+	7252.8 (11)	7395.3

[1] $(V_0^{T=1})_{ijkl}$ of nuclear Hamiltonian USD had been used as the ISB term and UCOM SRC scheme was applied on V_{coul}.
[2] Recently adopted g.s. mass excess data from Ref. [103] and excited levels from Ref. [104, 141]
[3] *Ibid.*, except excited levels are from Ref. [104, 142]
[4] *Ibid.*, except excited levels are from Ref. [104, 145]
[5] *Ibid.*, except excited levels are from Ref. [104, 174]

B.2 Fitted b and c Coefficients of $T = 1$ Triplets

Table B.2: *Fitted $T = 1$ Triplets*

mass, A	$2J^\pi$	b (exp) (keV)	b (fit) (keV)	c (exp) (keV)	c (fit) (keV)
18^2	0^+	3832.57 (18)	3844.63	352.74 (50)	339.28
	4^+	3785.2 (2)	3801.0	267.1 (6)	268.3
20^3	4^+	4216.5 (6)	4182.5	185.4 (20)	193.6
	6^+	4186 (4)	4187	200 (5)	211
	8^+	4206 (4)	4169	181 (5)	185
22^4	0^+	4594.74 (16)	4579.52	312.03 (26)	297.58
	4^+	4580.96 (16)	4572.70	277.86 (28)	265.95
	8^+	4570.0 (2)	4576.8	230.5 (4)	230.0
	4^+	4567.8 (3)	4582.3	224.1 (20)	235.8
24^5	8^+	4967.63 (55)	4953.27	184.61 (55)	196.81
	2^+	4944.4 (6)	4957.6	182.7 (6)	191.4
	4^+	4942 (2)	4969	179 (2)	163
26^6	0^+	5319.14 (6)	5316.15	304.05 (9)	307.97
	4^+	5312.7 (11)	5338.4	265.2 (1)	273.7
28^7	6^+	5633.85 (60)	5666.53	177.88 (61)	191.95
	4^+	5671.35 (61)	5662.88	180.39 (62)	186.26
30^8	0^+	5967.65 (150)	5976.12	275.93 (153)	272.84
	4^+	5955.3 (15)	5952.5	238.4 (16)	239.8
	4^+	5919.7 (15)	5946.1	220.6 (16)	229.7
32^9	2^+	6267.5 (3)	6246.9	193.2 (11)	199.7
	4^+	6273.4 (3)	6244.2	164.7 (12)	169.5
	0^+	6244.2 (3)	6246.8	149.4 (9)	153.1
34^6	0^+	6559.49 (17)	6560.29	285.50 (18)	271.63
	4^+	6541.2 (2)	6544.9	236.8 (3)	234.8
	4^+	6551.1 (3)	6573.8	198.1 (4)	204.2
	0^+	6537 (1)	6590	239 (1)	230
36^6	4^+	6834.7 (2)	6859.7	150.7 (4)	147.9
	6^+	6840 (8)	6862	219 (8)	220
	2^+	6808.6 (3)	6858.3	191.2 (7)	195.9
	2^+	6843.6 (2)	6849.0	239.2 (9)	235.7
38^{10}	0^+	7110.5 (2)	7103.4	283.7 (4)	268.5
	4^+	7133.23 (19)	7153.19	203.39 (35)	195.20

[1] $(V_0^{T=1})_{ijkl}$ of nuclear Hamiltonian USD had been used as the ISB term and UCOM SRC scheme was applied on V_{coul}.
[2] Recently adopted g.s. mass excess data from Ref. [103] and excited levels from Ref. [104, 141]
[3] *Ibid.*, except g.s. mass excess of ^{20}Na is from TABLE IV, column 4 of Ref. [172] and excited levels from Ref. [104, 160]
[4] Recently adopted g.s. mass excess data from Ref. [103] and excited levels from Ref. [104, 161]
[5] *Ibid.*, except g.s. mass excess of ^{24}Al is from TABLE IV, column 4 of Ref. [172] and excited levels from Ref. [104, 143]
[6] Recently adopted g.s. mass excess data from Ref. [103] and excited levels from Ref. [104, 145]
[7] *Ibid.*, except g.s. mass excess of ^{28}P is from TABLE IV, column 4 of Ref. [172] and excited levels from Ref. [104, 145]
[8] Recently adopted g.s. mass excess data from Ref. [103] and excited levels from Ref. [104, 162]
[9] All g.s. mass excess data were from TABLE I. of Ref. [112, 159, 173] and excited levels from Ref. [104, 145]
[10] Recently adopted g.s. mass excess data from Ref. [103] and excited levels from Ref. [104, ?]

B.3 Fitted b and c Coefficients of $T = 3/2$ Quartets

Table B.3: *Fitted $T = 3/2$ Quartets*

mass, A	$2J^\pi$	b (exp) (keV)	b (fit) (keV)	c (exp) (keV)	c (fit) (keV)
19[2]	5^+	3982.7 (40)	3930.0	240.7 (22)	233.6
	3^+	3987.3 (50)	3931.9	230.8 (27)	231.3
21[3]	5^+	4444.6 (23)	4382.8	243.1 (18)	230.5
	1^+	4399.6 (24)	4377.6	216.8 (19)	225.8
23[4]	5^+	4749.73 (12)	4754.66	225.99 (10)	223.77
25[5]	5^+	5174.1 (18)	5171.5	219.9 (11)	224.9
27[6]	1^+	5406.8 (29)	5483.1	210.4 (16)	226.6
29[6]	5^+	5812.5 (55)	5830.2	209.4 (50)	214.1
31[7]	3^+	6070.0 (87)	6056.4	199.2 (45)	207.0
	1^+	6047.1 (127)	6056.9	184.0 (65)	210.5
33[6]	1^+	6432.92 (37)	6404.15	210.32 (39)	209.89
35[6]	3^+	6673.41 (17)	6653.74	204.90 (39)	198.97
37[6]	3^+	6990.95 (27)	6980.92	203.03 (48)	198.32
	1^+	6953.7 (55)	6983.2	214.2 (56)	211.9

[1] $(V_0^{T=1})_{ijkl}$ of nuclear Hamiltonian USD had been used as the ISB term and UCOM SRC scheme was applied on V_{coul}.
[2] Recently adopted mass excess data Ref. [103] and excited states from Ref. [104, 141]
[3] *Ibid.*, except excited levels are from Ref. [104, 142]
[4] *Ibid.*, except excited levels are from Ref. [104, 143]
[5] *Ibid.*, except excited levels are from Ref. [104, 144]
[6] *Ibid.*, except excited levels are from Ref. [104, 145]
[7] *Ibid.*, except g.s. mass excess of ^{31}S is from Ref. [112] and excited states from Ref. [104, 145]

B.4 Fitted b and c Coefficients of $T = 2$ Quintets

Table B.4: *Fitted $T = 2$ Quintets*

mass, A	J^π	b (exp) (keV)	b (fit) (keV)	c (exp) (keV)	c (fit) (keV)
20[2]	0^+	4219.3 (41)	4179.2	244.5 (20)	234.0
24[3]	0^+	4960.9 (85)	4962.5	225.8 (37)	225.2
28[4]	0^+	5590.1 (20)	5651.9	215.6 (12)	219.0
32[5]	0^+	6254.08 (26)	6245.91	208.45 (14)	208.18
36[6]	0^+	6828.4 (19)	6865.0	201.4 (7)	199.3

[1] $(V_0^{T=1})_{ijkl}$ of nuclear Hamiltonian USD had been used as the ISB term and UCOM SRC scheme was applied on V_{coul}.
[2] Recently adopted g.s. mass excess data from Ref. [103], g.s. mass excess of ^{20}Na is from TABLE IV, column 4 of Ref. [172] and excited states from Ref. [104, 160]
[3] *Ibid.*, except g.s. mass excess of ^{24}Al is from TABLE IV, column 4 of Ref. [172] and excited states from Ref. [104, 143]
[4] *Ibid.*, except g.s. mass excess of ^{28}P is from TABLE IV, column 4 of Ref. [172] and excited states from Ref. [104]
[5] Mass excess data and excited states from TABLE I, set C of Ref. [112]
[6] Recently adopted mass excess data Ref. [103] and excited states from Ref. [104, 145]

References

References

162

Bibliography

[1] K. Nakamura, et al., (Particle Data Group), J. Phys. **G**: Nucl. Part. Phys. 37 (2010) 075021.

[2] W. Heisenberg, Z. Physik 77 (1932) 8.

[3] J. Chadwick, Nature 129 (1932) 312.

[4] R. Machleidt, D. R. Entem, Phys. Rep. 503 (2011) 1.

[5] E. P. Wigner, Phys. Rev. 51 (1937) 106.

[6] B. Cassen, E. U. Condon, Phys. Rev. 50 (1936) 846.

[7] E. M. Henley, *Charge Independence and Charge Symmetry of Nuclear Forces*, Isospin in Nuclear Physics, ed. D. H. Wilkinson, North-Holland, Amsterdam, 1969, p. 15.

[8] F. Iachello, *Lie Algebras and Applications*, Springer, Heidelberg, 2006.

[9] A. Frank, J. Jolie, P. V. Isacker, *Symmetries in Atomic Nuclei*, Springer-Verlag, Heidelberg, 2009.

[10] J. Jänecke, *Systematics of Coulomb Energies and Excitation Energies of Isobaric Analogue States*, Isospin in Nuclear Physics, ed. D. H. Wilkinson, North-Holland, Amsterdam, 1969, p. 297.

[11] A. R. Edmonds, *Angular Momentum in Quantum Mechanics*, Princeton University Press, New Jersey, 1957.

[12] E. P. Wigner, in: W. Milligan (Ed.), Proceedings of the Robert A. Welch Foundation Conference on Chemical Research, Vol. 1, Welch Foundation, Houston, 1958, p. 88.

[13] S. Weinberg, S. B. Treiman, Phys. Rev. 116 (1959) 465.

[14] G. A. Miller, B. Nefkens, I. Slaus, Phys. Rev. 194 (1990) 1.

[15] R. Machleidt, Phys. Rev. **C** 63 (2001) 024001.

[16] E. Epelbaum, H.-W. Hammer, U.-G. Meissner, Rev. Mod. Phys. 81 (2009) 1773.

[17] I. S. Towner, J. C. Hardy, Rep. Prog. Phys. 73 (2010) 046301.

[18] J. C. Hardy, I. S. Towner, Phys. Rev. **C** 79 (2009) 055502.

[19] O. Naviliat-Cuncic, N. Severijns, Phys. Rev. Lett. 102 (2009) 012502.

[20] I. S. Towner, Nucl. Phys. **A** 216 (1973) 589.

[21] N. Smirnova, C. Volpe, Nucl. Phys. **A** 714 (2003) 441.

[22] M. Bentley, S. Lenzi, Prog. Part. Nucl. Phys. 59 (2007) 497.

[23] B. Blank, M. Borge, Prog. Part. Nucl. Phys. 60 (2008) 403.

[24] E. Farnea, et al., Phys. Lett. **B** 551 (2004) 56.

[25] R. Orlandi, et al., Phys. Rev. Lett. 103 (2009) 052501.

[26] R. J. Blin-Stoyle, M. Rosina, Nucl. Phys. 70 (1965) 321.

[27] G. F. Bertsch, B. H. Wildenthal, Phys. Rev. **C** 8 (1973) 1023.

[28] I. S. Towner, J. C. Hardy, Nucl. Phys. **A** 205 (1973) 33.

[29] W. E. Ormand, B. A. Brown, Nucl. Phys. **A** 440 (1985) 274.

[30] W. E. Ormand, B. A. Brown, Nucl. Phys. **A** 491 (1989) 1.

[31] A. P. Zuker, et al., Phys. Rev. Lett. 89 (2002) 142502.

[32] I. S. Towner, J. C. Hardy, Phys. Rev. **C** 77 (2008) 025501.

[33] B. A. Brown, Phys. Rev. Lett. 65 (1990) 2753.

[34] W. E. Ormand, Phys. Rev. **C** 53 (1996) 214.

[35] W. E. Ormand, Phys. Rev. **C** 55 (1997) 2407.

[36] I. Hamamoto, H. Sagawa, Phys. Rev. **C** 48 (1993) R960.

[37] J. Dobaczewski, I. Hamamoto, Phys. Lett. **B** 345 (1995) 181.

[38] G. Colo, M. A. Nagarajan, P. V. Isacker, A. Vitturi, Phys. Rev. **C** 52 (1995) R1175.

[39] H. Sagawa, T. Suzuki, N. V. Giai, Phys. Rev. **C** 53 (1996) 2126.

[40] H. Liang, N. V. Giai, J. Meng, Phys. Rev. **C** 79 (2009) 064316.

[41] W. Satula, J. Dobaczewski, W. Nazarewicz, M. Rafalski, Phys. Rev. Lett. 103 (2009) 012502.

[42] W. Satula, J. Dobaczewski, W. Nazarewicz, M. Rafalski, nucl-th/1101.0939 (2011).

[43] A. Petrovici, K. Schmid, O.Radu, A. Faessler, Phys. Rev. **C** 78 (2008) 064311.

[44] E. Caurier, P. Navratil, W. Ormand, J. Vary, Phys. Rev. **C** 66 (2002) 024314.

[45] N. Michel, W. Nazarewicz, M. Ploszajczak, Phys. Rev. **C** 82 (2010) 044315.

[46] N. Auerbach, Phys. Rev. **C** 79 (2009) 035502.

[47] N. Auerbach, Phys. Rev. **C** 81 (2010) 067305.

[48] E. Caurier, G. Martínez-Pinedo, F. Nowacki, A. Poves, A. P. Zuker, The shell model as a unified view of nuclear structure, Rev. Mod. Phys. 77 (2005) 427.

[49] B. A. Brown, W. A. Richter, Phys. Rev. **C** 74 (2006) 034315.

[50] M. Honma, T. Otsuka, B. A. Brown, T. Mizusaki, Phys. Rev. **C** 69 (2004) 034335.

[51] F. Nowacki, A. Poves, Phys. Rev. **C** 79 (2009) 014310.

[52] R. Roth, T. Neff, H. Feldmeier, Prog. Part. Nucl. Phys. 65 (2010) 50.

[53] F. Šimkovic, A. Faessler, H. Műther, V. Rodin, M. Stauf, Phys. Rev. **C** 79 (2009) 055501.

[54] M. Goeppert Mayer, Phys. Rev. 75 (1949) 1969.

[55] O. Haxel, J. H. D. Jensen, H. E. Suess, Phys. Rev. 75 (1949) 1766.

[56] I. Talmi, *Fifty Years of the Shell Model – The Quest for the Effective Interaction*, Vol. 27, Kluwer Academic Press, New York, 2002.

[57] K. Heyde, *The Nuclear Shell Model*, second corrected and enlarged Edition, Springer-Verlag, Heidelberg, 2004.

[58] A. Bohr, B. Mottelson, *The Nuclear Structure*, second corrected and enlarged Edition, Springer-Verlag, Heidelberg, 1977.

[59] M. Taketani, Prog. Theor. Phys. Suppl. No. 3 (1956) 1.

[60] W. Weise, Prog. Theor. Phys. Suppl. No. 170 (2007) 161.

[61] K. Heyde, *Basic Ideas and Concepts in Nuclear Physics*, second edition Edition, Institute of Physics, Bristol and Philadelphia, 1999.

[62] W. O. Myers, W. J. Swiatecki, Nucl. Phys. 81 (1966) 1.

[63] P. J. Brussaard, P. W. M. Glaudemans, *Shell-Model Applications in Nuclear Spectroscopy*, North-Holland, Amsterdam, 1977.

[64] R. F. Casten, *Nuclear Structure from a Simple Perspective*, Oxford University Press, Oxford, 1990.

[65] P. F. A. Klingenberg, Rev. Mod. Phys. 24 (1952) 63.

[66] P. Navratil, S. Quaglioni, I. Stetcu, B. Barrett, nucl-th/0904.0463 (2009).

[67] E. Caurier, F. Nowacki, Acta Physica Polonica 30 (1999) 705.

[68] B. A. Brown, A. Etchegoyen, W. D. M. Rae, N. S. Godwin, W. A. Richter, C. H. Zimmerman, W. E. Ormand, J. S. Winfield, The computer code OXBASH. MSU-NSCL Report, No. 524, 1984.

[69] W. D. M. Rae, http://www.nscl.msu.edu/~brown/resources/resources.html.

[70] T. Mizusaki, RIKEN Accel. Prog. Rep., 33:14, 2000.

[71] W. E. Ormand, C. W. Johnson, REDSTICK, version 3.5, UCRL-CODE-230640.

[72] Oslo code, http://folk.uio.no/mhjensen/cp/software.html.

[73] R. R. Whitehead, A. Watt, B. J. Cole, I. Morrison, Adv. Nucl. Phys. 9 (1977) 123.

[74] B. H. Brandow, Rev. Mod. Phys. 39 (1967) 771.

[75] T. T. S. Kuo, Ann. Rev. Nucl. Part. Sci. 24 (1974) 101.

[76] M. Hjorth-Jensen, T. T. S. Kuo, E. Osnes, Phys. Rep. 261 (1995) 125.

[77] B. R. Barrett, M. W. Kirson, Adv. Nucl. Phys. 6 (1973) 219.

[78] T. T. S. Kuo, G. E. Brown, Nucl. Phys. 85 (1966) 40.

[79] S. K. Bogner, T. T. S. Kuo, A. Schwenk, Phys. Rep. 386 (2003) 1.

[80] H. Bethe, Ann. Rev. Nucl. Part. Sci. 21 (1971) 93.

[81] S. Weinberg, Phys. Lett. **B** 251 (1990) 288.

[82] D. R. Entem, R. Machleidt, Phys. Rev. **C** 68 (2003) 041001.

[83] E. Epelbaum, W. Gloeckle, U.-G. Meissner, Nucl. Phys. **A** 747 (2005) 362.

[84] U. van Kolck, Phys. Rev. **C** 49 (1994) 2932.

[85] J. L. Friar, D. Hűber, U. van Kolck, Phys. Rev. **C** 59 (1999) 53.

[86] L. Coraggio, A. Covello, A. Gargano, N. Itaco, T. T. S. Kuo, Prog. Part. Nucl. Phys. 62 (2009) 135.

[87] A. Poves, A. P. Zuker, Phys. Rep. 70 (1981) 235.

[88] G. Martínez-Pinedo, A. P. Zuker, A. Poves, E. Caurier, Phys. Rev. **C** 55 (1997) 187.

[89] F. Nowacki, *Description Microscopique des Processus Faibles dans les Noyaux Spheriques*, Ph.D. thesis, IReS, Strasbourg (1996).

[90] M. Honma, T. Otsuka, B. A. Brown, T. Mizusaki, Phys. Rev. **C** 65 (2002) 061301(R).

[91] T. Otsuka, M. Honma, T. Mizusaki, et al., Prog. Part. Nucl. Phys. 47 (2001) 319.

[92] B. A. Brown, B. H. Wildenthal, Ann. Rev. Nucl. Part. Sci. 38 (1988) 29.

[93] T. T. S. Kuo, Nucl. Phys. **A** 103 (1967) 71.

[94] S. Cohen, D. Kurath, Nucl. Phys. 73 (1965) 1.

[95] J. Blomqvist, A. Molinari, Nucl. Phys. **A** 106 (1968) 545.

[96] I. Angeli, At. Data Nucl. Data Tables 87 (2004) 185.

[97] M. W. Kirson, Nucl. Phys. **A** 781 (2007) 350.

[98] G. Miller, J. Spencer, Ann. Phys. (N.Y.) 100 (1976) 562.

[99] R. Roth, H. Hergert, P. Papakonstantinou, T. Neff, H. Feldmeier, Phys. Rev. **C** 72 (2005) 034002.

[100] F. Šimkovic, A. Faessler, V. Rodin, P. Vogel, J. Engel, Phys. Rev. **C** 77 (2008) 045503.

[101] J. Britz, A. Pape, M. S. Antony, At. Data Nucl. Data Tables 69 (1998) 125.

[102] K. Blaum, Phys. Rep. 425 (2006) 1.

[103] G. Audi, M. Wang, (private communication).

[104] NNDC, National Nuclear Data Center online, http://www.nndc.bnl.gov.

[105] Y. H. Lam, B. Blank, N. A. Smirnova, J. B. Bueb, M. S. Antony, (in preparation).

[106] H. A. Bethe, R. F. Bacher, Rev. Mod. Phys. 8 (1936) 82.

[107] J. Jänecke, Phys. Rev. 147 (1966) 735.

[108] S. Sengupta, Nucl. Phys. 21 (1960) 542.

[109] J. A. Nolen, J. P. Schiffer, Ann. Rev. Nucl. Sci. 19 (1969) 471.

[110] F. Everling, Nucl. Phys. **A** 144 (1970) 539.

[111] E. Henley, C. Lacy, Phys. Rev. 184 (1969) 1228.

[112] A. Kankainen, et al., Phys. Rev. **C** 82 (2010) 052501.

[113] S. Triambak, et al., Phys. Rev. **C** 73 (2006) 054313.

[114] W. E. Ormand, (private communication).

[115] B. A. Brown, R. Sherr, Nucl. Phys. **A** 322 (1979) 61.

[116] G. E. Brown, M. Rho, Phys. Rev. Lett. 66 (1991) 2720.

[117] J. W. Holt, G. E. Brown, J. D. Holt, T. T. S. Kuo, Nucl. Phys. **A** 785 (2007) 322.

[118] J. W. Holt, G. E. Brown, J. D. Holt, T. T. S. Kuo, R. Machleidt, Phys. Rev. Lett. 66 (2008) 062501.

[119] K. T. Hecht, Nucl. Phys. **A** 114 (1968) 280.

[120] B. C. Carlson, I. Talmi, Phys. Rev. 96 (1954) 436.

[121] K. T. Hecht, S. C. Pang, J. Math. Phys. 10 (1969) 1571.

[122] K. T. Hecht, *Isobaric Spin in Nuclear Physics*, ed. J. D. Fox and D. Robson, Academic Press, New York and London, 1966, p. 823.

[123] K. T. Hecht, Nucl. Phys. **A** 102 (1967) 11.

[124] R. Hemenger, Ph.D. thesis, The University of Michigan (1968).

[125] A. Signoracci, B. A. Brown, Phys. Rev. **C** 84 (2011) 031301.

[126] A. A. Kwiatkowski, et al., Phys. Rev. **C** 80 (2009) 051302.

[127] E. K. Warburton, J. A. Becker, B. A. Brown, Phys. Rev. **C** 41 (1990) 1147.

[128] B. H. Wildenthal, Prog. Part. Nucl. Phys. 11 (1984) 5.

[129] I. I. Y. Bigi, A. I. Sanda, *CP Violation*, Cambridge University Press, Cambridge, 2009.

[130] M. Kobayashi, T. Maskawa, Prog. Theor. Phys. 49 (1973) 652.

[131] L. Wolfenstein, Phys. Rev. Lett. 51 (1983) 1945.

[132] A. J. Buras, M. E. Lautenbacher, G. Ostermaier, Phys. Rev. **D** 50 (1994) 3433.

[133] W. E. Ormand, B. A. Brown, Phys. Rev. Lett. 62 (1989) 866.

[134] Y. H. Lam, N. A. Smirnova, B. Blank, E. Caurier, (in preparation).

[135] H. R. W. D. R. Tilley, H. H. Hasan, Nucl. Phys. **A** 474 (1987) 1.

[136] D. R. Tilley, C. M. Cheves, J. L. Godwin, G. M. Hale, H. M. Hofmann, J. H. Kelley, C. G. Sheu, H. R. Weller, Nucl. Phys. **A** 708 (2002) 3.

[137] D. R. Tilley, J. H. Kelley, J. L. Godwin, D. J. Millener, J. E. Purcell, C. G. Sheu, H. R. Weller, Nucl. Phys. **A** 745 (2004) 155.

[138] F. Ajzenberg-Selove, Nucl. Phys. **A** 506 (1990) 1.

[139] F. Ajzenberg-Selove, Nucl. Phys. **A** 523 (1991) 1.

[140] H. R. W. D. R. Tilley, C. M. Cheves, Nucl. Phys. **A** 564 (1993) 1.

[141] D. R. Tilley, et al., Nucl. Phys. **A** 595 (1995) 1.

[142] R. B. Firestone, Nuclear Data Sheets 103 (2004) 269.

[143] R. B. Firestone, Nuclear Data Sheets 108 (2007) 2319.

[144] R. B. Firestone, Nuclear Data Sheets 110 (2009) 1691.

[145] P. M. Endt, Nucl. Phys. **A** 633 (1998) 1.

[146] F. Della Vedova, et al., Phys. Rev. **C** 75 (2007) 034317.

[147] B. Singh, J. A. Cameron, Nuclear Data Sheets 107 (2006) 225.

[148] J. A. Cameron, B. Singh, Nuclear Data Sheets 94 (2001) 429.

[149] J. A. Cameron, B. Singh, Nuclear Data Sheets 92 (2001) 783.

[150] M. A. Bentley, et al., Phys. Rev. **C** 73 (2006) 024304.

[151] T. W. Burrows, Nuclear Data Sheets 109 (2008) 171.

[152] T. W. Burrows, Nuclear Data Sheets 108 (2007) 923.

[153] T. W. Burrows, Nuclear Data Sheets 109 (2008) 1879.

[154] X. Huang, Nuclear Data Sheets 107 (2006) 2131.

[155] J. Huo, Nuclear Data Sheets 110 (2009) 2689.

[156] J. Huo, Nuclear Data Sheets 109 (2008) 787.

[157] M. R. Bhat, Nuclear Data Sheets 85 (1998) 415.

[158] C. M. Baglin, Nuclear Data Sheets 95 (2002) 215.

[159] M. Redshaw, et al., Phys. Rev. Lett. 100 (2008) 093002.

[160] D. R. Tilley, C. Cheves, J. Kelley, S. Raman, H. Weller, Nucl. Phys. **A** 636 (1998) 249.

[161] R. B. Firestone, Nuclear Data Sheets 106 (2005) 1.

[162] M. S. Basunia, Nuclear Data Sheets 111 (2010) 2331.

[163] J. A. Cameron, B. Singh, Nuclear Data Sheets 109 (2008) 1.

[164] J. A. Cameron, B. Singh, Nuclear Data Sheets 102 (2004) 293.

[165] B. Singh, J. A. Cameron, Nuclear Data Sheets 92 (2001) 1.

[166] S. -C. WU, Nuclear Data Sheets 91 (2000) 1.

[167] P. E. Garrett, et al., Phys. Rev. Lett. 87 (2001) 132502.

[168] T. W. Burrows, Nuclear Data Sheets 107 (2006) 1747.

[169] B. Singh, Nuclear Data Sheets 112 (2011) 1.

[170] A. Gadea, et al., Phys. Rev. Lett. 97 (2006) 152501.

[171] C. D. Nesaraja, S. D. Geraedts, B. Singh, Nuclear Data Sheets 111 (2010) 897.

[172] C. Wrede, et al., Phys. Rev. **C** 81 (2010) 055503.

[173] W. Shi, M. Redshaw, E. G. Myers, Phys. Rev. **A** 72 (2005) 022510.

[174] B. Singh, J. A. Cameron, Nuclear Data Sheets 107 (2006) 225.

List of Figures

List of Figures

174

List of Tables